UNIVERSITY OF BELGRADE

FACULTY OF CIVIL ENGINEERING

Miroslav S. Marjanović

Nonlinear Analysis of Laminated Composite Plates and Shells with Delaminations using Finite Element Method

Doctoral Dissertation

Belgrade, 2016.

UNIVERZITET U BEOGRADU

GRADJEVINSKI FAKULTET

Miroslav S. Marjanović

Nelinearna analiza laminatnih kompozitnih ploča i ljuski sa delaminacijama primenom metode konačnih elemenata

Doktorska disertacija

Beograd, 2016.

Miroslav S. Marjanović

Nonlinear Analysis of Laminated Composite Plates and Shells with Delaminations using Finite Element Method

Advisors:

Prof. Dr. Djordje Vuksanović
University of Belgrade, Faculty of Civil Engineering

Prof. Dr.techn. Günther Meschke
Ruhr Universität Bochum, Institute for Structural Mechanics

Comitee:

Prof. Dr.techn. Günther Meschke
Ruhr Universität Bochum, Institute for Structural Mechanics

Prof. Dr. Branislav Pujević
University of Belgrade, Faculty of Civil Engineering

Prof. Dr. Mira Petronijević
University of Belgrade, Faculty of Civil Engineering

Prof. Dr. Djordje Ladjinović
University of Novi Sad, Faculty of Technical Sciences

Assist. Prof. Dr. Marija Nefovska-Danilović
University of Belgrade, Faculty of Civil Engineering

Belgrade, ____. ____. 2016.

Acknowledgments

I would like to express a very deep gratitude to my advisor, Prof. Dr. Djordje Vuksanović of the University of Belgrade, for introducing me to the theory of composite materials, continuous encouragement during the development of the thesis, and finally for being so strict and devoted to our joint work. I am grateful for the scientific freedom he gave me during the creation of this work which allowed me to grow as a researcher.

Djordje is not with us anymore. I will miss his selfless support and will always be proud to have a privilege to work under his dedicated guidance. Thank you *George*.

I express my gratitude to Prof. Dr. Günther Meschke of the Ruhr University Bochum for his enthusiastic guidance and valuable discussions. I am not only grateful for his willingness to be a coadvisor of my work, but also for having welcomed me several times in Bochum during 2012-2015. The research stays at the Institute for Structural Mechanics have been an invaluable experience in my career.

I appreciate Prof. Meschke's careful review of this thesis and several research papers, which helped me to broaden my view in the area of finite element analysis.

My sincerest thanks are addressed to Prof. Dr. Mira Petronijević of the University of Belgrade for encouraging me to start a research in a field of Theory of Structures and her support during my studies. Her valuable advises guided me to the true values of the scientific research, while her outstanding dedication, involvement and coordination of the SEEFORM project made my visits to the Ruhr University Bochum possible.

I would also like to specially thank my good friend Marko Radišić for his great effort to help me overcome a lot of programming difficulties in MATLAB and LaTeX.

Financial Support

To the Memory of

Professor Djordje Vuksanović

Nonlinear Analysis of Laminated Composite Plates and Shells with Delaminations using Finite Element Method

Abstract

Laminated composites play an important role in the construction of aircrafts, wind turbines, ships, cars and other components in mechanical and civil engineering. For example, the aerospace structures are made of thin-walled cylindrical or spherical composite shell components having an excellent stiffness-to-weight and strength-to-weight ratios. It is also well-known that Fiber Reinforced Polymer strengthening of the RC beams and slabs give excellent structural results, low time required and moderate cost. Finally, sandwich plates are widely used in civil engineering as roof and wall panels to provide the thermal isolation of the buildings. For these reasons, numerical analysis of laminated composite and sandwich structures attract the increasing attention of researchers in the various engineering disciplines.

It is very important that perfect bond between the adjacent layers within the laminate remain intact for the panel to perform on the designed level. However, the mismatch of material properties between the adjacent layers, along with some other factors, may cause a delamination that reduces the stiffness of the component and leads to the unexpected structural behavior. To predict the response of damaged structure, a computational model capable to describe the kinematics of the delaminated structures is required.

Several limitations of the Equivalent Single Layer (ESL) laminate theories motivated the researchers to derive the refined (layerwise) plate theories for the analysis of composite laminates. Therefore, the scope of this study is based on the reduction of the 3D elasticity problem to a 2D one using the Generalized Laminated Plate Theory (GLPT) of Reddy, capable to describe the delamination kinematics. The GLPT became the basis for the development of enriched layered finite elements, which are applied in the numerical solution of several structural problems. In addition, layered plate finite elements were applied in the numerical investigation of delaminated composite shells using the simple transformations presented in this study.

To accurately capture the buckling phenomena of the laminated composites, as

well as for investigation of the influence of large rotations on the transient response of delaminated composite and sandwich plates, the geometric nonlinearity is taken into account upon the von Kármán assumptions. Beside the numerical solution, the analytical (Navier) solution for linear transient analysis of intact rectangular simply supported composite plates is provided based on double Fourier series.

During the motion of the plate a small gap maybe formed between the adjacent layers in delaminated zones. Because the initially present embedded delamination can open and close in the dynamic loading environment, the node-to-node nonlinear frictionless contact algorithm which prevent the layer overlapping is introduced. In addition, energy criterion based on the Virtual Crack Closing Technique is applied in order to predict a delamination growth in static and dynamic loading environments. The algorithm allows for the change of the previously imposed delaminated zone. Finally, the differences between the solutions considering only the stationary delamination and these allowing for delamination propagation have been highlighted.

Pre- and post-processing phases of the simulations are performed using the GiD Pre/Post Processor software developed in CIMNE, Barcelona. All numerical models and solution procedures are coded in original object-oriented MATLAB solver. Theoretical considerations are validated in the variety of numerical examples for bending, free vibration, buckling and transient analysis of delaminated composite and sandwich plates and shells. Whenever possible, the obtained results are compared with the exact, analytical, numerical and experimental data from the literature. In addition, the variety of new results (especially for the damaged structures) is given as the benchmark for future investigations. Finally, conclusions and the recommendations for the future work in this field are proposed.

Keywords: laminate, composite plate, composite shell, delamination, GLPT, FEM, bending, free vibrations, buckling

Research Field: Civil Engineering

Expertise Research Field: Engineering Mechanics and Theory of Structures

UDC: 624.04:[519.61/.64:539.3(043.3)

Nelinearna analiza laminatnih kompozitnih ploča i ljuski sa delaminacijama primenom metode konačnih elemenata

Rezime

Laminatni kompoziti igraju važnu ulogu u izradi aviona, vetrogeneratora, brodova, automobila i različitih elemenata u mašinstvu i gradjevinarstvu. Na primer, delovi kosmičkih konstrukcija su izradjeni od tankozidnih cilindričnih ili sferičnih ljuski koje imaju odlične odnose krutost-težina i čvrstoća-težina. Takodje je dobro poznato da ojačanje armirano-betonskih greda ili ploča uz pomoć polimera ojačanih vlaknima daje odlične rezultate u konstrukcijama, uz mali utrošak vremena i umereno visoku cenu. Konačno, sendvič ploče se široko primenjuju u gradjevinarstvu u vidu krovnih ili fasadnih panela kako bi se obezbedila termička izolacija zgrada. Iz ovih razloga, numerička analiza laminatnih kompozitnih i sendvič konstrukcija sve više privlači pažnju istraživača u različitim inženjerskim disciplinama.

Veoma je važno da idealna veza susednih slojeva u laminatu ostane neoštećena kako bi se panel ponašao na projektovanom nivou. Medjutim, razlika u materijalnim osobinama susednih slojeva, uz uticaj nekih dodatnih faktora, može da izazove delaminaciju koja smanjuje krutost konstrukcije i dovodi do njenog neočekivanog ponašanja. Da bi se predvideo odgovor oštećene konstrukcije potreban je numerički model koji je u stanju da opiše kinematiku ploče ili ljuske sa delaminacijom.

Odredjena ograničenja teorija laminatnih ploča zasnovanih na jednom ekvivalentnom sloju (ESL) motivisala su istraživače da razvijaju složenije (slojevite) teorije ploča za analizu laminatnih kompozita. Iz ovog razloga, predmet ovog istraživanja zasniva se na redukciji trodimenzionalnog problema teorije elastičnosti na dvodimenzionalni problem primenom Redijeve Opšte Laminatne Teorije Ploča (GLPT), koja je u mogućnosti da opiše kinematiku delaminacije. GLPT predstavlja osnovu za razvijanje složenih slojevitih konačnih elemenata koji su primenjeni u numeričkom rešavanju različitih problema. Zatim su slojeviti konačni elementi ploče primenjeni u numeričkom ispitivanju laminatnih kompozitnih ljuski sa delaminacijama, primenom jednostavnih transformacija koje su prikazane u ovom istraživanju.

Kako bi se precizno ispitao problem izbočavanja laminatnih kompozita, kao i

za ispitivanje uticaja velikih rotacija na dinamički odgovor kompozitnih i sendvič ploča sa delaminacijama, u obzir je uzeta geometrijska nelinearnost bazirana na von Kármán-ovim pretpostavkama. Pored numeričkog resenja, dato je i analitičko (Navier-ovo) rešenje u linearnoj dinamičkoj analizi neoštećenih pravougaonih slobodno oslonjenih kompozitnih ploča pomoću dvostrukih Fourier-ovih redova.

Prilikom kretanja ploče može se formirati mali razmak izmedju susednih slojeva u zonama delaminacije. Kako se prethodno prisutna delaminacija može otvarati i zatvarati pri dinamičkom opterećenju, uveden je nelinearni čvor-čvor kontaktni algoritam koji sprečava medjusobno preklapanje slojeva. Zatim je primenjen energetski kriterijum zasnovan na metodi pod nazivom *Virtual Crack Closure Technique* kako bi se predvidelo širenje delaminacije pri statičkom i dinamičkom opterećenju. Algoritam omogućava promenu oblika prethodno ubačene delaminacije. Razlike izmedju rešenja koje razmatra jedino stacionarnu delaminaciju i rešenja koje omogućava propagaciju delaminacije su na kraju istaknute u ovom radu.

Pre- i post-processing faze u numeričkim simulacijama su sprovedene primenom programa GiD Pre/Post Processor razvijenog u CIMNE, Barselona. Svi numerički modeli i procedure rešavanja su kodirane u originalnom objektno-orjentisanom MAT-LAB programu. Teoretska razmatranja su potvrdjena kroz mnoštvo numeričkih primera savijanja, slobodnih vibracija, izbočavanja i dinamičke analize laminatnih kompozitnih i sendvič ploča i ljuski sa delaminacijama. Kada god je bilo moguće, dobijeni rezultati su uporedjeni sa tačnim, analitičkim, numeričkim i eksperimental-nim rezultatima iz literature. Zatim je prikazano mnoštvo novih rezultata (naročito za oštećene konstrukcije) koji će služiti kao odrednice za buduća istraživanja. Na kraju su izvedeni zaključci i date preporuke za budući rad u ovoj oblasti.

Ključne reči: laminat, kompozitna ploča, kompozitna ljuska, delaminacija, GLPT, MKE, savijanje, slobodne vibracije, izbočavanje

Naučna oblast: Gradjevinarstvo

Uža naučna oblast: Tehnička mehanika i teorija konstrukcija

UDK: 624.04:[519.61/.64:539.3(043.3)

Contents

List of Figures

vi

List of Tables

1 Introduction

Composite materials are those formed by combining two or more materials on a macroscopic scale to achieve better engineering properties (such as stiffness, strength, weight reduction or thermal properties) in comparison with some conventional materials. *Laminated composites* are generally made of thin layers (*laminae, plies*) of different *orthotropic* materials. These fundamental building blocks consists of high-strength *fibers* (oriented in some prescribed direction) embedded in a *matrix* material. In the scope of this study, laminated composite plates composed of thin unidirectional orthotropic layers will be discussed.

A *laminate* is a collection of laminae stacked to achieve the desired stiffness and thickness. The sequence of various orientations of layers in a laminate is called the *lamination scheme* or *stacking sequence*. The lamination scheme and material properties of individual plies provide the flexibility to designers to tailor the stiffness and strength of the laminate to match a variety of structural requirements.

Composite materials attract the increasing attention in the various engineering disciplines. They play an important role in the design and construction of aircrafts, wind turbines, ships, cars and many other parts in mechanical and civil engineering. The aerospace structures are generally made of thin-walled cylindrical or spherical shell components [1], which have an excellent fatigue and corrosion resistance properties, as well as high stiffness-to-weight and strength-to-weight ratios. Examples are carbon-fiber, glass-fiber, or fiber-reinforced polymers (FRP), which include carbon-fiber reinforced plastic (CFRP) and glass-reinforced plastic (GRP). It is well-known that FRP-strengthening of the reinforced-concrete or wooden beams and slabs give excellent structural results, low time required and moderate cost.

Another type of plate structures relevant for the numerical model discussed in this study are *sandwich panels*, i.e. structural members made of two stiff orthotropic *faces* separated by an isotropic *core*. The low weight of sandwich panels was first

exploited in the aircraft industry [2]. In civil engineering, the soft-core sandwich panels are used as light roof and wall panels usually designed to provide the thermal isolation of the buildings. It is of the great importance that the bond between the face sheets and the soft-core in sandwich panel remain intact for the panel to perform on the appropriate level.
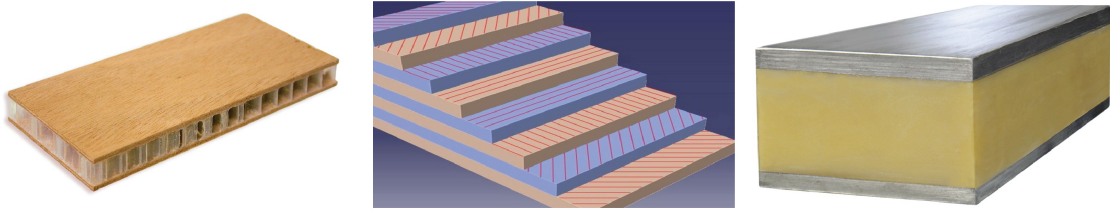
Figure 1.1: Different types of laminar composites: honeycomb sandwich plate (left), laminated composite plate (middle) and soft-core sandwich panel (right)

However, because of the mismatch of material properties between the adjacent layers, the shear stresses produced between the layers may cause *delamination*, which is the most common type of damage in laminated composite plates. Delamination may also result from the different fabrication induced faults in the joining of plies. Consideration of existing *interfacial damage* often is relevant for the assessment of the residual lifetime of such structures [3]. Once significant damage occurs at the ply level, the kinematic and material description of the problem must be changed before further analysis can proceed.

The delamination mechanics was first studied by Obreimoff [4], who estimated the specific work of interlaminar fracture. The development of production engineering of composites has aroused an interest in delamination mechanics [5]. Among other references, it is important to mention the work of Kachanov [6], in which the problem of a thin internal delamination in a circular shell was solved. An overview of delamination problems can be found in [7] (see references herein for details).

As the laminated composite plates are used for primary or secondary components of different engineering structures (which are generally loaded with transient loads), it is of the great importance to understand their fundamental dynamic characteristics, such as *natural frequencies*, *mode shapes* and *critical buckling loads*. Due to

their position in the structure, sandwich panels are also often exposed to dynamic forces such as turbulent wind loading. This requires the adequate computational models able to consider delamination of plates in dynamic loading environments in order to predict the *transient response* of the delaminated structure.

This dissertation is devoted to the numerical investigation of different types of laminated structures with the presence of delamination. The analysis is based on the reduction of the 3D-elasticity problem to a 2D one using the *Generalized Laminated Plate Theory* (GLPT) of Reddy [8], able to properly represent the kinematics of delamination [9]. The numerical solution based on the *Finite Element Method* (FEM) is proposed for the solution of differential equations of the problem. To accurately capture the buckling phenomena due to significant in-plane forces acting on the laminate, the *geometric nonlinearity* is taken into account using the nonlinear plate kinematics according to von Kármán [10].

The energy dissipated during the delamination propagation per unit of a newly created delaminated area is called *Strain Energy Release Rate* (SERR), which can be calculated using the direct or indirect methods that have been developed over years [11]. In the direct methods, special finite elements have to be implemented to predict the crack tip singularity [12, 13]. On the other hand, the indirect methods [14–17] calculate the stress intensity factors from the previously derived displacement or stress field. Within this study, the deformation field obtained from the numerical solution of the GLPT is used to predict the Strain Energy Release Rate components, which are further compared with the interlaminar fracture toughness, using the *fracture criteria* along the crack boundary. The Strain Energy Release Rates in delaminated composite plates with straight delamination front are derived analytically based on a third-order shear deformation theory by Szekrényes [18, 19].

Because the initially present embedded delamination within a plate can open and close in the dynamic loading environment, the *contact algorithms* which prevent the layer overlapping in the delaminated zone is incorporated in the numerical model. Finally, changing of the prescribed delamination shape due to the *propagation of the fracture* within a plate is predicted using the novel algorithm. These two algorithms, along with the finite element code, are implemented in a original com-

puter program (solver) which is used for all numerical calculations within this study.

The dissertation is organized as follows: in **Chapter 2** the overview of the literature and the previous research in this field is elaborated. Governing equations of the Generalized Laminated Plate Theory, which served for the derivation of analytical and numerical solutions, are given in **Chapter 3**. Analytical solution for transient response of laminated composite plates without any damage is presented in **Chapter 4**. The numerical model based on the finite element method as well as the solution procedures for different structural problems are elaborated in **Chapter 5**. Previously mentioned contact algorithm which prevents the layer overlapping in the delaminated zone is illustrated in **Chapter 6**. Delamination propagation algorithm which describe the change of the delamination shape under different types of loading is described in **Chapter 7**. After that, the proposed layered finite element of the plate is extended for the analysis of laminated composite shells in **Chapter 8**. The structure of the original object-oriented computer program used for the calculations in all numerical examples, as well as the development of the graphical user interface for the practical application of the developed computer program using GiD® Pre/Post Processor is elaborated in **Chapter 9**.

All theoretical considerations from mentioned Chapters are validated using the variety of numerical examples which are elaborated in **Chapter 10**. Whenever possible, the obtained results are compared with the existing data from the literature, and the variety of new results, especially for the delaminated structures, is given as the benchmark for future investigations. Finally, conclusions and the recommendations for the future work in this field are provided in **Chapters 11-12**.

2 Review of Previous Research

The structural response of laminated composite plates can be accurately determined by the use of simple *Equivalent-Single-Layer* (ESL) laminate theories, especially for laminates with high length-to-thickness ratios [20]. However, in the case of thicker structural components these theories are not adequate since they give too stiff structural response because of the simplifications associated with the classical plate kinematics. Example is the First-Order Shear Deformation Theory (FSDT) based on Mindlin-Reissner assumptions, where the transverse shear effects are accounted by means of shear correction factors. As shown in Refs. [21–23], ESL theories of higher order overestimate the fundamental frequencies of laminated composite and soft-core sandwich plates, especially for laminates with arbitrary layout [24]. For the extensive overview of ESL plate theories, the reader is referred to the monographs by Staab [25], Reddy [8], Gay, Hoa and Tsai [26], Leissa [27] and Carrera et al. [28], among other references. Due to the considerably different material characteristics of the adjacent layers within a laminate, discontinuities in transverse shear strains at the interfaces between layers may be significant, but this phenomenon is not accounted for in ESL theories. Another problem that arise is inability of the ESL theories to consider the local damage effects, such as matrix cracking, delamination or the free edge effects within a laminate. These limitations motivated the researchers to derive the refined (layerwise) plate theories.

The number of exact 3D elasticity solutions of the intact laminated composite plates is generally limited to the typical cases of plate geometry, loading or boundary conditions [29, 30]. Also, the exact 3D equations of elasticity which describe the shell behavior are generally complicated [31], and thus the analyses of the laminated composite shells are usually carried out using the two-dimensional shell theories. An overview of recent research in the field of dynamic analysis of laminated composite shells can be found in papers of Qatu [32–34].

The finite element solutions of the classical plate theory (CPT) based on the Kirchhoff's hypothesis overpredicts natural frequencies and buckling loads due to the neglecting of transverse shear strains [21, 35]. Reddy [36] developed the finite element based on the FSDT for geometrically nonlinear analysis of laminated composite and isotropic plates without consideration of delamination. Further, Ju et al. [37] divided the FSDT-based finite element into the delaminated and intact segments and calculated the natural frequencies and mode shapes of delaminated composite plates. Finally, Owen and Li [38] calculated the fundamental frequencies of laminated composite plates using different ESL theories and provided the comparison study.

In order to accurately incorporate the cross-sectional warping in the FSDT, Reddy [39] developed a Higher-Order Shear Deformation Theory (HSDT), where displacement expansion through the plate thickness is approximated using the cubic series expansion of thickness coordinate. Basar et al. [40] used these refined shear-deformation models with finite rotations, allowing for a quadratic shear deformation distribution across the thickness. Vuksanović also [21] investigated the single layer models of higher order based on the HSDT, and used the HSDT-based finite elements for the calculation of the dynamic response of intact composite plates. Beside the application to the analysis of laminated composite plates, HSDT-based finite elements were applied in the analysis of composite sandwich plates, for example in works of Nayak et al. [41, 42]

Reddy [43] used the shear deformable finite elements for the bending analysis of laminated composite shells, and derived the finite elements based on the various shell theories. Khdeir et al. [44] derived the analytical solutions for displacements, natural frequencies and buckling loads of cross-ply circular cylindrical shells using the CPT, FSDT and HSDT. The method of differential quadrature (DQM) [45, 46], which was improved to the Generalized Differential Quadrature Method (GDQM)[47–49], was also used for the calculation of natural frequencies of laminated composite conical shells based on different ESL shell theories in Refs. [50–53]. Several analytical solutions for the free vibration problems of laminated composite shells are derived by Tong [54, 55], based on the power series method on the basis of CPT and FSDT. Jin

et al. [56–58] have also developed a unified modified Fourier solution based on the FSDT for the vibration analysis of various composite laminated structure elements of revolution with general elastic restraints. The exact solution for free vibration analysis of thick cross-ply laminated composite cylindrical shells based on the dynamic stiffness method (DSM) is recently derived in work of Ich Thinh et al. [59].

The Generalized Laminated Plate Theory proposed by Reddy [8] and further improved by Barbero and Reddy [9] became the basis for the development of enriched *layered finite elements*, capable to describe the independent motion of every layer separately. Ćetković and Vuksanović [20] have derived both the analytical and numerical solution of the GLPT for the analysis of intact laminated composite and sandwich plates. Marjanović and Vuksanović [60] further improved this model to account for delamination kinematics and applied the model for the calculation of natural frequencies, mode shapes and critical buckling loads of delaminated composite and sandwich plates. The papers of Yam et al. [61], Lin et al. [62], Wei et al. [63] and Zhen et al. [64] served as the benchmark for comparison of the present model with experimental and numerical data. On the other hand, Alnefaie [65] used a full layerwise finite element model for the calculation of fundamental dynamic characteristics of laminated plates considering the interlaminar damage. Basar et al. [66, 67] also developed a family of multi-layer shell elements to calculate the interlaminar stresses with the high accuracy. They used the layerwise shell models to calculate the free vibration response of laminated structures. In order to reduce the computational cost arising in the GLPT, Botello et al. [68] derived the layerwise finite element model of intact composite plates using the triangular finite elements, introducing the substructuring technique to eliminate the in-plane degrees of freedom during the assembly process. Ghoshal et al. [69, 70] incorporated the interlaminar contact algorithm to enrich the plate kinematics during the so-called "breathing" phenomena in the delaminated zone of smart composite plates. Nonlinear contact conditions were incorporated in the analysis of sandwich panels using the high-order sandwich plate theory in Ref. [71].

Many authors investigated the delamination in laminated composite and sand-

wich plates using the shell formulation obtained from a degeneration of 3D solid elements. Klinkel et al. [72] derived a solid element for the nonlinear analysis of laminated shell structures, using natural strain and enhanced assumed strain methods to improve the element behavior. A refined eight-node continuum shell element with enhanced strain, capable to account for delamination using the interface element was presented in a work of Sprenger et al. [73]. The shell element with enhanced assumed strains for a geometrically non-linear theory has been presented by Klinkel and Wagner [72].

While the many researchers focused their attention on the analysis of laminated composite plate structures using the layered finite elements [9, 11, 20, 65, 74], there is still a lack of investigations regarding the applicability of layered finite elements for the analysis of laminated composite shells with delaminations. Basar et al. [66, 67] developed a family of layered shell elements to calculate the free vibration response of laminated composite cylindrical and hyperboloid shells without the delamination.

Regarding the programming issues, the first object-oriented finite element codes are proposed in [75–80], having some basic *classes* like `Node`, `Element`, `DispBC`, `ForcedBC`, `Material` and `Dof` as finite element components and some additional ones like `Gauss` and `ShapeFunction` for assisting in the numerical analysis. Dubois-Pèlerin et al. [81] have designed a structure for linear dynamic FE analysis, consisting of (1) FEM *objects*: `Node`, `Element`, `Load`, `LoadTimeFunction`, `Material`, `Dof`, `Domain`, and `LinearSolver`, (2) tools: `GaussPoint`, `Polynomial` and (3) collection classes: `Array`, `Matrix`, `String`. They also developed a nonlinear extension to a previously developed structure and presented it in Ref. [82].

In Refs. [83, 84] a more detailed codes are published for different algorithms in the dynamic analysis of structures, introducing some new numerical expressions for handling the common numerical operations in the FEM. Object-oriented nonlinear dynamic finite element code is introduced by Miller et al. [85, 86], with some new classes such as `TimeDependentLoad`, `Constrain`, `Assemblage` and `Material`, having the ability to handle both linear and nonlinear materials.

Archer et al. [87, 88] presented the another object-oriented structure for a finite element program dedicated to simulate a linear and nonlinear static and dynamic

analysis of structures. In the top level of *abstraction*, the `Analysis` class encapsulates the algorithms and the `Model` class represents the finite element components. In addition, different handlers are used to handle model dependent parts of the algorithm (`ReorderHandler`, `MatrixHandler`, `ConstraintHandler`).

Cardona et al. [89] developed the **O**bject **O**riented **F**inite **E**lements method **L**ed by **I**nteractive **E**xecutor (OOFELIE). They used this flexible tool for solving *coupled* problem where their high level language interpreting mechanism provides an extra flexibility in handling different algorithms in coupled problems. Further on, Patzák et al. [90] published an structure used in the **O**bject **O**riented **F**inite **E**lement **M**odeling (OOFEM) program which is oriented to structural analysis. Recently, Dadvand et al. [91, 92] designed a framework for building multi-disciplinary finite element programs called *Kratos*, which contains several tools for the easy implementation of different finite element applications.

3 Generalized Laminated Plate Theory

3.1 Introduction

In contrast to the ESL theories, the layerwise plate theories are developed by assuming that the displacement field exhibits only C^0-continuity through the laminate thickness. Thus the derivatives of displacement components with respect to the thickness coordinate may be discontinuous, allowing for the possibility of continuous transverse stresses at the interfaces between the adjacent layers. From the equilibrium of interlaminar forces the following continuity conditions hold between the stress field of adjacent layers at their interface [8]:

$$
\left\{ \begin{array}{c} \sigma_x \\ \sigma_y \\ \tau_{xy} \end{array} \right\}^{(k)} \neq \left\{ \begin{array}{c} \sigma_x \\ \sigma_y \\ \tau_{xy} \end{array} \right\}^{(k+1)} \quad , \quad \left\{ \begin{array}{c} \tau_{xz} \\ \tau_{yz} \\ \sigma_z \end{array} \right\}^{(k)} = \left\{ \begin{array}{c} \tau_{xz} \\ \tau_{yz} \\ \sigma_z \end{array} \right\}^{(k+1)} \tag{3.1}
$$

These conditions in turn imply that the strain field of adjacent layers satisfy the following conditions:

$$
\left\{ \begin{array}{c} \gamma_{xz} \\ \gamma_{yz} \\ \varepsilon_z \end{array} \right\}^{(k)} \neq \left\{ \begin{array}{c} \gamma_{xz} \\ \gamma_{yz} \\ \varepsilon_z \end{array} \right\}^{(k+1)} \tag{3.2}
$$

These continuity conditions can only be achieved by the use of layerwise theories or a 3-D elasticity theory. The displacement field of the GLPT allows that any desired number of layers, distribution of layers and order of interpolation can be achieved by specifying a particular mesh of one-dimensional finite elements through the thickness. The resulting strain field is kinematically correct: the in-plane strains are continuous, while the transverse strains are discontinuous through the thickness.

3.2 Assumptions and Restrictions

The Generalized Laminated Plate Theory in its extended version is based on the following assumptions:

1. All layers are perfectly bonded together, except in the previously imposed delaminated area, where the jump discontinuities (delamination openings) in three orthogonal directions may occur.

2. The previously imposed delaminated zone may change its shape during the loading process allowing for the propagation of delamination. Debonding of the boundary nodes is only possible for free plate boundaries.

3. The growth of the delamination can not change the essential boundary conditions along Γ (Dirichlet boundary) - see Figure 3.3.

4. Inextensibility of the transverse normal is imposed.

5. The overlapping of layers is prevented by a contact algorithm described in Chapter 6.

6. All layers are considered as homogeneous materials, without the possibility of transverse cracking.

The third assumption imply that the transverse displacement is independent of the thickness coordinate and the transverse normal strain $\varepsilon_{zz} = 0$. In the formulation of the theory, the following restrictions are imposed:

1. The material of each layer is linearly elastic and has three planes of material symmetry (orthotropic material).

2. Each layer is of uniform thickness.

3. Nonlinear kinematics according to von Kármán [10] are incorporated to account for moderately large rotations and small strains.

4. The transverse shear stresses on the top and the bottom surfaces of the laminate are zero ($\tau_{xz,top} = \tau_{yz,top} = \tau_{xz,bottom} = \tau_{yz,bottom} = 0$).

3.3 Formulation

This study deals with the laminated composite and composite sandwich plates composed of n orthotropic material layers with the principal coordinates of the kth lamina oriented at an angle θ_k to the laminate coordinate x (the x-axis of the local (material) coordinates of each lamina coincides with the fiber direction). The typical plates analyzed in this study are shown in Figures 3.2 and 3.3. Although not necessary, it is convenient to take the xy-plane of the problem in the mid-plane of the laminate Ω_0, while the z-axis is oriented upward. The overall plate thickness is denoted as h, while the thickness of the kth lamina is denoted as h_k. The adopted global coordinate system is Cartesian orthogonal coordinate system xyz.

The problem domain consists of the laminate domain $\overline{\Omega}_0 \equiv \Omega_0 \times (-h/2, h/2)$ and the domain boundaries: top surface $S_t(z = h/2)$, bottom surface $S_b(z = -h/2)$ and the edge $\overline{\Gamma} \equiv \Gamma \times (-h/2, h/2)$, where Γ is a curved edge surface with the outward normal $\hat{\mathbf{n}} = n_x \hat{e}_x + n_y \hat{e}_y$ (see Figure 3.1).
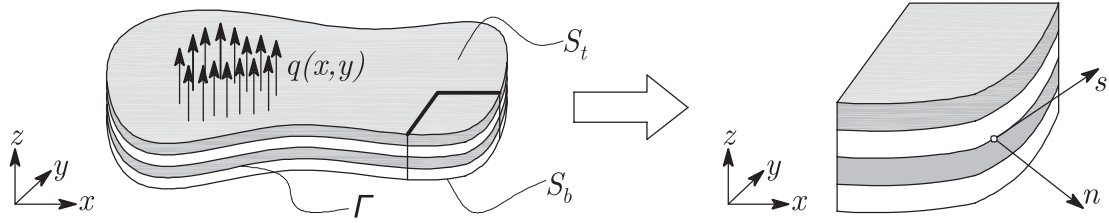
Figure 3.1: Laminated composite plate with a curved boundary
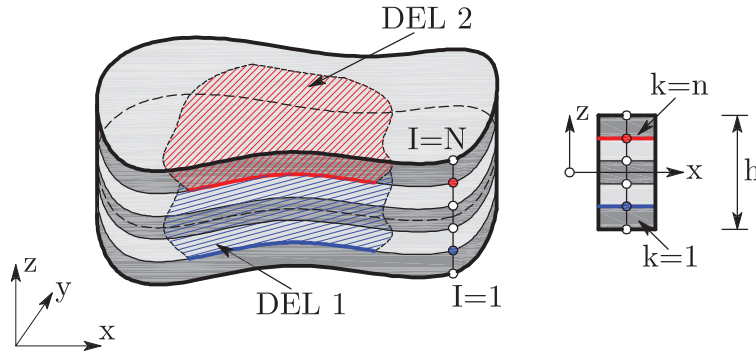
Figure 3.2: Laminated composite plate with delaminations in the global coordinate system xyz
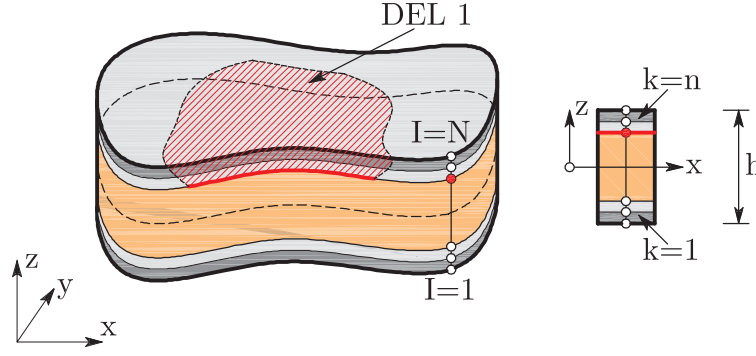
Figure 3.3: Composite sandwich plate with delamination in the global coordinate system xyz

3.4 Displacement Field

The displacement field of the arbitrary point of the laminate considering the arbitrary time point t, with coordinates (x, y, z) in the global coordinate system according to Figures 3.2 and 3.3 is adopted in this study. In the GLPT the displacements (u_1, u_2, u_3) of the arbitrary point of the plate in three orthogonal directions which coincide with the global coordinate system are denoted as follows:

$$
\begin{aligned}
u_1(x,y,z,t) &= u(x,y,t) + \sum_{I=1}^{N} u^I(x,y,t)\Phi^I(z) + \sum_{I=1}^{ND} U^I(x,y,t)H^I(z) \\
u_2(x,y,z,t) &= v(x,y,t) + \sum_{I=1}^{N} v(x,y,t)^I\Phi^I(z) + \sum_{I=1}^{ND} V^I(x,y,t)H^I(z) \qquad (3.3) \\
u_3(x,y,z,t) &= w(x,y,t) + \sum_{I=1}^{ND} W^I(x,y,t)H^I(z)
\end{aligned}
$$

In Eqs. (3.3), (u, v, w) represent the displacement components in the mid-plane of the laminate in directions x, y and z respectively, (u^I, v^I) represent the relative displacements of the Ith numerical layer through the plate thickness in relation to the middle plane of the laminate in directions x and y, respectively, and (U^I, V^I, W^I) are the jump discontinuities in the displacement field in the Ith delaminated interface in three orthogonal directions (see Figure 3.5). N is the number of interfaces between the layers including the top and bottom laminate surfaces (S_t and S_b) in which nodes through the thickness are located. These interfaces are usually denoted as numerical layers, and correspondingly $N = n + 1$. ND represents the number of numerical layers in which delamination is present.

The variable W^I is the *crack opening displacement* (COD), thus the condition $W^I \geqslant 0$ should be adopted to provide no-penetration boundary condition for delaminated surfaces of the Ith delamination. This means that if $W^I = 0$ the delaminated surfaces of the Ith delamination are in the contact condition. The *delamination front* is the boundary curve in the delamination plane, along which essential boundary conditions $U^I = V^I = W^I$ are enforced.

$\Phi^I(z)$ are selected to be layerwise continuous functions of z-coordinate. In this study, one-dimensional linear Lagrangian functions are adopted [8, 93], as shown in Figure 3.4:

$$
\begin{aligned}
&\Phi^1(z) = 1 - \frac{z}{h^{(1)}} \qquad \frac{d\Phi^1}{dz} = -\frac{1}{h^{(1)}} \qquad\qquad z_1 \leq z \leq z_2 \\
&\Phi^I = \begin{cases} \frac{z}{h^{(I-1)}} \\ 1 - \frac{z}{h^{(I)}} \end{cases} \quad \frac{d\Phi^I}{dz} = \begin{cases} \frac{1}{h^{(I-1)}} & z_{I-1} \leq z \leq z_I \\ -\frac{1}{h^{(I)}} & z_I \leq z \leq z_{I+1} \end{cases} \\
&\Phi^N(z) = \frac{z}{h^{(N-1)}} \qquad \frac{d\Phi^N}{dz} = \frac{1}{h^{(N-1)}} \qquad z_{N-1} \leq z \leq z_N
\end{aligned}
\tag{3.4}
$$

$H^I(z)$ are Heaviside step functions which describe the delamination kinematics in the Ith delaminated layer. These functions are defined as (see Figure 3.4):

$$
H^I(z) = \begin{cases} +1 & z_0 \leq z^I \leq h \\ -1 & 0 \leq z^I < z_0 \end{cases} \quad , \quad \frac{dH^I(z)}{dz} = 0
\tag{3.5}
$$
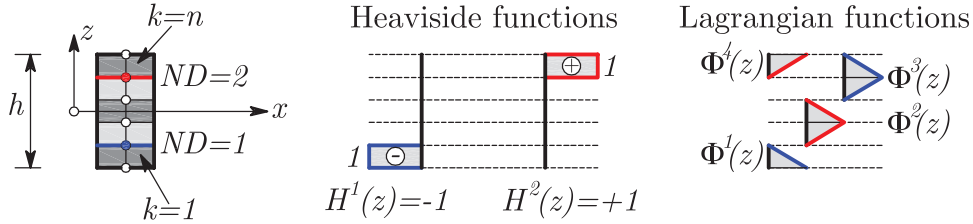
Figure 3.4: Heaviside step functions $H^I(z)$ to represent jump discontinuities (center) and Lagrangian functions $\Phi^I(z)$ to represent the layerwise change of the displacements (right)

As the consequence of the assumed displacement field, the in-plane displacements are piece-wise continuous through the thickness of the laminate in the intact region with the discontinuities at the delaminated interfaces (see Ref. [60] for details), while the transverse displacement is constant through the thickness, except in the delaminated zone. The proposed plate model allows for the consideration of an
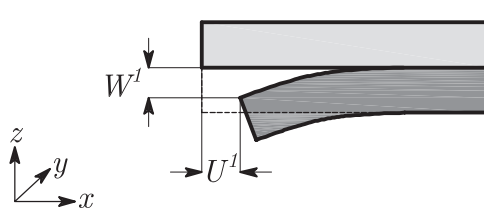
Figure 3.5: Physical interpretation of the displacements U^1 and W^1 at the delaminated interface

arbitrary number of delaminations between layers by using an arbitrary number of additional delamination expansions in the displacement field. The effect of the assumed displacement field is illustrated in Figure 3.6.
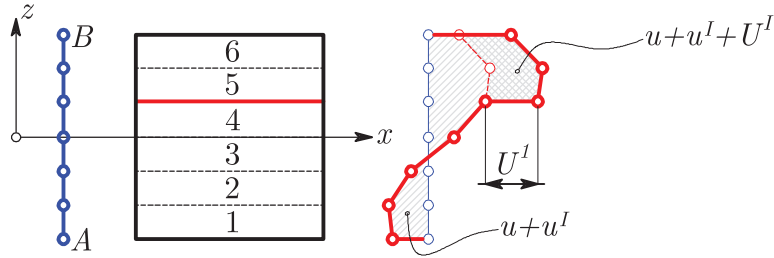
Figure 3.6: In-plane deformation of the transverse normal AB due to the assumed displacement field and the delamination between layers 4-5

3.5   Strain Field

For the plate-like structures investigated in this work, it is appropriate to consider small strains and moderately large rotations in the kinematics description [8]. This can be achieved by the use of von Kármán kinematic assumptions [10]. The strain field is divided into a linear and nonlinear part (superscripts L and NL), for the sake of simplicity. Note that transverse normal strain ε_z is equal to zero in this case, as a result of the assumption of the inextensibility of the transverse normal. The strains are discontinuous at the layer interfaces because of the layerwise definition of the functions $\Phi^I(z)$.

The von Kármán nonlinear strains associated with the assumed displacement

field can be written as follows:

$$
\varepsilon_x = \frac{\partial u_1}{\partial x} + \frac{1}{2}\left(\frac{\partial u_3}{\partial x}\right)^2 = \frac{\partial u}{\partial x} + \sum_{I=1}^{N}\frac{\partial u^I}{\partial x}\Phi^I + \sum_{I=1}^{ND}\frac{\partial U^I}{\partial x}H^I + \tag{3.6}
$$
$$
+\frac{1}{2}\left(\frac{\partial w}{\partial x}\right)^2 + \frac{\partial w}{\partial x}\sum_{I=1}^{ND}\frac{\partial W^I}{\partial x}H^I + \frac{1}{2}\sum_{I=1}^{ND}\sum_{J=1}^{ND}\frac{\partial W^I}{\partial x}\frac{\partial W^J}{\partial x}H^I H^J
$$

$$
\varepsilon_y = \frac{\partial u_2}{\partial y} + \frac{1}{2}\left(\frac{\partial u_3}{\partial y}\right)^2 = \frac{\partial v}{\partial y} + \sum_{I=1}^{N}\frac{\partial v^I}{\partial y}\Phi^I + \sum_{I=1}^{ND}\frac{\partial V^I}{\partial y}H^I + \tag{3.7}
$$
$$
+\frac{1}{2}\left(\frac{\partial w}{\partial y}\right)^2 + \frac{\partial w}{\partial y}\sum_{I=1}^{ND}\frac{\partial W^I}{\partial y}H^I + \frac{1}{2}\sum_{I=1}^{ND}\sum_{J=1}^{ND}\frac{\partial W^I}{\partial y}\frac{\partial W^J}{\partial y}H^I H^J
$$

$$
\varepsilon_z = \frac{\partial u_3}{\partial z} = 0 \tag{3.8}
$$

$$
\gamma_{yz} = \frac{\partial u_2}{\partial z} + \frac{\partial u_3}{\partial y} = \frac{\partial w}{\partial y} + \sum_{I=1}^{N}v^I\frac{d\Phi^I}{dz} + \sum_{I=1}^{ND}\frac{\partial W^I}{\partial y}H^I \tag{3.9}
$$

$$
\gamma_{xz} = \frac{\partial u_1}{\partial z} + \frac{\partial u_3}{\partial x} = \frac{\partial w}{\partial x} + \sum_{I=1}^{N}u^I\frac{d\Phi^I}{dz} + \sum_{I=1}^{ND}\frac{\partial W^I}{\partial x}H^I \tag{3.10}
$$

$$
\gamma_{xy} = \frac{\partial u_1}{\partial y} + \frac{\partial u_2}{\partial x} + \frac{\partial u_3}{\partial x}\frac{\partial u_3}{\partial y} = \frac{\partial u}{\partial y} + \frac{\partial v}{\partial x} + \sum_{I=1}^{N}\left(\frac{\partial u^I}{\partial y} + \frac{\partial v^I}{\partial x}\right)\Phi^I + \tag{3.11}
$$
$$
+\sum_{I=1}^{ND}\left(\frac{\partial U^I}{\partial y} + \frac{\partial V^I}{\partial x}\right)H^I + \frac{\partial w}{\partial x}\frac{\partial w}{\partial y} + \sum_{I=1}^{ND}\sum_{I=1}^{ND}\frac{\partial W^I}{\partial x}\frac{\partial W^I}{\partial y}H^I H^J
$$

3.6 Constitutive Equations of the Single Lamina

Before defining the constitutive equations of the single lamina, some comments regarding the selected constitutive model will be given. A *plane stress* model is adopted (see Ref. [94] and references herein for details). This choice is motivated by the fact, that for thin plates, the layerwise models which account for the transverse normal stress suffer numerical instabilities. This issue is caused by the presence

of spurious transverse normal and shear stiffness leading to the *shear locking phenomenon*. Spurious transverse normal and shear stiffness occurs when the span-to-thickness ratio of the analyzed domain (say single layer of the laminate) increases. Furthermore, in the delaminated area, the separated parts of the laminate behave as two independent thin plates, which can be correctly described using the plane stress assumptions. In some author's preliminary investigations [60] it was found that for the investigated cases the differences are minimal, with reduced computational costs for the plane stress model.

The constitutive relations for the kth orthotropic layer, for linear elastic material that follows Hooke's law, in local coordinate system of the single layer which coincides with fiber direction can be written as:

$$\overline{\sigma} = \begin{Bmatrix} \sigma_1 \\ \sigma_2 \\ \sigma_6 \\ \sigma_4 \\ \sigma_5 \end{Bmatrix}^{(k)} = \begin{bmatrix} Q_{11} & Q_{12} & 0 & 0 & 0 \\ Q_{12} & Q_{22} & 0 & 0 & 0 \\ 0 & 0 & Q_{66} & 0 & 0 \\ 0 & 0 & 0 & Q_{44} & 0 \\ 0 & 0 & 0 & 0 & Q_{55} \end{bmatrix}^{(k)} \begin{Bmatrix} \varepsilon_1 \\ \varepsilon_2 \\ \varepsilon_6 \\ \varepsilon_4 \\ \varepsilon_5 \end{Bmatrix}^{(k)} = Q\overline{\varepsilon} \quad (3.12)$$

In Eq. (3.12), $Q_{ij}^{(k)}$ are the reduced stiffness components for the plane stress case, calculated as: $Q_{11} = \frac{E_1}{1-\nu_{12}\nu_{21}}, Q_{12} = \frac{\nu_{12}E_2}{1-\nu_{12}\nu_{21}}, Q_{22} = \frac{E_2}{1-\nu_{12}\nu_{21}}, Q_{66} = G_{12}, Q_{44} = G_{23}$ and $Q_{55} = G_{13}$. In previous relations, E_1 and E_2 are moduli of elasticity of the material in two orthogonal directions, G_{12}, G_{13} and G_{23} are shear moduli, while ν_{12}, ν_{13} and ν_{23} are Poisson's ratios. Since the laminate is made of several orthotropic layers, with their material axes oriented arbitrarily with respect to the laminate coordinates, the constitutive relations must be transformed from the local (layer) to the global (laminate) coordinate system using the following relations:

$$\{\overline{\sigma}\} = [T]\{\sigma\}$$
$$\{\overline{\varepsilon}\} = [T]\{\varepsilon\}$$
$$(3.13)$$

In Eqs. (3.13), $\{\overline{\sigma}\}$ and $\{\overline{\varepsilon}\}$ are the vectors of stress and strain components in the global coordinate system, respectively, while $[T]$ is the following transformation

matrix of the kth orthotropic lamina:

$$
T = \begin{bmatrix}
\cos^2\theta & \sin^2\theta & 2\sin\theta\cos\theta & 0 & 0 \\
\sin^2\theta & \cos^2\theta & -2\sin\theta\cos\theta & 0 & 0 \\
-\sin\theta\cos\theta & \sin\theta\cos\theta & \cos^2\theta - \sin^2\theta & 0 & 0 \\
0 & 0 & 0 & \cos\theta & -\sin\theta \\
0 & 0 & 0 & \sin\theta & \cos\theta
\end{bmatrix}^{(k)}
\tag{3.14}
$$

In Eq. (3.14), θ is the angle between the fiber orientation in the kth lamina (material coordinate system) and x-axis in the global coordinate system. From here, the matrix of the plane stress stiffness coefficients of the kth layer in the global coordinate system is calculated as:

$$
\left[\overline{Q}\right] = [T]^{(k)^{-1}}[Q]^{(k)}[T]^{(k)}
\tag{3.15}
$$

The stress-strain relations in the kth orthotropic layer in global coordinate system can now be computed from the plane stress constitutive equations. For the kth orthotropic lamina the constitutive law is described as:

$$
\left\{\begin{array}{c}
\sigma_x \\
\sigma_y \\
\tau_{yz} \\
\tau_{xz} \\
\tau_{xy}
\end{array}\right\}^{(k)}
=
\begin{bmatrix}
\overline{Q}_{11} & \overline{Q}_{12} & 0 & 0 & \overline{Q}_{16} \\
\overline{Q}_{12} & \overline{Q}_{22} & 0 & 0 & \overline{Q}_{26} \\
0 & 0 & \overline{Q}_{44} & \overline{Q}_{45} & 0 \\
0 & 0 & \overline{Q}_{45} & \overline{Q}_{55} & 0 \\
\overline{Q}_{16} & \overline{Q}_{26} & 0 & 0 & \overline{Q}_{66}
\end{bmatrix}^{(k)}
\left\{\begin{array}{c}
\varepsilon_x \\
\varepsilon_y \\
\gamma_{yz} \\
\gamma_{xz} \\
\gamma_{xy}
\end{array}\right\}^{(k)}
\tag{3.16}
$$

The previous system of equations can be separated into two independent systems of equations according to:

$$
\left\{\begin{array}{c}
\sigma_x \\
\sigma_y \\
\tau_{xy}
\end{array}\right\}^{(k)}
=
\begin{bmatrix}
\overline{Q}_{11} & \overline{Q}_{12} & \overline{Q}_{16} \\
\overline{Q}_{12} & \overline{Q}_{22} & \overline{Q}_{26} \\
\overline{Q}_{16} & \overline{Q}_{26} & \overline{Q}_{66}
\end{bmatrix}^{(k)}
\left\{\begin{array}{c}
\varepsilon_x \\
\varepsilon_y \\
\gamma_{xy}
\end{array}\right\}^{(k)}
$$
$$
\left\{\begin{array}{c}
\tau_{xz} \\
\tau_{yz}
\end{array}\right\}^{(k)}
=
\begin{bmatrix}
\overline{Q}_{55} & \overline{Q}_{45} \\
\overline{Q}_{45} & \overline{Q}_{44}
\end{bmatrix}^{(k)}
\left\{\begin{array}{c}
\gamma_{xz} \\
\gamma_{yz}
\end{array}\right\}^{(k)}
\tag{3.17}
$$

The transformed plane stress stiffnesses from Eqs. 3.17 are [8]:

$$\overline{Q}_{11} = Q_{11} \cos^4 \theta + 2\left(Q_{12} + 2Q_{66}\right) \sin^2 \theta \cos^2 \theta + Q_{22} \sin^4 \theta$$

$$\overline{Q}_{12} = \left(Q_{11} + Q_{22} - 4Q_{66}\right) \sin^2 \theta \cos^2 \theta + Q_{12} \left(\sin^4 \theta + \cos^4 \theta\right)$$

$$\overline{Q}_{22} = Q_{11} \sin^4 \theta + 2\left(Q_{12} + 2Q_{66}\right) \sin^2 \theta \cos^2 \theta + Q_{22} \cos^4 \theta$$

$$\overline{Q}_{16} = \left(Q_{11} - Q_{12} - 2Q_{66}\right) \sin \theta \cos^3 \theta + \left(Q_{12} - Q_{22} + 2Q_{66}\right) \sin^3 \theta \cos \theta$$

$$\overline{Q}_{26} = \left(Q_{11} - Q_{12} - 2Q_{66}\right) \sin^3 \theta \cos \theta + \left(Q_{12} - Q_{22} + 2Q_{66}\right) \sin \theta \cos^3 \theta \qquad (3.18)$$

$$\overline{Q}_{66} = \left(Q_{11} + Q_{22} - 2Q_{12} - 2Q_{66}\right) \sin^2 \theta \cos^2 \theta + Q_{66} \left(\sin^4 \theta + cos^4\theta\right)$$

$$\overline{Q}_{44} = Q_{44} \cos^2 \theta + Q_{55} \sin^2 \theta$$

$$\overline{Q}_{45} = \left(Q_{55} - Q_{44}\right) \sin \theta \cos \theta$$

$$\overline{Q}_{55} = Q_{55} \cos^2 \theta + Q_{44} \sin^2 \theta$$

3.7 Equations of Motion

As noted before, the transverse normal strain ε_{zz} is equal to zero in the GLPT. Consequently, the variation of virtual strain is $\delta\varepsilon_{zz} = 0$ and do not enter the formulation. The governing equations of motion for the present theory can be derived using the dynamic version of the principle of virtual displacements:

$$0 = \int_0^T (\delta U + \delta V - \delta K)dt \qquad (3.19)$$

The virtual strain energy (virtual work of internal forces), virtual work of external forces and the virtual kinetic energy, respectively, are denoted as [8]:

$$\delta U = \int_\Omega \left[\int_{-h/2}^{h/2} \left(\sigma_x \delta\varepsilon_x + \sigma_y \delta\varepsilon_y + \tau_{xy} \delta\gamma_{xy} + \tau_{xz} \delta\gamma_{xz} + \tau_{yz} \delta\gamma_{yz}\right) dz \right] d\Omega \qquad (3.20)$$

$$\delta V = -\int_\Omega q(x,y) \delta w\, dx dy - \int_\Gamma \left[\int_{-h/2}^{h/2} \left(\hat{\sigma}_{nn} \delta u_n + \hat{\sigma}_{ns} \delta u_s + \hat{\sigma}_{nz} \delta w\right) dz \right] ds \qquad (3.21)$$

$$\delta K = -\int_\Omega \left[\int_{-h/2}^{h/2} \rho \left(\dot{u}_1 \delta\dot{u}_1 + \dot{u}_2 \delta\dot{u}_2 + \dot{u}_3 \delta\dot{u}_3\right) dz \right] d\Omega \qquad (3.22)$$

In Eqs. 3.19 - 3.21, $q(x, y)$ is the distributed transverse loading in the mid-plane of the laminate, $(\hat{\sigma}_{nn}, \hat{\sigma}_{ns}, \hat{\sigma}_{nz})$ are the specified stress components on the portion Γ_σ of the boundary Γ (see Figure 3.1), $(\delta u_n, \delta u_s)$ are the virtual displacements along the normal and tangential directions, respectively, on the boundary Γ, ρ is the mass density of the plate material, while the superposed dot on a variable indicates the time derivative.

The virtual displacements are zero on the portion of the boundary where the corresponding actual displacements are specified. For the time-dependent problems, the admissible virtual displacements must also vanish at times $t = 0$ and $t = T$. Having in mind that if a stress component is specified only on a part of the boundary, on the remaining part of the boundary the corresponding virtual displacements must be zero [8]. For the clear notation the derivation will be performed separately for all components which enter the principle of virtual displacements.

3.7.1 Virtual Strain Energy

Virtual strains are derived from the previously derived strain field (Eq. (3.8)):

$$
\begin{aligned}
\delta\varepsilon_x = {} & \frac{\partial \delta u}{\partial x} + \sum_{I=1}^{N} \frac{\partial \delta u^I}{\partial x} \Phi^I + \sum_{I=1}^{ND} \frac{\partial \delta U^I}{\partial x} H^I + \frac{\partial w}{\partial x} \frac{\partial \delta w}{\partial x} + \frac{\partial \delta w}{\partial x} \sum_{I=1}^{ND} \frac{\partial W^I}{\partial x} H^I + \\
& + \frac{1}{2} \sum_{I,J=1}^{ND} \left(\frac{\partial W^J}{\partial x} \frac{\partial \delta W^I}{\partial x} + \frac{\partial W^I}{\partial x} \frac{\partial \delta W^J}{\partial x} \right) H^I H^J
\end{aligned}
\tag{3.23}
$$

$$
\begin{aligned}
\delta\varepsilon_y = {} & \frac{\partial \delta v}{\partial y} + \sum_{I=1}^{N} \frac{\partial \delta v^I}{\partial y} \Phi^I + \sum_{I=1}^{ND} \frac{\partial \delta V^I}{\partial y} H^I + \frac{\partial w}{\partial y} \frac{\partial \delta w}{\partial y} + \frac{\partial \delta w}{\partial y} \sum_{I=1}^{ND} \frac{\partial W^I}{\partial y} H^I + \\
& + \frac{1}{2} \sum_{I,J=1}^{ND} \left(\frac{\partial W^J}{\partial y} \frac{\partial \delta W^I}{\partial y} + \frac{\partial W^I}{\partial y} \frac{\partial \delta W^J}{\partial y} \right) H^I H^J
\end{aligned}
\tag{3.24}
$$

$$\delta\gamma_{xy} = \frac{\partial\delta u}{\partial y} + \frac{\partial\delta v}{\partial x} + \sum_{I=1}^{N}\left(\frac{\partial\delta u^I}{\partial y} + \frac{\partial\delta v^I}{\partial x}\right)\Phi^I + \sum_{I=1}^{ND}\left(\frac{\partial\delta U^I}{\partial y} + \frac{\partial\delta V^I}{\partial x}\right)H^I +$$

$$+\frac{\partial w}{\partial y}\frac{\partial\delta w}{\partial x} + \frac{\partial w}{\partial x}\frac{\partial\delta w}{\partial y} + \sum_{I,J=1}^{ND}\left(\frac{\partial W^J}{\partial y}\frac{\partial\delta W^I}{\partial x} + \frac{\partial W^I}{\partial x}\frac{\partial\delta W^J}{\partial y}\right)H^I H^J +$$

$$+\frac{\partial\delta w}{\partial x}\sum_{I=1}^{ND}\frac{\partial W^I}{\partial y}H^I + \frac{\partial w}{\partial x}\sum_{I=1}^{ND}\frac{\partial\delta W^I}{\partial y}H^I +$$

$$+\frac{\partial\delta w}{\partial y}\sum_{I=1}^{ND}\frac{\partial W^I}{\partial x}H^I + \frac{\partial w}{\partial y}\sum_{I=1}^{ND}\frac{\partial\delta W^I}{\partial x}H^I \qquad (3.25)$$

$$\delta\gamma_{xz} = \frac{\partial\delta w}{\partial x} + \sum_{I=1}^{N}u^I\frac{d\Phi^I}{dz} + \sum_{I=1}^{ND}\frac{d\delta W^I}{dx}H^I \qquad (3.26)$$

$$\delta\gamma_{yz} = \frac{\partial\delta w}{\partial y} + \sum_{I=1}^{N}v^I\frac{d\Phi^I}{dz} + \sum_{I=1}^{ND}\frac{d\delta W^I}{dy}H^I \qquad (3.27)$$

After the incorporation of virtual strains from Eqs. (3.23) - (3.27) into the Eq. (3.20), the linear and nonlinear portions of the virtual strain energy are derived:

$$\delta U^L = \int_{\Omega}\int_{-h/2}^{h/2}\begin{bmatrix}\sigma_x\left(\frac{\partial\delta u}{\partial x} + \sum_{I=1}^{N}\frac{\partial\delta u^I}{\partial x}\Phi^I + \sum_{I=1}^{ND}\frac{\partial\delta U^I}{\partial x}H^I\right) + \\ +\sigma_y\left(\frac{\partial\delta v}{\partial y} + \sum_{I=1}^{N}\frac{\partial\delta v^I}{\partial y}\Phi^I + \sum_{I=1}^{ND}\frac{\partial\delta V^I}{\partial y}H^I\right) + \\ +\tau_{xy}\left(\frac{\partial\delta u}{\partial y} + \frac{\partial\delta v}{\partial x} + \sum_{I=1}^{N}\left(\frac{\partial\delta u^I}{\partial y} + \frac{\partial\delta v^I}{\partial x}\right)\Phi^I\right) + \\ +\tau_{xy}\sum_{I=1}^{ND}\left(\frac{\partial\delta U^I}{\partial y} + \frac{\partial\delta V^I}{\partial x}\right)H^I + \\ +\tau_{xz}\left(\frac{\partial\delta w}{\partial x} + \sum_{I=1}^{N}u^I\frac{d\Phi^I}{dz} + \sum_{I=1}^{ND}\frac{d\delta W^I}{dx}H^I\right) + \\ +\tau_{yz}\left(\frac{\partial\delta w}{\partial y} + \sum_{I=1}^{N}v^I\frac{d\Phi^I}{dz} + \sum_{I=1}^{ND}\frac{d\delta W^I}{dy}H^I\right)\end{bmatrix}dz d\Omega \qquad (3.28)$$

$$
\delta U^{NL} = \int_\Omega \int_{-h/2}^{h/2}
\begin{bmatrix}
\sigma_x \left(\frac{\partial w}{\partial x} \frac{\partial \delta w}{\partial x} + \frac{\partial \delta w}{\partial x} \sum_{I=1}^{ND} \frac{\partial W^I}{\partial x} H^I \right) + \\[2mm]
+ \sigma_x \left(\frac{1}{2} \sum_{I,J=1}^{ND} \left(\frac{\partial W^J}{\partial x} \frac{\partial \delta W^I}{\partial x} + \frac{\partial W^I}{\partial x} \frac{\partial \delta W^J}{\partial x} \right) H^I H^J \right) + \\[2mm]
+ \sigma_y \left(\frac{\partial w}{\partial y} \frac{\partial \delta w}{\partial y} + \frac{\partial \delta w}{\partial y} \sum_{I=1}^{ND} \frac{\partial W^I}{\partial y} H^I \right) + \\[2mm]
+ \sigma_y \left(\frac{1}{2} \sum_{I,J=1}^{ND} \left(\frac{\partial W^J}{\partial y} \frac{\partial \delta W^I}{\partial y} + \frac{\partial W^I}{\partial y} \frac{\partial \delta W^J}{\partial y} \right) H^I H^J \right) + \\[2mm]
+ \tau_{xy} \left(\frac{\partial w}{\partial y} \frac{\partial \delta w}{\partial x} + \frac{\partial w}{\partial x} \frac{\partial \delta w}{\partial y} \right) + \\[2mm]
+ \tau_{xy} \left(\sum_{I,J=1}^{ND} \left(\frac{\partial W^J}{\partial y} \frac{\partial \delta W^I}{\partial x} + \frac{\partial W^I}{\partial x} \frac{\partial \delta W^J}{\partial y} \right) H^I H^J \right) + \\[2mm]
+ \tau_{xy} \left(\frac{\partial \delta w}{\partial x} \sum_{I=1}^{ND} \frac{\partial W^I}{\partial y} H^I + \frac{\partial w}{\partial x} \sum_{I=1}^{ND} \frac{\partial \delta W^I}{\partial y} H^I \right) + \\[2mm]
+ \tau_{xy} \left(\frac{\partial \delta w}{\partial y} \sum_{I=1}^{ND} \frac{\partial W^I}{\partial x} H^I + \frac{\partial w}{\partial y} \sum_{I=1}^{ND} \frac{\partial \delta W^I}{\partial x} H^I \right)
\end{bmatrix}
dz\, d\Omega \quad (3.29)
$$

To reduce the 3D model to a 2D one, we eliminate the z-coordinate by the explicit integration of stress components multiplied with the corresponding functions $\Phi^I(z)$ or $H^I(z)$. In this way we introduce the following stress resultants as the integrals of the stress components through the thickness of the plate:

$$
\left\{ \begin{array}{ccccc} N_x & N_y & N_{xy} & Q_x & Q_y \end{array} \right\} = \sum_{k=1}^{n} \int_{z_k}^{z_{k+1}} \left\{ \begin{array}{ccccc} \sigma_x & \sigma_y & \tau_{xy} & \tau_{xz} & \tau_{yz} \end{array} \right\}^{(k)} dz
$$

$$
\left\{ \begin{array}{ccc} N_x^I & N_y^I & N_{xy}^I \end{array} \right\} = \sum_{k=1}^{n} \int_{z_k}^{z_{k+1}} \left\{ \begin{array}{ccc} \sigma_x & \sigma_y & \tau_{xy} \end{array} \right\}^{(k)} \Phi^I dz
$$

$$
\left\{ \begin{array}{cc} Q_x^I & Q_y^I \end{array} \right\} = \sum_{k=1}^{n} \int_{z_k}^{z_{k+1}} \left\{ \begin{array}{cc} \tau_{xz} & \tau_{yz} \end{array} \right\}^{(k)} \frac{d\Phi^I}{dz} dz
$$

$$
\left\{ \begin{array}{ccccc} \overline{N}_x^I & \overline{N}_y^I & \overline{N}_{xy}^I & \overline{Q}_x^I & \overline{Q}_y^I \end{array} \right\} = \sum_{k=1}^{n} \int_{z_k}^{z_{k+1}} \left\{ \begin{array}{ccccc} \sigma_x & \sigma_y & \tau_{xy} & \tau_{xz} & \tau_{yz} \end{array} \right\}^{(k)} H^I dz
$$

$$
\left\{ \begin{array}{ccc} \overline{N}_x^{IJ} & \overline{N}_y^{IJ} & \overline{N}_{xy}^{IJ} \end{array} \right\} = \sum_{k=1}^{n} \int_{z_k}^{z_{k+1}} \left\{ \begin{array}{ccc} \sigma_x & \sigma_y & \tau_{xy} \end{array} \right\}^{(k)} H^I H^J dz
$$

$$
\left\{ \begin{array}{cc} \overline{Q}_x^{IJ} & \overline{Q}_y^{IJ} \end{array} \right\} = \sum_{k=1}^{n} \int_{z_k}^{z_{k+1}} \left\{ \begin{array}{cc} \tau_{xz} & \tau_{yz} \end{array} \right\}^{(k)} H^I H^J dz
$$

$$(3.30)$$

In Eqs. (3.30), N_x, N_y, N_{xy}, Q_x, Q_y are the mid-plane stress resultants, N_x^I, N_y^I, N_{xy}^I, Q_x^I, Q_y^I are relative values of the stress resultants in the Ith delaminated interface, while the $\overline{N}_x^I$, $\overline{N}_y^I$, $\overline{N}_{xy}^I$, $\overline{Q}_x^I$, $\overline{Q}_y^I$ are the stress resultants in the Ith delaminated layer (the forces to hold the delaminated nodes together in the Ith delaminated interface). If we substitute the stress resultants of the laminate from (3.30) into the Eqs. (3.28)

- (3.29) we obtain the virtual strain energy in the following form:

$$
\delta U^L = \int\limits_{\Omega} \left\{
\begin{array}{l}
N_x \frac{\partial \delta u}{\partial x} + N_y \frac{\partial \delta v}{\partial y} + N_{xy}\left(\frac{\partial \delta u}{\partial y} + \frac{\partial \delta v}{\partial x}\right) + Q_x \frac{\partial \delta w}{\partial x} + Q_y \frac{\partial \delta w}{\partial y} + \\[2mm]
+ \sum\limits_{I=1}^{N}\left[
\begin{array}{l}
N_x^I \frac{\partial \delta u^I}{\partial x} + N_y^I \frac{\partial \delta v^I}{\partial y} + N_{xy}^I\left(\frac{\partial \delta u^I}{\partial y} + \frac{\partial \delta v^I}{\partial x}\right) + \\[1mm]
+ Q_x^I \delta u^I + Q_y^I \delta v^I
\end{array}
\right] + \\[2mm]
+ \sum\limits_{I=1}^{ND}\left[\overline{N}_x^I \frac{\partial \delta U^I}{\partial x} + \overline{N}_y^I \frac{\partial \delta V^I}{\partial y} + \overline{N}_{xy}^I\left(\frac{\partial \delta U^I}{\partial y} + \frac{\partial \delta V^I}{\partial x}\right)\right] + \\[2mm]
+ \sum\limits_{I=1}^{ND}\left(\overline{Q}_x^I \frac{\partial \delta W^I}{\partial x} + \overline{Q}_y^I \frac{\partial \delta W^I}{\partial y}\right)
\end{array}
\right\} d\Omega \quad (3.31)
$$

$$
\delta U^{NL} = \int\limits_{\Omega} \left\{
\begin{array}{l}
N_x \frac{\partial w}{\partial x}\frac{\partial \delta w}{\partial x} + N_y \frac{\partial w}{\partial y}\frac{\partial \delta w}{\partial y} + N_{xy}\left(\frac{\partial w}{\partial y}\frac{\partial \delta w}{\partial x} + \frac{\partial w}{\partial x}\frac{\partial \delta w}{\partial y}\right) + \\[2mm]
+ \overline{N}_x^I\left(\frac{\partial \delta w}{\partial x}\sum\limits_{I=1}^{ND}\frac{\partial W^I}{\partial x} + \frac{\partial w}{\partial x}\sum\limits_{I=1}^{ND}\frac{\partial \delta W^I}{\partial x}\right) + \\[2mm]
+ \overline{N}_y^I\left(\frac{\partial \delta w}{\partial y}\sum\limits_{I=1}^{ND}\frac{\partial W^I}{\partial y} + \frac{\partial w}{\partial y}\sum\limits_{I=1}^{ND}\frac{\partial \delta W^I}{\partial y}\right) + \\[2mm]
+ \overline{N}_{xy}^I\left(
\begin{array}{l}
\frac{\partial \delta w}{\partial x}\sum\limits_{I=1}^{ND}\frac{\partial W^I}{\partial y} + \frac{\partial w}{\partial x}\sum\limits_{I=1}^{ND}\frac{\partial \delta W^I}{\partial y} + \\[1mm]
+ \frac{\partial \delta w}{\partial y}\sum\limits_{I=1}^{ND}\frac{\partial W^I}{\partial x} + \frac{\partial w}{\partial y}\sum\limits_{I=1}^{ND}\frac{\partial \delta W^I}{\partial x}
\end{array}
\right) + \\[2mm]
+ \overline{N}_x^{IJ}\sum\limits_{I,J=1}^{ND}\frac{1}{2}\left(\frac{\partial W^J}{\partial x}\frac{\partial \delta W^I}{\partial x} + \frac{\partial W^I}{\partial x}\frac{\partial \delta W^J}{\partial x}\right) + \\[2mm]
+ \overline{N}_y^{IJ}\sum\limits_{I,J=1}^{ND}\frac{1}{2}\left(\frac{\partial W^J}{\partial y}\frac{\partial \delta W^I}{\partial y} + \frac{\partial W^I}{\partial y}\frac{\partial \delta W^J}{\partial y}\right) + \\[2mm]
+ \overline{N}_{xy}^{IJ}\sum\limits_{I,J=1}^{ND}\left(\frac{\partial W^J}{\partial y}\frac{\partial \delta W^I}{\partial x} + \frac{\partial W^I}{\partial x}\frac{\partial \delta W^J}{\partial y}\right)
\end{array}
\right\} d\Omega \quad (3.32)
$$

In previous equations the derivations of virtual displacements exist, which have to be eliminated. This is done by performing the integration by parts for the surface integral, using the following formulas:

$$
\begin{aligned}
\int\limits_{\Omega} F(x,y)\frac{\partial G(x,y)}{\partial x}d\Omega &= \oint\limits_{\Gamma} F(x,y)G(x,y)n_x ds - \int\limits_{\Omega} G(x,y)\frac{\partial F(x,y)}{\partial x}d\Omega \\
\int\limits_{\Omega} F(x,y)\frac{\partial G(x,y)}{\partial y}d\Omega &= \oint\limits_{\Gamma} F(x,y)G(x,y)n_y ds - \int\limits_{\Omega} G(x,y)\frac{\partial F(x,y)}{\partial y}d\Omega
\end{aligned}
\quad (3.33)
$$

After the integration by parts all members corresponding to the specific virtual

displacement are grouped. Consequently:

$$\delta U^L = \oint_{\Gamma} \left\{ \begin{aligned} &\delta u \left(N_x n_x + N_{xy} n_y\right) + \delta v \left(N_{xy} n_x + N_y n_y\right) + \\ &+ \delta w \left(Q_x n_x + Q_y n_y\right) + \\ &+ \sum_{I=1}^{N} \left[\delta u^I \left(N_x^I n_x + N_{xy}^I n_y\right) + \delta v^I \left(N_{xy}^I n_x + N_y^I n_y\right)\right] + \\ &+ \sum_{I=1}^{ND} \left[\delta U^I \left(\overline{N}_x^I n_x + \overline{N}_{xy}^I n_y\right) + \delta V^I \left(\overline{N}_{xy}^I n_x + \overline{N}_y^I n_y\right)\right] + \\ &+ \sum_{I=1}^{ND} \left[\delta W^I \left(\overline{Q}_x^I n_x + \overline{Q}_y^I n_y\right)\right] \end{aligned} \right\} ds -$$

$$- \int_{\Omega} \left\{ \begin{aligned} &\delta u \left(\frac{\partial N_x}{\partial x} + \frac{\partial N_{xy}}{\partial y}\right) + \delta v \left(\frac{\partial N_{xy}}{\partial x} + \frac{\partial N_y}{\partial y}\right) + \delta w \left(\frac{\partial Q_x}{\partial x} + \frac{\partial Q_y}{\partial y}\right) + \\ &+ \sum_{I=1}^{N} \left[\delta u^I \left(\frac{\partial N_x^I}{\partial x} + \frac{\partial N_{xy}^I}{\partial y} - Q_x^I\right) + \delta v^I \left(\frac{\partial N_{xy}^I}{\partial x} + \frac{\partial N_y^I}{\partial y} - Q_y^I\right)\right] + \\ &+ \sum_{I=1}^{ND} \left[\delta U^I \left(\frac{\partial \overline{N}_x^I}{\partial x} + \frac{\partial \overline{N}_{xy}^I}{\partial y}\right) + \delta V^I \left(\frac{\partial \overline{N}_{xy}^I}{\partial x} + \frac{\partial \overline{N}_y^I}{\partial y}\right)\right] + \\ &+ \sum_{I=1}^{ND} \delta W^I \left(\frac{\partial \overline{Q}_x^I}{\partial x} + \frac{\partial \overline{Q}_y^I}{\partial y}\right) \end{aligned} \right\} d\Omega$$

$$(3.34)$$

$$\delta U^{NL} = \oint_{\Gamma} \left\{ \begin{aligned} &\delta w \left[N_x \frac{\partial w}{\partial x} n_x + N_y \frac{\partial w}{\partial y} n_y + N_{xy} \left(\frac{\partial w}{\partial y} n_x + \frac{\partial w}{\partial x} n_y\right)\right] + \\ &+ \sum_{I=1}^{ND} \delta w \left[\overline{N}_x^I \frac{\partial W^I}{\partial x} n_x + \overline{N}_y^I \frac{\partial W^I}{\partial y} n_y + \overline{N}_{xy}^I \left(\frac{\partial W^I}{\partial y} n_x + \frac{\partial W^I}{\partial x} n_y\right)\right] + \\ &+ \sum_{I=1}^{ND} \delta W^I \left[\overline{N}_x^I \frac{\partial w}{\partial x} n_x + \overline{N}_y^I \frac{\partial w}{\partial y} n_y + \overline{N}_{xy}^I \left(\frac{\partial w}{\partial y} n_x + \frac{\partial w}{\partial x} n_y\right)\right] + \\ &+ \sum_{I,J=1}^{ND} \delta W^I \left[\begin{aligned} &\overline{N}_x^{IJ} \frac{\partial W^J}{\partial x} n_x + \overline{N}_y^{IJ} \frac{\partial W^J}{\partial y} n_y + \\ &+ \overline{N}_{xy}^{IJ} \left(\frac{\partial W^J}{\partial y} n_x + \frac{\partial W^J}{\partial x} n_y\right) \end{aligned}\right] \end{aligned} \right\} ds -$$

$$- \int_{\Omega} \left\{ \begin{aligned} &\delta w \left[\frac{\partial}{\partial x}\left(N_x \frac{\partial w}{\partial x} + N_{xy}\frac{\partial w}{\partial y}\right) + \frac{\partial}{\partial y}\left(N_{xy}\frac{\partial w}{\partial x} + N_y\frac{\partial w}{\partial y}\right)\right] + \\ &+ \sum_{I=1}^{ND} \delta w \left[\frac{\partial}{\partial x}\left(\overline{N}_x^I \frac{\partial W^I}{\partial x} + \overline{N}_{xy}^I\frac{\partial W^I}{\partial y}\right) + \frac{\partial}{\partial y}\left(\overline{N}_{xy}^I\frac{\partial W^I}{\partial x} + \overline{N}_y^I\frac{\partial W^I}{\partial y}\right)\right] + \\ &+ \sum_{I=1}^{ND} \delta W^I \left[\frac{\partial}{\partial x}\left(\overline{N}_x^I \frac{\partial w}{\partial x} + \overline{N}_{xy}^I\frac{\partial w}{\partial y}\right) + \frac{\partial}{\partial y}\left(\overline{N}_{xy}^I\frac{\partial w}{\partial x} + \overline{N}_y^I\frac{\partial w}{\partial y}\right)\right] + \\ &+ \sum_{I,J=1}^{ND} \delta W^I \left[\frac{\partial}{\partial x}\left(\overline{N}_x^{IJ} \frac{\partial W^J}{\partial x} + \overline{N}_{xy}^{IJ}\frac{\partial W^J}{\partial y}\right) + \frac{\partial}{\partial y}\left(\overline{N}_{xy}^{IJ}\frac{\partial W^J}{\partial x} + \overline{N}_y^{IJ}\frac{\partial W^J}{\partial y}\right)\right] \end{aligned} \right\} d\Omega$$

$$(3.35)$$

Now $(\delta u, \delta v)$ should be expressed in terms of $(\delta u_{0n}, \delta u_{0s})$. If the unit outward normal vector $\hat{\mathbf{n}}$ is oriented at an angle θ from the x-axis, then its direction cosines are $n_x = \cos\theta$ and $n_y = \sin\theta$. Since there exists the relations:

$$\left\{ \begin{array}{c} \delta u \\ \delta v \end{array} \right\} = \left[\begin{array}{cc} n_x & -n_y \\ n_y & n_x \end{array} \right] \left\{ \begin{array}{c} \delta u_{0n} \\ \delta u_{0s} \end{array} \right\} \tag{3.36}$$

$$\left\{ \begin{array}{c} \delta u^I \\ \delta v^I \end{array} \right\} = \left[\begin{array}{cc} n_x & -n_y \\ n_y & n_x \end{array} \right] \left\{ \begin{array}{c} \delta u_n^I \\ \delta u_s^I \end{array} \right\} \tag{3.37}$$

$$\left\{ \begin{array}{c} \delta U^I \\ \delta V^I \end{array} \right\} = \left[\begin{array}{cc} n_x & -n_y \\ n_y & n_x \end{array} \right] \left\{ \begin{array}{c} \delta U_n^I \\ \delta U_s^I \end{array} \right\} \tag{3.38}$$

Also, from the fact that the stresses $(\sigma_{nn}, \sigma_{ns})$ are related to $(\sigma_x, \sigma_y, \tau_{xy})$ by the transformation:

$$\left\{ \begin{array}{c} \sigma_{nn} \\ \sigma_{ns} \end{array} \right\} = \left[\begin{array}{ccc} n_x^2 & n_y^2 & 2n_x n_y \\ -n_x n_y & n_x n_y & n_x^2 - n_y^2 \end{array} \right] \left\{ \begin{array}{c} \sigma_x \\ \sigma_y \\ \tau_{xy} \end{array} \right\} \tag{3.39}$$

the transformations of force resultants is expressed as:

$$\left\{ \begin{array}{c} N_{nn} \\ N_{ns} \end{array} \right\} = \left[\begin{array}{ccc} n_x^2 & n_y^2 & 2n_x n_y \\ -n_x n_y & n_x n_y & n_x^2 - n_y^2 \end{array} \right] \left\{ \begin{array}{c} N_x \\ N_y \\ N_{xy} \end{array} \right\} \tag{3.40}$$

$$\left\{ \begin{array}{c} N_{nn}^I \\ N_{ns}^I \end{array} \right\} = \left[\begin{array}{ccc} n_x^2 & n_y^2 & 2n_x n_y \\ -n_x n_y & n_x n_y & n_x^2 - n_y^2 \end{array} \right] \left\{ \begin{array}{c} N_x^I \\ N_y^I \\ N_{xy}^I \end{array} \right\} \tag{3.41}$$

$$\left\{ \begin{array}{c} \overline{N}_{nn}^I \\ \overline{N}_{ns}^I \end{array} \right\} = \left[\begin{array}{ccc} n_x^2 & n_y^2 & 2n_x n_y \\ -n_x n_y & n_x n_y & n_x^2 - n_y^2 \end{array} \right] \left\{ \begin{array}{c} \overline{N}_x^I \\ \overline{N}_y^I \\ \overline{N}_{xy}^I \end{array} \right\} \tag{3.42}$$

Similarly, the normal and tangential derivatives $\left(\frac{\partial w}{\partial x}, \frac{\partial w}{\partial y} \right)$ and $\left(\frac{\partial W^I}{\partial x}, \frac{\partial W^I}{\partial y} \right)$ are related to the derivatives $\left(\frac{\partial w}{\partial n}, \frac{\partial w}{\partial s} \right)$ and $\left(\frac{\partial W^I}{\partial n}, \frac{\partial W^I}{\partial s} \right)$ by:

$$\left\{ \begin{array}{c} \frac{\partial w}{\partial x} \\ \frac{\partial w}{\partial y} \end{array} \right\} = \left[\begin{array}{cc} n_x & -n_y \\ n_y & n_x \end{array} \right] \left\{ \begin{array}{c} \frac{\partial w}{\partial n} \\ \frac{\partial w}{\partial s} \end{array} \right\}, \quad \left\{ \begin{array}{c} \frac{\partial W^I}{\partial x} \\ \frac{\partial W^I}{\partial y} \end{array} \right\} = \left[\begin{array}{cc} n_x & -n_y \\ n_y & n_x \end{array} \right] \left\{ \begin{array}{c} \frac{\partial W^I}{\partial n} \\ \frac{\partial W^I}{\partial s} \end{array} \right\}$$
$$\tag{3.43}$$

Finally the following form of the virtual strain energy is obtained:

$$
\delta U^L = \oint_\Gamma \left\{
\begin{array}{l}
N_{nn}\delta u_{0n} + N_{ns}\delta u_{0s} + \left(Q_x n_x + Q_y n_y\right)\delta w + \\
+ \sum\limits_{I=1}^{N} \left(N_{nn}^I \delta u_n^I + N_{ns}^I \delta u_s^I\right) + \\
+ \sum\limits_{I=1}^{ND} \left[\overline{N}_{nn}^I \delta U_n^I + \overline{N}_{ns}^I \delta U_s^I + \left(\overline{Q}_x^I n_x + \overline{Q}_y^I n_y\right)\delta W^I\right]
\end{array}
\right\} ds -
$$

$$
- \int_\Omega \left\{
\begin{array}{l}
\delta u\left(\frac{\partial N_x}{\partial x} + \frac{\partial N_{xy}}{\partial y}\right) + \delta v\left(\frac{\partial N_{xy}}{\partial x} + \frac{\partial N_y}{\partial y}\right) + \delta w\left(\frac{\partial Q_x}{\partial x} + \frac{\partial Q_y}{\partial y}\right) + \\
+ \sum\limits_{I=1}^{N}\left[\delta u^I\left(\frac{\partial N_x^I}{\partial x} + \frac{\partial N_{xy}^I}{\partial y} - Q_x^I\right) + \delta v^I\left(\frac{\partial N_{xy}^I}{\partial x} + \frac{\partial N_y^I}{\partial y} - Q_y^I\right)\right] + \\
+ \sum\limits_{I=1}^{ND}\left[\delta U^I\left(\frac{\partial \overline{N}_x^I}{\partial x} + \frac{\partial \overline{N}_{xy}^I}{\partial y}\right) + \delta V^I\left(\frac{\partial \overline{N}_{xy}^I}{\partial x} + \frac{\partial \overline{N}_y^I}{\partial y}\right)\right] + \\
+ \sum\limits_{I=1}^{ND}\delta W^I\left(\frac{\partial \overline{Q}_x^I}{\partial x} + \frac{\partial \overline{Q}_y^I}{\partial y}\right)
\end{array}
\right\} d\Omega
\tag{3.44}
$$

$$
\delta U^{NL} = \oint_\Gamma \left\{
\begin{array}{l}
\delta w\left[N_{nn}\frac{\partial w}{\partial n} + N_{ns}\frac{\partial w}{\partial s} + \sum\limits_{I=1}^{ND}\left(\overline{N}_{nn}^I\frac{\partial W^I}{\partial n} + \overline{N}_{ns}^I\frac{\partial W^I}{\partial s}\right)\right] + \\
+ \sum\limits_{I=1}^{ND}\delta W^I\left(\overline{N}_{nn}^I\frac{\partial w}{\partial n} + \overline{N}_{ns}^I\frac{\partial w}{\partial s}\right) + \\
+ \sum\limits_{I,J=1}^{ND}\delta W^I\left(\overline{N}_{nn}^{IJ}\frac{\partial W^J}{\partial n} + \overline{N}_{ns}^{IJ}\frac{\partial W^J}{\partial s}\right)
\end{array}
\right\} ds -
$$

$$
- \int_\Omega \left\{
\begin{array}{l}
\delta w\left[\frac{\partial}{\partial x}\left(N_x\frac{\partial w}{\partial x} + N_{xy}\frac{\partial w}{\partial y}\right) + \frac{\partial}{\partial y}\left(N_{xy}\frac{\partial w}{\partial x} + N_y\frac{\partial w}{\partial y}\right)\right] + \\
+ \sum\limits_{I=1}^{ND}\delta w\left[\frac{\partial}{\partial x}\left(\overline{N}_x^I\frac{\partial W^I}{\partial x} + \overline{N}_{xy}^I\frac{\partial W^I}{\partial y}\right) + \frac{\partial}{\partial y}\left(\overline{N}_{xy}^I\frac{\partial W^I}{\partial x} + \overline{N}_y^I\frac{\partial W^I}{\partial y}\right)\right] + \\
+ \sum\limits_{I=1}^{ND}\delta W^I\left[\frac{\partial}{\partial x}\left(\overline{N}_x^I\frac{\partial w}{\partial x} + \overline{N}_{xy}^I\frac{\partial w}{\partial y}\right) + \frac{\partial}{\partial y}\left(\overline{N}_{xy}^I\frac{\partial w}{\partial x} + \overline{N}_y^I\frac{\partial w}{\partial y}\right)\right] + \\
+ \sum\limits_{I,J=1}^{ND}\delta W^I\left[\frac{\partial}{\partial x}\left(\overline{N}_x^{IJ}\frac{\partial W^J}{\partial x} + \overline{N}_{xy}^{IJ}\frac{\partial W^J}{\partial y}\right) + \frac{\partial}{\partial y}\left(\overline{N}_{xy}^{IJ}\frac{\partial W^J}{\partial x} + \overline{N}_y^{IJ}\frac{\partial W^J}{\partial y}\right)\right]
\end{array}
\right\} d\Omega
$$

$$
\tag{3.45}
$$

3.7.2 Constitutive Equations of the Laminate

Before proceeding with the derivation of the virtual work components, it is convenient now to introduce the constitutive equations of the laminate, which relates the stress resultants of the laminate with the deformation components. The laminate constitutive equations can be derived by the substitution of the constitutive equations of the single lamina from Eq. (3.16) in the expressions for stress resultants

from Eq. (3.30). Here we obtain:

$$
\begin{Bmatrix} N_x \\ N_y \\ N_{xy} \end{Bmatrix} = \begin{bmatrix} A_{11} & A_{12} & A_{16} \\ & A_{22} & A_{26} \\ & & A_{66} \end{bmatrix} \begin{Bmatrix} \frac{\partial u}{\partial x} + \frac{1}{2}\left(\frac{\partial w}{\partial x}\right)^2 \\ \frac{\partial v}{\partial y} + \frac{1}{2}\left(\frac{\partial w}{\partial y}\right)^2 \\ \frac{\partial u}{\partial y} + \frac{\partial v}{\partial x} + \frac{\partial w}{\partial x}\frac{\partial w}{\partial y} \end{Bmatrix} + \tag{3.46}
$$

$$
+ \sum_{I=1}^{N} \begin{bmatrix} B_{11}^I & B_{12}^I & B_{16}^I \\ & B_{22}^I & B_{26}^I \\ & & B_{66}^I \end{bmatrix} \begin{Bmatrix} \frac{\partial u^I}{\partial x} \\ \frac{\partial v^I}{\partial y} \\ \frac{\partial u^I}{\partial y} + \frac{\partial v^I}{\partial x} \end{Bmatrix} +
$$

$$
+ \sum_{I=1}^{ND} \begin{bmatrix} E_{11}^I & E_{12}^I & E_{16}^I \\ & E_{22}^I & E_{26}^I \\ & & E_{66}^I \end{bmatrix} \begin{Bmatrix} \frac{\partial U^I}{\partial x} + \frac{\partial w}{\partial x}\frac{\partial W^I}{\partial x} \\ \frac{\partial V^I}{\partial y} + \frac{\partial w}{\partial y}\frac{\partial W^I}{\partial y} \\ \frac{\partial U^I}{\partial y} + \frac{\partial V^I}{\partial x} + \frac{\partial w}{\partial x}\frac{\partial W^I}{\partial y} + \frac{\partial w}{\partial y}\frac{\partial W^I}{\partial x} \end{Bmatrix} +
$$

$$
+ \sum_{I,J=1}^{ND} \begin{bmatrix} F_{11}^{IJ} & F_{12}^{IJ} & F_{16}^{IJ} \\ & F_{22}^{IJ} & F_{26}^{IJ} \\ & & F_{66}^{IJ} \end{bmatrix} \begin{Bmatrix} \frac{1}{2}\frac{\partial W^I}{\partial x}\frac{\partial W^J}{\partial x} \\ \frac{1}{2}\frac{\partial W^I}{\partial y}\frac{\partial W^J}{\partial y} \\ \frac{\partial W^I}{\partial x}\frac{\partial W^J}{\partial y} \end{Bmatrix}
$$

$$
\begin{Bmatrix} Q_x \\ Q_y \end{Bmatrix} = \begin{bmatrix} A_{55} & A_{45} \\ & A_{44} \end{bmatrix} \begin{Bmatrix} \frac{\partial w}{\partial x} \\ \frac{\partial w}{\partial y} \end{Bmatrix} + \sum_{I=1}^{N} \begin{bmatrix} \overline{B}_{55}^I & \overline{B}_{45}^I \\ & \overline{B}_{44}^I \end{bmatrix} \begin{Bmatrix} u^I \\ v^I \end{Bmatrix} +
$$

$$
+ \sum_{I=1}^{ND} \begin{bmatrix} E_{55}^I & E_{45}^I \\ & E_{44}^I \end{bmatrix} \begin{Bmatrix} \frac{\partial W^I}{\partial x} \\ \frac{\partial W^I}{\partial y} \end{Bmatrix} \tag{3.47}
$$

$$
\left\{
\begin{array}{c}
N_x^I \\
N_y^I \\
N_{xy}^I
\end{array}
\right\}
=
\left[
\begin{array}{ccc}
B_{11}^I & B_{12}^I & B_{16}^I \\
 & B_{22}^I & B_{26}^I \\
 & & B_{66}^I
\end{array}
\right]
\left\{
\begin{array}{c}
\frac{\partial u}{\partial x} + \frac{1}{2}\left(\frac{\partial w}{\partial x}\right)^2 \\
\frac{\partial v}{\partial y} + \frac{1}{2}\left(\frac{\partial w}{\partial y}\right)^2 \\
\frac{\partial u}{\partial y} + \frac{\partial v}{\partial x} + \frac{\partial w}{\partial x}\frac{\partial w}{\partial y}
\end{array}
\right\}
+
\tag{3.48}
$$

$$
+\sum_{J=1}^{N}
\left[
\begin{array}{ccc}
D_{11}^{IJ} & D_{12}^{IJ} & D_{16}^{IJ} \\
 & D_{22}^{IJ} & D_{26}^{IJ} \\
 & & D_{66}^{IJ}
\end{array}
\right]
\left\{
\begin{array}{c}
\frac{\partial u^J}{\partial x} \\
\frac{\partial v^J}{\partial y} \\
\frac{\partial u^J}{\partial y} + \frac{\partial v^J}{\partial x}
\end{array}
\right\}
+
$$

$$
+\sum_{J=1}^{ND}
\left[
\begin{array}{ccc}
L_{11}^{IJ} & L_{12}^{IJ} & L_{16}^{IJ} \\
 & L_{22}^{IJ} & L_{26}^{IJ} \\
 & & L_{66}^{IJ}
\end{array}
\right]
\left\{
\begin{array}{c}
\frac{\partial U^J}{\partial x} + \frac{\partial w}{\partial x}\frac{\partial W^J}{\partial x} \\
\frac{\partial V^J}{\partial y} + \frac{\partial w}{\partial y}\frac{\partial W^J}{\partial y} \\
\frac{\partial U^J}{\partial y} + \frac{\partial V^J}{\partial x} + \frac{\partial w}{\partial x}\frac{\partial W^J}{\partial y} + \frac{\partial w}{\partial y}\frac{\partial W^J}{\partial x}
\end{array}
\right\}
+
$$

$$
+\sum_{J,K=1}^{ND}
\left[
\begin{array}{ccc}
L_{11}^{IJK} & L_{12}^{IJK} & L_{16}^{IJK} \\
 & L_{22}^{IJK} & L_{26}^{IJK} \\
 & & L_{66}^{IJK}
\end{array}
\right]
\left\{
\begin{array}{c}
\frac{1}{2}\frac{\partial W^J}{\partial x}\frac{\partial W^K}{\partial x} \\
\frac{1}{2}\frac{\partial W^J}{\partial y}\frac{\partial W^K}{\partial y} \\
\frac{\partial W^J}{\partial x}\frac{\partial W^K}{\partial y}
\end{array}
\right\}
$$

$$
\left\{
\begin{array}{c}
Q_x^I \\
Q_y^I
\end{array}
\right\}
=
\left[
\begin{array}{cc}
\overline{B}_{55}^I & \overline{B}_{45}^I \\
 & \overline{B}_{44}^I
\end{array}
\right]
\left\{
\begin{array}{c}
\frac{\partial w}{\partial x} \\
\frac{\partial w}{\partial y}
\end{array}
\right\}
+
\sum_{J=1}^{N}
\left[
\begin{array}{cc}
\overline{D}_{55}^{IJ} & \overline{D}_{45}^{IJ} \\
 & \overline{D}_{44}^{IJ}
\end{array}
\right]
\left\{
\begin{array}{c}
u^J \\
v^J
\end{array}
\right\}
+
$$

$$
+\sum_{J=1}^{ND}
\left[
\begin{array}{cc}
\overline{L}_{55}^{IJ} & \overline{L}_{45}^{IJ} \\
 & \overline{L}_{44}^{IJ}
\end{array}
\right]
\left\{
\begin{array}{c}
\frac{\partial W^J}{\partial x} \\
\frac{\partial W^J}{\partial y}
\end{array}
\right\}
\tag{3.49}
$$

$$
\left\{
\begin{array}{c}
\overline{N}_x^I \\
\overline{N}_y^I \\
\overline{N}_{xy}^I
\end{array}
\right\}
=
\left[
\begin{array}{ccc}
E_{11}^I & E_{12}^I & E_{16}^I \\
 & E_{22}^I & E_{26}^I \\
 & & E_{66}^I
\end{array}
\right]
\left\{
\begin{array}{c}
\frac{\partial u}{\partial x} + \frac{1}{2}\left(\frac{\partial w}{\partial x}\right)^2 \\
\frac{\partial v}{\partial y} + \frac{1}{2}\left(\frac{\partial w}{\partial y}\right)^2 \\
\frac{\partial u}{\partial y} + \frac{\partial v}{\partial x} + \frac{\partial w}{\partial x}\frac{\partial w}{\partial y}
\end{array}
\right\}
+
\tag{3.50}
$$

$$
+\sum_{J=1}^{N}
\left[
\begin{array}{ccc}
L_{11}^{JI} & L_{12}^{JI} & L_{16}^{JI} \\
 & L_{22}^{JI} & L_{26}^{JI} \\
 & & L_{66}^{JI}
\end{array}
\right]
\left\{
\begin{array}{c}
\frac{\partial u^J}{\partial x} \\
\frac{\partial v^J}{\partial y} \\
\frac{\partial u^J}{\partial y} + \frac{\partial v^J}{\partial x}
\end{array}
\right\}
+
$$

$$
+\sum_{J=1}^{ND}
\left[
\begin{array}{ccc}
F_{11}^{IJ} & F_{12}^{IJ} & F_{16}^{IJ} \\
 & F_{22}^{IJ} & F_{26}^{IJ} \\
 & & F_{66}^{IJ}
\end{array}
\right]
\left\{
\begin{array}{c}
\frac{\partial U^J}{\partial x} + \frac{\partial w}{\partial x}\frac{\partial W^J}{\partial x} \\
\frac{\partial V^J}{\partial y} + \frac{\partial w}{\partial y}\frac{\partial W^J}{\partial y} \\
\frac{\partial U^J}{\partial y} + \frac{\partial V^J}{\partial x} + \frac{\partial w}{\partial x}\frac{\partial W^J}{\partial y} + \frac{\partial w}{\partial y}\frac{\partial W^J}{\partial x}
\end{array}
\right\}
+
$$

$$
+\sum_{J,K=1}^{ND}
\left[
\begin{array}{ccc}
F_{11}^{IJK} & F_{12}^{IJK} & F_{16}^{IJK} \\
 & F_{22}^{IJK} & F_{26}^{IJK} \\
 & & F_{66}^{IJK}
\end{array}
\right]
\left\{
\begin{array}{c}
\frac{1}{2}\frac{\partial W^J}{\partial x}\frac{\partial W^K}{\partial x} \\
\frac{1}{2}\frac{\partial W^J}{\partial y}\frac{\partial W^K}{\partial y} \\
\frac{\partial W^J}{\partial x}\frac{\partial W^K}{\partial y}
\end{array}
\right\}
$$

$$
\left\{ \begin{array}{c} \overline{Q}_x^I \\ \overline{Q}_y^I \end{array} \right\} = \left[\begin{array}{cc} E_{55}^I & E_{45}^I \\ & E_{44}^I \end{array} \right] \left\{ \begin{array}{c} \frac{\partial w}{\partial x} \\ \frac{\partial w}{\partial y} \end{array} \right\} + \sum_{J=1}^{N} \left[\begin{array}{cc} \overline{L}_{55}^{JI} & \overline{L}_{45}^{JI} \\ & \overline{L}_{44}^{JI} \end{array} \right] \left\{ \begin{array}{c} u^J \\ v^J \end{array} \right\} +
$$
$$
+ \sum_{J=1}^{ND} \left[\begin{array}{cc} F_{55}^{IJ} & F_{45}^{IJ} \\ & F_{44}^{IJ} \end{array} \right] \left\{ \begin{array}{c} \frac{\partial W^J}{\partial x} \\ \frac{\partial W^J}{\partial y} \end{array} \right\} \tag{3.51}
$$

$$
\left\{ \begin{array}{c} \overline{N}_x^{IJ} \\ \overline{N}_y^{IJ} \\ \overline{N}_{xy}^{IJ} \end{array} \right\} = \left[\begin{array}{ccc} F_{11}^{IJ} & F_{12}^{IJ} & F_{16}^{IJ} \\ & F_{22}^{IJ} & F_{26}^{IJ} \\ & & F_{66}^{IJ} \end{array} \right] \left\{ \begin{array}{c} \frac{\partial u}{\partial x} + \frac{1}{2}\left(\frac{\partial w}{\partial x}\right)^2 \\ \frac{\partial v}{\partial y} + \frac{1}{2}\left(\frac{\partial w}{\partial y}\right)^2 \\ \frac{\partial u}{\partial y} + \frac{\partial v}{\partial x} + \frac{\partial w}{\partial x}\frac{\partial w}{\partial y} \end{array} \right\} + \tag{3.52}
$$
$$
+ \sum_{K=1}^{N} \left[\begin{array}{ccc} L_{11}^{KIJ} & L_{12}^{KIJ} & L_{16}^{KIJ} \\ & L_{22}^{KIJ} & L_{26}^{KIJ} \\ & & L_{66}^{KIJ} \end{array} \right] \left\{ \begin{array}{c} \frac{\partial u^K}{\partial x} \\ \frac{\partial v^K}{\partial y} \\ \frac{\partial u^K}{\partial y} + \frac{\partial v^K}{\partial x} \end{array} \right\} +
$$
$$
+ \sum_{K=1}^{ND} \left[\begin{array}{ccc} F_{11}^{IJK} & F_{12}^{IJK} & F_{16}^{IJK} \\ & F_{22}^{IJK} & F_{26}^{IJK} \\ & & F_{66}^{IJK} \end{array} \right] \left\{ \begin{array}{c} \frac{\partial U^K}{\partial x} + \frac{\partial w}{\partial x}\frac{\partial W^K}{\partial x} \\ \frac{\partial V^K}{\partial y} + \frac{\partial w}{\partial y}\frac{\partial W^K}{\partial y} \\ \frac{\partial U^K}{\partial y} + \frac{\partial V^K}{\partial x} + \frac{\partial w}{\partial x}\frac{\partial W^K}{\partial y} + \frac{\partial w}{\partial y}\frac{\partial W^K}{\partial x} \end{array} \right\} +
$$
$$
+ \sum_{K,L=1}^{ND} \left[\begin{array}{ccc} F_{11}^{IJKL} & F_{12}^{IJKL} & F_{16}^{IJKL} \\ & F_{22}^{IJKL} & F_{26}^{IJKL} \\ & & F_{66}^{IJKL} \end{array} \right] \left\{ \begin{array}{c} \frac{1}{2}\frac{\partial W^K}{\partial x}\frac{\partial W^L}{\partial x} \\ \frac{1}{2}\frac{\partial W^K}{\partial y}\frac{\partial W^L}{\partial y} \\ \frac{\partial W^K}{\partial x}\frac{\partial W^L}{\partial y} \end{array} \right\}
$$

Note that in the Eqs. (3.47) - (3.53) the laminate stiffness matrices are introduced, which respective components are calculated as follows:

$$
\left\{ \begin{array}{cccc} A_{ij} & B_{ij}^I & \overline{B}_{ij}^I & D_{ij}^{IJ} & \overline{D}_{ij}^{IJ} \end{array} \right\} = \sum_{k=1}^{n} \int_{z_k}^{z_{k+1}} \overline{Q}_{ij}^{(k)} \left\{ \begin{array}{ccccc} 1 & \Phi^I & \frac{d\Phi^I}{dz} & \Phi^I\Phi^J & \frac{d\Phi^I}{dz}\frac{d\Phi^J}{dz} \end{array} \right\} dz
$$
$$
\left\{ \begin{array}{cccc} E_{ij}^I & F_{ij}^{IJ} & L_{ij}^{IJ} & \overline{L}_{ij}^{IJ} \end{array} \right\} = \sum_{k=1}^{n} \int_{z_k}^{z_{k+1}} \overline{Q}_{ij}^{(k)} \left\{ \begin{array}{cccc} H^I & H^I H^J & \Phi^I H^J & \frac{d\Phi^I}{dz}H^J \end{array} \right\} dz \tag{3.53}
$$

Nonlinear terms:

$$
\left\{ \begin{array}{ccc} L_{ij}^{IJK} & F_{ij}^{IJK} & F_{ij}^{IJKL} \end{array} \right\} = \sum_{k=1}^{n} \int_{z_k}^{z_{k+1}} \overline{Q}_{ij}^{(k)} \left\{ \begin{array}{ccc} \Phi^I H^J H^K & H^I H^J H^K & H^I H^J H^K H^L \end{array} \right\} dz \tag{3.54}
$$

For the linear functions Φ^I through the thickness of the laminate, elements of

the laminate stiffness matrices are:

$$
\begin{aligned}
A_{ij} &= \sum_{k=1}^{n} \overline{Q}_{ij}^{(k)} h^{(k)} \\
B_{ij}^1 &= \overline{Q}_{ij}^{(1)} \frac{h^{(1)}}{2} & B_{ij}^I &= \overline{Q}_{ij}^{(I-1)} \frac{h^{(I-1)}}{2} + \overline{Q}_{ij}^{(I)} \frac{h^{(I)}}{2} & B_{ij}^N &= \overline{Q}_{ij}^{(N-1)} \frac{h^{(N-1)}}{2} \\
\overline{B}_{ij}^1 &= -\overline{Q}_{ij}^{(1)} & \overline{B}_{ij}^I &= \overline{Q}_{ij}^{(I-1)} - \overline{Q}_{ij}^{(I)} & \overline{B}_{ij}^N &= \overline{Q}_{ij}^{(N-1)} \\
D_{ij}^{11} &= \overline{Q}_{ij}^{(1)} \frac{h^{(1)}}{3} & D_{ij}^{12} &= \overline{Q}_{ij}^{(1)} \frac{h^{(1)}}{6} \\
D_{ij}^{I-1,I} &= \overline{Q}_{ij}^{(I-1)} \frac{h^{(I-1)}}{6} & D_{ij}^{II} &= \overline{Q}_{ij}^{(I-1)} \frac{h^{(I-1)}}{6} + \overline{Q}_{ij}^{(I)} \frac{h^{(I)}}{3} & D_{ij}^{I,I+1} &= \overline{Q}_{ij}^{(I)} \frac{h^{(I)}}{6} \\
& & D_{ij}^{N-1,N} &= \overline{Q}_{ij}^{(N-1)} \frac{h^{(N-1)}}{6} & D_{ij}^{NN} &= \overline{Q}_{ij}^{(N-1)} \frac{h^{(N-1)}}{3} \\
\overline{D}_{ij}^{11} &= \frac{\overline{Q}_{ij}^{(1)}}{h^{(1)}} & \overline{D}_{ij}^{12} &= -\frac{\overline{Q}_{ij}^{(1)}}{h^{(1)}} \\
\overline{D}_{ij}^{I-1,I} &= -\frac{\overline{Q}_{ij}^{(I-1)}}{h^{(I-1)}} & \overline{D}_{ij}^{II} &= \frac{\overline{Q}_{ij}^{(I-1)}}{h^{(I-1)}} + \frac{\overline{Q}_{ij}^{(I)}}{h^{(I)}} & \overline{D}_{ij}^{I,I+1} &= -\frac{\overline{Q}_{ij}^{(I)}}{h^{(I)}} \\
\overline{D}_{ij}^{N-1,N} &= -\frac{\overline{Q}_{ij}^{(N-1)}}{h^{(N-1)}} & \overline{D}_{ij}^{NN} &= \frac{\overline{Q}_{ij}^{(N-1)}}{h^{(N-1)}}
\end{aligned}
\tag{3.55}
$$

The elements of the laminate stiffness matrices which take into account the delamination are calculated in a similar way (see Barbero [9]). Note that when von Kármán nonlinearity is not accounted, all laminate stiffnesses with three or four superscripts will not enter the governing equations. For the sake of simplicity, the following vectors of deformations and rotations are introduced:

$$
\begin{aligned}
\{\varepsilon\} &= \left\{ \begin{array}{ccccc} \frac{\partial u}{\partial x} & \frac{\partial v}{\partial y} & \frac{\partial u}{\partial y} + \frac{\partial v}{\partial x} & \frac{\partial w}{\partial x} & \frac{\partial w}{\partial y} \end{array} \right\}^T \\
\{\varepsilon^I\} &= \left\{ \begin{array}{ccccc} \frac{\partial u^I}{\partial x} & \frac{\partial v^I}{\partial y} & \frac{\partial u^I}{\partial y} + \frac{\partial v^I}{\partial x} & u^I & v^I \end{array} \right\}^T \\
\{\overline{\varepsilon^I}\} &= \left\{ \begin{array}{ccccc} \frac{\partial U^I}{\partial x} & \frac{\partial V^I}{\partial y} & \frac{\partial U^I}{\partial y} + \frac{\partial V^I}{\partial x} & \frac{\partial W^I}{\partial x} & \frac{\partial W^I}{\partial y} \end{array} \right\}^T \\
\{\eta\} &= \left\{ \begin{array}{ccccc} \frac{1}{2}\left(\frac{\partial w}{\partial x}\right)^2 & \frac{1}{2}\left(\frac{\partial w}{\partial y}\right)^2 & \frac{\partial w}{\partial x}\frac{\partial w}{\partial y} & 0 & 0 \end{array} \right\}^T \\
\{\overline{\eta}^I\} &= \left\{ \begin{array}{ccccc} \frac{\partial w}{\partial x}\frac{\partial W^I}{\partial x} & \frac{\partial w}{\partial y}\frac{\partial W^I}{\partial y} & \frac{\partial w}{\partial x}\frac{\partial W^I}{\partial y} + \frac{\partial w}{\partial y}\frac{\partial W^I}{\partial x} & 0 & 0 \end{array} \right\}^T \\
\{\overline{\eta}^{IJ}\} &= \left\{ \begin{array}{ccccc} \frac{1}{2}\frac{\partial W^I}{\partial x}\frac{\partial W^J}{\partial x} & \frac{1}{2}\frac{\partial W^I}{\partial y}\frac{\partial W^J}{\partial y} & \frac{\partial W^I}{\partial x}\frac{\partial W^J}{\partial y} & 0 & 0 \end{array} \right\}^T
\end{aligned}
\tag{3.56}
$$

Laminate constitutive relations now can be re-written in the matrix form:

$$
\{N\} = [A]\left(\{\epsilon\} + \{\eta\}\right) + \sum_{I=1}^{N} \left[B^I\right] \left\{\epsilon^I\right\} +
$$

$$
+ \sum_{I=1}^{ND} \left[E^I\right] \left(\{\overline{\epsilon}^I\} + \{\overline{\eta}^I\}\right) + \sum_{I,J=1}^{ND} \left[F^{IJ}\right] \{\overline{\eta}^{IJ}\} \tag{3.57}
$$

$$\{N^I\} = [B^I]\,(\{\epsilon\} + \{\eta\}) + \sum_{J=1}^{N} [D^{IJ}]\,\{\epsilon^J\} +$$

$$+ \sum_{J=1}^{ND} [L^{IJ}]\,(\{\bar{\epsilon}^J\} + \{\bar{\eta}^J\}) + \sum_{J,K=1}^{ND} [L^{IJK}]\,\{\bar{\eta}^{JK}\} \quad (3.58)$$

$$\{\overline{N}^I\} = [E^I]\,(\{\epsilon\} + \{\eta\}) + \sum_{J=1}^{N} [L^{JI}]\,\{\epsilon^J\} +$$

$$+ \sum_{J=1}^{ND} [F^{IJ}]\,(\{\bar{\epsilon}^J\} + \{\bar{\eta}^J\}) + \sum_{J,K=1}^{ND} [F^{IJK}]\,\{\bar{\eta}^{JK}\} \quad (3.59)$$

$$\{\overline{N}^{IJ}\} = [F^{IJ}]\,(\{\epsilon\} + \{\eta\}) + \sum_{K=1}^{N} [L^{KIJ}]\,\{\epsilon^K\} +$$

$$+ \sum_{K=1}^{ND} [F^{IJK}]\,(\{\bar{\epsilon}^K\} + \{\bar{\eta}^K\}) + \sum_{K,L=1}^{ND} [F^{IJKL}]\,\{\bar{\eta}^{KL}\} \quad (3.60)$$

3.7.3   Virtual Work of External Forces

The virtual displacements along the normal and tangential directions δu_n and δu_s in the GLPT follow from the assumed displacement field from Eq. (3.3):

$$\delta u_n = \delta u_{0n} + \sum_{I=1}^{N} \delta u_n^I \Phi^I + \sum_{I=1}^{ND} \delta U_n^I H^I$$
$$\delta u_s = \delta u_{0s} + \sum_{I=1}^{N} \delta u_s^I \Phi^I + \sum_{I=1}^{ND} \delta U_s^I H^I$$

(3.61)

After incorporation of the virtual displacements along the normal and tangential directions from Eqs. (3.61) into the Eq. (3.21), the virtual work of external forces is derived:

$$\delta V = -\int_{\Omega} q(x,y)\delta w\, d\Omega - \int_{\Gamma_\sigma} \left[\int_{-h/2}^{h/2} \hat{\sigma}_{nz} \left(\delta w + \sum_{I=1}^{ND} \delta W^I H^I \right) dz \right] ds -$$

$$- \int_{\Gamma_\sigma} \left[\int_{-h/2}^{h/2} \hat{\sigma}_{nn} \left(\delta u_{0n} + \sum_{I=1}^{N} \delta u_n^I \Phi^I + \sum_{I=1}^{ND} \delta U_n^I H^I \right) dz \right] ds -$$

$$- \int_{\Gamma_\sigma} \left[\int_{-h/2}^{h/2} \hat{\sigma}_{ns} \left(\delta u_{0s} + \sum_{I=1}^{N} \delta u_s^I \Phi^I + \sum_{I=1}^{ND} \delta U_s^I H^I \right) dz \right] ds \quad (3.62)$$

To reduce the 3D model to a 2D one, the z-coordinate is again eliminatd by the explicit integration of stress components multiplied with the corresponding functions $\Phi^I(z)$ or $H^I(z)$, and derive the following stress resultants:

$$
\left\{ \begin{array}{ccc} \hat{N}_{nn} & \hat{N}_{ns} & \hat{Q}_n \end{array} \right\} = \sum_{k=1}^{n} \int_{z_k}^{z_{k+1}} \left\{ \begin{array}{ccc} \hat{\sigma}_{nn} & \hat{\sigma}_{ns} & \hat{\sigma}_{nz} \end{array} \right\}^{(k)} dz
$$

$$
\left\{ \begin{array}{cc} \hat{N}_{nn}^I & \hat{N}_{ns}^I \end{array} \right\} = \sum_{k=1}^{n} \int_{z_k}^{z_{k+1}} \left\{ \begin{array}{cc} \hat{\sigma}_{nn} & \hat{\sigma}_{ns} \end{array} \right\}^{(k)} \Phi^I dz \qquad (3.63)
$$

$$
\left\{ \begin{array}{ccc} \hat{\bar{N}}_{nn}^I & \hat{\bar{N}}_{ns}^I & \hat{\bar{Q}}_n^I \end{array} \right\} = \sum_{k=1}^{n} \int_{z_k}^{z_{k+1}} \left\{ \begin{array}{ccc} \hat{\sigma}_{nn} & \hat{\sigma}_{ns} & \hat{\sigma}_{nz} \end{array} \right\}^{(k)} H^I dz
$$

After the substitution of the stress resultants from Eqs. (3.63), the virtual work of external forces is obtained as follows:

$$
\delta V = - \int_{\Omega} q(x,y) \delta w d\Omega - \int_{\Gamma_\sigma} \left[\hat{N}_{nn} \delta u_{0n} + \hat{N}_{ns} \delta u_{0s} + \hat{Q}_n \delta w \right] ds -
$$
$$
- \int_{\Gamma_\sigma} \left[\sum_{I=1}^{N} \left(\hat{N}_{nn}^I \delta u_n^I + \hat{N}_{ns}^I \delta u_s^I \right) + \sum_{I=1}^{ND} \left(\hat{\bar{N}}_{nn}^I \delta U_n^I + \hat{\bar{N}}_{ns}^I \delta U_s^I + \hat{\bar{Q}}_n \delta W^I \right) \right] ds \qquad (3.64)
$$

3.7.4 Virtual Kinetic Energy

The time derivatives of displacements components (*velocities*) and their respective virtual velocities are:

$$
\dot{u}_1(x,y,z,t) = \dot{u}(x,y,t) + \sum_{I=1}^{N} \dot{u}^I(x,y,t)\Phi^I(z) + \sum_{I=1}^{ND} \dot{U}^I(x,y,t)H^I(z)
$$
$$
\dot{u}_2(x,y,z,t) = \dot{v}(x,y,t) + \sum_{I=1}^{N} \dot{v}^I(x,y,t)\Phi^I(z) + \sum_{I=1}^{ND} \dot{V}^I(x,y,t)H^I(z) \qquad (3.65)
$$
$$
\dot{u}_3(x,y,z,t) = \dot{w}(x,y,t) + \sum_{I=1}^{ND} \dot{W}^I(x,y,t)H^I(z)
$$

$$
\delta\dot{u}_1(x,y,z,t) = \delta\dot{u}(x,y,t) + \sum_{I=1}^{N} \delta\dot{u}^I(x,y,t)\Phi^I(z) + \sum_{I=1}^{ND} \delta\dot{U}^I(x,y,t)H^I(z)
$$
$$
\delta\dot{u}_2(x,y,z,t) = \delta\dot{v}(x,y,t) + \sum_{I=1}^{N} \delta\dot{v}^I(x,y,t)\Phi^I(z) + \sum_{I=1}^{ND} \delta\dot{V}^I(x,y,t)H^I(z) \qquad (3.66)
$$
$$
\delta\dot{u}_3(x,y,z,t) = \delta\dot{w}(x,y,t) + \sum_{I=1}^{ND} \delta\dot{W}^I(x,y,t)H^I(z)
$$

After the substitution of the time derivatives and the respective virtual velocities

from Eqs. (3.65) - (3.66), the virtual kinetic energy is obtained as follows:

$$
\begin{aligned}
\delta K = \\
-\int_\Omega \left\{ \int_{-h/2}^{h/2} \rho \left(\dot{u} + \sum_{I=1}^{N} \dot{u}^I \Phi^I + \sum_{I=1}^{ND} \dot{U}^I H^I \right) \left(\delta\dot{u} + \sum_{I=1}^{N} \delta\dot{u}^I \Phi^I + \sum_{I=1}^{ND} \delta\dot{U}^I H^I \right) dz \right\} d\Omega - \\
-\int_\Omega \left\{ \int_{-h/2}^{h/2} \rho \left(\dot{v} + \sum_{I=1}^{N} \dot{v}^I \Phi^I + \sum_{I=1}^{ND} \dot{V}^I H^I \right) \left(\delta\dot{v} + \sum_{I=1}^{N} \delta\dot{v}^I \Phi^I + \sum_{I=1}^{ND} \delta\dot{V}^I H^I \right) dz \right\} d\Omega - \\
-\int_\Omega \left\{ \int_{-h/2}^{h/2} \rho \left(\dot{w} + \sum_{I=1}^{ND} \dot{W}^I H^I(z) \right) \left(\delta\dot{w} + \sum_{I=1}^{ND} \delta\dot{W}^I H^I \right) dz \right\} d\Omega
\end{aligned}
$$

$$(3.67)$$

Finally, the z-coordinate is eliminated by the explicit integration of mass density of the material multiplied with the corresponding functions $\Phi^I(z)$ or $H^I(z)$. During this procedure, the following mass moments of inertia are derived:

$$
\left\{ \begin{array}{ccc} I_0 & I^I & I^{IJ} \end{array} \right\} = \sum_{k=1}^{n} \int_{z_k}^{z_{k+1}} \rho^{(k)} \left\{ \begin{array}{ccc} 1 & \Phi^I & \Phi^I\Phi^J \end{array} \right\} dz
$$
$$
\left\{ \begin{array}{ccc} \bar{I}^I & \bar{I}^{IJ} & \tilde{I}^{IJ} \end{array} \right\} = \sum_{k=1}^{n} \int_{z_k}^{z_{k+1}} \rho^{(k)} \left\{ \begin{array}{ccc} H^I & \Phi^I H^J & H^I H^J \end{array} \right\} dz
$$

$$(3.68)$$

After the substitution of the mass moments of inertia from Eqs. (3.68), the virtual kinetic energy is obtained in the following form:

$$
\delta K = -\int_\Omega \left\{ \begin{array}{l} I_0 \left(\dot{u}\delta\dot{u} + \dot{v}\delta\dot{v} + \dot{w}\delta\dot{w} \right) + \sum_{I=1}^{N} I^I \left(\dot{u}^I\delta\dot{u} + \dot{v}^I\delta\dot{v} + \dot{u}\delta\dot{u}^I + \dot{v}\delta\dot{v}^I \right) + \\[2mm]
+ \sum_{I,J=1}^{N} I^{IJ} \left(\dot{u}^I\delta\dot{u}^J + \dot{v}^I\delta\dot{v}^J \right) + \\[2mm]
+ \sum_{I=1}^{ND} \bar{I}^I \left(\dot{U}^I\delta\dot{u} + \dot{V}^I\delta\dot{v} + \dot{W}^I\delta\dot{w} + \dot{u}\delta\dot{U}^I + \dot{v}\delta\dot{V}^I + \dot{w}\delta\dot{W}^I \right) + \\[2mm]
+ \sum_{I=1}^{N}\sum_{J=1}^{ND} \bar{I}^{IJ} \left(\dot{u}^I\delta\dot{U}^J + \dot{v}^I\delta\dot{V}^J \right) + \sum_{I=1}^{ND}\sum_{J=1}^{N} \bar{I}^{JI} \left(\dot{U}^I\delta\dot{u}^J + \dot{V}^I\delta\dot{v}^J \right) + \\[2mm]
+ \sum_{I,J=1}^{ND} \tilde{I}^{IJ} \left(\dot{U}^I\delta\dot{U}^J + \dot{V}^I\delta\dot{V}^J + \dot{W}^I\delta\dot{W}^J \right)
\end{array} \right\} d\Omega
$$

$$(3.69)$$

Now the time integration by parts should be performed to eliminate the time derivatives of virtual displacements. Note that all terms evaluated at $t = 0$ and $t = T$ are zero because the virtual displacements are zero there:

$$
\int_0^T \dot{F}(t)\dot{G}(t)dt = - \int_0^T \ddot{F}(t)G(t)dt.
$$

$$(3.70)$$

Finally, the expression for the virtual kinetic energy is obtained:

$$
\delta K = -\int_{\Omega} \left\{
\begin{aligned}
& I_0 \left(\ddot{u}\delta u + \ddot{v}\delta v + \ddot{w}\delta w \right) + \sum_{I=1}^{N} I^I \left(\ddot{u}^I \delta u + \ddot{v}^I \delta v + \ddot{u}\delta u^I + \ddot{v}\delta v^I \right) + \\
& + \sum_{I,J=1}^{N} I^{IJ} \left(\ddot{u}^I \delta u^J + \ddot{v}^I \delta v^J \right) + \\
& + \sum_{I=1}^{ND} \overline{I}^I \left(\ddot{U}^I \delta u + \ddot{V}^I \delta v + \ddot{W}^I \delta w + \ddot{u}\delta U^I + \ddot{v}\delta V^I + \ddot{w}\delta W^I \right) + \\
& + \sum_{I=1}^{N}\sum_{J=1}^{ND} \left(\overline{I}^{IJ} \left(\ddot{u}^I \delta U^J + \ddot{v}^I \delta V^J \right) + \overline{I}^{JI} \left(\ddot{U}^J \delta u^I + \ddot{V}^J \delta v^I \right) \right) + \\
& + \sum_{I,J=1}^{ND} \widetilde{I}^{IJ} \left(\ddot{U}^I \delta U^J + \ddot{V}^I \delta V^J + \ddot{W}^I \delta W^J \right)
\end{aligned}
\right\} d\Omega
$$

$$(3.71)$$

3.7.5 Strong Formulation

All components of the virtual work are summed, collecting the coefficients of each of the virtual displacements. The *in-plane stress resultants* acting on the second order strains are now introduced:

$$
\begin{aligned}
\overline{P}(w, W^I) &= N_{nn}\frac{\partial w}{\partial n} + N_{ns}\frac{\partial w}{\partial s} + \sum_{I=1}^{ND}\left(\overline{N}_{nn}^I \frac{\partial W^I}{\partial n} + \overline{N}_{ns}^I \frac{\partial W^I}{\partial s} \right) \\
\overline{P}^I(w, W^J) &= \overline{N}_{nn}^I \frac{\partial w}{\partial n} + \overline{N}_{ns}^I \frac{\partial w}{\partial s} + \sum_{J=1}^{ND}\left(\overline{N}_{nn}^{IJ} \frac{\partial W^J}{\partial n} + \overline{N}_{ns}^{IJ} \frac{\partial W^J}{\partial s} \right) \\
N(w) &= \frac{\partial}{\partial x}\left(N_x \frac{\partial w}{\partial x} + N_{xy}\frac{\partial w}{\partial y} \right) + \frac{\partial}{\partial y}\left(N_{xy}\frac{\partial w}{\partial x} + N_y \frac{\partial w}{\partial y} \right) \\
\overline{N}(W^I) &= \sum_{I=1}^{ND}\left[\frac{\partial}{\partial x}\left(\overline{N}_x^I \frac{\partial W^I}{\partial x} + \overline{N}_{xy}^I \frac{\partial W^I}{\partial y} \right) + \frac{\partial}{\partial y}\left(\overline{N}_{xy}^I \frac{\partial W^I}{\partial x} + \overline{N}_y^I \frac{\partial W^I}{\partial y} \right) \right] \\
\overline{N}^I(w) &= \frac{\partial}{\partial x}\left(\overline{N}_x^I \frac{\partial w}{\partial x} + \overline{N}_{xy}^I \frac{\partial w}{\partial y} \right) + \frac{\partial}{\partial y}\left(\overline{N}_{xy}^I \frac{\partial w}{\partial x} + \overline{N}_y^I \frac{\partial w}{\partial y} \right) \\
\overline{N}^I(W^J) &= \sum_{J=1}^{ND}\left[\frac{\partial}{\partial x}\left(\overline{N}_x^{IJ} \frac{\partial W^J}{\partial x} + \overline{N}_{xy}^{IJ} \frac{\partial W^J}{\partial y} \right) + \frac{\partial}{\partial y}\left(\overline{N}_{xy}^{IJ} \frac{\partial W^J}{\partial x} + \overline{N}_y^{IJ} \frac{\partial W^J}{\partial y} \right) \right]
\end{aligned}
$$

$$(3.72)$$

After summation, the following form of the principle of virtual displacements is

obtained:

$$
\begin{aligned}
0 = \int\limits_0^T &\left\{ \oint\limits_\Gamma \left[
\begin{array}{l}
N_{nn}\delta u_{0n} + N_{ns}\delta u_{0s} + \left[Q_x n_x + Q_y n_y + \overline{P}(w, W^I)\right]\delta w + \\
+ \sum\limits_{I=1}^N \left(N_{nn}^I \delta u_n^I + N_{ns}^I \delta u_s^I\right) + \sum\limits_{I=1}^{ND}\left(\overline{N}_{nn}^I \delta U_n^I + \overline{N}_{ns}^I \delta U_s^I\right) + \\
+ \sum\limits_{I=1}^{ND}\left(\overline{Q}_x^I n_x + \overline{Q}_y^I n_y + \overline{P}^I(w, W^J)\right)\delta W^I
\end{array}
\right] ds \right\} dt - \\
&- \int\limits_0^T \left\{ \int\limits_{\Gamma_\sigma} \left[\hat{N}_{nn}\delta u_{0n} + \hat{N}_{ns}\delta u_{0s} + \hat{Q}_n \delta w\right] ds \right\} dt - \\
&- \int\limits_0^T \left\{ \int\limits_{\Gamma_\sigma} \left[
\begin{array}{l}
\sum\limits_{I=1}^N \left(\hat{N}_{nn}^I \delta u_n^I + \hat{N}_{ns}^I \delta u_s^I\right) + \\
+ \sum\limits_{I=1}^{ND}\left(\hat{\overline{N}}_{nn}^I \delta U_n^I + \hat{\overline{N}}_{ns}^I \delta U_s^I + \hat{\overline{Q}}_n^I \delta W^I\right)
\end{array}
\right] ds \right\} dt -
\end{aligned}
$$

$$
- \int\limits_0^T \left\{ \int\limits_\Omega \left[
\begin{array}{l}
\delta u \left(\frac{\partial N_x}{\partial x} + \frac{\partial N_{xy}}{\partial y} - I_0\ddot{u} - \sum\limits_{I=1}^N I^I \ddot{u}^I - \sum\limits_{I=1}^{ND} \overline{I}^I \ddot{U}^I\right) + \\
+ \delta v \left(\frac{\partial N_{xy}}{\partial x} + \frac{\partial N_y}{\partial y} - I_0\ddot{v} - \sum\limits_{I=1}^N I^I \ddot{v}^I - \sum\limits_{I=1}^{ND} \overline{I}^I \ddot{V}^I\right) + \\
+ \delta w \left(\begin{array}{l}\frac{\partial Q_x}{\partial x} + \frac{\partial Q_y}{\partial y} + q(x,y,t) + N(w) + \overline{N}(W^I) - \\ -I_0\ddot{w} - \sum\limits_{I=1}^{ND} \overline{I}^I \ddot{W}^I \end{array}\right) + \\
+ \sum\limits_{I=1}^N \delta u^I \left(\frac{\partial N_x^I}{\partial x} + \frac{\partial N_{xy}^I}{\partial y} - Q_x^I - I^I \ddot{u} - \sum\limits_{J=1}^{ND} \overline{I}^{JI} \ddot{U}^J - \sum\limits_{J=1}^N I^{IJ} \ddot{u}^J\right) + \\
+ \sum\limits_{I=1}^N \delta v^I \left(\frac{\partial N_{xy}^I}{\partial x} + \frac{\partial N_y^I}{\partial y} - Q_y^I - I^I \ddot{v} - \sum\limits_{J=1}^{ND} \overline{I}^{JI} \ddot{V}^J - \sum\limits_{J=1}^N I^{IJ} \ddot{v}^J\right) + \\
+ \sum\limits_{I=1}^{ND} \delta U^I \left(\frac{\partial \overline{N}_x^I}{\partial x} + \frac{\partial \overline{N}_{xy}^I}{\partial y} - \overline{I}^I \ddot{u} - \sum\limits_{J=1}^N \overline{I}^{JI} \ddot{u}^J - \sum\limits_{J=1}^{ND} \widetilde{I}^{IJ} \ddot{U}^J\right) + \\
+ \sum\limits_{I=1}^{ND} \delta V^I \left(\frac{\partial \overline{N}_{xy}^I}{\partial x} + \frac{\partial \overline{N}_y^I}{\partial y} - \overline{I}^I \ddot{v} - \sum\limits_{J=1}^N \overline{I}^{JI} \ddot{v}^J - \sum\limits_{J=1}^{ND} \widetilde{I}^{IJ} \ddot{V}^J\right) + \\
+ \sum\limits_{I=1}^{ND} \delta W^I \left(\begin{array}{l}\frac{\partial \overline{Q}_x^I}{\partial x} + \frac{\partial \overline{Q}_y^I}{\partial y} + \overline{N}^I(w) + \overline{N}^I(W^J) - \\ -\overline{I}^I \ddot{w} - \sum\limits_{J=1}^{ND} \widetilde{I}^{IJ} \ddot{W}^J \end{array}\right)
\end{array}
\right] d\Omega \right\} dt
$$

$$(3.73)$$

All virtual displacements δu, δv, δw, δu^I, δv^I, δU^I, δV^I and δW^I except one are now set to zero separately. To satisfy the previous equation, the coefficients of δu, δv, δw, δu^I, δv^I, δU^I, δV^I and δW^I must be zero. For example, if $\delta w \neq 0$ and $\delta u = \delta v = \delta u^I = \delta v^I = \delta U^I = \delta V^I = \delta W^I = 0$ it follows:

$$
\begin{aligned}
0 = \int\limits_0^T &\oint\limits_\Gamma \delta w \left[Q_x n_x + Q_y n_y + \overline{P}(w, W^I) - \hat{Q}_n\right] ds\, dt - \\
&- \int\limits_0^T \int\limits_\Omega \delta w \left(\frac{\partial Q_x}{\partial x} + \frac{\partial Q_y}{\partial y} + q(x,y,t) + N(w) + \overline{N}(W^I) - I_0\ddot{w} - \sum\limits_{I=1}^{ND} \overline{I}^I \ddot{W}^I\right) d\Omega\, dt
\end{aligned}
$$

$$(3.74)$$

The coefficient of δw from the contour integral $\oint_\Gamma$ must be zero to satisfy the previous expression. From this the natural (force) boundary condition of the theory is derived. Also, the coefficient of δw from the surface integral $\int_\Omega$ must be zero, and from this the equation of motion of the theory is derived.

Repeating the procedure for all virtual displacements, $3 + 2N + 3ND$ Euler Lagrange equations of the theory are derived, as well as the natural (force) boundary conditions. The Euler Lagrange equations of the theory define the **"strong"** form of the geometrically nonlinear problem of the laminated composite plate:

$$
\begin{aligned}
&\frac{\partial N_x}{\partial x} + \frac{\partial N_{xy}}{\partial y} = I_0\ddot{u} + \sum_{I=1}^{N} I^I \ddot{u}^I + \sum_{I=1}^{ND} \overline{I}^I \ddot{U}^I \\
&\frac{\partial N_{xy}}{\partial x} + \frac{\partial N_y}{\partial y} = I_0\ddot{v} + \sum_{I=1}^{N} I^I \ddot{v}^I + \sum_{I=1}^{ND} \overline{I}^I \ddot{V}^I \\
&\frac{\partial Q_x}{\partial x} + \frac{\partial Q_y}{\partial y} + q(x,y,t) + N(w) + \overline{N}(W^I) = I_0\ddot{w} + \sum_{I=1}^{ND} \overline{I}^I \ddot{W}^I \\
&\frac{\partial N_x^I}{\partial x} + \frac{\partial N_{xy}^I}{\partial y} - Q_x^I = I^I \ddot{u} + \sum_{J=1}^{ND} \overline{I}^{JI} \ddot{U}^J + \sum_{J=1}^{N} I^{IJ} \ddot{u}^J \\
&\frac{\partial N_{xy}^I}{\partial x} + \frac{\partial N_y^I}{\partial y} - Q_y^I = I^I \ddot{v} + \sum_{J=1}^{ND} \overline{I}^{JI} \ddot{V}^J + \sum_{J=1}^{N} I^{IJ} \ddot{v}^J \\
&\frac{\partial \overline{N}_x^I}{\partial x} + \frac{\partial \overline{N}_{xy}^I}{\partial y} = \overline{I}^I \ddot{u} + \sum_{J=1}^{N} \overline{I}^{JI} \ddot{u}^J + \sum_{J=1}^{ND} \widetilde{I}^{IJ} \ddot{U}^J \\
&\frac{\partial \overline{N}_{xy}^I}{\partial x} + \frac{\partial \overline{N}_y^I}{\partial y} = \overline{I}^I \ddot{v} + \sum_{J=1}^{N} \overline{I}^{JI} \ddot{v}^J + \sum_{J=1}^{ND} \widetilde{I}^{IJ} \ddot{V}^J \\
&\frac{\partial \overline{Q}_x^I}{\partial x} + \frac{\partial \overline{Q}_y^I}{\partial y} + \overline{N}^I(w) + \overline{N}^I(W^J) = \overline{I}^I \ddot{w} + \sum_{J=1}^{ND} \widetilde{I}^{IJ} \ddot{W}^J
\end{aligned}
\tag{3.75}
$$

Several structural problems may be considered based on the Euler-Lagrange equations, taking into account some restrictions:

1. **Geometrically Nonlinear Bending Analysis** - Inertia forces are neglected, while the transverse loading is static.

   $$
   \begin{aligned}
   &\frac{\partial N_x}{\partial x} + \frac{\partial N_{xy}}{\partial y} = 0 \\
   &\frac{\partial N_{xy}}{\partial x} + \frac{\partial N_y}{\partial y} = 0 \\
   &\frac{\partial Q_x}{\partial x} + \frac{\partial Q_y}{\partial y} + q(x,y) + N(w) + \overline{N}(W^I) = 0 \\
   &\frac{\partial N_x^I}{\partial x} + \frac{\partial N_{xy}^I}{\partial y} - Q_x^I = 0 \\
   &\frac{\partial N_{xy}^I}{\partial x} + \frac{\partial N_y^I}{\partial y} - Q_y^I = 0
   \end{aligned}
   \qquad
   \begin{aligned}
   &\frac{\partial \overline{N}_x^I}{\partial x} + \frac{\partial \overline{N}_{xy}^I}{\partial y} = 0 \\
   &\frac{\partial \overline{N}_{xy}^I}{\partial x} + \frac{\partial \overline{N}_y^I}{\partial y} = 0 \\
   &\frac{\partial \overline{Q}_x^I}{\partial x} + \frac{\partial \overline{Q}_y^I}{\partial y} + \overline{N}^I(w) + \overline{N}^I(W^J) = 0
   \end{aligned}
   $$

2. **Linear Bending Analysis** - Inertia forces are neglected, as well as the in-plane loading acting on the second order strains. The transverse loading is

static.

$$\frac{\partial N_x}{\partial x} + \frac{\partial N_{xy}}{\partial y} = 0 \qquad \frac{\partial N_x^I}{\partial x} + \frac{\partial N_{xy}^I}{\partial y} - Q_x^I = 0 \qquad \frac{\partial \overline{N}_x^I}{\partial x} + \frac{\partial \overline{N}_{xy}^I}{\partial y} = 0$$

$$\frac{\partial N_{xy}}{\partial x} + \frac{\partial N_y}{\partial y} = 0 \qquad \frac{\partial N_{xy}^I}{\partial x} + \frac{\partial N_y^I}{\partial y} - Q_y^I = 0 \qquad \frac{\partial \overline{N}_{xy}^I}{\partial x} + \frac{\partial \overline{N}_y^I}{\partial y} = 0$$

$$\frac{\partial Q_x}{\partial x} + \frac{\partial Q_y}{\partial y} + q(x,y) = 0 \qquad\qquad\qquad\qquad \frac{\partial \overline{Q}_x^I}{\partial x} + \frac{\partial \overline{Q}_y^I}{\partial y} = 0$$

3. **Linear Buckling Analysis** - Inertia forces are neglected. The only loading acting on the plate are the initial in-plane force resultants $N(w^0) = \frac{\partial}{\partial x}\left(N_x^0 \frac{\partial w}{\partial x} + N_{xy}^0 \frac{\partial w}{\partial y}\right) + \frac{\partial}{\partial y}\left(N_{xy}^0 \frac{\partial w}{\partial x} + N_y^0 \frac{\partial w}{\partial y}\right)$, corresponding to the initial in-plane stresses σ_x^0, σ_y^0 and τ_{xy}^0.

$$\frac{\partial N_x}{\partial x} + \frac{\partial N_{xy}}{\partial y} = 0 \qquad \frac{\partial N_x^I}{\partial x} + \frac{\partial N_{xy}^I}{\partial y} - Q_x^I = 0 \qquad \frac{\partial \overline{N}_x^I}{\partial x} + \frac{\partial \overline{N}_{xy}^I}{\partial y} = 0$$

$$\frac{\partial N_{xy}}{\partial x} + \frac{\partial N_y}{\partial y} = 0 \qquad \frac{\partial N_{xy}^I}{\partial x} + \frac{\partial N_y^I}{\partial y} - Q_y^I = 0 \qquad \frac{\partial \overline{N}_{xy}^I}{\partial x} + \frac{\partial \overline{N}_y^I}{\partial y} = 0$$

$$\frac{\partial Q_x}{\partial x} + \frac{\partial Q_y}{\partial y} + N(w^0) = 0 \qquad\qquad\qquad\qquad \frac{\partial \overline{Q}_x^I}{\partial x} + \frac{\partial \overline{Q}_y^I}{\partial y} = 0$$

4. **Linear Free Vibration Analysis** - There is no loading acting on the plate.

$$\frac{\partial N_x}{\partial x} + \frac{\partial N_{xy}}{\partial y} = I_0 \ddot{u} + \sum_{I=1}^{N} I^I \ddot{u}^I + \sum_{I=1}^{ND} \overline{I}^I \ddot{U}^I$$

$$\frac{\partial N_{xy}}{\partial x} + \frac{\partial N_y}{\partial y} = I_0 \ddot{v} + \sum_{I=1}^{N} I^I \ddot{v}^I + \sum_{I=1}^{ND} \overline{I}^I \ddot{V}^I$$

$$\frac{\partial Q_x}{\partial x} + \frac{\partial Q_y}{\partial y} = I_0 \ddot{w} + \sum_{I=1}^{ND} \overline{I}^I \ddot{W}^I$$

$$\frac{\partial N_x^I}{\partial x} + \frac{\partial N_{xy}^I}{\partial y} - Q_x^I = I^I \ddot{u} + \sum_{J=1}^{ND} \overline{I}^{JI} \ddot{U}^J + \sum_{J=1}^{N} I^{IJ} \ddot{u}^J$$

$$\frac{\partial N_{xy}^I}{\partial x} + \frac{\partial N_y^I}{\partial y} - Q_y^I = I^I \ddot{v} + \sum_{J=1}^{ND} \overline{I}^{JI} \ddot{V}^J + \sum_{J=1}^{N} I^{IJ} \ddot{v}^J$$

$$\frac{\partial \overline{N}_x^I}{\partial x} + \frac{\partial \overline{N}_{xy}^I}{\partial y} = \overline{I}^I \ddot{u} + \sum_{J=1}^{N} \overline{I}^{JI} \ddot{u}^J + \sum_{J=1}^{ND} \widetilde{I}^{IJ} \ddot{U}^J$$

$$\frac{\partial \overline{N}_{xy}^I}{\partial x} + \frac{\partial \overline{N}_y^I}{\partial y} = \overline{I}^I \ddot{v} + \sum_{J=1}^{N} \overline{I}^{JI} \ddot{v}^J + \sum_{J=1}^{ND} \widetilde{I}^{IJ} \ddot{V}^J$$

$$\frac{\partial \overline{Q}_x^I}{\partial x} + \frac{\partial \overline{Q}_y^I}{\partial y} = \overline{I}^I \ddot{w} + \sum_{J=1}^{ND} \widetilde{I}^{IJ} \ddot{W}^J$$

5. **Geometrically Nonlinear Transient Analysis**

$$\frac{\partial N_x}{\partial x} + \frac{\partial N_{xy}}{\partial y} = I_0\ddot{u} + \sum_{I=1}^{N} I^I \ddot{u}^I + \sum_{I=1}^{ND} \overline{I}^I \ddot{U}^I$$

$$\frac{\partial N_{xy}}{\partial x} + \frac{\partial N_y}{\partial y} = I_0\ddot{v} + \sum_{I=1}^{N} I^I \ddot{v}^I + \sum_{I=1}^{ND} \overline{I}^I \ddot{V}^I$$

$$\frac{\partial Q_x}{\partial x} + \frac{\partial Q_y}{\partial y} + q(x,y,t) + N(w) + \overline{N}(W^I) = I_0\ddot{w} + \sum_{I=1}^{ND} \overline{I}^I \ddot{W}^I$$

$$\frac{\partial N_x^I}{\partial x} + \frac{\partial N_{xy}^I}{\partial y} - Q_x^I = I^I \ddot{u} + \sum_{J=1}^{ND} \overline{I}^{JI} \ddot{U}^J + \sum_{J=1}^{N} I^{IJ} \ddot{u}^J$$

$$\frac{\partial N_{xy}^I}{\partial x} + \frac{\partial N_y^I}{\partial y} - Q_y^I = I^I \ddot{v} + \sum_{J=1}^{ND} \overline{I}^{JI} \ddot{V}^J + \sum_{J=1}^{N} I^{IJ} \ddot{v}^J$$

$$\frac{\partial \overline{N}_x^I}{\partial x} + \frac{\partial \overline{N}_{xy}^I}{\partial y} = \overline{I}^I \ddot{u} + \sum_{J=1}^{N} \overline{I}^{JI} \ddot{u}^J + \sum_{J=1}^{ND} \widetilde{I}^{IJ} \ddot{U}^J$$

$$\frac{\partial \overline{N}_{xy}^I}{\partial x} + \frac{\partial \overline{N}_y^I}{\partial y} = \overline{I}^I \ddot{v} + \sum_{J=1}^{N} \overline{I}^{JI} \ddot{v}^J + \sum_{J=1}^{ND} \widetilde{I}^{IJ} \ddot{V}^J$$

$$\frac{\partial \overline{Q}_x^I}{\partial x} + \frac{\partial \overline{Q}_y^I}{\partial y} + \overline{N}^I(w) + \overline{N}^I(W^J) = \overline{I}^I \ddot{w} + \sum_{J=1}^{ND} \widetilde{I}^{IJ} \ddot{W}^J$$

6. **Geometrically Linear Transient Analysis** - The in-plane loading acting on the second order strains is neglected.

$$\frac{\partial N_x}{\partial x} + \frac{\partial N_{xy}}{\partial y} = I_0\ddot{u} + \sum_{I=1}^{N} I^I \ddot{u}^I + \sum_{I=1}^{ND} \overline{I}^I \ddot{U}^I$$

$$\frac{\partial N_{xy}}{\partial x} + \frac{\partial N_y}{\partial y} = I_0\ddot{v} + \sum_{I=1}^{N} I^I \ddot{v}^I + \sum_{I=1}^{ND} \overline{I}^I \ddot{V}^I$$

$$\frac{\partial Q_x}{\partial x} + \frac{\partial Q_y}{\partial y} + q(x,y,t) = I_0\ddot{w} + \sum_{I=1}^{ND} \overline{I}^I \ddot{W}^I$$

$$\frac{\partial N_x^I}{\partial x} + \frac{\partial N_{xy}^I}{\partial y} - Q_x^I = I^I \ddot{u} + \sum_{J=1}^{ND} \overline{I}^{JI} \ddot{U}^J + \sum_{J=1}^{N} I^{IJ} \ddot{u}^J$$

$$\frac{\partial N_{xy}^I}{\partial x} + \frac{\partial N_y^I}{\partial y} - Q_y^I = I^I \ddot{v} + \sum_{J=1}^{ND} \overline{I}^{JI} \ddot{V}^J + \sum_{J=1}^{N} I^{IJ} \ddot{v}^J$$

$$\frac{\partial \overline{N}_x^I}{\partial x} + \frac{\partial \overline{N}_{xy}^I}{\partial y} = \overline{I}^I \ddot{u} + \sum_{J=1}^{N} \overline{I}^{JI} \ddot{u}^J + \sum_{J=1}^{ND} \widetilde{I}^{IJ} \ddot{U}^J$$

$$\frac{\partial \overline{N}_{xy}^I}{\partial x} + \frac{\partial \overline{N}_y^I}{\partial y} = \overline{I}^I \ddot{v} + \sum_{J=1}^{N} \overline{I}^{JI} \ddot{v}^J + \sum_{J=1}^{ND} \widetilde{I}^{IJ} \ddot{V}^J$$

$$\frac{\partial \overline{Q}_x^I}{\partial x} + \frac{\partial \overline{Q}_y^I}{\partial y} = \overline{I}^I \ddot{w} + \sum_{J=1}^{ND} \widetilde{I}^{IJ} \ddot{W}^J$$

All previous expressions are valid for the appropriate boundary conditions of the

theory. The boundary integral from the Eq. (3.74) can be re-written as:

$$
0 = \int_0^T \left\{ \oint_\Gamma \left[\begin{array}{l} \left(N_{nn} - \hat{N}_{nn}\right) \delta u_{0n} + \left(N_{ns} - \hat{N}_{ns}\right) \delta u_{0s} + \\ + \left[Q_x n_x + Q_y n_y + \overline{P}(w, W^I) - \hat{Q}_n\right] \delta w + \\ + \sum_{I=1}^N \left[\left(N_{nn}^I - \hat{N}_{nn}^I\right) \delta u_n^I + \left(N_{ns}^I - \hat{N}_{ns}^I\right) \delta u_s^I\right] + \\ + \sum_{I=1}^{ND} \left[\left(\overline{N}_{nn}^I - \hat{\overline{N}}_{nn}^I\right) \delta U_n^I + \left(\overline{N}_{ns}^I - \hat{\overline{N}}_{ns}^I\right) \delta U_s^I\right] + \\ + \sum_{I=1}^{ND} \left(\overline{Q}_x^I n_x + \overline{Q}_y^I n_y + \overline{P}^I(w, W^J) - \hat{\overline{Q}}_n^I\right) \delta W^I \end{array} \right] ds \right\} dt \quad (3.76)
$$

The natural boundary conditions are given by:

$$
N_{nn} - \hat{N}_{nn} = 0, \quad N_{ns} - \hat{N}_{ns} = 0, \quad Q_n - \hat{Q}_n = 0
$$
$$
N_{nn}^I - \hat{N}_{nn}^I = 0, \quad N_{ns}^I - \hat{N}_{ns}^I = 0 \qquad (3.77)
$$
$$
\overline{N}_{nn}^I - \hat{\overline{N}}_{nn}^I = 0, \quad \overline{N}_{ns}^I - \hat{\overline{N}}_{ns}^I = 0, \quad \overline{Q}_n^I - \hat{\overline{Q}}_n^I = 0
$$

on the boundary Γ, where:

$$
Q_n = Q_x n_x + Q_y n_y + \overline{P}(w, W^I)
$$
$$
\overline{Q}_n^I = \overline{Q}_x^I n_x + \overline{Q}_y^I n_y + \overline{P}^I(w, W^J) \qquad (3.78)
$$

The *primary variables* (*generalized displacements*) of the theory are u_n, u_s, w, u_n^I, u_s^I, U_n^I, U_s^I and W^I, while the *secondary variables* (*generalized forces*) of the theory are N_{nn}, N_{ns}, Q_n, N_{nn}^I, N_{ns}^I, $\overline{N}_{nn}^I$, $\overline{N}_{ns}^I$ and $\overline{Q}_n^I$. The initial conditions of the theory involve specifying the values of the displacements and their first derivatives with the respect to time at $t = 0$.

4 Analytical Solution for Linear Transient Analysis of Intact Plates

---

In this chapter the analytical solution of the GLPT for the intact, rectangular, cross-ply simply supported laminated composite plates is discussed. Linear transient analysis is performed. The governing partial differential equations of motion are reduced to a set of ordinary differential equations in time using Newmark's integration schemes for the second order differential equations. The Navier solution method is used to determine the spatial variation of the transient solution, while the initial displacements and velocities are known from the initial conditions.

After the displacement field of the laminated plate is determined, the stress field can be derived using the constitutive equations in each time step. The time evolution of the stresses in any point of the plate is exactly the same as for the time history plot of the displacements. The solution is numerically validated through several examples in Chapter 10.4. The part of the presented results is taken from the works of Marjanović and Vuksanović [95–97].

4.1 Equations of Motion

The development of analytical solution of the GLPT is by no means simple, especially for the arbitrary boundary conditions. Here the analytical solution of the GLPT for the rectangular simply supported laminated composite plate is discussed, taking into account the following restrictions:

4. Analytical Solution for Linear Transient Analysis of Intact Plates

1. cross-ply laminates are considered, in which fibers are oriented alternately with angles of 0° and 90°,

2. the plate is intact,

3. geometrically linear transient analysis is performed.

From the first restriction follows that the following elements of constitutive matrix of the laminate are identically zero: $A_{16} = A_{26} = A_{45} = B_{16}^I = B_{26}^I = \overline{B}_{45}^I = D_{16}^{IJ} = D_{26}^{IJ} = \overline{D}_{45}^{IJ}$. The previously derived Euler-Lagrange equations are then simplified:

$$\frac{\partial N_x}{\partial x} + \frac{\partial N_{xy}}{\partial y} = I_0 \ddot{u} + \sum_{I=1}^{N} I^I \ddot{u}^I$$

$$\frac{\partial N_{xy}}{\partial x} + \frac{\partial N_y}{\partial y} = I_0 \ddot{v} + \sum_{I=1}^{N} I^I \ddot{v}^I$$

$$\frac{\partial Q_x}{\partial x} + \frac{\partial Q_y}{\partial y} + q(x, y, t) = I_0 \ddot{w} \tag{4.1}$$

$$\frac{\partial N_x^I}{\partial x} + \frac{\partial N_{xy}^I}{\partial y} - Q_x^I = I^I \ddot{u} + \sum_{J=1}^{N} I^{IJ} \ddot{u}^J$$

$$\frac{\partial N_{xy}^I}{\partial x} + \frac{\partial N_y^I}{\partial y} - Q_y^I = I^I \ddot{v} + \sum_{J=1}^{N} I^{IJ} \ddot{v}^J$$

Also the expressions for stress resultants are simplified:

$$N_x = A_{11}\frac{\partial u}{\partial x} + A_{12}\frac{\partial v}{\partial y} + \sum_{I=1}^{N} \left(B_{11}^I \frac{\partial u^I}{\partial x} + B_{12}^I \frac{\partial v^I}{\partial y} \right)$$

$$N_y = A_{12}\frac{\partial u}{\partial x} + A_{22}\frac{\partial v}{\partial y} + \sum_{I=1}^{N} \left(B_{12}^I \frac{\partial u^I}{\partial x} + B_{22}^I \frac{\partial v^I}{\partial y} \right)$$

$$N_{xy} = A_{66} \left(\frac{\partial u}{\partial y} + \frac{\partial v}{\partial x} \right) + \sum_{I=1}^{N} B_{66}^I \left(\frac{\partial u^I}{\partial y} + \frac{\partial v^I}{\partial x} \right)$$

$$N_x^I = B_{11}^I \frac{\partial u}{\partial x} + B_{12}^I \frac{\partial v}{\partial y} + \sum_{J=1}^{N} \left(D_{11}^{JI} \frac{\partial u^I}{\partial x} + D_{12}^{JI} \frac{\partial v^I}{\partial y} \right) \tag{4.2}$$

$$N_y^I = B_{12}^I \frac{\partial u}{\partial x} + B_{22}^I \frac{\partial v}{\partial y} + \sum_{J=1}^{N} \left(D_{12}^{JI} \frac{\partial u^I}{\partial x} + D_{22}^{JI} \frac{\partial v^I}{\partial y} \right)$$

$$N_{xy}^I = B_{66}^I \left(\frac{\partial u}{\partial y} + \frac{\partial v}{\partial x} \right) + \sum_{J=1}^{N} D_{66}^{JI} \left(\frac{\partial u^I}{\partial y} + \frac{\partial v^I}{\partial x} \right)$$

$$Q_x = A_{55}\frac{\partial w}{\partial x} + \sum_{I=1}^{N} \overline{B}_{55}^I u^I$$

$$Q_y = A_{44}\frac{\partial w}{\partial y} + \sum_{I=1}^{N} \overline{B}_{44}^I v^I$$

$$Q_x^I = \overline{B}_{55}^I \frac{\partial w}{\partial x} + \sum_{J=1}^{N} \overline{D}_{55}^{JI} u^I \tag{4.3}$$

$$Q_y^I = \overline{B}_{44}^I \frac{\partial w}{\partial y} + \sum_{J=1}^{N} \overline{D}_{44}^{JI} v^I$$

There are two major steps in the solution process: (1) assume the spatial variation of the displacements and reduce the governing partial differential equations to a set of ordinary differential equations in time, and (2) solve the ordinary differential equations numerically.

The *Navier solution method* is used to determine the spatial variation of the transient solution. The coefficients of the double *Fourier series* are assumed to be functions of time. The solution is derived for rectangular simply supported laminates, with dimensions $a \times b$, under uniformly distributed transverse loading $q(x, y, t)$. In this case, the boundary conditions are (see Figure 4.1):
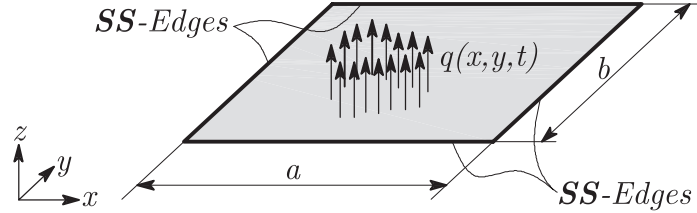
Figure 4.1: Rectangular plate $a \times b$ considered in the analytical solution

$$
\begin{aligned}
x = 0, x = a: & \quad v = w = v^I = N_x = N_x^I = 0 \\
y = 0, y = b: & \quad u = w = u^I = N_y = N_y^I = 0
\end{aligned}
\tag{4.4}
$$

The displacement field which satisfy the boundary conditions on the edges of the simply supported plate and Euler-Lagrange equations of motion is given as:

$$
\begin{aligned}
u(x, y, t) &= \sum_{m=1}^{\infty} \sum_{n=1}^{\infty} X_{mn}(t) \cos \alpha x \sin \beta y \\
v(x, y, t) &= \sum_{m=1}^{\infty} \sum_{n=1}^{\infty} Y_{mn}(t) \sin \alpha x \cos \beta y \\
w(x, y, t) &= \sum_{m=1}^{\infty} \sum_{n=1}^{\infty} W_{mn}(t) \sin \alpha x \sin \beta y \\
u^I(x, y, t) &= \sum_{m=1}^{\infty} \sum_{n=1}^{\infty} R_{mn}^I(t) \cos \alpha x \sin \beta y \\
v^I(x, y, t) &= \sum_{m=1}^{\infty} \sum_{n=1}^{\infty} S_{mn}^I(t) \sin \alpha x \cos \beta y
\end{aligned}
\tag{4.5}
$$

In previous equations, m and n denote number of members in double Fourier series, X_{mn}, Y_{mn}, W_{mn}, R_{mn}^I and S_{mn}^I are Fourier coefficients which are chosen only in a way that u, v, w, u^I and v^I satisfy the boundary conditions, $\alpha = \frac{m\pi}{a}$, $\beta = \frac{n\pi}{b}$. The second part of the expansion determines the spatial variation of transient solution.

In a same manner the loading is expanded in the double trigonometric series:

$$q(x, y, t) = \sum_{m=1}^{\infty} \sum_{n=1}^{\infty} q_{mn}(t) \sin \alpha x \sin \beta y \tag{4.6}$$

where

$$q_{mn}(t) = \frac{4}{ab} \int_0^a \int_0^b q(x, y) \sin \alpha x \sin \beta y dx dy \tag{4.7}$$

If we substitute the simplified stress resultants into the Euler-Lagrange equations, and incorporate the assumed expansions of displacements, we derive the matrix form of the governing equations of the problem:

$$\begin{bmatrix} k & k^I \\ k^I & k^{JI} \end{bmatrix} \begin{Bmatrix} X_{mn}(t) \\ Y_{mn}(t) \\ W_{mn}(t) \\ R^I_{mn}(t) \\ S^I_{mn}(t) \end{Bmatrix} + \begin{bmatrix} m & m^I \\ m^I & m^{JI} \end{bmatrix} \begin{Bmatrix} \ddot{X}_{mn}(t) \\ \ddot{Y}_{mn}(t) \\ \ddot{W}_{mn}(t) \\ \ddot{R}^I_{mn}(t) \\ \ddot{S}^I_{mn}(t) \end{Bmatrix} = \begin{Bmatrix} 0 \\ 0 \\ -q_{mn}(t) \\ 0 \\ 0 \end{Bmatrix} \tag{4.8}$$

where:

$$k = \begin{bmatrix} A_{11}\alpha^2 + A_{66}\beta^2 & A_{12}\alpha\beta + A_{66}\alpha\beta & 0 \\ A_{12}\alpha\beta + A_{66}\alpha\beta & A_{22}\beta^2 + A_{66}\alpha^2 & 0 \\ 0 & 0 & A_{44}\alpha^2 + A_{55}\beta^2 \end{bmatrix} \tag{4.9}$$

$$k^I = \begin{bmatrix} B^I_{11}\alpha^2 + B^I_{66}\beta^2 & B^I_{12}\alpha\beta + B^I_{66}\alpha\beta \\ B^I_{12}\alpha\beta + B^I_{66}\alpha\beta & B^I_{22}\beta^2 + B^I_{66}\alpha^2 \\ \overline{B}^I_{44}\alpha & \overline{B}^I_{55}\beta \end{bmatrix} \tag{4.10}$$

$$k^{JI} = \begin{bmatrix} D^{JI}_{11}\alpha^2 + D^{JI}_{66}\beta^2 + \overline{D}^{JI}_{44} & D^{JI}_{12}\alpha\beta + D^{JI}_{66}\alpha\beta \\ D^{JI}_{12}\alpha\beta + D^{JI}_{66}\alpha\beta & D^{JI}_{22}\beta^2 + D^{JI}_{66}\alpha^2 + \overline{D}^{JI}_{55} \end{bmatrix} \tag{4.11}$$

$$m = \begin{bmatrix} I_0 & & \\ & I_0 & \\ & & I_0 \end{bmatrix}, \quad m^I = \begin{bmatrix} I^I & 0 \\ 0 & I^I \\ 0 & 0 \end{bmatrix}, \quad m^{JI} = \begin{bmatrix} I^{JI} & \\ & I^{JI} \end{bmatrix} \tag{4.12}$$

The previous system of equations can be re-written in the compact matrix form:

$$[M]\{\ddot{d}\} + [K]\{d\} = \{f\} \tag{4.13}$$

4.2 Numerical Time Integration

The system of algebraic matrix equations in time are solved numerically using *Newmark's integration scheme* for second order differential equations [98]. The time derivatives are approximated using the truncated Taylor's series, thus the solution is obtained only for discrete time points and not as a continuous function of time. If we assume that the mass matrix $[M]$ and the stiffness matrix $[K]$ do not change through time and that the transient loading is defined as a time function in discrete time points $0 \le t \le T$, the governing system of equations in time point t_{n+1} is:

$$[M]\left\{\ddot{d}_{n+1}\right\} + [K]\left\{d_{n+1}\right\} = \left\{f_{n+1}\right\} \tag{4.14}$$

In the Newmark's *constant average acceleration method* the time function and its first derivative are approximated using truncated Taylor's series where only terms up to the second derivative are included:

$$\begin{aligned}
\{d_{n+1}\} &= \{d_n\} + \Delta t\left\{\dot{d}_n\right\} + \tfrac{\Delta t^2}{2}\left\{\ddot{d}_{n+\frac{1}{2}}\right\} \\
\left\{\dot{d}_{n+1}\right\} &= \left\{\dot{d}_n\right\} + \Delta t\left\{\ddot{d}_{n+\frac{1}{2}}\right\} \\
\left\{\ddot{d}_{n+\frac{1}{2}}\right\} &= \tfrac{1}{2}\left(\left\{\ddot{d}_n\right\} + \left\{\ddot{d}_{n+1}\right\}\right)
\end{aligned} \tag{4.15}$$

where Δt is the time increment and indexes n and $n+1$ denote the current and the next time points in which the solution is calculated, respectively. It is assumed that the solution at time t_n is known. Substituting the third equation from (4.15) into the first two and solving for $\left\{\ddot{d}\right\}$ the following equations are obtained:

$$\begin{aligned}
\left\{\dot{d}_{n+1}\right\} &= \left\{\dot{d}_n\right\} + \tfrac{1}{2}\Delta t\left\{\ddot{d}_n\right\} + \tfrac{1}{2}\Delta t\left\{\ddot{d}_{n+1}\right\} \\
\left\{\ddot{d}_{n+1}\right\} &= \tfrac{4}{(\Delta t)^2}\left(\{d_{n+1}\} - \{d_n\}\right) - \tfrac{4}{\Delta t}\left\{\dot{d}_n\right\} - \left\{\ddot{d}_n\right\}
\end{aligned} \tag{4.16}$$

If the second equation from the previous system is multiplied with $[M]$ and substituted in Eq. (4.13), the following equation is obtained:

$$[M]\left[\frac{4}{\Delta t^2}\{d_{n+1}\} - \frac{4}{\Delta t^2}\{d_n\} - \frac{4}{\Delta t}\left\{\dot{d}_n\right\} - \left\{\ddot{d}_n\right\}\right] + [K]\{d_{n+1}\} = \{f_{n+1}\} \tag{4.17}$$

and finally:

$$\left[\frac{4}{\Delta t^2}[M] + [K]\right]\{d_{n+1}\} = \{f_{n+1}\} + [M]\left[\frac{4}{\Delta t^2}\{d_n\} + \frac{4}{\Delta t}\left\{\dot{d}_n\right\} + \left\{\ddot{d}_n\right\}\right] \tag{4.18}$$

Equation (4.18) represents the system of algebraic equations among the discrete values of $\{d\}$ at time t_{n+1} in terms of known values at time t_n (recurrent formula). For the completion of solution, the initial values of $\{d\}$, $\{\dot{d}\}$ and $\{\ddot{d}\}$ are needed. The initial displacements and velocities are known from the initial conditions, while the initial acceleration are calculated from:

$$\left\{\ddot{d}_0\right\} = [M]^{-1}\left(\{f_0\} - [K]\{d_0\}\right) \tag{4.19}$$

4.3 Computation of the Interlaminar Stresses

After the displacement field of the laminated plate is calculated, the stress field can be derived using the constitutive equations (3.16), as shown in [93]. The stress field should be derived in each time step, substituting the Eqs. (4.5) in Eqs. (3.16). The in-plane stresses are then:

$$\sigma_x^{(k)}(x,y,z,t) = -\sum_{m=1}^{\infty}\sum_{n=1}^{\infty}\left[\begin{array}{c}\overline{Q}_{11}^{(k)}\alpha\left(X_{mn}(t) + \sum_{I=1}^{N}R_{mn}^{I}(t)\Phi^{I}(z)\right) + \\ +\overline{Q}_{12}^{(k)}\beta\left(Y_{mn}(t) + \sum_{I=1}^{N}S_{mn}^{I}(t)\Phi^{I}(z)\right)\end{array}\right]\sin\alpha x\sin\beta y$$

$$\sigma_y^{(k)}(x,y,z,t) = -\sum_{m=1}^{\infty}\sum_{n=1}^{\infty}\left[\begin{array}{c}\overline{Q}_{12}^{(k)}\alpha\left(X_{mn}(t) + \sum_{I=1}^{N}R_{mn}^{I}(t)\Phi^{I}(z)\right) + \\ +\overline{Q}_{22}^{(k)}\beta\left(Y_{mn}(t) + \sum_{I=1}^{N}S_{mn}^{I}(t)\Phi^{I}(z)\right)\end{array}\right]\sin\alpha x\sin\beta y$$

$$\tau_{xy}^{(k)}(x,y,z,t) = \overline{Q}_{66}^{(k)}\sum_{m=1}^{\infty}\sum_{n=1}^{\infty}\left[\begin{array}{c}\beta\left(X_{mn}(t) + \sum_{I=1}^{N}R_{mn}^{I}(t)\Phi^{I}(z)\right) + \\ +\alpha\left(Y_{mn}(t) + \sum_{I=1}^{N}S_{mn}^{I}(t)\Phi^{I}(z)\right)\end{array}\right]\cos\alpha x\cos\beta y$$

$$\tag{4.20}$$

In addition, the transverse shear stresses are defined as given in [93]:

$$\tau_{xz}^{(k)}(x,y,z,t) = \overline{Q}_{55}^{(k)}\sum_{m=1}^{\infty}\sum_{n=1}^{\infty}\left[\alpha W_{mn}(t) + \sum_{I=1}^{N}R_{mn}^{I}(t)\frac{d\Phi^{I}}{dz}(z)\right]\cos\alpha x\sin\beta y$$

$$\tau_{yz}^{(k)}(x,y,z,t) = \overline{Q}_{44}^{(k)}\sum_{m=1}^{\infty}\sum_{n=1}^{\infty}\left[\beta W_{mn}(t) + \sum_{I=1}^{N}S_{mn}^{I}(t)\frac{d\Phi^{I}}{dz}(z)\right]\sin\alpha x\cos\beta y$$

$$\tag{4.21}$$

The definition of functions $\Phi^{I}(z)$ from Eqs. (3.4) implies the discontinuity of in-plane stresses at the layer interfaces if different materials or different fiber orientations are used, while the transverse shear stresses are constant within each material layer. For the calculation of transverse shear stresses, the algorithm presented in [20,

74, 93] can be used. Because the stress field is derived directly from the previously calculated displacement field, the time evolution of the stresses in any point of the plate is exactly the same as for the time history plot of the displacements.

This completes the derivation of the analytical solution for the linear transient analysis of the intact, simply supported cross-ply laminated composite plates. The solution will be numerically validated through several examples in Chapter 10.4. The stress distribution will be also presented through the examples to illustrate the layerwise change of stresses through the thickness of the plate.

5 Finite Element Model

5.1 Introduction

As shown in **Chapter 4**, analytical solution of the GLPT exists only for the relatively simple plate geometries, loading and boundary conditions. However, for the analysis of structural elements of arbitrary shape, loading, boundary conditions, as well as for the analysis of laminated composite plates with delaminations of arbitrary shape and arbitrary positioned within a plate, numerical solution is required.

The Finite Element Method [99] is a powerful computational technique for the solution of differential and integral equations. The basic idea of the FEM is to approximate the given domain as an assemblage of simple geometric shapes (finite elements). The advantage of this concept is the possibility to systematically generate the *approximation functions* for the chosen domains. The approximation functions are constructed using the ideas of the interpolation theory [8], and hence they are also called the *interpolation functions*.

For a given differential equation, it is possible to develop different finite element approximations (models), depending on the choice of a particular variational and weighted-residual method. The FEM allows coupling of various physical problems because finite elements based on the different problems can be easily generated in the same computer program.

In **Chapter 3**, the Euler-Lagrange differential equations of motion are derived, which define the "strong" formulation of the geometrically nonlinear problem of the laminated composite plate. These governing equations will serve as a basis for the development of a numerical solution based on FEM. The weighted-integral or **"weak"** formulation of the governing differential equations over a typical finite element domain Ω^e will be defined as follows.

5.2 Weak Formulation

When deriving the "weak" form, first we multiply the $3 + 2N + 3ND$ governing differential equations of the problem from (3.75) with δu, δv, δw, δu^I, δv^I, δU^I, δV^I and δW^I, respectively, and integrate over the finite element domain Ω^e:

$$
0 = \int_{\Omega^e} \delta u \left[-\frac{\partial N_x}{\partial x} - \frac{\partial N_{xy}}{\partial y} + I_0 \ddot{u} + \sum_{I=1}^{N} I^I \ddot{u}^I + \sum_{I=1}^{ND} \overline{I}^I \ddot{U}^I \right] d\Omega^e
$$

$$
0 = \int_{\Omega^e} \delta v \left[-\frac{\partial N_{xy}}{\partial x} - \frac{\partial N_y}{\partial y} + I_0 \ddot{v} + \sum_{I=1}^{N} I^I \ddot{v}^I + \sum_{I=1}^{ND} \overline{I}^I \ddot{V}^I \right] d\Omega^e
$$

$$
0 = \int_{\Omega^e} \delta w \left[-\frac{\partial Q_x}{\partial x} - \frac{\partial Q_y}{\partial y} - q(x,y,t) - N(w) - \overline{N}(W^I) + I_0 \ddot{w} + \sum_{I=1}^{ND} \overline{I}^I \ddot{W}^I \right] d\Omega^e
$$

$$
0 = \int_{\Omega^e} \delta u^I \left[-\frac{\partial N_x^I}{\partial x} - \frac{\partial N_{xy}^I}{\partial y} + Q_x^I + I^I \ddot{u} + \sum_{J=1}^{ND} \overline{I}^{JI} \ddot{U}^J + \sum_{J=1}^{N} I^{IJ} \ddot{u}^J \right] d\Omega^e
$$

$$
0 = \int_{\Omega^e} \delta v^I \left[-\frac{\partial N_{xy}^I}{\partial x} - \frac{\partial N_y^I}{\partial y} + Q_y^I + I^I \ddot{v} + \sum_{J=1}^{ND} \overline{I}^{JI} \ddot{V}^J + \sum_{J=1}^{N} I^{IJ} \ddot{v}^J \right] d\Omega^e
$$

$$
0 = \int_{\Omega^e} \delta U^I \left[-\frac{\partial \overline{N}_x^I}{\partial x} - \frac{\partial \overline{N}_{xy}^I}{\partial y} + \overline{I}^I \ddot{u} + \sum_{J=1}^{N} \overline{I}^{JI} \ddot{u}^J + \sum_{J=1}^{ND} \widetilde{I}^{IJ} \ddot{U}^J \right] d\Omega^e
$$

$$
0 = \int_{\Omega^e} \delta V^I \left[-\frac{\partial \overline{N}_{xy}^I}{\partial x} - \frac{\partial \overline{N}_y^I}{\partial y} + \overline{I}^I \ddot{v} + \sum_{J=1}^{N} \overline{I}^{JI} \ddot{v}^J + \sum_{J=1}^{ND} \widetilde{I}^{IJ} \ddot{V}^J \right] d\Omega^e
$$

$$
0 = \int_{\Omega^e} \delta W^I \left[-\frac{\partial \overline{Q}_x^I}{\partial x} - \frac{\partial \overline{Q}_y^I}{\partial y} - \overline{N}^I(w) - \overline{N}^I(W^J) + \overline{I}^I \ddot{w} + \sum_{J=1}^{ND} \widetilde{I}^{IJ} \ddot{W}^J \right] d\Omega^e
$$

$$(5.1)$$

Here the virtual displacements δu, δv, δw, δu^I, δv^I, δU^I, δV^I and δW^I take the role of the weight functions. Integration by parts to weaken the differentiability of u, v, w, u^I, v^I, U^I, V^I and W^I results in the following expressions (n_x and n_y denote the direction cosines of the unit normal on the element boundary Γ^e):

$$
0 = \int_{\Omega^e} \left[\begin{array}{l} \frac{\partial \delta u}{\partial x} N_x + \frac{\partial \delta u}{\partial y} N_{xy} + I_0 \delta u \ddot{u} + \\ + \sum_{I=1}^{N} I^I \delta u \ddot{u}^I + \sum_{I=1}^{ND} \overline{I}^I \delta u \ddot{U}^I \end{array} \right] d\Omega^e - \oint_{\Gamma^e} \delta u \left(N_x n_x + N_{xy} n_y \right) ds
$$

$$
0 = \int_{\Omega^e} \left[\begin{array}{l} \frac{\partial \delta v}{\partial y} N_y + \frac{\partial \delta v}{\partial x} N_{xy} + I_0 \delta v \ddot{v} + \\ + \sum_{I=1}^{N} I^I \delta v \ddot{v}^I + \sum_{I=1}^{ND} \overline{I}^I \delta v \ddot{V}^I \end{array} \right] d\Omega^e - \oint_{\Gamma^e} \delta v \left(N_{xy} n_x + N_y n_y \right) ds
$$

$$
0 = \int\limits_{\Omega^e} \left[\begin{array}{l} \frac{\partial \delta w}{\partial x} Q_x + \frac{\partial \delta w}{\partial y} Q_y + \frac{\partial \delta w}{\partial x} \left(N_x \frac{\partial w}{\partial x} + N_{xy} \frac{\partial w}{\partial y} \right) + \frac{\partial \delta w}{\partial y} \left(N_{xy} \frac{\partial w}{\partial x} + N_y \frac{\partial w}{\partial y} \right) + \\ + \sum\limits_{I=1}^{ND} \left[\frac{\partial w}{\partial x} \left(\overline{N}_x^I \frac{\partial W^I}{\partial x} + \overline{N}_{xy}^I \frac{\partial W^I}{\partial y} \right) + \frac{\partial w}{\partial y} \left(\overline{N}_{xy}^I \frac{\partial W^I}{\partial x} + \overline{N}_y^I \frac{\partial W^I}{\partial y} \right) \right] - \\ -\delta w q(x,y,t) + I_0 \delta w \ddot{w} + \sum\limits_{I=1}^{ND} \overline{I}^I \delta w \ddot{W}^I \end{array} \right] d\Omega^e -
$$

$$
- \oint\limits_{\Gamma^e} \delta w \left\{ \begin{array}{l} Q_x n_x + Q_y n_y + \left(N_x \frac{\partial w}{\partial x} + N_{xy} \frac{\partial w}{\partial y} \right) n_x + \left(N_{xy} \frac{\partial w}{\partial x} + N_y \frac{\partial w}{\partial y} \right) n_y + \\ + \sum\limits_{I=1}^{ND} \left[\left(\overline{N}_x^I \frac{\partial W^I}{\partial x} + \overline{N}_{xy}^I \frac{\partial W^I}{\partial y} \right) n_x + \left(\overline{N}_{xy}^I \frac{\partial W^I}{\partial x} + \overline{N}_y^I \frac{\partial W^I}{\partial y} \right) n_y \right] \end{array} \right\} ds
$$

$$
0 = \int\limits_{\Omega^e} \left[\begin{array}{l} \frac{\partial \delta u^I}{\partial x} N_x^I + \frac{\partial \delta u^I}{\partial y} N_{xy}^I + \delta u^I Q_x^I + I^I \delta u^I \ddot{u} + \\ + \sum\limits_{J=1}^{ND} \overline{I}^{JI} \delta u^I \ddot{U}^J + \sum\limits_{J=1}^{N} I^{IJ} \delta u^I \ddot{u}^J \end{array} \right] d\Omega^e - \oint\limits_{\Gamma^e} \delta u^I \left(N_x^I n_x + N_{xy}^I n_y \right) ds
$$

$$
0 = \int\limits_{\Omega^e} \left[\begin{array}{l} \frac{\partial \delta v^I}{\partial y} N_y^I + \frac{\partial \delta v^I}{\partial x} N_{xy}^I + \delta v^I Q_y^I + I^I \delta v^I \ddot{v} + \\ + \sum\limits_{J=1}^{ND} \overline{I}^{JI} \delta v^I \ddot{V}^J + \sum\limits_{J=1}^{N} I^{IJ} \delta v^I \ddot{v}^J \end{array} \right] d\Omega^e - \oint\limits_{\Gamma^e} \delta v^I \left(N_{xy}^I n_x + N_y^I n_y \right) ds
$$

$$
0 = \int\limits_{\Omega^e} \left[\begin{array}{l} \frac{\partial \delta U^I}{\partial x} \overline{N}_x^I + \frac{\partial \delta U^I}{\partial y} \overline{N}_{xy}^I + \overline{I}^I \delta U^I \ddot{u} + \\ + \sum\limits_{J=1}^{N} \overline{I}^{JI} \delta U^I \ddot{u}^J + \sum\limits_{J=1}^{ND} \widetilde{I}^{IJ} \delta U^I \ddot{U}^J \end{array} \right] d\Omega^e - \oint\limits_{\Gamma^e} \delta U^I \left(\overline{N}_x^I n_x + \overline{N}_{xy}^I n_y \right) ds
$$

$$
0 = \int\limits_{\Omega^e} \left[\begin{array}{l} \frac{\partial \delta V^I}{\partial y} \overline{N}_y^I + \frac{\partial \delta V^I}{\partial x} \overline{N}_{xy}^I + \overline{I}^I \delta V^I \ddot{v} + \\ + \sum\limits_{J=1}^{N} \overline{I}^{JI} \delta V^I \ddot{v}^J + \sum\limits_{J=1}^{ND} \widetilde{I}^{IJ} \delta V^I \ddot{V}^J \end{array} \right] d\Omega^e - \oint\limits_{\Gamma^e} \delta V^I \left(\overline{N}_{xy}^I n_x + \overline{N}_y^I n_y \right) ds
$$

$$
0 = \int\limits_{\Omega^e} \left[\begin{array}{l} \frac{\partial \delta W^I}{\partial x} \left(\overline{N}_x^I \frac{\partial w}{\partial x} + \overline{N}_{xy}^I \frac{\partial w}{\partial y} \right) + \frac{\partial \delta W^I}{\partial y} \left(\overline{N}_{xy}^I \frac{\partial w}{\partial x} + \overline{N}_y^I \frac{\partial w}{\partial y} \right) + \\ + \sum\limits_{J=1}^{ND} \left[\begin{array}{l} \frac{\partial \delta W^I}{\partial x} \left(\overline{N}_x^{IJ} \frac{\partial W^J}{\partial x} + \overline{N}_{xy}^{IJ} \frac{\partial W^J}{\partial y} \right) + \\ + \frac{\partial \delta W^I}{\partial y} \left(\overline{N}_{xy}^{IJ} \frac{\partial W^J}{\partial x} + \overline{N}_y^{IJ} \frac{\partial W^J}{\partial y} \right) \end{array} \right] + \\ + \frac{\partial \delta W^I}{\partial x} \overline{Q}_x^I + \frac{\partial \delta W^I}{\partial y} \overline{Q}_y^I + \overline{I}^I \delta W^I \frac{\partial^2 w}{\partial t^2} + \sum\limits_{J=1}^{ND} \widetilde{I}^{IJ} \frac{\partial^2 W^J}{\partial t^2} \end{array} \right] d\Omega^e -
$$

$$
- \oint\limits_{\Gamma^e} \delta W^I \left\{ \begin{array}{l} \overline{Q}_x^I n_x + \overline{Q}_y^I n_y + \\ + \sum\limits_{J=1}^{ND} \left[\left(\overline{N}_x^{IJ} \frac{\partial W^J}{\partial x} + \overline{N}_{xy}^{IJ} \frac{\partial W^J}{\partial y} \right) n_x + \left(\overline{N}_{xy}^{IJ} \frac{\partial W^J}{\partial x} + \overline{N}_y^{IJ} \frac{\partial W^J}{\partial y} \right) n_y \right] \end{array} \right\} ds
$$

$$
\tag{5.2}
$$

The primary variables of the problem are u, v, w, u^I, v^I, U^I, V^I and W^I. The coefficients of the virtual displacements δu, δv, δw, δu^I, δv^I, δU^I, δV^I and δW^I in the contour integrals $\oint\limits_{\Gamma^e}$ are the secondary variables (generalized forces) of the

problem. If we re-write the forces on the boundary of the finite element Γ^e as:

$$N_n = N_x n_x + N_{xy} n_y, \quad N_s = N_{xy} n_x + N_y n_y, \quad Q_n = Q_x n_x + Q_y n_y$$

$$P_n = \left(N_x \frac{\partial w}{\partial x} + N_{xy} \frac{\partial w}{\partial y} \right) n_x + \left(N_{xy} \frac{\partial w}{\partial x} + N_y \frac{\partial w}{\partial y} \right) n_y$$

$$\overline{P}_n^I = \left(\overline{N}_x^I \frac{\partial W^I}{\partial x} + \overline{N}_{xy}^I \frac{\partial W^I}{\partial y} \right) n_x + \left(\overline{N}_{xy}^I \frac{\partial W^I}{\partial x} + \overline{N}_y^I \frac{\partial W^I}{\partial y} \right) n_y$$

$$\overline{P}_n^{IJ} = \left(\overline{N}_x^{IJ} \frac{\partial W^J}{\partial x} + \overline{N}_{xy}^{IJ} \frac{\partial W^J}{\partial y} \right) n_x + \left(\overline{N}_{xy}^{IJ} \frac{\partial W^J}{\partial x} + \overline{N}_y^{IJ} \frac{\partial W^J}{\partial y} \right) n_y \qquad (5.3)$$

$$N_n^I = N_x^I n_x + N_{xy}^I n_y, \quad N_s = N_{xy}^I n_x + N_y^I n_y$$

$$\overline{N}_n^I = \overline{N}_x^I n_x + \overline{N}_{xy}^I n_y, \quad \overline{N}_s^I = \overline{N}_{xy}^I n_x + \overline{N}_y^I n_y, \overline{Q}_n^I = \overline{Q}_x^I n_x + \overline{Q}_y^I n_y$$

we finally obtain the "**weak**" formulation in the following form:

$$0 = \int_{\Omega^e} \left[\frac{\partial \delta u}{\partial x} N_x + \frac{\partial \delta u}{\partial y} N_{xy} + I_0 \delta u \ddot{u} + \sum_{I=1}^{N} I^I \delta u \ddot{u}^I + \sum_{I=1}^{ND} \overline{I}^I \delta u \ddot{U}^I \right] d\Omega^e - \oint_{\Gamma^e} \delta u N_n ds$$

$$0 = \int_{\Omega^e} \left[\frac{\partial \delta v}{\partial y} N_y + \frac{\partial \delta v}{\partial x} N_{xy} + I_0 \delta v \ddot{v} + \sum_{I=1}^{N} I^I \delta v \ddot{v}^I + \sum_{I=1}^{ND} \overline{I}^I \delta v \ddot{V}^I \right] d\Omega^e - \oint_{\Gamma^e} \delta v N_s ds$$

$$0 = \int_{\Omega^e} \left[\begin{array}{l} \frac{\partial \delta w}{\partial x} Q_x + \frac{\partial \delta w}{\partial y} Q_y - \delta w q(x,y,t) + I_0 \delta w \ddot{w} + \sum_{I=1}^{ND} \overline{I}^I \delta w \ddot{W}^I + \\[2mm] + \frac{\partial \delta w}{\partial x} \left(N_x \frac{\partial w}{\partial x} + N_{xy} \frac{\partial w}{\partial y} \right) + \frac{\partial \delta w}{\partial y} \left(N_{xy} \frac{\partial w}{\partial x} + N_y \frac{\partial w}{\partial y} \right) + \\[2mm] + \sum_{I=1}^{ND} \left[\frac{\partial w}{\partial x} \left(\overline{N}_x^I \frac{\partial W^I}{\partial x} + \overline{N}_{xy}^I \frac{\partial W^I}{\partial y} \right) + \frac{\partial w}{\partial y} \left(\overline{N}_{xy}^I \frac{\partial W^I}{\partial x} + \overline{N}_y^I \frac{\partial W^I}{\partial y} \right) \right] \end{array} \right] d\Omega^e -$$

$$- \oint_{\Gamma^e} \delta w \left[Q_n + P_n \right] ds$$

$$0 = \int_{\Omega^e} \left[\begin{array}{l} \frac{\partial \delta u^I}{\partial x} N_x^I + \frac{\partial \delta u^I}{\partial y} N_{xy}^I + \delta u^I Q_x^I + \\[2mm] + I^I \delta u^I \ddot{u} + \sum_{J=1}^{ND} \overline{I}^{JI} \delta u^I \ddot{U}^J + \sum_{J=1}^{N} I^{IJ} \delta u^I \ddot{u}^J \end{array} \right] d\Omega^e - \oint_{\Gamma^e} \delta u^I N_n^I ds$$

$$0 = \int_{\Omega^e} \left[\begin{array}{l} \frac{\partial \delta v^I}{\partial y} N_y^I + \frac{\partial \delta v^I}{\partial x} N_{xy}^I + \delta v^I Q_y^I + \\[2mm] + I^I \delta v^I \ddot{v} + \sum_{J=1}^{ND} \overline{I}^{JI} \delta v^I \ddot{V}^J + \sum_{J=1}^{N} I^{IJ} \delta v^I \ddot{v}^J \end{array} \right] d\Omega^e - \oint_{\Gamma^e} \delta v^I N_s^I ds$$

$$0 = \int_{\Omega^e} \left[\begin{array}{l} \frac{\partial \delta U^I}{\partial x} \overline{N}_x^I + \frac{\partial \delta U^I}{\partial y} \overline{N}_{xy}^I + \\[2mm] + \overline{I}^I \delta U^I \ddot{u} + \sum_{J=1}^{N} \overline{I}^{JI} \delta U^I \ddot{u}^J + \sum_{J=1}^{ND} \widetilde{I}^{IJ} \delta U^I \ddot{U}^J \end{array} \right] d\Omega^e - \oint_{\Gamma^e} \delta U^I \overline{N}_n^I ds$$

$$
0 \quad = \quad \int_{\Omega^e} \left[\begin{array}{c} \frac{\partial \delta V^I}{\partial y} \overline{N}_y^I + \frac{\partial \delta V^I}{\partial x} \overline{N}_{xy}^I + \\ + \overline{I}^I \delta V^I \ddot{v} + \sum_{J=1}^{N} \overline{I}^{JI} \delta V^I \ddot{v}^J + \sum_{J=1}^{ND} \widetilde{I}^{IJ} \delta V^I \ddot{V}^J \end{array} \right] d\Omega^e \quad - \quad \oint_{\Gamma^e} \delta V^I \overline{N}_s^I ds
$$

$$
0 = \int_{\Omega^e} \left[\begin{array}{c} \frac{\partial \delta W^I}{\partial x} \overline{Q}_x^I + \frac{\partial \delta W^I}{\partial y} \overline{Q}_y^I + \overline{I}^I \delta W^I \ddot{w} + \sum_{J=1}^{ND} \widetilde{I}^{IJ} \ddot{W}^J + \\ + \frac{\partial \delta W^I}{\partial x} \left(\overline{N}_x^I \frac{\partial w}{\partial x} + \overline{N}_{xy}^I \frac{\partial w}{\partial y} \right) + \frac{\partial \delta W^I}{\partial y} \left(\overline{N}_{xy}^I \frac{\partial w}{\partial x} + \overline{N}_y^I \frac{\partial w}{\partial y} \right) + \\ + \sum_{J=1}^{ND} \left[\begin{array}{c} \frac{\partial \delta W^I}{\partial x} \left(\overline{N}_x^{IJ} \frac{\partial W^J}{\partial x} + \overline{N}_{xy}^{IJ} \frac{\partial W^J}{\partial y} \right) + \\ + \frac{\partial \delta W^I}{\partial y} \left(\overline{N}_{xy}^{IJ} \frac{\partial W^J}{\partial x} + \overline{N}_y^{IJ} \frac{\partial W^J}{\partial y} \right) \end{array} \right] \end{array} \right] d\Omega^e -
$$

$$
- \oint_{\Gamma^e} \delta W^I \left[\overline{Q}_n^I + \overline{P}_n^{IJ} \right] ds \quad (5.4)
$$

5.3 Spatial Approximation

As shown before, the primary variables of the problem are u, v, w, u^I, v^I, U^I, V^I and W^I. Thus the proposed theory allows adopting only translation components in three orthogonal directions as generalized displacements in the nodes. Nodal variables (*degrees of freedom* - DOFs) are the displacement components (u, v, w) in the middle plane, relative displacements (u^I, v^I) in I^{th} numerical layer (node) through the thickness of the plate, and displacement jumps (U^I, V^I, W^I) in I^{th} delaminated numerical layer, which means that the number of nodal variables is layer-dependent: $3 + 2N + 3ND$.
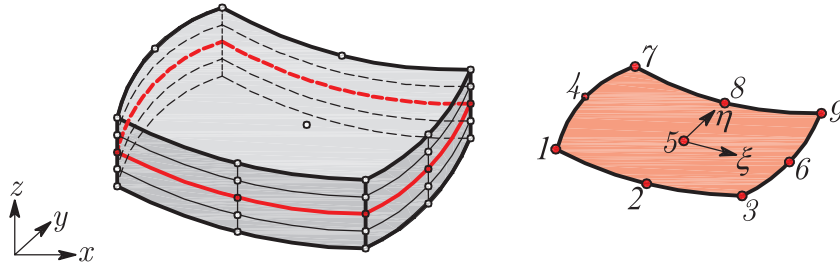
Figure 5.1: Typical layered finite element with nine nodes (quadratic interpolation)

The displacement based finite element model is derived in a following way: we substitute the assumed interpolation of the displacement field into the previously

derived weak formulation, for the single finite element of the plate. The finite element *mesh* is generated only in the 2D plane, and the adopted interpolation functions through the plate thickness are used for out-of-plane interpolation of the unknown variables (which eliminates the z-coordinate from the calculation). This assumption allows interpolating the unknown field variables independently for the in-plane and out-of-plane distribution.

We assume that all generalized displacements are interpolated using same interpolation functions, for the sake of simplicity:

$$\left(u, v, w, u^I, v^I, U^I, V^I, W^I\right) = \sum_{i=1}^{m} \left(u_i, v_i, w_i, u_i^I, v_i^I, U_i^I, V_i^I, W_i^I\right) \psi_i \qquad (5.5)$$

In the previous interpolation, m is the number of nodes per 2D finite element, while $\left(u_i, v_i, w_i, u_i^I, v_i^I, U_i^I, V_i^I, W_i^I\right)$ are the ith node values of the displacements $\left(u, v, w, u^I, v^I, U^I, V^I, W^I\right)$, respectively. The natural coordinate system $\xi - \eta$ of the single FE is located at the centroid of the element, as shown in Figure 5.1. The functions ψ_i are the 2-D Lagrangian interpolation polynomials associated with the ith node of the 2-D finite element. For the clear notation, the displacements (u, v, w), (u^I, v^I) and (U^I, V^I, W^I) are interpolated separately in the following way:

$$\left\{ \begin{array}{c} u \\ v \\ w \end{array} \right\} = \left\{ \begin{array}{c} \sum_{i=1}^{m} u_i \psi_i \\ \sum_{i=1}^{m} v_i \psi_i \\ \sum_{i=1}^{m} w_i \psi_i \end{array} \right\} = [\Psi] \{\Delta\}, \qquad \left\{ \begin{array}{c} u^I \\ v^I \end{array} \right\} = \left\{ \begin{array}{c} \sum_{i=1}^{m} u_i^I \psi_i \\ \sum_{i=1}^{m} v_i^I \psi_i \end{array} \right\} = \left[\overline{\Psi}\right] \{\Delta^I\}$$

$$\left\{ \begin{array}{c} u \\ v \end{array} \right\} = \left[\overline{\overline{\Psi}}\right] \{\Delta\}, \qquad \left\{ \begin{array}{c} U^I \\ V^I \end{array} \right\} = \left[\overline{\overline{\Psi}}\right] \left\{\overline{\Delta}^I\right\}$$

$$\left\{ \begin{array}{c} U^I \\ V^I \\ W^I \end{array} \right\} = \left\{ \begin{array}{c} \sum_{i=1}^{m} U_i^I \psi_i \\ \sum_{i=1}^{m} V_i^I \psi_i \\ \sum_{i=1}^{m} W_i^I \psi_i \end{array} \right\} = [\Psi] \left\{\overline{\Delta}^I\right\}$$

$$(5.6)$$

In Eqs. (5.6), $\{\Delta\}$, $\{\Delta^I\}$ and $\{\overline{\Delta}^I\}$ are displacement vectors in the mid-plane, the

5. Finite Element Model

I^{th} numerical layer and the Ith delaminated interface, respectively:

$$\{\Delta\} = \begin{Bmatrix} u_1 \\ v_1 \\ w_1 \\ \vdots \end{Bmatrix}_{3m \times 1} , \quad \{\Delta^I\} = \begin{Bmatrix} u_1^I \\ v_1^I \\ \vdots \end{Bmatrix}_{2m \times 1} , \quad \{\overline{\Delta}^I\} = \begin{Bmatrix} U_1^I \\ V_1^I \\ W_1^I \\ \vdots \end{Bmatrix}_{3m \times 1} \tag{5.7}$$

In this study, four-node and nine-node Lagrange quadrilateral finite elements are derived. $[\Psi]$, $[\overline{\Psi}]$ and $[\overline{\overline{\Psi}}]$ are the matrices of Lagrangian interpolation functions:

$$[\Psi] = \begin{bmatrix} \psi_1 & 0 & 0 \\ 0 & \psi_1 & 0 & \cdots \\ 0 & 0 & \psi_1 \end{bmatrix}_{3 \times 3m} , \quad [\overline{\Psi}] = \begin{bmatrix} \psi_1 & 0 \\ 0 & \psi_1 & \cdots \end{bmatrix}_{2 \times 2m}$$

$$[\overline{\overline{\Psi}}] = \begin{bmatrix} \psi_1 & 0 & 0 \\ 0 & \psi_1 & 0 & \cdots \end{bmatrix}_{2 \times 3m} \tag{5.8}$$

Interpolation of Strain Field

If we incorporate the displacement interpolations from Eqs. (5.6) into the kinematic relations from Eqs. (3.7) - (3.12), we obtain the discretized version of strain matrices:

$$\{\epsilon\}_{5 \times 1} = [B]_{5 \times 3m} \{\Delta\}_{3m \times 1}$$
$$\{\epsilon^I\}_{5 \times 1} = [\overline{B}]_{5 \times 2m} \{\Delta^I\}_{2m \times 1}$$
$$\{\overline{\epsilon}^I\}_{5 \times 1} = [B]_{5 \times 3m} \{\overline{\Delta}^I\}_{3m \times 1}$$
$$\{\eta\}_{5 \times 1} = [B_{NL}]_{5 \times 3m} \{\Delta\}_{3m \times 1} \tag{5.9}$$
$$\{\overline{\eta}^I\}_{5 \times 1} = [B_{NL}]_{5 \times 3m} \{\overline{\Delta}^I\}_{3m \times 1} + \left[\overline{B}_{NL}^I\right]_{5 \times 3m} \{\Delta\}_{3m \times 1}$$
$$\{\overline{\eta}^{IJ}\}_{5 \times 1} = \tfrac{1}{2} \left(\left[\overline{B}_{NL}^I\right]_{5 \times 3m} \{\overline{\Delta}^J\}_{3m \times 1} + \left[\overline{B}_{NL}^J\right]_{5 \times 3m} \{\overline{\Delta}^I\}_{3m \times 1} \right)$$

The corresponding variations of strain matrices are:

$$\{\delta\epsilon\}_{5 \times 1} = [B]_{5 \times 3m} \{\delta\Delta\}_{3m \times 1}$$
$$\{\delta\epsilon^I\}_{5 \times 1} = [\overline{B}]_{5 \times 2m} \{\delta\Delta^I\}_{2m \times 1}$$
$$\{\delta\overline{\epsilon}^I\}_{5 \times 1} = [B]_{5 \times 3m} \{\delta\overline{\Delta}^I\}_{3m \times 1}$$
$$\{\delta\eta\}_{5 \times 1} = 2 [B_{NL}]_{5 \times 3m} \{\delta\Delta\}_{3m \times 1} \tag{5.10}$$
$$\{\delta\overline{\eta}^I\}_{5 \times 1} = 2 [B_{NL}]_{5 \times 3m} \{\delta\overline{\Delta}^I\}_{3m \times 1} + 2 \left[\overline{B}_{NL}^I\right]_{5 \times 3m} \{\delta\Delta\}_{3m \times 1}$$
$$\{\delta\overline{\eta}^{IJ}\}_{5 \times 1} = \left[\overline{B}_{NL}^J\right]_{5 \times 3m} \{\delta\overline{\Delta}^I\}_{3m \times 1} + \left[\overline{B}_{NL}^I\right]_{5 \times 3m} \{\delta\overline{\Delta}^J\}_{3m \times 1}$$

In the previous expressions, kinematic matrices $[B]$, $[\overline{B}]$, $[B_{NL}]$ and $\left[\overline{B}_{NL}^I\right]$ relate generalized displacements (degrees of freedom) with the respective strain resultants:

$$[B] = \begin{bmatrix} \frac{\partial\psi_1}{\partial x} & 0 & 0 \\ 0 & \frac{\partial\psi_1}{\partial y} & 0 \\ \frac{\partial\psi_1}{\partial y} & \frac{\partial\psi_1}{\partial x} & 0 & \cdots \\ 0 & 0 & \frac{\partial\psi_1}{\partial x} \\ 0 & 0 & \frac{\partial\psi_1}{\partial y} \end{bmatrix}_{5\times 3m} , \quad [\overline{B}] = \begin{bmatrix} \frac{\partial\psi_1}{\partial x} & 0 \\ 0 & \frac{\partial\psi_1}{\partial y} \\ \frac{\partial\psi_1}{\partial y} & \frac{\partial\psi_1}{\partial x} & \cdots \\ \psi_1 & 0 \\ 0 & \psi_1 \end{bmatrix}_{5\times 2m}$$

$$[B_{NL}] = \frac{1}{2} \begin{bmatrix} 0 & 0 & \frac{\partial w}{\partial x}\frac{\partial\psi_1}{\partial x} \\ 0 & 0 & \frac{\partial w}{\partial y}\frac{\partial\psi_1}{\partial y} \\ 0 & 0 & \frac{\partial w}{\partial x}\frac{\partial\psi_1}{\partial y} + \frac{\partial w}{\partial y}\frac{\partial\psi_1}{\partial x} & \cdots \\ 0 & 0 & 0 \\ 0 & 0 & 0 \end{bmatrix}_{5\times 3m} \tag{5.11}$$

$$\left[\overline{B}_{NL}^I\right] = \frac{1}{2} \begin{bmatrix} 0 & 0 & \frac{\partial W^I}{\partial x}\frac{\partial\psi_1}{\partial x} \\ 0 & 0 & \frac{\partial W^I}{\partial y}\frac{\partial\psi_1}{\partial y} \\ 0 & 0 & \frac{\partial W^I}{\partial x}\frac{\partial\psi_1}{\partial y} + \frac{\partial W^I}{\partial y}\frac{\partial\psi_1}{\partial x} & \cdots \\ 0 & 0 & 0 \\ 0 & 0 & 0 \end{bmatrix}_{5\times 3m}$$

Substituting the approximations (5.10) into the weak formulation, and introducing the vectors of external nodal loading $\{\mathbf{q}\}$, mid-plane nodal loading $\{\mathbf{t}\}$ on the boundary of the element Γ^e, nodal loading $\{\mathbf{t}^I\}$ of the Ith layer on the boundary of the element Γ^e and nodal loading $\left\{\overline{\mathbf{t}}^I\right\}$ of the Ith delaminated interface on the boundary of the element Γ^e, respectively:

$$\{\mathbf{q}\} = \left\{ \begin{matrix} 0 & 0 & q_1 & \cdots \end{matrix} \right\}_{3m\times 1}^T, \{\mathbf{t}\} = \left\{ \begin{matrix} N_{n1} & N_{s1} & Q_{n1}+P_{n1} & \cdots \end{matrix} \right\}_{3m\times 1}^T \tag{5.12}$$

$$\{\mathbf{t}^I\} = \left\{ \begin{matrix} N_{n1}^I & N_{s1}^I & \cdots \end{matrix} \right\}_{2m\times 1}^T, \left\{\overline{\mathbf{t}}^I\right\} = \left\{ \begin{matrix} \overline{N}_{n1}^I & \overline{N}_{s1}^I & \overline{Q}_{n1}^I+\overline{P}_{n1}^I & \cdots \end{matrix} \right\}_{3m\times 1}^T$$

and introducing the kinematic matrix $[G]$ and the matrix of initial mid-plane force resultants acting on the second order strains $[N^0]$:

$$[G] = \begin{bmatrix} 0 & 0 & \frac{\partial\psi_1}{\partial x} & \cdots \\ 0 & 0 & \frac{\partial\psi_1}{\partial y} & \cdots \end{bmatrix}_{2\times 3m} , \quad [N^0] = \begin{bmatrix} N_x^0 & N_{xy}^0 \\ N_{xy}^0 & N_y^0 \end{bmatrix}_{2\times 2} \tag{5.13}$$

the matrix form of the weak formulation is obtained:

$$
0 = \int_{\Omega^e} \left[\begin{array}{l} (\{\delta\epsilon\} + \{\delta\eta\})^T \{N\} + \sum_{I=1}^{N} \{\delta\epsilon^I\}^T \{N^I\} + \\ + \sum_{I=1}^{ND} (\{\delta\overline{\epsilon}^I\} + \{\delta\overline{\eta}^I\})^T \{\overline{N}^I\} + \sum_{I,J=1}^{ND} \{\delta\overline{\eta}^{IJ}\}^T \{\overline{N}^{IJ}\} \end{array} \right] d\Omega^e +
$$

$$
+ \int_{\Omega^e} \left[\begin{array}{l} I_0 \{\delta\Delta\}^T [\Psi]^T [\Psi] \{\ddot{\Delta}\} + \sum_{I=1}^{N} I^I \{\delta\Delta\}^T \left[\overline{\overline{\Psi}}\right]^T [\Psi] \{\ddot{\Delta}\} + \\ + \sum_{I=1}^{N} I^I \{\delta\Delta^I\}^T \left[\overline{\Psi}\right]^T \left[\overline{\overline{\Psi}}\right] \{\ddot{\Delta}\} + \sum_{I=1}^{ND} \overline{I}^I \{\delta\Delta\}^T [\Psi]^T [\Psi] \left\{\ddot{\overline{\Delta}}^I\right\} + \\ + \sum_{I=1}^{ND} \overline{I}^I \left\{\delta\overline{\Delta}^I\right\}^T [\Psi]^T [\Psi] \{\ddot{\Delta}\} + \sum_{I,J=1}^{N} I^{IJ} \{\delta\Delta^I\}^T \left[\overline{\Psi}\right]^T \left[\overline{\Psi}\right] \{\Delta^I\} + \\ + \sum_{I=1}^{N} \sum_{J=1}^{ND} \overline{I}^{JI} \left(\{\delta\Delta^I\}^T \left[\overline{\Psi}\right]^T \left[\overline{\overline{\Psi}}\right] \{\overline{\Delta}^J\} + \left\{\delta\overline{\Delta}^J\right\}^T \left[\overline{\overline{\Psi}}\right]^T \left[\overline{\Psi}\right] \{\Delta^J\} \right) + \\ + \sum_{I,J=1}^{ND} \widetilde{I}^{IJ} \left\{\delta\overline{\Delta}^I\right\}^T [\Psi]^T [\Psi] \left\{\overline{\Delta}^J\right\} \end{array} \right] d\Omega^e +
$$

$$
+ \int_{\Omega^e} [G]^T [N^0] [G] \{\Delta\} d\Omega^e - \int_{\Omega^e} \left[\{\delta\Delta\}^T [\Psi]^T [\Psi] \{\mathbf{q}\} \right] d\Omega^e -
$$

$$
- \oint_{\Gamma^e} \left[\{\delta\Delta\}^T [\Psi]^T [\Psi] \{\mathbf{t}\} + \sum_{I=1}^{N} \{\delta\Delta^I\}^T \left[\overline{\Psi}\right]^T \left[\overline{\Psi}\right] \{\mathbf{t}^I\} + \sum_{I=1}^{ND} \left\{\delta\overline{\Delta}^I\right\}^T [\Psi]^T [\Psi] \left\{\overline{\mathbf{t}}^I\right\} \right] ds
$$

$$
(5.14)
$$

By considering the matrix form of the laminate constitutive equations from Eqs. (3.57) - (3.60) and substituting into Eq. (5.14) the discretized weak formulation is obtained:

$$
\int_{\Omega^e} (\mathbf{I}_1 + \mathbf{I}_2) d\Omega^e + \int_{\Omega^e} [G]^T [N^0] [G] \{\Delta\} d\Omega^e = \int_{\Omega^e} \left[\{\delta\Delta\}^T [\Psi]^T [\Psi] \{\mathbf{q}\} \right] d\Omega^e +
$$

$$
+ \oint_{\Gamma^e} \left[\{\delta\Delta\}^T [\Psi]^T [\Psi] \{\mathbf{t}\} + \sum_{I=1}^{N} \{\delta\Delta^I\}^T \left[\overline{\Psi}\right]^T \left[\overline{\Psi}\right] \{\mathbf{t}^I\} + \sum_{I=1}^{ND} \left\{\delta\overline{\Delta}^I\right\}^T [\Psi]^T [\Psi] \left\{\overline{\mathbf{t}}^I\right\} \right] ds
$$

$$
(5.15)
$$

where the integrand $\mathbf{I}_1 =$

$$
\begin{aligned}
&\{\delta\Delta\}^T \left[B + 2B_{NL}\right]^T [A] \left[B + B_{NL}\right] \{\Delta\} + \sum_{I=1}^{N} \{\delta\Delta\}^T \left[B + 2B_{NL}\right]^T \left[B^I\right] \left[\overline{B}\right] \{\Delta^I\} + \\
&+ \sum_{I=1}^{ND} \{\delta\Delta\}^T \left[B + 2B_{NL}\right]^T \left[E^I\right] \left(\left[B + B_{NL}\right] \{\overline{\Delta}^I\} + \left[\overline{B}_{NL}^I\right] \{\Delta\}\right) + \\
&+ \sum_{I,J=1}^{ND} \tfrac{1}{2} \{\delta\Delta\}^T \left[B + 2B_{NL}\right]^T \left[F^{IJ}\right] \left(\left[\overline{B}_{NL}^I\right] \{\overline{\Delta}^J\} + \left[\overline{B}_{NL}^J\right] \{\overline{\Delta}^I\}\right) + \\
&+ \sum_{I=1}^{N} \{\delta\Delta^I\}^T \left[\overline{B}\right]^T \left[B^I\right] \left[B + B_{NL}\right] \{\Delta\} + \sum_{I,J=1}^{N} \{\delta\Delta^I\}^T \left[\overline{B}\right]^T \left[D^{IJ}\right] \left[\overline{B}\right] \{\Delta^J\} + \\
&+ \sum_{I=1}^{N} \sum_{J=1}^{ND} \{\delta\Delta^I\}^T \left[\overline{B}\right]^T \left[L^{IJ}\right] \left(\left[B + B_{NL}\right] \{\overline{\Delta}^J\} + \left[\overline{B}_{NL}^J\right] \{\Delta\}\right) + \\
&+ \sum_{I=1}^{N} \sum_{J,K=1}^{ND} \tfrac{1}{2} \{\delta\Delta^I\}^T \left[\overline{B}\right]^T \left[L^{IJK}\right] \left(\left[\overline{B}_{NL}^J\right] \{\overline{\Delta}^K\} + \left[\overline{B}_{NL}^K\right] \{\overline{\Delta}^J\}\right) + \\
&+ \sum_{I=1}^{ND} \{\delta\overline{\Delta}^I\}^T [B]^T \left[E^I\right] \left[B + B_{NL}\right] \{\Delta\} + \sum_{I=1}^{ND} \sum_{J=1}^{N} \{\delta\overline{\Delta}^I\}^T [B]^T \left[L^{JI}\right] \left[\overline{B}\right] \{\Delta^J\} + \\
&+ \sum_{I,J=1}^{ND} \{\delta\overline{\Delta}^I\}^T [B]^T \left[F^{IJ}\right] \left(\left[B + B_{NL}\right] \{\overline{\Delta}^J\} + \left[\overline{B}_{NL}^J\right] \{\Delta\}\right) + \\
&+ \sum_{I,J,K=1}^{ND} \tfrac{1}{2} \{\delta\overline{\Delta}^I\}^T [B]^T \left[F^{IJK}\right] \left(\left[\overline{B}_{NL}^J\right] \{\overline{\Delta}^K\} + \left[\overline{B}_{NL}^K\right] \{\overline{\Delta}^J\}\right) + \\
&+ \sum_{I=1}^{ND} 2 \left(\{\delta\Delta\}^T \left[\overline{B}_{NL}^I\right]^T + \{\delta\overline{\Delta}^I\}^T [B_{NL}]^T\right) \left[E^I\right] \left[B + B_{NL}\right] \{\Delta\} + \\
&+ \sum_{I=1}^{ND} \sum_{J=1}^{N} 2 \left(\{\delta\Delta\}^T \left[\overline{B}_{NL}^I\right]^T + \{\delta\overline{\Delta}^I\}^T [B_{NL}]^T\right) \left[L^{JI}\right] \left[\overline{B}\right] \{\Delta^J\} + \\
&+ \sum_{I,J=1}^{ND} 2 \{\delta\Delta\}^T \left[\overline{B}_{NL}^I\right]^T \left[F^{IJ}\right] \left(\left[B + B_{NL}\right] \{\overline{\Delta}^J\} + \left[\overline{B}_{NL}^J\right] \{\Delta\}\right) + \\
&+ \sum_{I,J=1}^{ND} 2 \{\delta\overline{\Delta}^I\}^T [B_{NL}]^T \left[F^{IJ}\right] \left(\left[B + B_{NL}\right] \{\overline{\Delta}^J\} + \left[\overline{B}_{NL}^J\right] \{\Delta\}\right) + \\
&+ \sum_{I,J,K=1}^{ND} \left(\{\delta\Delta\}^T \left[\overline{B}_{NL}^I\right]^T + \{\delta\overline{\Delta}^I\}^T [B_{NL}]^T\right) \left[F^{IJK}\right] 2 \left[\overline{B}_{NL}^J\right] \{\overline{\Delta}^K\} + \\
&+ \sum_{I,J=1}^{ND} \left(\{\delta\overline{\Delta}^J\}^T \left[\overline{B}_{NL}^I\right]^T + \{\delta\overline{\Delta}^I\}^T \left[\overline{B}_{NL}^J\right]^T\right) \left[F^{IJ}\right] \left[B + B_{NL}\right] \{\Delta\} + \\
&+ \sum_{I,J=1}^{ND} \sum_{K=1}^{N} \left(\{\delta\overline{\Delta}^J\}^T \left[\overline{B}_{NL}^I\right]^T + \{\delta\overline{\Delta}^I\}^T \left[\overline{B}_{NL}^J\right]^T\right) \left[L^{KIJ}\right] \left[\overline{B}\right] \{\Delta^K\} + \\
&+ \sum_{I,J,K=1}^{ND} 2 \{\delta\overline{\Delta}^I\}^T \left[\overline{B}_{NL}^J\right]^T \left[F^{IJK}\right] \left(\left[B + B_{NL}\right] \{\overline{\Delta}^K\} + \left[\overline{B}_{NL}^K\right] \{\Delta\}\right) + \\
&+ \sum_{I,J,K,L=1}^{ND} \{\delta\overline{\Delta}^I\}^T \left[\overline{B}_{NL}^J\right]^T \left[F^{IJKL}\right] \left(\left[\overline{B}_{NL}^K\right] \{\overline{\Delta}^L\} + \left[\overline{B}_{NL}^L\right] \{\overline{\Delta}^K\}\right)
\end{aligned}
$$

$$(5.16)$$

and integrand $\mathbf{I}_2 =$

$$
I_0 \{\delta\Delta\}^T [\Psi]^T [\Psi] \{\ddot{\Delta}\} + \sum_{I=1}^{N} I^I \{\delta\Delta\}^T \left[\overline{\overline{\Psi}}\right]^T [\Psi] \{\ddot{\Delta}\} +
$$
$$
+ \sum_{I=1}^{N} I^I \{\delta\Delta^I\}^T [\overline{\Psi}]^T [\overline{\overline{\Psi}}] \{\ddot{\Delta}\} + \sum_{I=1}^{ND} \overline{I}^I \{\delta\Delta\}^T [\Psi]^T [\Psi] \left\{\ddot{\overline{\Delta}}^I\right\} +
$$
$$
+ \sum_{I=1}^{ND} \overline{I}^I \left\{\delta\overline{\Delta}^I\right\}^T [\Psi]^T [\Psi] \{\ddot{\Delta}\} + \sum_{I,J=1}^{N} I^{IJ} \{\delta\Delta^I\}^T [\overline{\Psi}]^T [\overline{\Psi}] \{\Delta^J\} + \qquad (5.17)
$$
$$
+ \sum_{I=1}^{N} \sum_{J=1}^{ND} \overline{I}^{JI} \left(\{\delta\Delta^I\}^T [\overline{\Psi}]^T [\overline{\overline{\Psi}}] \left\{\overline{\Delta}^J\right\} + \left\{\delta\overline{\Delta}^J\right\}^T [\overline{\overline{\Psi}}]^T [\overline{\Psi}] \{\Delta^J\} \right) +
$$
$$
+ \sum_{I,J=1}^{ND} \widetilde{I}^{IJ} \left\{\delta\overline{\Delta}^I\right\}^T [\Psi]^T [\Psi] \left\{\overline{\Delta}^J\right\} .
$$

Collecting the coefficients of all displacement vectors from the previous equations, the matrix form of the finite element model is derived:

$$
\begin{bmatrix} [K_{11}] & \left[K_{12}^I\right] & \left[K_{13}^I\right] \\ \left[K_{21}^I\right] & \left[K_{22}^{IJ}\right] & \left[K_{23}^{IJ}\right] \\ \left[K_{31}^I\right] & \left[K_{32}^{IJ}\right] & \left[K_{33}^{IJ}\right] \end{bmatrix}^e \left\{ \begin{array}{c} \{\Delta\} \\ \{\Delta^I\} \\ \{\overline{\Delta}^I\} \end{array} \right\}^e + \begin{bmatrix} [M_{11}] & \left[M_{12}^I\right] & \left[M_{13}^I\right] \\ \left[M_{21}^I\right] & \left[M_{22}^{IJ}\right] & \left[M_{23}^{IJ}\right] \\ \left[M_{31}^I\right] & \left[M_{32}^{IJ}\right] & \left[M_{33}^{IJ}\right] \end{bmatrix}^e \left\{ \begin{array}{c} \{\ddot{\Delta}\} \\ \{\ddot{\Delta}^I\} \\ \{\ddot{\overline{\Delta}}^I\} \end{array} \right\}^e +
$$
$$
+ \begin{bmatrix} [G]^T [N^0] [G] & [0] & [0] \\ [0] & [0] & [0] \\ [0] & [0] & [0] \end{bmatrix}^e \left\{ \begin{array}{c} \{\Delta\} \\ \{\Delta^I\} \\ \{\overline{\Delta}^I\} \end{array} \right\}^e = \left\{ \begin{array}{c} \{F\} \\ \{F^I\} \\ \{\overline{F}^I\} \end{array} \right\}^e \qquad (5.18)
$$

or in the following form:

$$
\left[K^{NL}\right]^e \{d\}^e + \left[K^G\right]^e \{d\}^e + [M]^e \left\{\ddot{d}\right\}^e = \{f\}^e \qquad (5.19)
$$

In Eq. (5.19), $\left[K^{NL}\right]^e$ is the nonlinear element stiffness matrix, $\left[K^G\right]$ is the element geometric stiffness matrix (which describe the initial in-plane forces acting on the second-order strains), $[M]^e$ is the element mass matrix, $\{d\}^e$ is the vector of generalized displacements, $\left\{\ddot{d}\right\}^e$ is the element acceleration vector and finally $\{f\}^e$ is the element force vector.

Element Stiffness Matrix

Submatrices of the stiffness matrix of the single, representative finite element of the laminated composite plate with embedded delaminations are:

$$[K_{11}] = \int\limits_{\Omega^e} \left(\begin{array}{c} [B+B_{NL}]^T \, [A] \, [B+B_{NL}] + \sum\limits_{I=1}^{ND} [B]^T \, [E^I] \, \left[\overline{B}_{NL}^I\right] + \\ \sum\limits_{I=1}^{ND} 2\,[B_{NL}]^T \, [E^I] \, \left[\overline{B}_{NL}^I\right] + \sum\limits_{I=1}^{ND} 2\,\left[\overline{B}_{NL}^I\right]^T [E^I] \, [B+B_{NL}] + \\ + \sum\limits_{I,J=1}^{ND} 2\,\left[\overline{B}_{NL}^I\right]^T \left[F^{IJ}\right] \left[\overline{B}_{NL}^J\right] \end{array} \right) d\Omega^e$$

$$\left[K_{12}^I\right] = \int\limits_{\Omega^e} \left([B+2B_{NL}]^T \, [B^I] \, \left[\overline{B}\right] + \sum\limits_{J=1}^{ND} 2\,\left[\overline{B}_{NL}^J\right]^T \left[L^{IJ}\right] \left[\overline{B}\right] \right) d\Omega^e$$

$$\left[K_{13}^I\right] = \int\limits_{\Omega^e} \left(\begin{array}{c} [B+2B_{NL}]^T \, [E^I] \, [B+B_{NL}] + \sum\limits_{J=1}^{ND} [B]^T \left[F^{IJ}\right] \left[\overline{B}_{NL}^J\right] + \\ + \sum\limits_{J=1}^{ND} 2\,[B_{NL}]^T \left[F^{IJ}\right] \left[\overline{B}_{NL}^J\right] + \sum\limits_{J=1}^{ND} 2\,\left[\overline{B}_{NL}^J\right]^T \left[F^{IJ}\right] [B+B_{NL}] + \\ + \sum\limits_{J,K=1}^{ND} 2\,\left[\overline{B}_{NL}^J\right]^T \left[F^{IJK}\right] \left[\overline{B}_{NL}^K\right] \end{array} \right) d\Omega^e$$

$$\left[K_{21}^I\right] = \int\limits_{\Omega^e} \left(\left[\overline{B}\right]^T \, [B^I] \, [B+B_{NL}] + \sum\limits_{J=1}^{ND} \left[\overline{B}\right]^T \left[L^{JI}\right] \left[\overline{B}_{NL}^J\right] \right) d\Omega^e$$

$$\left[K_{22}^{IJ}\right] = \int\limits_{\Omega^e} \left(\left[\overline{B}\right]^T \left[D^{IJ}\right] \left[\overline{B}\right] \right) d\Omega^e$$

$$\left[K_{23}^{IJ}\right] = \int\limits_{\Omega^e} \left(\left[\overline{B}\right]^T \left[L^{IJ}\right] [B+B_{NL}] + \sum\limits_{K=1}^{ND} \left[\overline{B}\right]^T \left[L^{IJK}\right] \left[\overline{B}_{NL}^K\right] \right) d\Omega^e$$

$$\left[K_{31}^I\right] = \int\limits_{\Omega^e} \left(\begin{array}{c} [B+2B_{NL}]^T \, [E^I] \, [B+B_{NL}] + \sum\limits_{J=1}^{ND} [B]^T \left[F^{IJ}\right] \left[\overline{B}_{NL}^J\right] + \\ \sum\limits_{J=1}^{ND} 2\,[B_{NL}]^T \left[F^{IJ}\right] \left[\overline{B}_{NL}^J\right] + \sum\limits_{J=1}^{ND} 2\,\left[\overline{B}_{NL}^J\right]^T \left[F^{IJ}\right] [B+B_{NL}] + \\ \sum\limits_{J,K=1}^{ND} 2\,\left[\overline{B}_{NL}^J\right]^T \left[F^{IJK}\right] \left[\overline{B}_{NL}^K\right] \end{array} \right) d\Omega^e$$

$$\left[K_{32}^{IJ}\right] = \int\limits_{\Omega^e} \left([B+2B_{NL}]^T \left[L^{JI}\right] \left[\overline{B}\right] + \sum\limits_{K=1}^{ND} 2\,\left[\overline{B}_{NL}^I\right]^T \left[L^{JIK}\right] \left[\overline{B}\right] \right) d\Omega^e$$

$$\left[K_{33}^{IJ}\right] = \int\limits_{\Omega^e} \left(\begin{array}{c} [B+2B_{NL}]^T \left[F^{IJ}\right] [B+B_{NL}] + \sum\limits_{K=1}^{ND} [B]^T \left[F^{IJK}\right] \left[\overline{B}_{NL}^K\right] + \\ \sum\limits_{K=1}^{ND} 2\,[B_{NL}]^T \left[F^{IJK}\right] \left[\overline{B}_{NL}^K\right] + \sum\limits_{K=1}^{ND} 2\,\left[\overline{B}_{NL}^I\right]^T \left[F^{IJK}\right] [B+B_{NL}] + \\ + \sum\limits_{K,L=1}^{ND} 2\,\left[\overline{B}_{NL}^I\right]^T \left[F^{IJKL}\right] \left[\overline{B}_{NL}^L\right] \end{array} \right) d\Omega^e$$

$$(5.20)$$

Element Mass Matrix

Mass matrix of the single, representative FE of the laminated composite plate with embedded delaminations is:

$$
[M]^e = \int\limits_{\Omega^e}
\begin{bmatrix}
I_0 \left[\Psi^T\right][\Psi] & \sum\limits_{I=1}^{N} I^I \left[\overline{\overline{\Psi}}\right]^T [\Psi] & \sum\limits_{I=1}^{ND} \overline{I}^I [\Psi]^T [\Psi] \\[2ex]
\sum\limits_{I=1}^{N} I^I [\Psi]^T \left[\overline{\overline{\Psi}}\right] & \sum\limits_{I,J=1}^{N} I^{IJ} [\Psi]^T [\Psi] & \sum\limits_{I=1}^{N}\sum\limits_{J=1}^{ND} \overline{I}^{IJ} [\Psi]^T \left[\overline{\overline{\Psi}}\right] \\[2ex]
\sum\limits_{I=1}^{ND} \overline{I}^I [\Psi]^T [\Psi] & \sum\limits_{I=1}^{ND}\sum\limits_{J=1}^{N} \overline{I}^{JI} \left[\overline{\overline{\Psi}}\right]^T [\Psi] & \sum\limits_{I,J=1}^{ND} \widetilde{I}^{IJ} [\Psi]^T [\Psi]
\end{bmatrix}
d\Omega^e
$$

$$(5.21)$$

Element Force Vector

Force vector of the single layered finite element of the laminated composite plate with embedded delaminations is:

$$
\{f\}^e =
\left\{
\begin{array}{c}
\{F\} \\[1ex]
\{F^I\} \\[1ex]
\{\overline{F}^I\}
\end{array}
\right\}
=
\left\{
\begin{array}{c}
\int\limits_{\Omega^e} [\Psi]^T [\Psi]\{\mathbf{q}\}\, d\Omega^e + \oint\limits_{\Gamma^e} [\Psi]^T [\Psi]\{\mathbf{t}\}\, d\Gamma^e \\[2ex]
\oint\limits_{\Gamma^e} \left[\overline{\Psi}\right]^T \left[\overline{\Psi}\right]\{\mathbf{t}^I\}\, d\Gamma^e \\[2ex]
\oint\limits_{\Gamma^e} [\Psi]^T [\Psi]\{\overline{\mathbf{t}}^I\}\, d\Gamma^e
\end{array}
\right\}
$$

$$(5.22)$$

5.4 Coordinate Transformations

When solving a structural problem using the conventional finite element method, an accurate representation of irregular domains can be accomplished by the use of refined meshes and irregularly shaped elements. A nonrectangular region cannot be accurately represented using all rectangular elements, so triangular or quadrilateral elements should be used. On the other hand, it is convenient to derive the interpolation functions for a rectangular element, as well as to evaluate integrals over rectangular geometries than over irregular ones. Therefore quadrilateral elements with straight or curved sides are used, but the interpolation functions are generated over the rectangular elements. A coordinate transformation between the coordinates (x, y) in the global coordinate system and the element coordinates (ξ, η)

results in the algebraically complex expressions which cannot be solved analytically. Therefore, the numerical integration is performed to evaluate these expressions.

Numerical integration schemes, such as the *Gauss-Legendre numerical integration*, require the integral to be evaluated on a specific domain or with respect to a specific coordinate system. Gauss-Legendre quadrature requires the integral to be expressed over a square region $\overline{\Omega}$ of dimensions 2×2 and the coordinate system be such that $-1 \leq (\xi, \eta) \leq 1$. The element $\overline{\Omega}$ is called a *master element*.

The transformation between Ω^e and $\overline{\Omega}$ is done using the following coordinate transformation:

$$x = \sum_{i=1}^{m} x_i \overline{\psi}_i(\xi, \eta), \quad y = \sum_{i=1}^{m} y_i \overline{\psi}_i(\xi, \eta) \tag{5.23}$$

while some dependent variable $var(x, y)$ is approximated according to:

$$var(x, y) = \sum_{i=1}^{m} var_i \psi_i(x, y) = \sum_{i=1}^{m} var_i \psi_i \left(x(\xi, \eta), y(\xi, \eta) \right) \tag{5.24}$$

In Eqs. (5.23)-(5.24), $\overline{\psi}_i$ denote the interpolation functions of the master element $\overline{\Omega}$ and ψ_i are the interpolation functions of the typical element Ω^e, m is the number of nodes per element, while (x_i, y_i, var_i) denote the (x, y) coordinates and the value of the variable var of the ith node, respectively. The above transformations exist if the Jacobian of the transformation is a positive-definite. The positive-definite requirement of the Jacobian dictates the admissible geometries of the elements in a finite element mesh. Also, note that in this study a *isoparametric* formulation of the finite elements is used, where equal degree of approximation is used both for the geometry and the dependent variables.

The linear and quadratic Lagrange shape functions of rectangular element are:

$$
\begin{Bmatrix} \psi_1 \\ \psi_2 \\ \psi_3 \\ \psi_4 \end{Bmatrix} = \frac{1}{4} \begin{Bmatrix} (1-\xi)(1-\eta) \\ (1+\xi)(1-\eta) \\ (1+\xi)(1+\eta) \\ (1-\xi)(1+\eta) \end{Bmatrix}, \quad
\begin{Bmatrix} \psi_1 \\ \psi_2 \\ \psi_3 \\ \psi_4 \\ \psi_5 \\ \psi_6 \\ \psi_7 \\ \psi_8 \\ \psi_9 \end{Bmatrix} = \frac{1}{4} \begin{Bmatrix} (\xi-\xi^2)(\eta-\eta^2) \\ (\xi+\xi^2)(\eta^2-\eta) \\ (\xi+\xi^2)(\eta+\eta^2) \\ (\xi^2-\xi)(\eta+\eta^2) \\ 2(1-\xi^2)(\eta^2-\eta) \\ 2(\xi+\xi^2)(1-\eta^2) \\ 2(1-\xi^2)(\eta+\eta^2) \\ 2(\xi^2-\xi)(1-\eta^2) \\ 4(1-\xi^2)(1-\eta^2) \end{Bmatrix} \quad (5.25)
$$

Gauss-Legendre Quadrature

The coefficients of the algebraic equations in the finite element model contain integrals of the physical parameters and the functions used for the approximation of primary variables. These complicated integral expressions are solved numerically. First the integral from Ω^e is transformed to the master element $\overline{\Omega}$. The integrand usually contains not only $\psi_i(x,y)$, but also their derivatives with respect to the global coordinates (x,y). The relations between the derivatives of ψ_i with respect to global coordinates and the derivatives of ψ_i with respect to natural coordinates are derived by the chain rule of partial differentiation:

$$
\begin{Bmatrix} \frac{\partial \psi_i}{\partial \xi} \\ \frac{\partial \psi_i}{\partial \eta} \end{Bmatrix} = \begin{bmatrix} \frac{\partial x}{\partial \xi} & \frac{\partial y}{\partial \xi} \\ \frac{\partial x}{\partial \eta} & \frac{\partial y}{\partial \eta} \end{bmatrix} \begin{Bmatrix} \frac{\partial \psi_i}{\partial x} \\ \frac{\partial \psi_i}{\partial y} \end{Bmatrix} \quad (5.26)
$$

The coefficient matrix in Eq. (5.26) is called the *Jacobian matrix*, while its determinant is called the *Jacobian*, which must be greater than zero in order to invert Eq. (5.26). Inverting the Eq. (5.26) we obtain:

$$
\begin{Bmatrix} \frac{\partial \psi_i}{\partial x} \\ \frac{\partial \psi_i}{\partial y} \end{Bmatrix} = [J]^{-1} \begin{Bmatrix} \frac{\partial \psi_i}{\partial \xi} \\ \frac{\partial \psi_i}{\partial \eta} \end{Bmatrix} \quad (5.27)
$$

This requires the Jacobian matrix [J] to be nonsingular.

While evaluating the integral $\int_{\Omega^e} F(x,y)d\Omega^e$, the element area $d\Omega^e = dxdy$ in element Ω^e is transformed to $d\Omega^e = dxdy = det[J]d\xi d\eta$ in the master element $\overline{\Omega}$.

Table 5.1: Gauss points (ξ_I, η_J) and corresponding weighting factors W_I and W_J of the Gauss-Legendre quadrature

$n \times n$	ξ_I	η_J	W_I	W_J
1×1	$\xi_1 = 0$	$\eta_1 = 0$	$W_1 = 2$	$W_1 = 2$
2×2	$\xi_1 = -1/\sqrt{3}$	$\eta_1 = -1/\sqrt{3}$	$W_1 = 1$	$W_1 = 1$
	$\xi_2 = 1/\sqrt{3}$	$\eta_2 = 1/\sqrt{3}$	$W_2 = 1$	$W_2 = 1$
3×3	$\xi_1 = -\sqrt{3/5}$	$\eta_1 = -\sqrt{3/5}$	$W_1 = 5/9$	$W_1 = 5/9$
	$\xi_2 = 0$	$\eta_2 = 0$	$W_2 = 8/9$	$W_2 = 8/9$
	$\xi_3 = \sqrt{3/5}$	$\eta_3 = \sqrt{3/5}$	$W_3 = 5/9$	$W_3 = 5/9$

Using the Gauss quadrature formula for integrals defined over a rectangular master element $\overline{\Omega}$, we obtain:

$$
\int_{\Omega^e} F(x,y)dxdy = \int_{\overline{\Omega}} F(\xi,\eta)d\xi d\eta = \int_{-1}^{1} \int_{-1}^{1} F(\xi,\eta)d\eta d\xi \det[J] \longrightarrow
$$
$$
\int_{\Omega^e} F(x,y)dxdy \approx \sum_{I=1}^{M} \sum_{J=1}^{N} F_{ij}\left(\xi_I, \eta_J\right) W_I W_J
$$

(5.28)

In Eq. (5.28), M and N denote the number of Gauss quadrature points in the ξ and η directions, (ξ_I, η_J) are the natural coordinates of the Gauss point, while W_I and W_J denote the corresponding Gauss weights (see Table (5.1)).

Shear Locking

Although the layerwise model may be primarily indended for thick plate situations $(a/h < 20)$, it is important to determine the limits of the layerwise model's applicability to thin plate situations $(a/h > 20)$. Generally, finite elements which possess full 3D modeling capability can exhibit spurious transverse shear stiffness, spurious transverse normal stiffness and ill-conditioned stiffness matrices as the span-to-thickness ratio increases (see [8] for details).

The *spurious shear stiffness* phenomenon is caused by the interpolation inconsistency that prevents the finite element from modeling a state of zero transverse shear stress in the presence of general nonzero bending strains. As the plate's span-to-thickness ratio approaches the thin plate limit, the transverse shear deformation

must tend toward zero relative to the bending deformation. The elements which are poor approximators of this condition are known to exhibit shear locking, while elements which are better approximators may exhibit a slight overstiffness. As the span-to-thickness ratio increases, the computed solution tends to suppress the higher-order terms of the interpolation. If a *reduced quadrature* is used to evaluate the terms contributing to the transverse shear energy, then the Kirchhoff's condition will not be enforced as stringently as in the case of the full quadrature [8]. The reduced quadrature is required only when integrating the transverse shear terms with respect to x and y (not the thickness coordinate z), because the transverse interpolation inconsistency is insignificant compared with the in-plane inconsistencies. The problem of the spurious transverse normal stiffness is explained in detail in Ref. [8].

Within this study, element stiffness and mass matrices were evaluated using full integration (3×3 Gauss-Legendre quadrature for 9-node quadrilateral finite element, or 2×2 quadrature for 4-node quadrilateral finite element) and reduced integration (2×2 Gauss-Legendre quadrature for 9-node or 1×1 quadrature for 4-node element).

5.5 Assembly Procedure

After the derivation of the characteristic element matrices, the assembly procedure is done in a usual manner. After the assembly procedure of the characteristic element matrices and vectors, we obtain the mathematical model on the structural level:

$$\left[K^{NL} \right] \{d\} + [M] \left\{ \ddot{d} \right\} = \{f\} \tag{5.29}$$

From the previous equation several structural problems may be considered, using the same restrictions as in the "strong" formulation, see Section 3.7.5:

1. Geometrically Nonlinear Bending Analysis

   $\left[K^L + K^{NL} \right] \{d\} = \{f\},$

2. Linear Bending Analysis

   $\left[K^L \right] \{d\} = \{f\},$

3. Linear Buckling Analysis

   $\left(\left[K^L \right] - \lambda \left[K^G \right] \right) \{d\} = 0,$

4. Linear Free Vibration Analysis

$$\left(\left[K^L \right] - \omega^2 \left[M \right] \right) \{d\} = 0,$$

5. Geometrically Nonlinear Transient Analysis

$$\left[K^L + K^{NL} \right] \{d\} + \left[M \right] \left\{ \ddot{d} \right\} = \{f\},$$

6. Geometrically Linear Transient Analysis

$$\left[K^L \right] \{d\} + \left[M \right] \left\{ \ddot{d} \right\} = \{f\}.$$

5.6 Assignment of Boundary Conditions

The FE model represents the system of algebraic equations, where unknown param-
eters are displacement components (degrees of freedom). To solve this system we
need to assign the appropriate boundary conditions. The natural (displacement)
boundary conditions constrain the nodal displacements, which lead to the unique
solution of the system of governing equations (the matrix of coefficients of gov-
erning equations becomes regular). The displacement boundary conditions can be
homogeneous or *non-homogeneous*.

For the rectangular plate, in general case exist three types of natural boundary
conditions on the plate edges:

1. Simply-Supported Edge (**SS**)

   for $x = 0$ and $x = a$: $v = w = v^I = U^I = V^I = W^I = 0$;

   for $y = 0$ and $y = b$: $u = w = u^I = U^I = V^I = W^I = 0$.

2. Simply-Supported Edge (**NN**)

   for $x = 0$ and $x = a$: $u = v = w = v^I = U^I = V^I = W^I = 0$;

   for $y = 0$ and $y = b$: $u = v = w = u^I = U^I = V^I = W^I = 0$.

3. Clamped Edge (**CC**)

   for $x = 0$ and $x = a$: $u = v = w = u^I = v^I = U^I = V^I = W^I = 0$;

   for $y = 0$ and $y = b$: $u = v = w = u^I = v^I = U^I = V^I = W^I = 0$.

Also, on delamination boundary the following boundary condition are enforced:

1. Delamination Front: $U^I = V^I = W^I = 0$
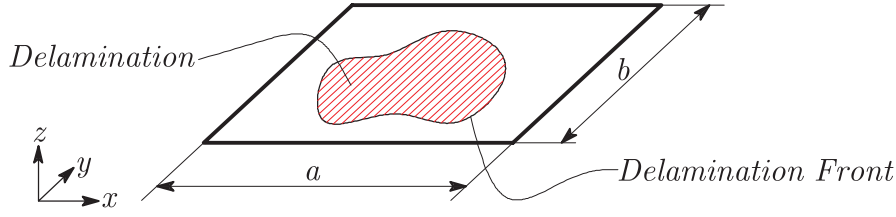
Figure 5.2: Rectangular plate $a \times b$ with delamination

5.7   Solution Procedure for the Time Independent Problems

In the nonlinear formulation based on a GLPT, the geometric nonlinearity in the form of the von Kármán strains is included. For small strains and moderately large deflections and rotations, these assumptions yield good results [8].

The spatial discretization of the problem using finite elements results in a system of ordinary differential equations in time, given in Eq. (5.29). If the time dependency of the problem can be neglected, then the system of nonlinear ordinary differential equations reduces to a system of nonlinear algebraic equations on the structural level:

$$\left[K^{NL}\right]\{d\} = \{f\} \tag{5.30}$$

We note that the nonlinearity of the stiffness matrix $\left[K^{NL}\right]$ is solely due to the transverse deflection w and the Crack Opening Displacements W^I, as can be seen from Eqs. (5.11). The stiffness matrix $\left[K^{NL}\right]$ is not symmetric because:

$$\left[K_{12}^{I,NL}\right] = 2\left[K_{21}^{I,NL}\right], \quad \left[K_{32}^{IJ,NL}\right] = 2\left[K_{23}^{IJ,NL}\right] \tag{5.31}$$

After the assignment of boundary conditions defined in the previous Section, the Eq. (5.30) must be solved using the numerical methods for the solution of nonlinear algebraic equations. Generally, the nonlinear system of equations can be written in the following form [93]:

$$K(d) \cdot d = R(d) = F \quad \longrightarrow \quad R(d, F) = R(d) - \lambda \cdot F = 0 \tag{5.32}$$

where d is the unknown solution for the displacements, $K(d)$ is the known function of d (known from the previous iteration), F is the known force, λ is the loading

parameter, $R(d)$ is the internal force vector and $R(d, F)$ is the unbalanced loading (residuum). The procedures for solving the Eq. (5.31) can generally be divided in two main categories:

1. The *iteration methods*, for finding the equilibrium states for an incremental load change, such as *Picard method* and *Newton-Raphson method*,

2. The *control methods* or *control procedures*, which describe the successive load application, such as *Arc-length method*.

5.7.1   Iteration Methods

In the **Direct Iteration (Picard) Method**, the solution (displacement) vector from the previous iteration is used to evaluate the stiffness matrix, and the solution at the subsequent iteration is determined by solving the assembled equations after the imposition of boundary conditions:

$$\left[K(d^{iter-1})\right]\left\{d^{iter}\right\} = \left\{f^{iter}\right\} \tag{5.33}$$

where $\{d^{iter}\}$ denotes the solution vector from the current iteration, and *iter* is the iteration index. The coefficients K_{ij} are obtained by evaluating the element stiffness matrix coefficients using the solution $\{d^{iter-1}\}$. The solution of the current iteration is obtained by solving:

$$\{d^{iter}\} = \left[K(d^{iter-1})\right]^{-1}\left\{f^{iter}\right\} \tag{5.34}$$

At the beginning of the loading step ($iter = 0$), we assume the homogeneous initial conditions so that the solution at the first iteration is the linear solution ($\left[K^{NL}\right] = 0$). The iteration process is continued until the convergence criterion is satisfied (the error is less than or equal to some prescribed tolerance (say $\varepsilon < 1\%$)):

$$\sqrt{\frac{(d^{iter} - d^{iter-1})^2}{(d^{iter})^2}} < \varepsilon \quad (say 10^{-3}) \tag{5.35}$$

Newton-Raphson method is based on the multi-dimensional Taylor series expansion of the internal forces vector R at a deformation state determined by the structural displacement vector d_{step}^{iter} [100]:

$$R\left(d_{step}^{iter}\right) = R\left(d_{step}^{iter-1}\right) + \frac{\partial R\left(d_{step}^{iter-1}\right)}{\partial d_{step}^{iter-1}}\left(d_{step}^{iter} - d_{step}^{iter-1}\right) + \cdots \tag{5.36}$$

The result of a Taylor series is approximated by the vector of internal forces of the displacements state d_{step}^{iter} in the neighborhood of the point d_{step}^{iter-1}, where index *iter* stands for the *iteration index* in dealing with the iteration procedure, while index *step* denotes the current loading step. To generate the iteration procedure, the Taylor row expansion is truncated after the linear term, and the *displacement increment* can be defined as $\Delta d^{iter} = d_{step}^{iter} - d_{step}^{iter-1}$. The internal force vector can now be re-written as:

$$R(d_{step}^{iter}) = R(d_{step}^{iter-1}) + \frac{\partial R(d_{step}^{iter-1})}{\partial d_{step}^{iter-1}}\Delta d^{iter} = R(d_{step}^{iter-1}) + [K_T](d_{step}^{iter-1})\Delta d^{iter} \tag{5.37}$$

where $[K_T]$ is the *tangent stiffness matrix*. This completes the linearisation of the internal force vector $\Delta R(d_{step}^{iter-1})$. Now the Eq. (5.32) can be re-written as:

$$R(d_{step}^{iter-1}) + [K_T](d_{step}^{iter-1})\Delta d^{iter} = F_{step} \tag{5.38}$$

From the previous equation follows:

$$\Delta d^{iter} = \left[[K_T](d_{step}^{iter-1})\right]^{-1} \cdot \left(F_{step} - R(d_{step}^{iter-1})\right) \tag{5.39}$$

and the displacement vector in the current iteration can be calculated

$$d_{step}^{iter} = d_{step}^{iter-1} + \left[[K_T](d_{step}^{iter-1})\right]^{-1} \cdot \left(F_{step} - R(d_{step}^{iter-1})\right). \tag{5.40}$$

The iteration process is continued until the convergence criterion is satisfied (the error is less than or equal to some prescribed tolerance (say $\varepsilon < 1\%$)):

$$\sqrt{\frac{(d_{step}^{iter} - d_{step}^{iter-1})^2}{(d_{step}^{iter})^2}} < \varepsilon \tag{5.41}$$

To complete the formulation, the internal force vector in the first iteration (*predictor*) is calculated as the converged solution from the previous step:

$$R(d_{step}^{0}) = R(d_{step-1}) \tag{5.42}$$

5.7.2   Control Methods

The application of the iterative methods is not possible when the structure becomes unstable (the stiffness matrix becomes singular), i.e. at the *snap through* points on the load-displacement curve. In this cases, Control Methods such as Arc-Length Controlling Method are used. These methods will not be discussed in this study.

5.8   Solution Procedure for the Time Dependent Problems

When the weak formulation is spatially discretized using the finite elements, a system of ordinary differential equations in time is obtained:

$$\left[K^{NL}\right]\{d\} + [M]\left\{\ddot{d}\right\} = \{f\} \tag{5.43}$$

From the experimental evidence it is known that damping effects occur in the structures undergoing dynamic motion, due to the viscose effects in the material or the internal friction. Then an additional term in the previous equation has to be introduced. It is usually done by introducing the damping matrix $[C]$, which is proportional to mass and stiffness matrices $[C] = \alpha[M] + \beta\left[K^{NL}\right]$ (*Rayleigh damping*).

However, if the structure is loaded with a single pulse, the effect of damping is usually not important, unless the system is highly damped [101]. Maximum response to an impulsive load will be reached in a very short time, before the damping forces can absorb the energy from the structure [102]. Consequently, in further calculations only the undamped structural response will be considered.

The Eq. (5.43) in the time point t_{n+1} should be re-written to obtain the following discretized form of the governing equations system:

$$[M]\left\{\ddot{d}_{n+1}\right\} + \{R\}(d_{n+1}) = \{f_{n+1}\} \tag{5.44}$$

where $\{R\}(d_{n+1})$ is the vector of internal forces in the time point t_{n+1} defined as:

$$\{R\}(d_{n+1}) = \left[K^{NL}\right]\{d_{n+1}\} \tag{5.45}$$

Finally, the initial conditions have to be described. These are the values of the displacements $\{d\}$ and velocities $\{\dot{d}\}$ at time t_0:

$$\{d\}\,(t=0) = \{d_0\}, \quad \{\dot{d}\}\,(t=0) = \{\dot{d}_0\} \tag{5.46}$$

Basically, two options are available for the solution of Eq. (5.44), which are known as *explicit* and *implicit* integration schemes. In the scope of this study, an implicit integration scheme is employed, which replaces the time derivatives by quantities which depend on quantities from the last time step in time t_n as well as from the still unknown quantities at time $t_{n+\alpha}$. This requires the solution of a nonlinear algebraic system at every time step - the implicit methods have to be combined with the iterative methods described in the Section 5.8. The advantage of implicit methods is that they can be constructed such that they are unconditionally stable (see [8, 36, 98, 101–103] and references herein).

In the implementation of the proposed plate model the Newmark's method [98] is used, in which accelerations and velocities are approximated using truncated Taylors series. The governing differential equations of the system are then satisfied in discrete time points t_{n+1}. Displacements and velocities at time t_{n+1} are approximated as:

$$\begin{aligned}
\{d_{n+1}\} &= \{d_n\} + \Delta t\{\dot{d}_n\} + \tfrac{\Delta t^2}{2}\left[(1-2\beta)\{\ddot{d}_n\} + 2\beta\{\ddot{d}_{n+1}\}\right], \\
\{\dot{d}_{n+1}\} &= \{\dot{d}_n\} + \Delta t\left[(1-\gamma)\{\ddot{d}_n\} + \gamma\{\ddot{d}_{n+1}\}\right]
\end{aligned} \tag{5.47}$$

In Eqs. (5.47), β and γ are constants which determine the behavior of the integration method, and they are chosen as $\beta = \gamma = 0.5$ because of the proven mathematical stability. Then the Eqs. (5.47) become:

$$\begin{aligned}
\{d_{n+1}\} &= \{d_n\} + \Delta t\{\dot{d}_n\} + \tfrac{\Delta t^2}{2}\{\ddot{d}_{n+1}\}, \\
\{\dot{d}_{n+1}\} &= \{\dot{d}_n\} + \tfrac{\Delta t}{2}\left[\{\ddot{d}_n\} + \{\ddot{d}_{n+1}\}\right]
\end{aligned} \tag{5.48}$$

The Eqs. (5.48) are re-written in the following form:

$$\begin{aligned}
\{\ddot{d}_{n+1}\} &= \tfrac{2}{\Delta t^2}\left(\{d_{n+1}\} - \{d_n\}\right) - \tfrac{2}{\Delta t}\{\dot{d}_n\}, \\
\{\dot{d}_{n+1}\} &= \tfrac{1}{\Delta t}\left(\{d_{n+1}\} - \{d_n\}\right) + \tfrac{\Delta t}{2}\{\ddot{d}_n\}
\end{aligned} \tag{5.49}$$

By incorporation of the approximations for $\{\ddot{d}_{n+1}\}$ and $\{\dot{d}_{n+1}\}$ in Eq. (5.43), we

obtain the following:

$$[M]\left[\frac{2}{\Delta t^2}\left(\{d_{n+1}\}-\{d_n\}\right)-\frac{2}{\Delta t}\{\dot{d}_n\}\right]+\left[K^{NL}\right]\{d_{n+1}\}-\{f_{n+1}\}=0 \quad \longrightarrow$$

$$\left[[M]\frac{2}{\Delta t^2}+\left[K^{NL}\right]\right]\{d_{n+1}\}=\{f_{n+1}\}+[M]\left[\frac{2}{\Delta t}\{\dot{d}_n\}+\frac{2}{\Delta t^2}\{d_n\}\right]$$

$$(5.50)$$

The Eq. (5.50) represents a system of algebraic equations at t_{n+1}, in terms of known values at t_n. In this study, homogeneous initial conditions are prescribed. Because $\left[K^{NL}\right]$ depends on the unknown solution $\{d_{n+1}\}$, the assembled equation must be solved iteratively until the convergence criterion is satisfied (the error is less than or equal to some prescribed tolerance (say $\varepsilon < 1\%$)).

5.9 Post Processing of Interlaminar Stresses

As previously shown in Chapter 4, the interlaminar stresses in the GLPT can be calculated using the constitutive equations (3.16) from the previously derived displacement field, as shown in [9, 93]. The definition of $\Phi^I(z)$ leads to the discontinuity of in-plane stresses at layer interfaces, while the transverse shear stresses are approximated as constant within each material layer. For the approximate solution for transverse shear stresses, the algorithm presented in [20, 74, 93] can be used, which use the previously derived in-plane stress information from the finite element solution to provide the approximation of transverse shear stresses.

6 Contact Algorithm

This chapter explains the node-to-node nonlinear frictionless contact algorithm which prevent the layer overlapping in the delaminated zone of the composite plate, during its motion in transient loading environment. The contact condition is iteratively enforced in every solution step, until the convergence criterion is satisfied. After the global equilibrium in the current step is satisfied, the next time step is computed where the contact status is again checked. The advantage of the proposed method is that it can be implemented easily into the geometrically nonlinear transient analysis algorithm. The efficiency of the contact algorithm is illustrated in Chapter 10.4, while the part of the results is already published by author in [94, 104, 105].

Obviously, during the transient response of laminated composite or sandwich plates with delamination, a small gap maybe formed between the adjacent layers in delaminated zones of the plate. After that, the separated layers may unload and again contact each other at that delaminated interface. This phenomenon is referred to as "breathing" of a delamination (see [69, 70] for details).

In this study, the node-to-node nonlinear frictionless contact algorithm is enforced, as illustrated in Figure 6.1. For the sake of simplicity, the algorithm will be illustrated using the example of a restrained simply-supported beam under transient forces $F(t)$ as shown in Figure 6.1. In the first iteration (predictor phase), the displacement field is calculated without any contact restraints, from:

$$[M_{uu}]\{\ddot{d}_u\} + [K_{uu}]\{d_u\} = \{F_u\}, \qquad (6.1)$$

where $[M_{uu}]$ and $[K_{uu}]$ are the system mass and stiffness matrices, respectively, while $\{\ddot{d}_u\}$ is the acceleration vector. $\{d_u\}$ is the displacement vector and $\{F_u\}$ is the vector of external transient loadings, where the subscript u refers to the

unknown displacement components. In the contact detection algorithm all nodes with the overlap are detected and the gap is computed and stored in a vector $\{d_c\}$ (the subscript c refers to the *contact nodes*). At the respective set of contact nodes the negative values of the gap are assigned as the prescribed displacements and computed as transient forces $F_c(t)$, as shown in Figure 6.1. The extended governing equations of the system are then obtained in the format:

$$[M_{uu}]\{\ddot{d}_u\} + [K_{uu}]\{d_u\} - [K_{uk}]\{d_k\} = \{F_u\}$$
$$[M_{uu}]\{\ddot{d}_u\} + [K_{uu}]\{d_u\} = \{F_u\} + \{F_{c,u}\}$$

(6.2)

where the subscript k refers to the *known displacement components.*
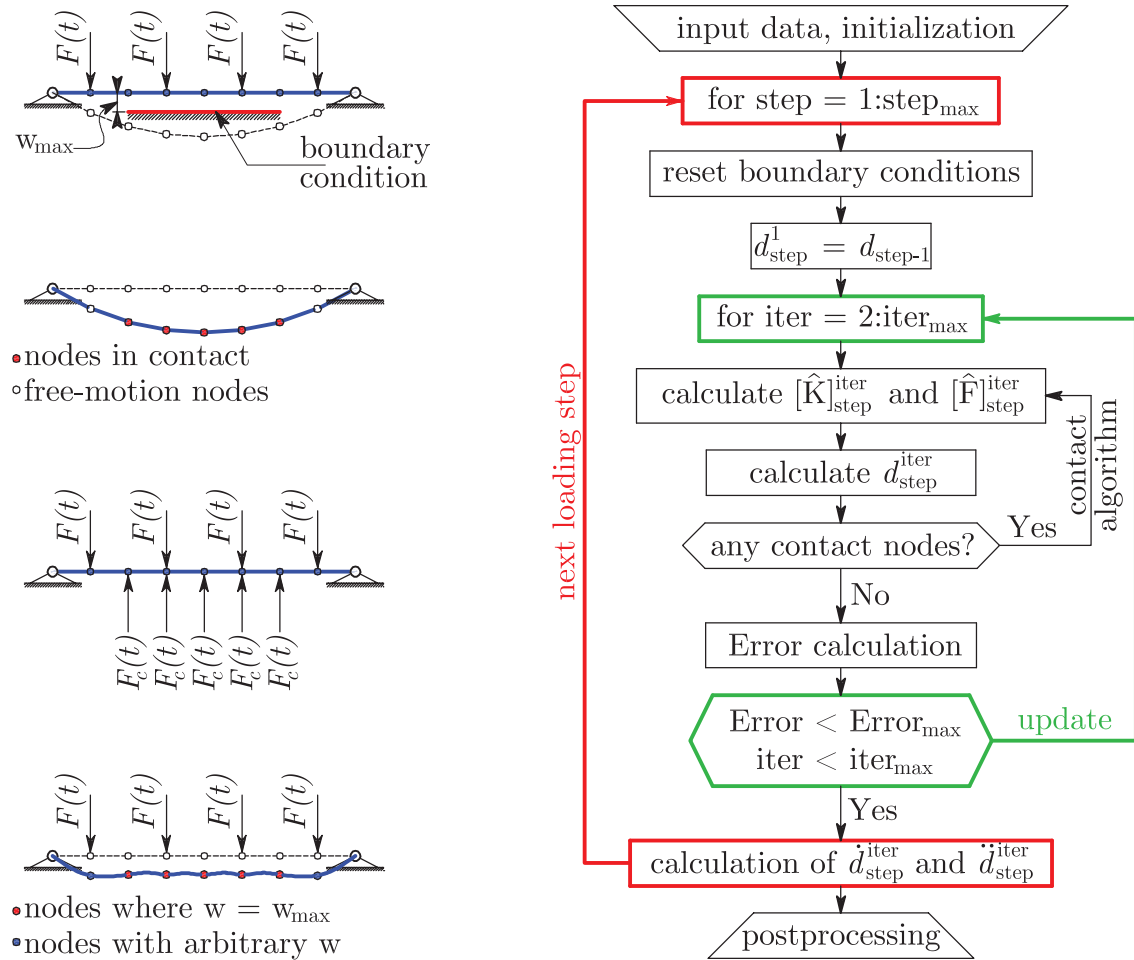
Figure 6.1: Contact algorithm to prevent overlapping in delaminated interfaces (left) and the flowchart of the program (right)

Eq. (6.2) replaces Eq. 6.1 if any overlapping occurs. The contact condition is iteratively enforced until the convergence criterion is satisfied (the error is less than

or equal to some prescribed tolerance (say $\varepsilon < 1\%$). After the iterative enforcement of the contact condition and the global equilibrium in the current step is satisfied, the next time step is computed, where the contact status is again checked. The advantage of the proposed method is that it can be implemented easily into the geometrically nonlinear transient analysis algorithm explained in this study. Figure 6.1 illustrates the flowchart of the program.

The efficiency of the contact algorithm will be illustrated in Example 10.4.1., which purpose is only to highlight the difference between the behavior of delaminated adjacent interfaces with and without the implementation of the contact algorithm. The parametric study of the influence of delamination position and size will be further discussed in several examples in Section 10.4.

7 Delamination Propagation

In this chapter, the method for tracking the moving delamination front is presented as the extension of the algorithm proposed by Xie et al. [106, 107] which was restricted to the structured FE meshes. The displacement field obtained from finite element calculation is used for the computation of three components G_i of the Strain Energy Release Rate along the delamination front, using the Virtual Crack Closure Technique, which requires the calculation of the delamination opening behind the crack front, the nodal forces along the front and the virtually closed area in front of the existing delamination. To predict the delamination growth the calculated G_i components are compared with the interlaminar fracture toughness. The direction in which delamination will grow is described by the vector normal to the delamination front, which components are accurately calculated in this study unlike the majority of the models from the literature. The virtually closed area is determined using 6 control points for every node along the delamination front. After that, the forces along the delamination front, as well as the delamination openings behind the front, are computed. The G_i components are approximated as the product of the calculated forces and the delamination openings, in the region of the virtually closed area. A mixed-mode fracture criterion is applied next in all considered nodes. The algorithm is repeated until there are no more propagating nodes in the current step of the analysis. Subsequently, the analysis continues with the next time or loading increment. Some basics of the proposed algorithm are published by author in [108].

7.1 Introduction

To predict the delamination growth, the Strain Energy Release Rate distribution along the delamination front must be derived first. The total Strain Energy Release

Rate (G) is divided into three components G_I, G_{II} and G_{III}, depending on the fracture mode (see Figure 7.1). In order to predict delamination growth, the calculated G_i components are compared with the interlaminar fracture toughness, which is a material property obtained experimentally. For simple examples such as the Double-Cantilever-Beam (DCB) problem, some components of the Strain Energy Release Rates can be also calculated analytically [109–113]).
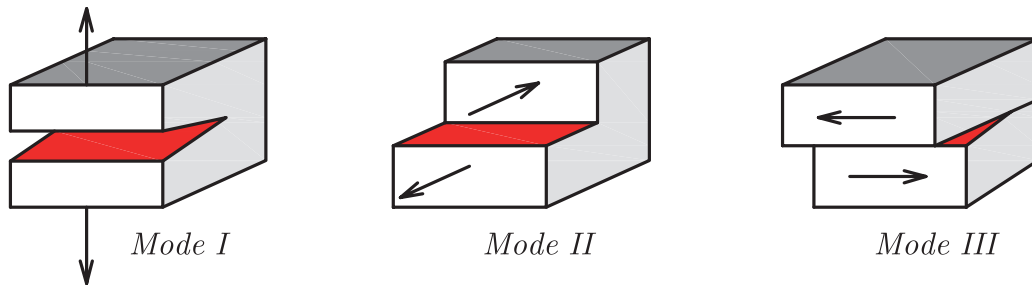
Figure 7.1: Different modes of delamination

For the modeling of delamination growth in laminated structures a number of computational strategies exist (see [114] and references therein). The Virtual Crack Closing Technique (VCCT) is an approximate method which is derived from the more fundamental Crack Closure Technique (CCT), assuming that the strain energy released during the delamination growth is equal to the work required to close the crack to its original length [115]. The VCCT approach was originally proposed by Rybicki and Kanninen [17] and was extended to 3D analysis by Shivakumar et al. [116]. For an overview of the history and applications of the VCCT we refer [117] among other references. The VCCT approach is advantageous because only a single FE solution step is used for the derivation of the G_i components. In [118] it is shown that the distributions of the Strain Energy Release Rate along the delamination front calculated using the CCT and VCCT are similar . This method is used in [13, 106, 107, 111, 115, 119–124].

In the non-linear spring approach the 1D interface element between upper and lower nodes in the delaminated zone is defined as a spring with a very small stiffness in tension and a high stiffness in compression to prevent the interlaminar penetration of the adjacent layers [125, 126]. These elements are usually combined with the

VCCT, because the forces in the nodes on the delamination front can be easily extracted [114]. Using this approach, a node-to-node discontinuous propagation can be modeled.

In the cohesive zone model, zero thickness interface elements are placed between solid composite layers in the delaminated zone [113, 114, 117, 127–129]. A softening interface law is generally adopted, characterized by an initial high positive stiffness until a critical stress level is reached, followed by a negative tangent stiffness representing the gradual loss of bonding strength between the laminae. To place an interface element between adjacent "layers" in the plate/shell formulation, the additional degrees of freedom are needed to describe the relative displacements between the upper and lower portions of the composite laminate in the delaminated zone, which can be achieved using the GLP Theory. Tenchev and Falzon [112] provide an extensive overview of cohesive interface elements, while numerical aspects are elaborated in [130].

The method for tracking of the moving delamination front which is proposed in this study is the extension of the previously proposed algorithm by Xie et al. [106, 107] that was used by Hosseini et al. in [122–124]. The previous algorithm was restricted to structured FE meshes, with maximum of four elements connected to the considered node. Although the previously proposed method covers the majority of typical structural applications, in this study it is extended to the unstructured meshes of 4- and 9-node quadrilateral elements. The algorithm has been implemented in the previously derived MATLAB code for the transient analysis of damaged composite plates, using a layered finite element model.

7.2   Assumptions

In this study, the displacement field obtained in the finite element calculation is used for the computation of three modes of the Strain Energy Release Rate along the crack front using the Virtual Crack Closure Technique. The VCCT requires the calculation of the delamination opening behind the crack front, the nodal forces in the nodes at the front and the virtually closed area in front of the existing delamination. The

delamination front is the curve in the delamination plane, along which essential boundary conditions $U^I = V^I = W^I = 0$ are enforced. The algorithm presented here is based on the following assumptions:

1. The energy released during the delamination extension from $(A + \Delta A)$ to $(A + 2\Delta A)$ is identically equal to the energy required to close the delamination of the same area ΔA.

2. The forces required to close the crack are identical to the forces acting on the upper and lower surfaces of the closed crack. In the GLPT, these are the forces to hold the delaminated nodes together in the delaminated area [129] and these forces correspond with the displacements U^I, V^I and W^I.

3. The specified crack extension does not change the stress and displacement state at the crack tip significantly. The displacements behind the crack tip at the observed node are approximately equal to the displacements behind the original crack tip.

4. There exists the previously imposed delamination area between two layers of the laminated composite plate. Because the displacement-based FE model is used it is convenient to impose the delaminated area by selecting the nodes in which the prescribed structural debonding exist (see Figure 7.2, left).

The post-processing algorithm presented in this study for the detection of the delamination front, calculation of G_i components, and the prediction of the delamination growth should be applied in all nodes of the finite element model after the each calculation step. The procedure is repeated for all delamination zones in the plate. For the sake of simplicity, the procedure is explained here only for a single embedded delamination zone.

7.3 Detection of Delamination Front

To start, the algorithm detects all nodes in which the essential condition $U^I = V^I = W^I = 0$ is satisfied. This is performed by checking the vicinity of each a

priori imposed delaminated node (red dots in Figure 7.2, left). The detected nodes are intact nodes defining the undamaged area of the plate. Nodes dividing the undamaged from the delaminated plate area are the nodes which define the node-to-node delamination front (blue dots in Figure 7.2, center). The delaminated zone is encapsulated by the polygonal line connecting the nodes along the delamination front (blue line in Figure 7.2, center). Finally, the shape of the delamination front is slightly corrected by excluding the nodes from the front for which the virtually closed area will become small (close to zero), according to Figures 7.6 and 7.7. The status of these nodes is changed to delaminated and a new polygonal line to represent the delamination front is generated (see Figure 7.2, right) and used in further calculations.
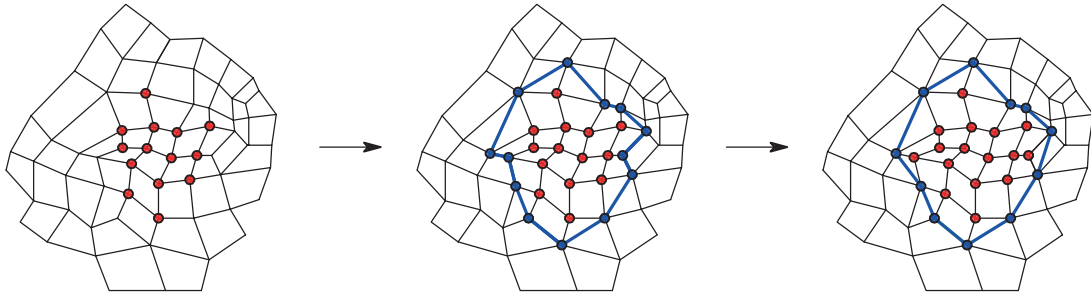
Figure 7.2: Detection of the delamination front (blue line) according to the debonded nodes (red circles)

7.4 Calculation of Two Direction Vectors and the Local Coordinate System

In the majority of the previously proposed models [111, 114, 115, 129], the orientation of the normal vector which defines the direction in which delamination will grow is assumed a priori. For example, in [129], a variety of crack front patterns and the delamination growth areas for different combinations of bonded and delaminated nodes in the vicinity of the node on the delamination front are listed. This approach is convenient when the delamination front is of regular shape and when the finite element mesh is structured.

However, for embedded delaminations of arbitrary shape (which generally occur in structural applications), the orientation of the normal vector is also arbitrary. The delamination front in node N is defined by two vectors pointing away from point N to two adjacent points on the delamination front. These vectors divide the bonded nodes from the debonded ones, and they are denoted as $\overrightarrow{v_1}$ and $\overrightarrow{v_2}$, respectively. After checking of the status of the nodes in the vicinity of the node N (i.e. the nodes belonging to the element which contain the node N), the proposed algorithm detects the adjacent nodes on the delamination front, which are denoted as A_1 and A_2. Figure 7.3 illustrates the situation for a 4-node and 9-node element (red nodes are delaminated, while the yellow nodes are intact).
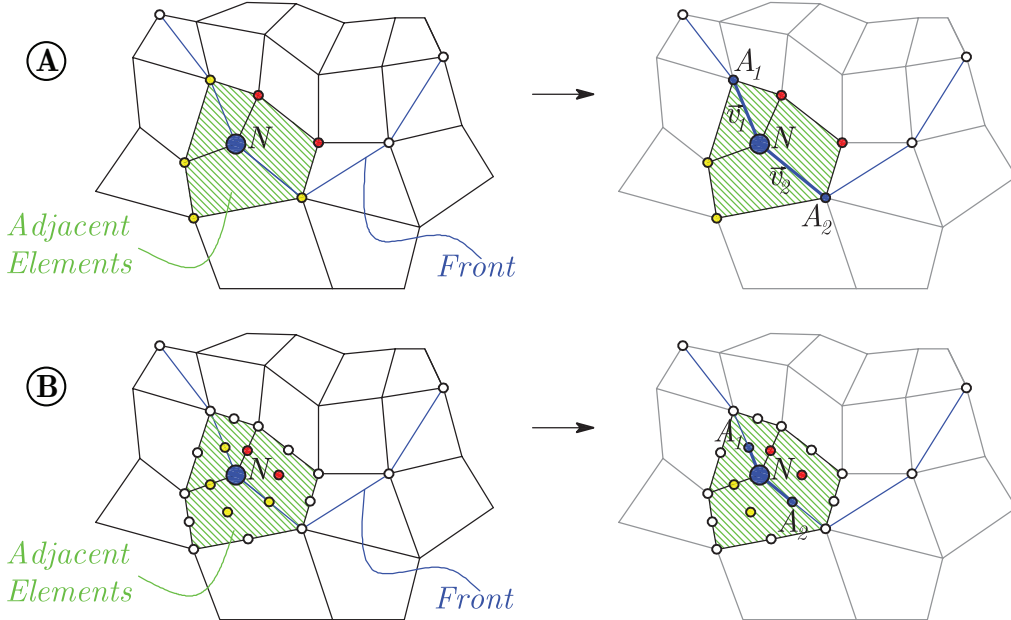
Figure 7.3: Calculation of auxiliary vectors $\overrightarrow{v_1}$ and $\overrightarrow{v_2}$ to describe the direction of the delamination propagation

After the derivation of the vectors $\overrightarrow{v_1}$ and $\overrightarrow{v_2}$, the vector that is normal to the delamination front at node N is calculated as a unit vector laying on the symetral of the angle defined by $\overrightarrow{v_1}$ and $\overrightarrow{v_2}$. After the derivation of the normal vector $\overrightarrow{n}$, its corresponding *tangent vector* $\overrightarrow{t}$ is defined from the vector $\overrightarrow{n} = n_x \overrightarrow{i} + n_y \overrightarrow{j}$ as:

$$\overrightarrow{t} = -n_y \overrightarrow{i} + n_x \overrightarrow{j} \tag{7.1}$$
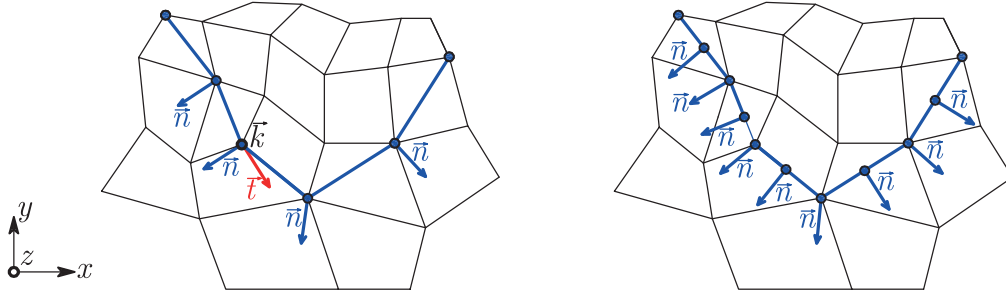
Figure 7.4: Normal vectors determined at the nodes along the delamination front and the local coordinate system defined by $\vec{n}$ and $\vec{t}$ (left: 4-node, right: 9-node element)

The vector $\vec{k}$ is the vector perpendicular to the delamination plane. Three unit vectors ($\vec{n}$, $\vec{t}$, $\vec{k}$) form a base of the local coordinate system, in which all G_i components will be calculated.

7.5   Determination of the Virtually Closed Area

To determine G_I, G_{II} and G_{III} the virtually closed area needs to be calculated. It is defined using 6 control points for every node N along the delamination front. The first three control points are known after the calculation of the vectors $\vec{v_1}$ and $\vec{v_2}$. The point P_1 coincides with the node N, while the points P_2 and P_3 are the mid-points of the segments $N - A_1$ and $N - A_2$, respectively.

The control points P_4 and P_5 are derived based on the status of the nodes in the vicinity of node N. To find these two points, first we find the finite elements corresponding to the vectors $\vec{v_1}$ and $\vec{v_2}$ (denoted as Elements 1 and Elements 2). If the delamination front crosses through the adjacent element, the control point P_4 (or P_5) is the only intact node from the current element. On the other hand, if the delamination front is located on the boundary between two elements, the control point P_4 (or P_5) is is located in the middle of the current element. Respective examples are illustrated in the Figure 7.5 for a 4-node element. An analogous procedure is performed for the 9-node element.

Finally, to find the point P_6, first we calculate the location of the points P_{6a}
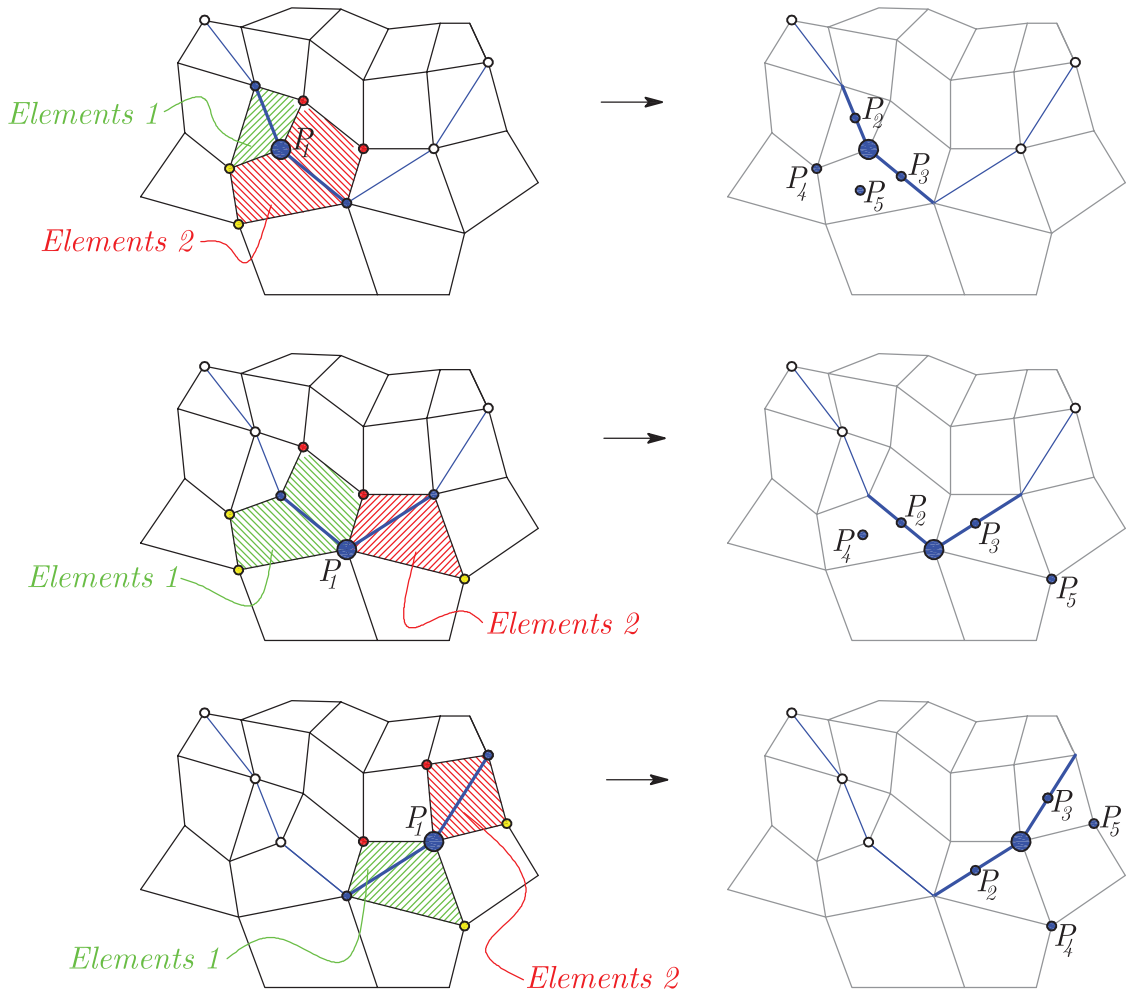
Figure 7.5: Detection of control points P_4 and P_5 considering different nodes on delamination front, for 4-node elements (red color: delaminated nodes, yellow color: intact nodes)

and P_{6b} (see Figure 7.6). The point P_{6a} is the intersection point of the direction of the normal vector $\overrightarrow{n}$ and the line parallel to $\overrightarrow{v_1}$ through the point P_4. On the other hand, the point P_{6b} is the intersection point of the direction of $\overrightarrow{n}$, and the line parallel to $\overrightarrow{v_2}$ through P_5. The point P_6 is the midpoint of the line $P_{6a} - P_{6b}$. The point P_0 is on the direction of vector $\overrightarrow{n}$, anti-symmetric to the point P_6 about node N. This point is also essential because the delamination openings behind the crack front are calculated in P_0.

After the six control points $P_1 - P_6$ are determined, the virtually closed area
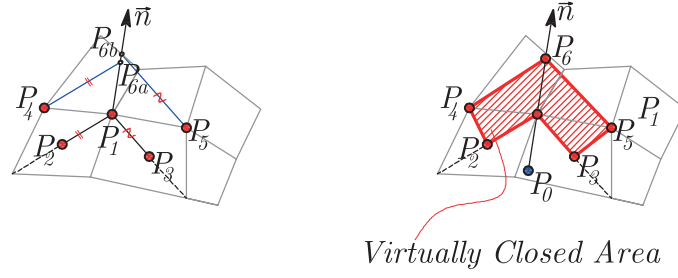
Figure 7.6: Calculation of locations of the control points P_{6a} and P_{6b} based on the previously derived control points P_1-P_5 (left) and the virtually closed area with the point P_0 (right)

is calculated using the MATLAB® function. Note that an overlap of the virtually closed areas corresponding to the adjacent nodes on the delamination front is a priori prevented (see Figure 7.7, left).

7.6 Calculation of Forces and Opening Displacements

After the the virtually closed area is determined one needs to compute the forces $\overline{Q}_x^I$, $\overline{Q}_y^I$ and $\overline{Q}_z^I$ (which correspond to the displacements U^I, V^I and W^I) in the nodes on the crack front, as well as the delamination openings behind the crack front. The forces and the displacements are calculated in the global coordinate system.

The reaction force $\overline{Q}_z^I$ corresponding to the delamination opening W^I can be used directly because the global z-axis coincides with the vector $\overrightarrow{k}$ in the local coordinate system. However, the in-plane reaction forces $\overline{Q}_x^I$ and $\overline{Q}_y^I$ must be transformed into the local coordinate system $(\overrightarrow{n}, \overrightarrow{t}, \overrightarrow{k})$ to reflect the true crack opening mechanisms according to

$$
\begin{aligned}
Q_x &= n_x \overline{Q}_x^I + n_y \overline{Q}_y^I, \\
Q_y &= n_y \overline{Q}_x^I - n_x \overline{Q}_y^I.
\end{aligned}
\tag{7.2}
$$

The delamination openings behind the crack front are calculated in the point P_0, which is anti-symmetric to the point P_6 with respect to the node N. When the point P_0 is defined (see Figure 7.6), the required jump displacement components are

evaluated from the nodal values of the finite element in which the point P_0 is located. For the calculation of G_I, the crack opening displacement W^I can be used directly. In-plane delamination openings must be transformed to the local coordinate system $(\overrightarrow{n}, \overrightarrow{t}, \overrightarrow{k})$ to calculate G_{II} and G_{III}:

$$
\begin{aligned}
\Delta u &= n_x U^I + n_y V^I \\
\Delta v &= n_y U^I - n_x V^I
\end{aligned}
\tag{7.3}
$$

7.7 Calculation of Strain Energy Release Rate Components and Application of the Fracture Mechanics Criteria

The three components of the strain energy release rate G_I, G_{II} and G_{III} are approximated as the product of the nodal forces at node N and the delamination openings at point P_0 in the region of the virtually closed area A:

$$
G_I \approx \frac{1}{2A} Q_z W^I, \quad G_{II} \approx \frac{1}{2A} Q_x \Delta u, \quad G_{III} \approx \frac{1}{2A} Q_y \Delta v
\tag{7.4}
$$

Once the G_i components are calculated, a mixed-mode fracture criterion for delamination propagation is applied:

$$
E_d = \frac{G_I}{G_{Ic}} + \frac{G_{II}}{G_{IIc}} + \frac{G_{III}}{G_{IIIc}} \geq 1
\tag{7.5}
$$

G_{Ic}, G_{IIc} and G_{IIIc} are the critical values of the strain energy release rate corresponding to Mode I, Mode II and Mode III fracture, respectively. They are assumed to be constant during the delamination growth and their derivation is not in a scope of this study. If the criterion (7.5) is satisfied, the status of the considered node on the delamination front is changed. The node in which the criterion is satisfied is referred as a *propagating node* (green color in Figure 7.7, right). After moving to the next calculation step, the new front is set and the calculation of the G_i components in all nodes along the delamination front is repeated for the same level of loading.

Next, the method to advance the delamination front once the propagating nodes are identified is discussed. As mentioned before, in this study the propagating
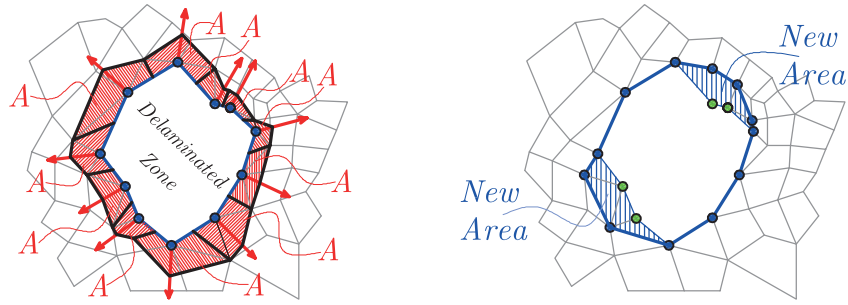
Figure 7.7: Non-overlapping virtually closed areas along the delamination front (left) and the generation of new delaminated zones after the propagating nodes are identified (right)

nodes are only those in which the criterion (7.5) is satisfied. However, the previous investigations [131] showed that this approach may be quite conservative due to the fact that the assumption of the similarity of the crack before and after the propagation is violated.

In addition to the previously described method, Orifici et al. [129] consider another two node-to-node propagation mechanisms. If any of the nodes on the delamination front is released, either all nodes on the front are released subsequently, irrespective of whether or not these nodes had also failed (option 1), or only two adjacent nodes on the delamination front are released (option 2). They force crack growth of the nodes in which the fracture criterion from Eq. (7.5) is not satisfied, which underestimates the fracture toughness G_{ic} of the material. These mechanisms can significantly accelerate the solution process leading to a smaller number of nodes to be checked, but they do not represent the real state at the crack tip. On the other hand, they more or less provide the self-similar crack growth which is one of the assumptions of the VCCT.

In this study, option 2 is adopted as soon as the delamination front reaches the plate boundary (see Figure 7.8, center). If any node on the delamination front, which is also in the vicinity of the boundary node, is released (see green node in Figure 7.8, center), the boundary node is also released (Figure 7.8, right). As previously mentioned, debonding of the boundary nodes is only possible for free (F) plate boundaries, without the possibility to change the previously prescribed essential

boundary conditions along Γ_u (e.g. along clamped (C) boundaries).

The algorithm is repeated until there are no more propagating nodes in the current step of the analysis. Subsequently, the analysis continues with the next time or loading increment.
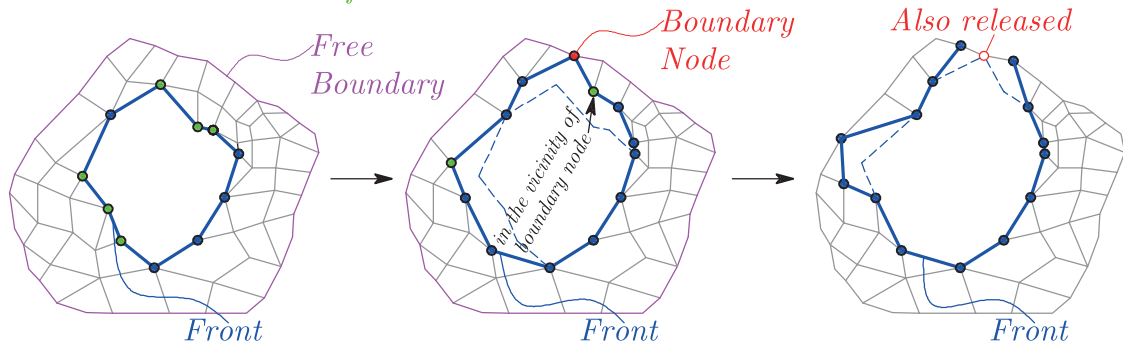
Figure 7.8: Debonding mechanism of the boundary nodes (left: delamination front with the new debonding nodes, center: creation of the new delamination front which reached the plate boundary, right: additional release of the boundary node)

The algorithm is looped until there are no more propagating nodes in the current calculation step. After that, depending on the analysis type, the loading is increased to the next solution step (bending), or the calculation is forwarded to the next time step (transient analysis).

8 Analysis of Laminated Composite Shells

In this chapter the possibility to represent the continuously curved shell surfaces using the assembly of small flat triangular finite elements is presented. The same assumptions as used in the analysis of plates (regarding the transverse distribution of strains and stresses) are valid in the consideration of shells. Some properties of the vector algebra are used for the transformation of the coordinates and characteristic element matrices. The shape functions of a triangular element are formulated in the natural coordinate system (on a master or unit triangle) of the local element plane. However, in the proposed formulation the difficulty arises if all the elements meeting in a node are co-planar. This situation will arise for shallow shell structures, flat (folded) shell segments and at straight boundaries of developable surfaces. The proposed model is applied in the free vibration analysis of laminated composite shells (see examples in Section 10.5). The part of the presented results is already published by Marjanović and Vuksanović in [132, 133].

8.1 Introduction

A shell is generally a structure that can be derived from a plate by initially forming the middle surface as a doubly (spherical) or singly (cylindrical) curved surface. The same assumptions as used in thin plates regarding the transverse distribution of strains and stresses are valid in the consideration of the shells. However, the way in which the shell supports the external loads is quite different from that of a plate, because the stress resultants acting in the middle surface of the shell have both tangential and normal components.

The classical derivation of governing equations for the curved shells will not be discussed in this study, and the reader is referred to the monographs of Timoshenko and Woinowsky-Krieger [134] and Reddy [135]. A different ways for the formulation of curved shell elements arised so far and they are presented in Refs. [136–140]. As shown in these works, the shallow shell elements are slightly more efficient than the flat ones because of the coupling of the effects of membrane and bending strain (also stated in the monograph of Zienkiewicz and Taylor [99]).

However, in this study it is assumed that the behavior of a continuously curved surface can be more or less accurately represented using the assembly of small flat (plate) elements. Although the author is aware that this is not the perfect idealization of the shell structure, the main motivation is the ease of the extension of the previously derived rotation-free layered plate element for the analysis of laminated composite shells.

Laminated composite shells of constant height, composed of n orthotropic laminas, are considered. The global coordinate system is a Cartesian coordinate system, denoted as xyz. In the treatment of shells, it is convenient to introduce the local coordinate system of a single FE. This coordinate system is denoted as $\overline{xyz}$, and it defines the "reference plane" in which all characteristic element matrices and vectors will be derived before the assembly.

The fiber direction of each lamina coincides with the local $\overline{x}$-axis of material coordinates. The overall shell thickness is denoted as h, while the thickness of the kth lamina is denoted as h_k (see Figure 8.1).
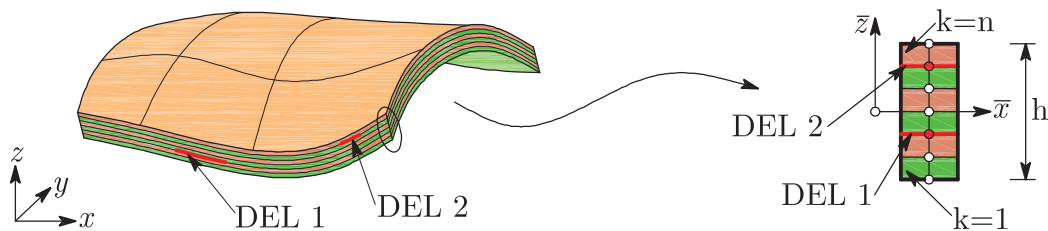
Figure 8.1: Laminated composite shell with embedded delaminations

8.2 The Geometry of Triangular Finite Element

Each finite element has an orientation in which the angles with the coordinate planes are arbitrary. To deal with this problem, some properties of the vector algebra are used. The local axis directions are specified that the $\bar{x}$-axis is directed along the side $1 - 2$ of the triangle, as shown in Figure 8.2.
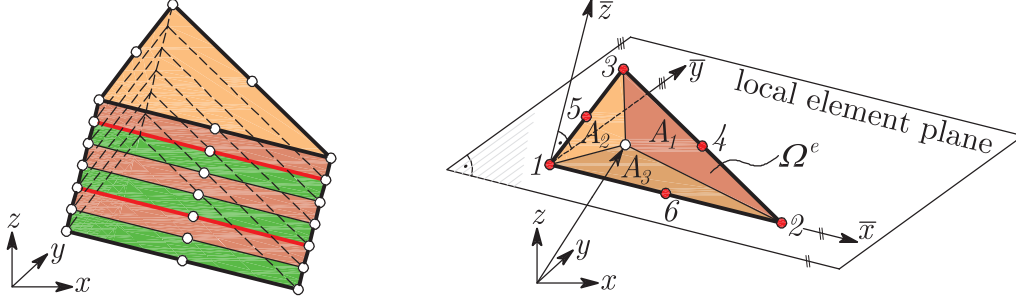
Figure 8.2: Triangular layered element for the modeling of composite shells

The vector $\mathbf{V}_{21}$ defines the element side $1 - 2$, which is in the global coordinates:

$$\mathbf{V}_{21} = \left\{ \begin{array}{c} x_2 - x_1 \\ y_2 - y_1 \\ z_2 - z_1 \end{array} \right\} = \left\{ \begin{array}{c} x_{21} \\ y_{21} \\ z_{21} \end{array} \right\} \tag{8.1}$$

The direction cosines are given as:

$$\mathbf{v}_{\bar{x}} = \left\{ \begin{array}{c} \Lambda_{\bar{x}x} \\ \Lambda_{\bar{x}y} \\ \Lambda_{\bar{x}z} \end{array} \right\} = \frac{1}{l_{21}} \left\{ \begin{array}{c} x_{21} \\ y_{21} \\ z_{21} \end{array} \right\}, \tag{8.2}$$

where $l_{21} = \sqrt{x_{21}^2 + y_{21}^2 + z_{21}^2}$.

The $\bar{z}$ direction is normal to the local element plane (see Figure 8.2), and it is obtained by the vector cross product of two sides of the triangle:

$$\mathbf{V}_{\bar{z}} = \mathbf{V}_{21} \times \mathbf{V}_{31} = \left\{ \begin{array}{c} y_{21}z_{31} - z_{21}y_{31} \\ z_{21}x_{31} - x_{21}z_{31} \\ x_{21}y_{31} - y_{21}x_{31} \end{array} \right\} = \left\{ \begin{array}{c} yz_{123} \\ zx_{123} \\ xy_{123} \end{array} \right\}, \tag{8.3}$$

where $\mathbf{V}_{\bar{z}}$ represents a vector normal to the element plane, whose length is $l_z = 2\Delta = \sqrt{(yz_{123})^2 + (zx_{123})^2 + (xy_{123})^2}$, as given in [99]. The direction cosines of the

$\overline{z}$-axis are:

$$\mathbf{v}_{\overline{z}} = \left\{ \begin{array}{c} \Lambda_{\overline{z}x} \\ \Lambda_{\overline{z}y} \\ \Lambda_{\overline{z}z} \end{array} \right\} = \frac{1}{2\Delta} \left\{ \begin{array}{c} y_{21}z_{31} - z_{21}y_{31} \\ z_{21}x_{31} - x_{21}z_{31} \\ x_{21}y_{31} - y_{21}x_{31} \end{array} \right\} \tag{8.4}$$

The direction cosines of the $\overline{y}$-axis are established as the direction cosines of a vector normal both to the $\overline{x}$ and $\overline{z}$ directions:

$$\mathbf{v}_{\overline{y}} = \left\{ \begin{array}{c} \Lambda_{\overline{y}x} \\ \Lambda_{\overline{y}y} \\ \Lambda_{\overline{y}z} \end{array} \right\} = \mathbf{v}_{\overline{z}} \times \mathbf{v}_{\overline{x}} = \left\{ \begin{array}{c} \Lambda_{\overline{z}y}\Lambda_{\overline{x}z} - \Lambda_{\overline{z}z}\Lambda_{\overline{x}y} \\ \Lambda_{\overline{z}z}\Lambda_{\overline{x}x} - \Lambda_{\overline{z}x}\Lambda_{\overline{x}z} \\ \Lambda_{\overline{z}x}\Lambda_{\overline{x}y} - \Lambda_{\overline{z}y}\Lambda_{\overline{x}x} \end{array} \right\} \tag{8.5}$$

8.3 Calculation of Element Matrices

In the division of an arbitrary shell into flat elements only triangular elements can be used for the doubly curved surfaces, so the triangular finite elements are considered within this study. Taking into account that the elements of arbitrary shape and size are considered, the shape functions of the triangular element are formulated in the natural coordinate system (on a master or unit triangle) of the element plane. The natural coordinates ξ_i for an arbitrary material point $(\overline{x}, \overline{y}, \overline{z})$ of the triangle are the areas of partial triangles A_i, created by connecting the point $(\overline{x}, \overline{y}, \overline{z})$ with triangle corners, as shown in Figure 8.2. A_i is the partial area of the triangle lying opposite to the node i, so there exist the following conditions [141]:

$$\sum_{i=1}^{3} A_i = \sum_{i=1}^{3} \xi_i A = A, \quad \sum_{i=1}^{3} \xi_i = \xi_1 + \xi_2 + \xi_3 = 1, \quad \xi_3 = 1 - \xi_1 - \xi_2 \tag{8.6}$$

From the geometrical considerations it follows that if the observed material point is located at the node i, the area A_i is equal to area A, and thereby $\xi_i = 1$. On the other hand, if the observed material point is placed at the element edge opposite to the node i, the area A_i and hence the natural coordinate ξ_i are equal to zero. Because of that, the triangle can be completely described by natural coordinates $\xi_i \in [0, 1]$.

On the element level, the submatrices of the element stiffness matrix $[K]^e$ and the consistent element mass matrix $[M]^e$ are derived using 2D Gauss-Legendre quadra-

Table 8.1: Natural coordinates and the weighting factors of triangular element

Accuracy	Points	ξ_1	ξ_2	W_I
Linear	a	1/3	1/3	1/2
	a	1/2	1/2	1/6
Quadratic	b	0	1/2	1/6
	c	1/2	0	1/6

ture over single triangular finite element domain Ω^e (see Figure 8.2). This procedure is explained in detail in Section 5.4.

The Gauss-Legendre quadrature for triangular domain is:

$$\int_{\Omega^e} F(\overline{x}, \overline{y}) dx dy = \int_0^1 \int_0^{1-\xi_2} F(\xi_1, \xi_2) d\xi_2 d\xi_1 det[J] \approx \sum_{I=1}^M F\left(\xi_1^I, \xi_2^I\right) W_I, \qquad (8.7)$$

where $F(\overline{x}, \overline{y})$ is the function to be calculated numerically, $[J]$ is the Jacobian matrix, M and N denote the number of Gauss quadrature points in the ξ_1 and ξ_2 directions, (ξ_1^I, ξ_2^I) are the natural coordinates of the Gauss point, while W_I denotes the corresponding Gauss weights. Table 8.1 shows the coordinates and the weighting factors used for the calculation of element matrices, for linear and quadratic triangular element [142], as shown in Figure 8.3.

Figure 8.3: Linear and quadratic triangular finite elements with corresponding integration points

The unknown displacement components are interpolated in the local element plane. For the sake of simplicity, the same shape functions are used for the discretization of all generalized displacements.

8.4 Transformation to Global Coordinates and the Assembly Procedure

It is now convenient to define the transformation matrices for each finite element. Following the preceding considerations, the number of nodal degrees of freedom in the local coordinate system is $N_{DOF,local} = 3 + 2N + 3ND$ (see Figure 8.4).
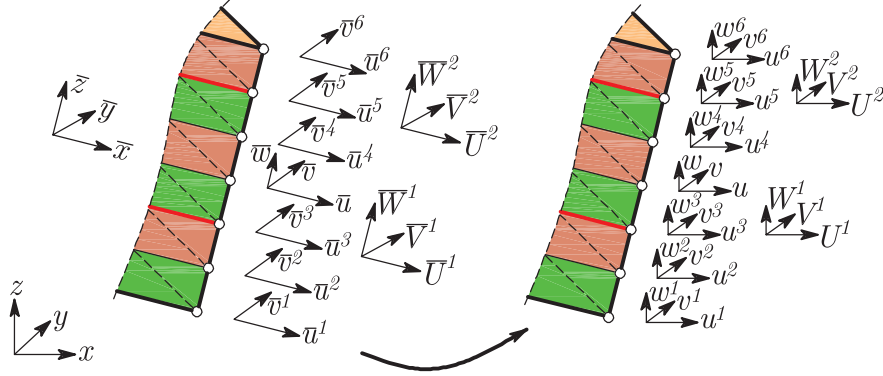
Figure 8.4: Transformation of nodal degrees of freedom of the layered triangular element (6 material layers with two delaminations)

The local displacement components should be transformed using the element transformation matrix into the following global displacement components (nodal degrees of freedom in the global coordinate system): $N_{DOF,global} = 3 + 3N + 3ND$.

This leads to the following transformation matrix:

$$
\left[\hat{T}\right] =
\begin{bmatrix}
\begin{bmatrix} T & 0 \\ 0 & \ddots \end{bmatrix} & & & \\
& \begin{bmatrix} \overline{T} & 0 & 0 \\ 0 & \overline{T} & 0 \\ 0 & 0 & \ddots \end{bmatrix} & \\
& & \begin{bmatrix} T & 0 \\ 0 & \ddots \end{bmatrix}
\end{bmatrix}
\tag{8.8}
$$

where

$$
[T] =
\begin{bmatrix}
\Lambda_{\overline{x}x} & \Lambda_{\overline{x}y} & \Lambda_{\overline{x}z} \\
\Lambda_{\overline{y}x} & \Lambda_{\overline{y}y} & \Lambda_{\overline{y}z} \\
\Lambda_{\overline{z}x} & \Lambda_{\overline{z}y} & \Lambda_{\overline{z}z}
\end{bmatrix},
\quad
[\overline{T}] =
\begin{bmatrix}
\Lambda_{\overline{x}x} & \Lambda_{\overline{x}y} & \Lambda_{\overline{x}z} \\
\Lambda_{\overline{y}x} & \Lambda_{\overline{y}y} & \Lambda_{\overline{y}z}
\end{bmatrix}.
\tag{8.9}
$$

In previous equations, Λ_{ij} is the direction cosine of the angle between the global axis i and the local axis j. Now the global element matrices/vectors of the triangular finite element can be calculated as follows:

$$[K]^e_{global} = [\hat{T}]^T[K]^e[\hat{T}], \quad [M]^e_{global} = [\hat{T}]^T[M]^e[\hat{T}], \quad \{f\}^e_{global} = [\hat{T}]^T\{f\}^e \quad (8.10)$$

The global matrices are obtained from the assembly of the respective element matrices in a usual manner.

8.5   Some Limitations of the Model

In the proposed formulation the difficulty arises if all the elements meeting in a node are co-planar. This situation will arise for shallow shell structures, flat (folded) shell segments and at straight boundaries of developable surfaces [99]. The assembled system of equations become singular in this case, and the detection of this singularity sometimes depends on round-off errors in each computer system. Within this study, this phenomenon is noticed in the free vibration analysis of the intact shallow cylindrical and spherical panels. The results are presented and commented in Section 10.5.

9 Object-Oriented Computer Program

Performance and memory efficiency are two crucial requirements for the finite element programs. Therefore the code should be well organized to increase the flexibility and reduce its maintenance cost. It should be extendable to new formulations, algorithms and concepts. The solution process in the FEM can be split into several steps, which are more or less complicated to perform in original codes:

1. **Pre-Processing** - geometry definition (points, lines, surfaces, volumes), definition of attributes or conditions (BC, loads...), their assignment to the geometrical entities and finally generation of the finite element mesh.

2. **Simulation** - Calculation in solver.

3. **Post-processing** - Visualization of the results.

All these steps must be carried out carefully, and must be easy for the user to perform. Within this study, the pre- and post-processing phases are performed using the GiD Pre/Post Processor software developed in CIMNE, Barcelona. Typical algorithm of the GiD-based finite element program is shown in Figure 9.1.
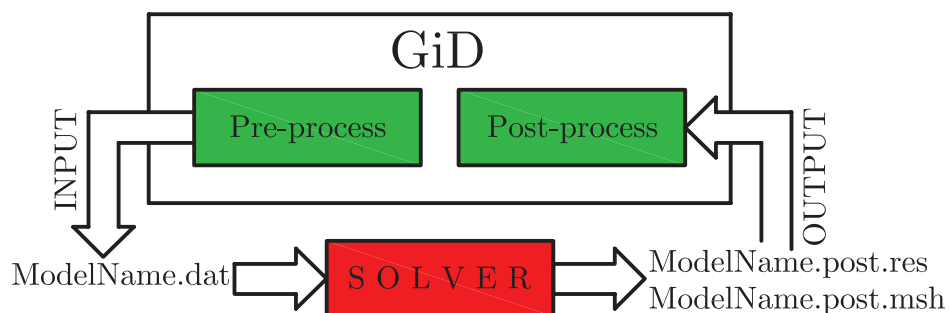
Figure 9.1: The algorithm of the GiD-based finite element program

9.1 GiD as the Pre-Processing Tool

GiD is a geometrical system in the sense that, having defined the geometry, all the attributes and conditions are applied to the geometrical entities without any reference or knowledge of a mesh. When the geometrical domain is defined, the meshing is performed. GiD allows changing of the geometry while maintaining the attributes or conditions definitions, as well as the creation of the new meshes on the same geometrical domain. Once the mesh is generated, new attributes or conditions can be assigned directly on mesh.

The *geometrical domain* in GiD is based on four geometrical levels of entities: points, lines, surfaces and volumes. Note that within this study volume entities are not used because the 3D structure is modeled using only plate finite elements. All domains are considered in 3D space (shell analysis) or in 2D space (analysis of plates). For the visualization purposes, all results are visualized in 3D space to describe the layered structure of the laminates.

The major strength of GiD is the ability for the users to **define and configure their own GUI within GiD**. This is done by creating several configuration files which define new windows where final user will enter data, such as materials, conditions or load assignments. The collection of these files is called `problemtype`. The simulation program coded in MATLAB is then executed to perform the necessary calculations, while the final phase consists of writing the results information in the format required by the GiD graphic visualizer.

9.1.1 GiD problemtype `layerwiseFE`

When GiD is to be used for a particular type of the analysis, it is necessary to predefine all the information required and to define the way the final information is given to the solver. To do so, a variety of configuration files are used to describe conditions, materials, general data, units, symbols and the format of the input file to the solver. In this study, the `layerwiseFE` problem type is designed. The configuration for the analysis is performed according to the particular specifications of MATLAB solver, regarding the syntax of the programming language. In this

study, several configuration files are written and will be explained.

`layerwiseFE.cnd` file contains all the information about the conditions that can be applied to different entities. The condition can adopt different field values for every entity. The conditions used in the `layerwiseFE.cnd` file are: **LaminateDefinition**, **DistributedLoadings**, **NodalForces**, **CrackOpeningDisplacement**, **ClampedEdge**, **SimplySupportedEdge** and **DelaminatedNode**. The graphical interface for the assignment of different conditions in GiD is shown in Figure 9.2, right, while `layerwiseFE.cnd` file is given in the Appendix.
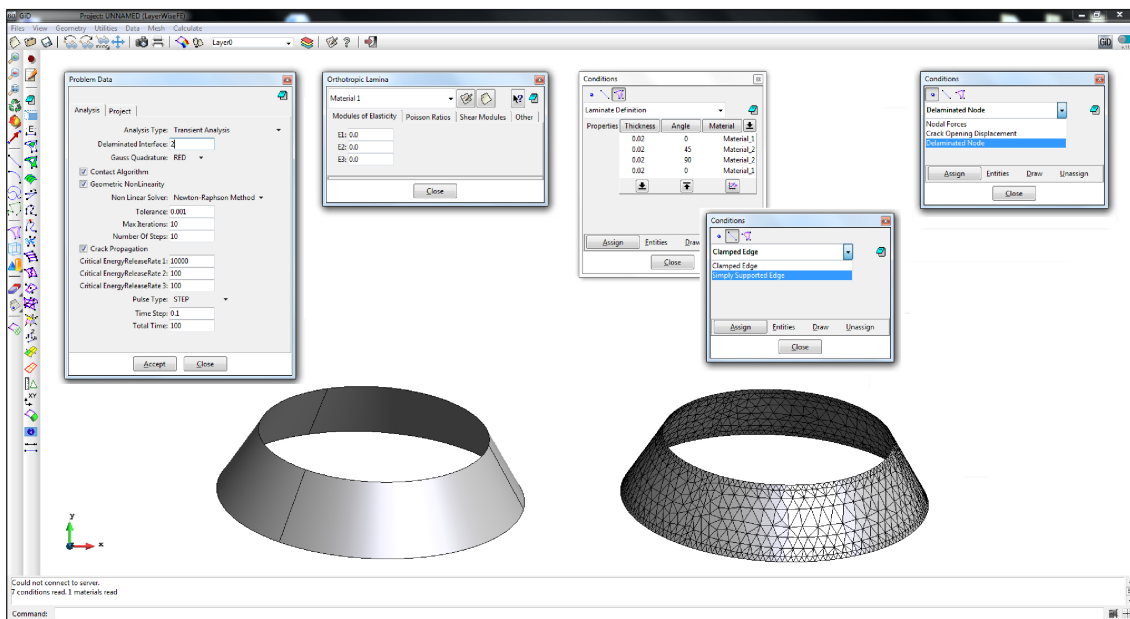
Figure 9.2: The graphical interface in GiD for the assignment of problem data (left), materials (center) and conditions (right). The geometrical domain of the conical shell with meshed model is shown below.

`layerwiseFE.mat` file include the definition of different materials that can be applied within a numerical model. Multiple materials can be defined, but it is not mandatory to use all predefined materials in the simulation, while it is useful to generate them for the materials library. The same material can be assigned to different geometrical entities. The `layerwiseFE.mat` allows the user to input the mechanical properties of the orthotropic material. Arbitrary number of material sets can be inserted. After that, the material can be assigned to the particular lamina using the **LaminateDefinition** condition. The `layerwiseFE.mat` file is given in

the Appendix, while the graphical interface for the material definition is shown in Figure 9.2, middle.

`layerwiseFE.prb` file contains all the information regarding the general problem and the intervals data. This data is required for performing of the analysis and it does not concern any particular geometrical entity. The general problem data options which can be assigned within the `layerwiseFE.prb` file are: **AnalysisType**, **DelaminatedInterface**, **GaussQuadrature**, **ContactAlgorithm**, **Geometric-NonLinearity**, **NonLinearSolver**, **Tolerance**, **MaxIterations**, **CrackPropagation**, **NumberOfSteps**, **CriticalERR1**, **CriticalERR2**, **CriticalERR3**, **Multiplicator**, **NumberOfModeShapes**, **NumberOfBucklingModes**, **PulseType**, **Nx**, **Ny**, **Nxy**, **TimeStep**, **TotalTime**, **DampingFactor**. The `layerwiseFE.prb` file is given in the Appendix, while the Problem Data user interface is shown in Figure 9.2, left.

At the beginning of the modeling process, the user defines the general problem data for the simulation. Once the geometry is created and after assignment of the materials and the conditions, the user generates the mesh using a variety of meshing options provided by GiD (Mesh Regularity, Quadratic Type, Element Type, Element Size, Mesh Criteria). It is now necessary to produce the data input files to be processed by the solver within a simulation. To manage this, GiD interprets the `layerwiseFE.bas` file, which describes the format and the structure of the required data input file for the solver in MATLAB. For this purpose, the `layerwiseFE.bas` file is generally written using the MATLAB syntax due to the fact that any information written in the `layerwiseFE.bas` file is reproduced exactly in the output file `ModelName.dat` (where `ModelName` is the chosen file name of the model, see Figure 9.1), apart from the so-called *GiD commands*. The GiD commands are the core of the GiD user interface, and they return one or multiple values obtained from the pre-processing (for example: condition field values, number of nodes in the model, FE connectivities). The `ModelName.dat` file is used later in the solver as the input file, transfering all the important data from the pre-processing to particular objects within the solver. The `layerwiseFE.bas` file is given in the Appendix.

To run the solver directly inside from GiD, it is neccesary to create the shell

script `layerwiseFE.bat`. The GiD will automatically write the `ModelName.dat` file inside the model directory, and after that the shell script will be executed.

`*.tcl` files are generally used in GiD to add some new functions or functionalities to the program. These files are written in TCL programming language [143]. In this study, the `layerwiseFE.tcl` file is used to remove some unimportant menus from the program environment, in order to simplify the program for the end user.

9.2   Using GiD in the Post-Processing

The communication between the solver and the GiD Post-Processing module is made using two output files: `ModelName.post.res`, which store the results of different calculations and the optional `ModelName.post.msh` file, in which the data regarding the post-process mesh is stored (see Figure 9.1). Note that the post-process mesh can be different from the pre-process mesh. For example, within this study, the pre-process mesh of the laminated plate model is 2D, but the post-process mesh is 3D, treating every layer as the three-dimensional volume.

In the `ModelName.post.msh` file, meshes of different element types can be handled: points, lines, triangles, quadrilaterals etc. Within this file, the 3D nodal coordinates and elements' connectivities are stored. In the `ModelName.post.res` file, the nodal variables (results) are stored. GiD allows the user to define as many nodal variables as desired, several calculation steps and analysis cases. When the post-processing of stresses is performed, Gauss points' coordinates and the results on these Gauss points are also stored in the `ModelName.post.res` file.

In this study, two MATLAB functions `MakePostRes.m` and `MakePostMsh.m` are written to prepare the post-processing files after the calculation in solver. These functions extract necessary information from the solver and they are provided in the Appendix. The applicability of `layerwiseFE` problemtype is illustrated in Figure 9.3 showing the 2D pre-process mesh (left) in GiD, 3D post-process mesh (middle) created using the `MakePostMsh.m` function, and finally the results of the simulation (right) of the DCB, calculated using the MATLAB solver and generated using the `MakePostRes.m` function.
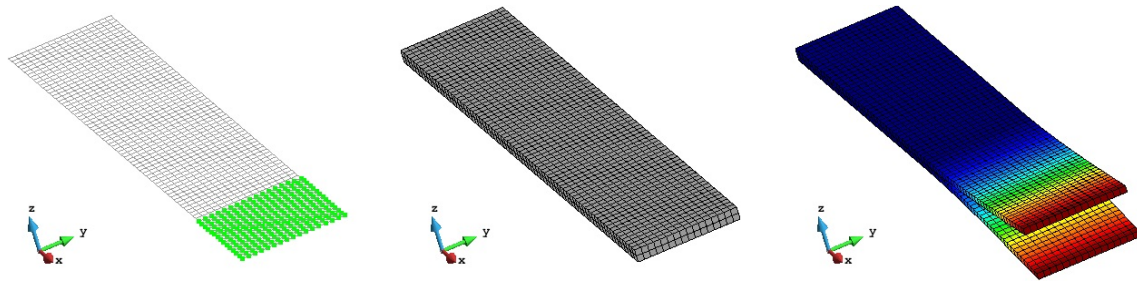
Figure 9.3: 2D pre-process mesh (left), 3D post-process mesh (middle) and the deformed shape of the Double-Cantilever-Beam (right) in GiD

9.3 MATLAB Solver

Previously derived layered finite elements served as a basis for originally coded object-oriented MATLAB solver, for the bending, free vibrations, buckling and transient analysis of laminated composite and sandwich plates with delaminations. Useful procedures for MATLAB programming of the FEM can be found in books of Ferreira [144] and Kwon and Bang [145].

The main author's motivation for chosing the object-oriented structure was motivated by the tendency to split the whole problem into several classes, in order to create objects and to define their *interfaces*. The classes that have been used in the solver are grouped in four categories:

1. modeling classes,

2. finite element model classes,

3. analysis classes,

4. numerical classes and functions.

9.3.1 Modeling Classes

The modeling classes store the global information of the considered project, mathematical model and the materials used in the analysis. The modeling classes used in the solver are `BuildProject`, `BuildModel`, `Orthotropic`, `CoefficientsL1` and `OrthotropicLaminaPlaneStress`. The *instances* of `BuildProject` and `BuildModel`

classes are objects `MyProject` and `MyModel`, which generally represent the main driver of the solver, extracting the majority of the input data from `ModelName.dat` input file during the initialization of the solver. Each simulation have only one `MyProject` and only one `MyModel` object.

`MyModel` object store the *properties* regarding the different aspects of the FE simulation: geometry(`StartCoord`, `DeformedShape`), FE model (`NumLayer`, `NumEl`, `Delamination`, `NodesPerElem`, `NumNode`, `ConnectivityInPlane`, `NodesNumericalZ`, `GiDNumEl`, `NDOF`, `SDOF`, `PlotNodes`, `ElemString`), global matrices (`GlobalK`, `GlobalM`, `GlobalKG`, `GlobalQ`, `GlobalP`), results (`Result`, `Reactions`) and boundary conditions (`CCNodes`, `SSEdges`, `DELNodes`, `ERR1`, `ERR2`, `ERR3`). The *methods* used in the `MyModel` are: `calcNumberOfDOF()`, `calcSystemMatrices()`, `assignPenalty()`, `calcSystemVectors()`, `calcStartCoord()` and `calcDeformedShape()`.

`MyProject` object is the instance of `BuildProject` class, which is an *abstract* class, for which no code is supplied to implement some of the methods. `MyProject` object is used to store the basic info regarding the FE simulation: `FileName`, `AnalysisType`, `SolverType`, `ElementShape`, `Integration`, `Interpolation`, `Steps`, `CrackPropagation`, `GeometricNonlinearity`, `Contact`, `Iterations`, `Tolerance`, `TimeStep`, `TimeTotal`, `PulseType` and `DampingFactor`.

`Orthotropic` represents the class which *encapsulates* the information regarding the material used in the analysis, with the following properties: `E1`, `E2`, `E3`, `ni12`, `ni13`, `ni23`, `G12`, `G13`, `G23`, `rho`. The methods `setni21()`, `setni32()` and `setni31()` are used to calculate the remaining Poisson's ratios of the orthotropic material.

`OrthotropicLaminaPlaneStress` is the *descendant class* of the `Orthotropic` class, storing the geometrical and mechanical info of the single lamina in the model, with the following properties: `ID`, `FiberAngle`, `Thickness`, `matrixC`, `matrixQ` and `matrixT`. The methods `setMatC()`, `setMatQ()`, `setMatT()` and `assignMat()` are used to calculate the lamina transformation matrix, compliance matrices in the local and the global coordinate system and to assign the material to the lamina.

`CoefficientsL1` encapsulates the characteristic matrices of the laminate in the following properties: `matrixApq`, `matrixBpq`, `matrixDpq`, `matrixEpq`, `matrixLpq`,

`matrixFpq`, `matrixLLpq`, `matrixFFpq`, `matrixFFFpq`, as well as `coeffI0`, `coeffIi`, `coefIij`, `coeffIIi`, `coeffIIij` and `IIIIij`.

9.3.2 Finite Element Model Classes

For the abstraction of the FE model, several main classes are used within the solver, which will be explained as follows:

`DOF` object represents a degree of freedom. It is a lightweight object which holds only its `ID` and *boolean* `Free` (True/False).

`Node` object represents the disreete point in the domain (3D space) at which DOFs are defined. It uses the info from `DOF` objects, but also encapsulates the additional information: `ID`, `DOFS`, `DamageStatus`, coordinates `XCoord`, `YCoord`, `ZCoord`, assigned loadings `ForceX`, `ForceY`, `ForceZ`. The `Node` object provides the following methods: `assignDOF()`, `assignDamageStatus()`, `changeToDEL()`, `changeToFront()`, `changeToIntact()` and `assignNodalForces()`. The `Node` class allows `Node` objects to be created in all types of the analysis used in the present study.

`LWL1PlaneStress` class is the **core** of the FE model, which encapsulates the element formulation of the **L**ayer-**W**ise **L**inear **Plane Stress** finite element with only **1** node per lamina through the thickness. It stores the data regarding the model (`ID`, `Nodes`, `NodeDOF`, `IndexDOF`, `NumLayers`, `NumNum`, `NumNumRed`, `ElementType`, `NNodes` and `NodalCoord`) and local matrices(`matrixKtang`, `vectorQ`, `matrixK`, `matrixM`, `matrixKG`, `matrixN0`). The instances of `LWL1PlaneStress` class are `Element` objects, which provide an interface for calculating the local matrices and vectors necessary for assembling the global system of equations: `calcMatrixK()`, `calcMatrixM()`, `calcTangentMatrixK()`, `calcMatrixKG()` and `calcVectorQ()`, as well as the interface for setting of the nodal coordinates and DOFs within the particular element: `deriveIndexDOF` and `setNodalCoord`. When the analysis of shells is performed, the additional `calcStartCoordofFE`, `calcDeformedCoordofFE` and `calcMatrixT` are used to keep track of the element's local coordinate system. Each `Element` object is associated with the number of `Node` objects.

9.3.3 Analysis Classes

When the global matrices are formed within the `MyModel` object, the solution procedure is called based on the global data from `MyProject` object. `SOLVER` class is a base class having the following properties: `KNOWN`, `UNKNOWN`, `Result`, `ResultType`, `NumberOfRecords`, and providing the method `SolveSystem()` which communicate with `MyModel`, `MyProject`, `Element` and `CoefficientsL1` objects.

Several descendent classes are provided based on the `SOLVER` class, which represent different types of the analysis. Some of these classes have the additional properties (`Reactions`) and provide some additional methods (`correctContactNodes()`). These classes are `LinearSolver`, `LinearSolverWithPropagation`, `TransientSolver`, `TransientSolverWithPropagation`, `BucklingSolver`, `FreeVibSolver`, `NRSolver`, `NRSolverWithPropagation`, `NonLinearTransientSolverWithPropagation` and finally `NonLinearTransientSolver`. These classes solve the governing equations of the FE model, using the MATLAB's numerical classes (`Vector`, `Matrix`...). They also describe the general flow of the solution process and update the results in the data structure. Some of these classes are very similar to each other, with the difference only in some local solution steps.

9.3.4 Numerical Classes and Functions

A finite element program has several common procedures that should be implemented as basic tools to be used by other parts of the program, for example for integrating, calculating shape functions and other geometrical parameters. While many of this tools are used in the most inner parts of the code, their performance has a great importance for the general execution of a program. For example integration tools are called inside the element objects and any overhead in their performance will cause a great overhead in program executing time. In this study, four main groups of functions are used within a code: **integration (quadrature) tools**, **geometry tools**, **delamination propagation tools** and finally **ConstraintHandler** function.

ConstraintHandler

This function is very important in the flow of the FE code. It communicates with `Node` and `MyModel` objects, collects the prescribed data regarding the boundary conditions and assigns the `Free/Restrained` status to the `DOF` objects.

Integration (quadrature) tools

Evaluation of the characteristic element matrices is usually done by integrating some function over the element domain or boundary. This makes necessary the designing and implementing an efficient integration tool which handle integration with less overhead as possible. As stated before, Gauss-Legendre quadrature is used within this study. The functions used in order to handle numerical integration over quadrilateral or triangular domains are: `ShapeQ4()`, `ShapeQ9()`, `ShapeT3()`, `ShapeT6()`, `GaussCoordinatesQuad()`, `GaussCoordinatesTriangle()`, `findNaturalCoord()` and `evaluate()`.

Geometry tools

The variety of geometry functions are implemented in solver to handle some geometrical operations, such as `findAngle()`, `findSymetral()`, `isPointInTriangle()`, `isIntersection()` and `isCounterClockWise()`.

Delamination propagation tools

The additional set of tools is implemented in order to perform the delamination propagation algorithm, which requires a lot of geometry checking during the consecutive solution steps. The functions designed for this purpose are: `FrontDetection()`, `PerformFrontChecking()`, `ContourDetection()`, `NodesToFix()`, `findPoints45()`, `findPoints60()`, `findAdjacent()`, `findDelaminated()`, `findPropagatingNodes()`, `findDelaminatedNodesBehindCrack()`, `findElementsWithCentralNodeOnFront()`. In addition, `vicinity()`, `narrowvicinity()` and `opposite()` are the tools used to extract the nodes in the vicinity of the considered node of the finite element model, in order to perform delamination propagation checking.

The classes and their relationships are shown in Figure 9.4. A simple line between

two rectangles represents the *knows-a relation*, a line with the triangle represents the *is-a relation* (*inheritance*) between the *descendant* and the *ancestor* class, while a diamond and a line represent the **has-a relation** (*aggregation*) between the *aggregation* and the *component* classes.
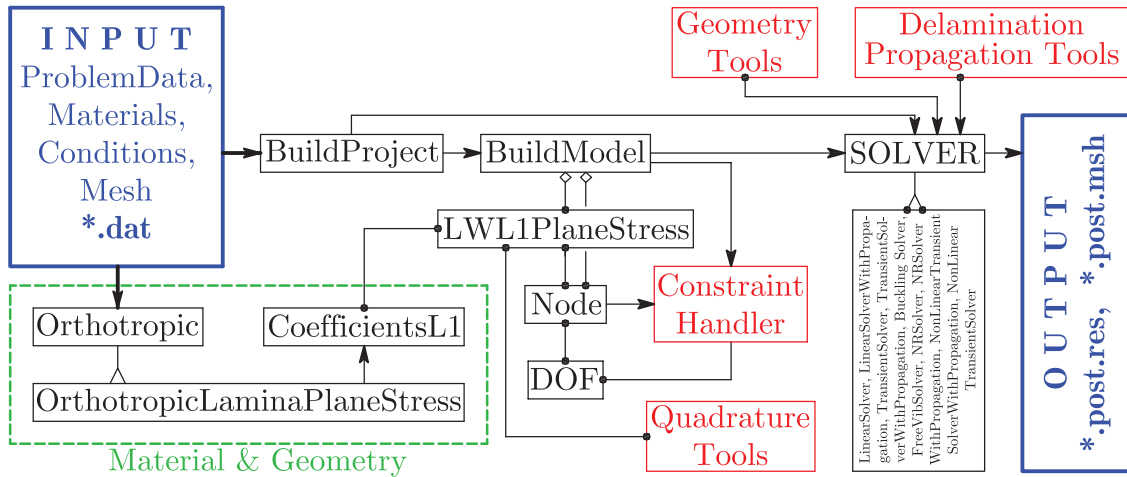
Figure 9.4: The main classes and their relationships

10 Numerical Examples

Theoretical considerations presented in this study are validated through a variety of numerical examples presented in this chapter. All calculations have been made using the original computer codes written by author. Whenever possible, obtained results are compared against existing exact, analytical, numerical and experimental data from the literature. The number of results is selected from author's publications [60, 94–97, 104, 105, 108, 132, 133, 146]. Note should be made of the fact that the numerical model presented herein is not restricted to any particular boundary condition, lamination scheme, geometry or loading type.

10.1 Linear and Geometrically Nonlinear Static Analysis

Bending Analysis of Intact Plates

Example 10.1.1. In the first validation example, the linear and nonlinear bending of a fully clamped four-layer cross-ply (0/90/90/0) square laminate is analyzed. Plate dimensions are $a = b = 12in$, while the overall plate thickness is $h = 0.096in$ (see Ref. [8] for details). All layers are of equal thickness and made of the orthotropic material with the following mechanical characteristics: $E_1 = 1.8282 \times 10^6 psi, E_2 = 1.8315 \times 10^6 psi, G_{12} = G_{13} = G_{23} = 0.3125 \times 10^6 psi, \nu_{12} = \nu_{13} = \nu_{23} = 0.2395$. The plate is discretized using different mesh densities (6×6, 8×8 and 10×10) of 9-node layered finite elements with reduced integration. The boundary conditions are prescribed along clamped edges by constraining all degrees of freedom in edge nodes.

Linear transverse deflection of the plate center is calculated for 6×6 mesh (red solid line in Figure 10.1) and compared with the existing solutions using ESL plate theories. After that, the nonlinear response is calculated for different mesh densities (red dashed lines in Figure 10.1), using $20 \times 0.2psi$ load increments. The nonlinear solution is obtained using Newton-Raphson iterative method (see subsection 5.7.1). The results are compared with numerical results using CLPT and FSDT laminate theories [8], as well as with the experimental data from [8].
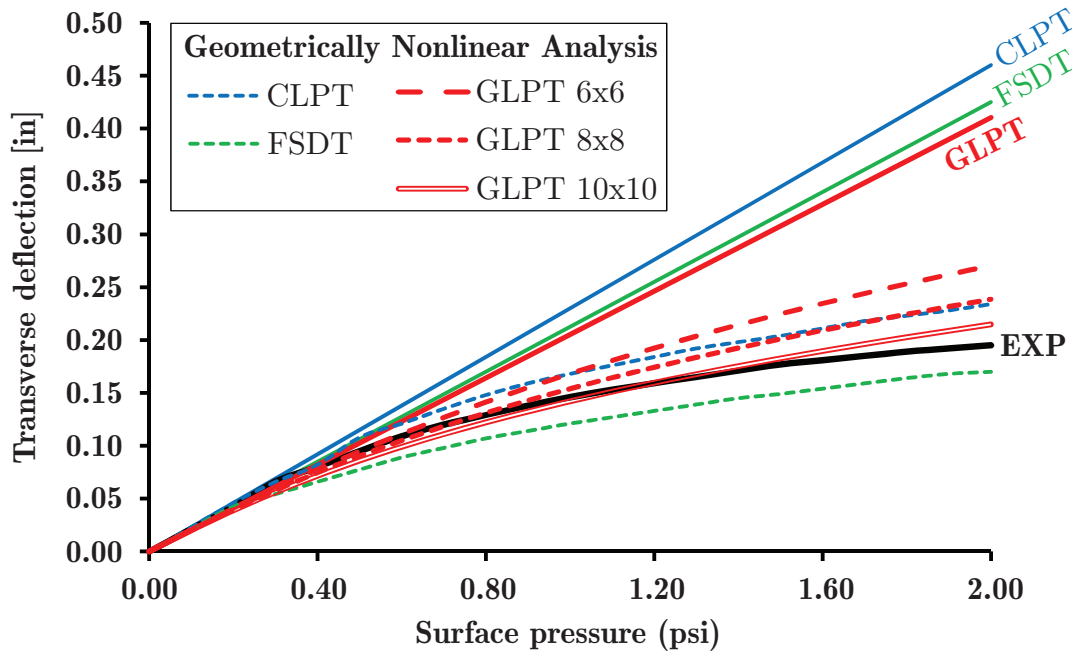
Figure 10.1: Load-deflection curves for fully clamped cross-ply (0/90/90/0) square composite plates under uniformly distributed transverse loading, for different numerical models

From Figure 10.1 it is obvious that the linear response is in agreement with the results obtained using FSDT. The nonlinear response converge to the experimental solution with refining the mesh density. The results obtained using 10×10 mesh are in excellent agreement with the experimental data from [8].

105

Bending Analysis of the Double-Cantilever-Beam

Example 10.1.2. In the second validation example DCB problem is analyzed. Geometry and the loading are shown in Figure 10.2. The T300/976 graphite/epoxy material is used, with the following material properties: $E_1 = 139300 N/mm^2$, $E_2 = E_3 = 9720 N/mm^2$, $G_{12} = G_{13} = 5580 N/mm^2$, $G_{23} = 3450 N/mm^2$, $\nu = 0.29$. The critical values of the Strain Energy Release Rates are: $G_{Ic} = 0.0876 N/mm$, $G_{IIc} = G_{IIIc} = 0.3152 N/mm$ [123]. The fibers are oriented along the length of the plate (fiber orientation $\theta = 0^o$).
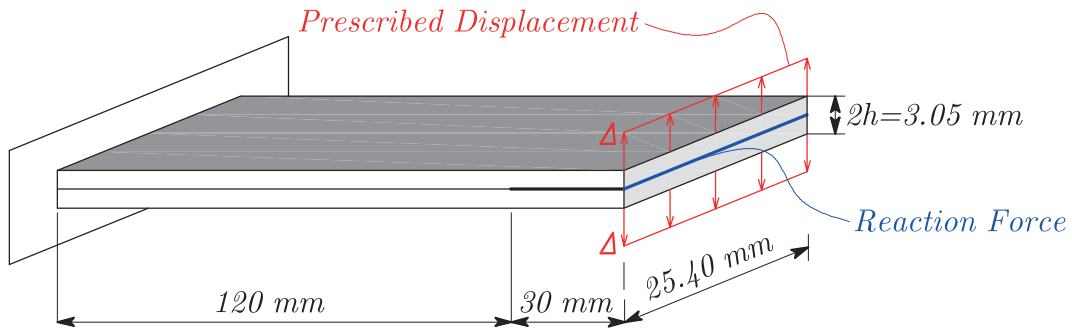
Figure 10.2: Double Cantilever Beam benchmark: Geometry, boundary conditions and prescribed delamination zone

The cantilever plate is discretized using different mesh densities (30×6, 50×10 and 75×16) of 4-node and, for comparison, 9-node layered finite elements with reduced integration. The boundary conditions are prescribed along clamped edge by constraining all degrees of freedom in edge nodes. The delamination is prescribed by allowing the motion of displacements U^I, V^I and W^I in the delaminated zone, as shown in Figure 10.2.

In the first part of this example, the plate is loaded by applying Crack Opening Displacements (COD) in 50 steps in increments of $W^I = 0.1\ mm$ along the nodes I on the free edge of the cantilever. The reaction force is measured in the nodes where the prescribed displacements are applied and then plotted versus the COD in Figure 10.3. For comparison, the analytical solution of the DCB test based on the Bernoulli

10. Numerical Examples

beam theory and Linear Elastic Fracture Mechanics [111–113] is calculated as:

$$R_{el} = \frac{3}{2}\frac{E_1 I}{a_0^3}\cdot\Delta, \quad R_{del} = \sqrt{\frac{2}{3}\frac{(bG_{Ic}E_1 I)^{3/2}}{E_1 I\Delta}} \tag{10.1}$$

In Eq. (10.1), R_{el} is the linear part of the $R - \Delta$ chart (before the delamination propagates), R_{del} is the nonlinear part of the $R - \Delta$ chart (during the delamination propagation), Δ is the prescribed displacement, $I = \frac{bh^3}{12}$ is the moment of inertia of one delaminated part of the cantilever, $h = 1.525mm$ is the height of one delaminated part of the cantilever, $b = 25.4mm$ is the width of the specimen, $a_0 = 30mm$ is the prescribed delamination length and $G_{Ic} = 0.0876N/mm$ is the critical value of the Strain Energy Release Rate for Mode I conditions.
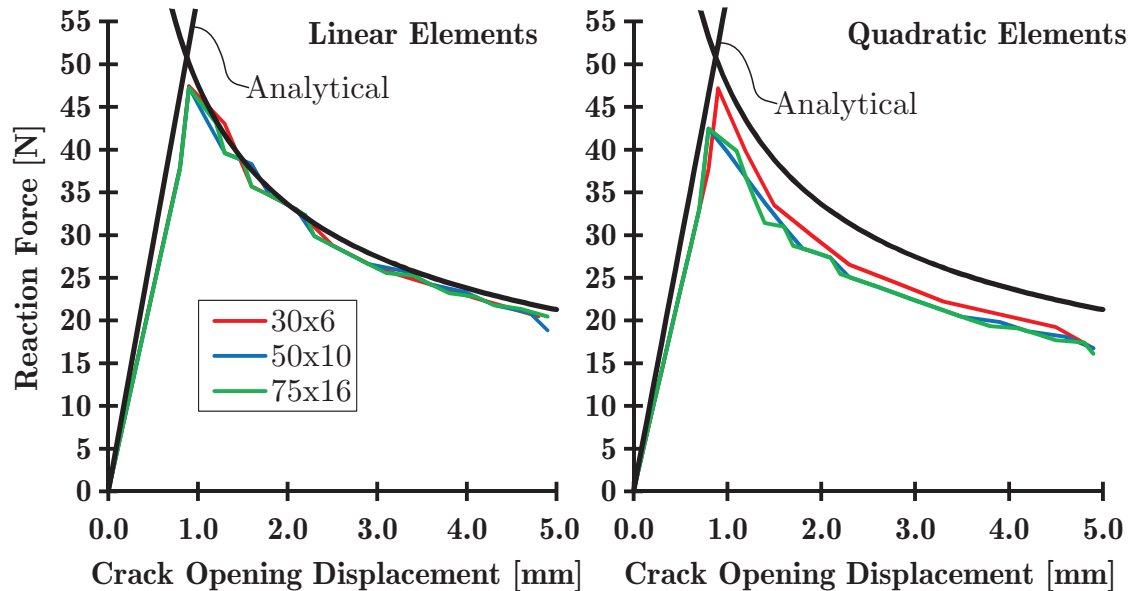
Figure 10.3: Double Cantilever Beam benchmark: Reaction Force versus Crack Opening Displacement for different element types and different mesh densities

Figure 10.3 shows the comparisons of the numerical and the analytical results of the DCB test for different mesh densities of the 4-node elements (left) and the 9-node elements (right). All models generally displayed similar behavior regardless of the mesh size, resulting in (1) the linear part of the load-displacement diagram until the initiation of the delamination growth and (2) nonlinear part where the delamination growth is accompanied by the reduction in the load-carrying behavior.

Mesh refinement in the longitudinal direction generally results in a smoother load-displacement curve because of the shorter distances between two consecutive stable delamination fronts.

As shown in Figure 10.3, the elastic branch of the force-displacement curve is slightly softer in the finite element solutions in comparison with the analytical solution. This has two main reasons:

- The analytical solution is based on the Bernoulli beam model, where the transverse shear deformation is not accounted. Therefore, the Bernoulli beam model is stiffer in comparison with the numerical solution based on the GLPT.

- The analytical solution does not take into account the orthotropic properties of the material. Only a single elasticity modulus E_1 is accounted, which assumes that $E_2 = E_3 = E_1$. Therefore, the plate model, which accounts for $E_2/E_1 < 1$ ratio, is slightly softer.

Obviously, slightly higher values of the reaction force are obtained if the model is discretized using linear elements (left hand side of Figure 10.3). For the fine discretizations (50×10 and 75×16) using the quadratic elements, the model underestimates the critical forces corresponding to the onset of delamination propagation as compared to the analytical solution due to the same reasons as mentioned above.

In the second part of this validation analysis, the influence of the mesh density along the width of the cantilever beam on the G_I distribution over the width of the plate is illustrated. The G_I distribution is measured along the delamination front in the moment of the creation of the first propagating node. Six different numerical models are considered, covering both linear and quadratic layered finite elements.

During the DCB test, consecutive straight delamination fronts should be created [129]. As shown in Figure 10.4 left, the distribution of the G_I along the plate width using linear (4-node) elements is nearly constant, leading to the debonding of all nodes along the delamination front (red nodes). However, Figure 10.4 (middle) shows, that for the quadratic (9-node) elements the distribution of G_I is not constant due to the differences in nodal force values of the mid-nodes and the corner-nodes of the 9-node quadrilateral element . This effect is well known for node-to-node de-
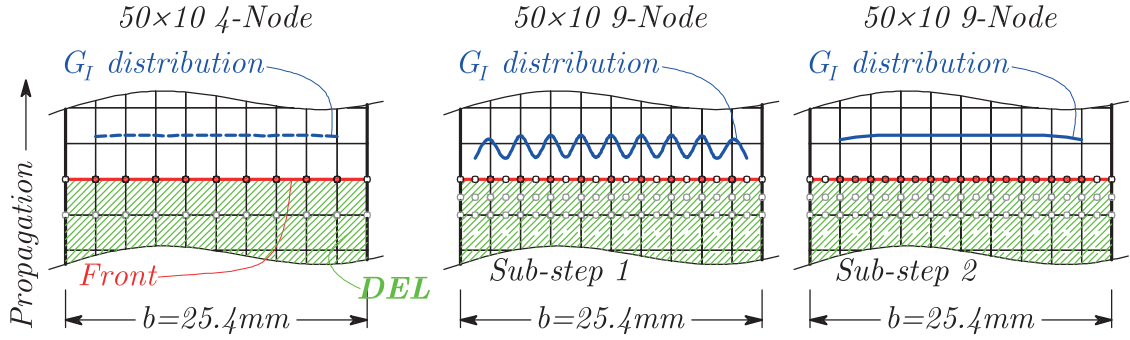
Figure 10.4: Creation of the stable delamination fronts for different numerical models (left: 4-node elements, middle: 9-node elements, Sub-step 1, right: 9-node elements, Sub-step 2, red circles: debonding nodes)

lamination propagation strategies when quadratic elements are applied. In this step (Sub-step 1), only one half of the nodes debond. After Sub-step 1 the delamination front is changed, causing the increase of the G_I in the remaining intact nodes, leading to the final distribution of G_I as illustrated in Figure 10.4 (right) after Sub-step 2.

The influence of the mesh refinement in the width direction on the G_I distribution is illustrated in Figure 10.5. The refinement does not seem to significantly influence the distribution of the G_I along the plate width. The Figure 10.5 shows that the G_I distribution is fairly constant in the center part of the specimen progressively decreasing towards the edges. There is a deviation in G_I (about 15%) at the nodes of free edge. The same behavior is detected in [147]. The non-uniform distribution of the G_I along the plate width is also experimentally proved in [148].

In the final part of this example the influence of the load step on the delamination propagation is investigated numerically. The plate is discretized using 50×10 4-node layered finite elements and loaded using different increment sizes of the applied crack mouth opening displacements. The reaction force is plotted versus the crack opening displacement in Figure 10.6 and compared with the analytical solution according to Eq. (10.1). It shows, that the reduction of the displacement increment improves the agreement with the analytical solution in the nonlinear portion of the chart, while the elastic branch is still softer due to simplifications in the analytical solution regarding both the transverse shear deformation and the material properties.
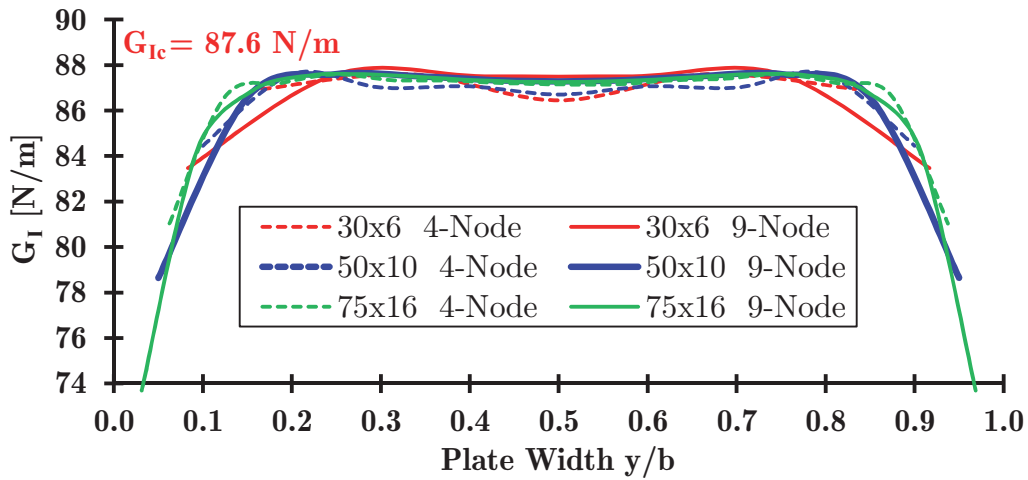
Figure 10.5: G_I distribution in the DCB test along the plate width considering different mesh densities and different numerical models
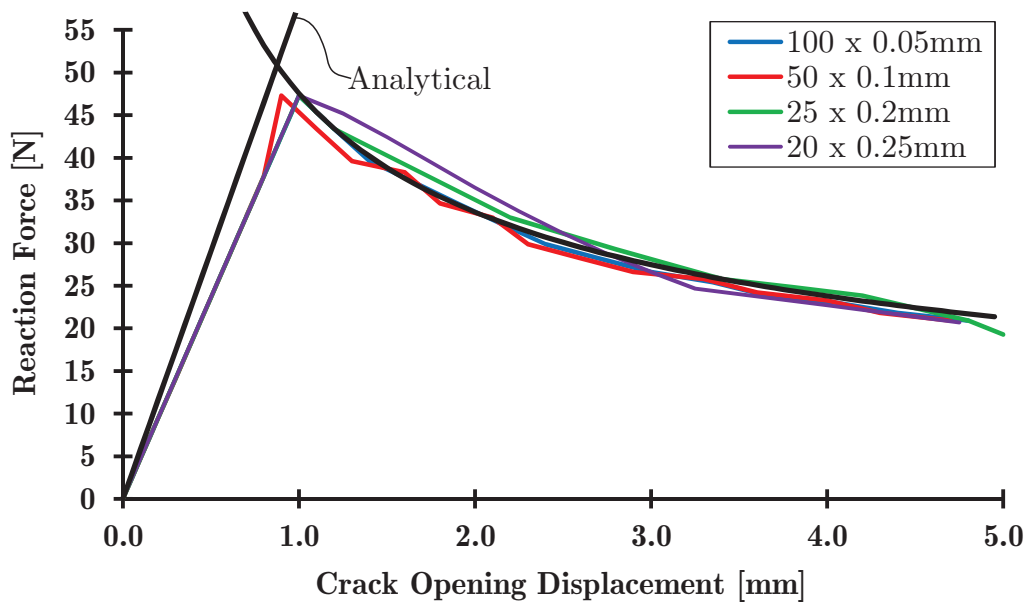
Figure 10.6: Reaction force versus COD considering different displacement increments (50×10 4-node elements)

From previous considerations it is obvious that the proposed algorithm, combined both with linear and quadratic quadrilateral layered finite elements, is capable to describe both pre- and post-propagation behavior of the laminated composite plate.

10.2   Free Vibrations

Free Vibrations of Intact Plates

Example 10.2.1. The effect of incorporated transverse shear deformation on fundamental frequencies of intact laminated composite plates is analyzed in this example. Simply supported square plate is considered, with symmetric cross-ply lamination scheme and laminas of equal thickness. For comparison, different numbers of layers through the overall plate height h are considered, as well as different E_1/E_2 ratios.

Each layer is made of material with the following mechanical characteristics [21]: $G_{12}/E_2 = 0.6, G_{13}/E_2 = G_{23}/E_2 = 0.5, \nu_{12} = 0.25, \rho = 1.0$. The fundamental frequencies are presented in the non-dimenzionalized form:

$$\overline{\omega} = \omega\sqrt{\rho h^2/E_2} \tag{10.2}$$

The effects of orthotropy and lamination scheme of simply supported cross-ply laminated composite plate with $a/h = 5$ are presented in Table 10.1. It is obvious that incorporation of the transverse shear deformation reduces the fundamental frequencies. This reduction is more pronounced for the plates with higher level of orthotropy. The same trend is obtained in both schemes of lamination shown in Table 10.1. Natural frequencies are overpredicted in all cases where ESL model is used.

Example 10.2.2. In the second benchmark example, a sensitivity analysis is performed to study the effects of mesh density and integration scheme on fundamental frequencies. Natural frequencies obtained using the proposed model are compared with the existing results obtained using commercial software ABAQUS® [65].

An eight-layer free square plate with a side length of $178mm$ and a total thickness $h = 1.58mm$ is considered. All plies are of 0° orientation and of equal thickness and made of material with following mechanical characteristics: $E_1 = 172.7GPa, E_2 = E_3 = 7.2GPa, G_{12} = G_{13} = 3.76GPa, G_{23} = 2.71GPa, \nu_{12} = \nu_{13} = 0.30, \nu_{23} = 0.33, \rho = 1566kg/m^3$ [65].

Table 10.2 shows the natural frequencies of the first six modes for different mesh densities. The agreement with experimental results of Lin et al. [62] even for the

Table 10.1: Non-dimenzionalized fundamental frequencies of the intact (0/90/0) simply supported square laminates with three and five orthotropic layers using different E_1/E_2 ratios

Source	Layers	E_1/E_2			
		3	10	20	30
Vuksanović - CLPT [21]		0.2920	0.4126	0.5404	0.6434
Owen and Li - Refined [38]		0.2695	0.3392	0.3898	0.4194
Vuksanović - HSDT [21]		0.2673	0.3318	0.3749	0.4015
Noor - 3D elasticity [30]	3	0.2647	0.3284	0.3842	0.4109
Present (9-node; 5×5 FE)		0.2621	0.3262	0.3691	0.3927
Present (4-node; 10×10 FE)		0.2683	0.3297	0.3685	0.3886
Vuksanović - CLPT [21]		0.2920	0.4126	0.5404	0.6434
Owen and Li - Refined [38]		0.2699	0.3453	0.4030	0.4370
Vuksanović - HSDT [21]		0.2684	0.3442	0.3939	0.4269
Noor - 3D elasticity [30]	5	0.2659	0.3409	0.3979	0.4314
Present (9-node; 5×5 FE)		0.2618	0.3330	0.3858	0.4166
Present (4-node; 10×10 FE)		0.2683	0.3396	0.3918	0.4219

Table 10.2: Comparison of natural frequencies (Hz) of the intact (0/0/0/0)s free square plate using different mesh densities and different integration schemes

Source	FE	Mode					
		1	2	3	4	5	6
	25	78.51	100.17	277.31	316.42	489.29	581.06
Alnefaie [65]	100	81.23	107.20	207.72	294.01	422.93	523.91
	400	81.48	109.20	199.50	300.46	391.40	533.89
	4	82.47	131.69	229.99	351.18	445.07	639.06
Present (9-node; full)	25	82.01	112.06	202.69	326.36	413.83	545.47
	100	81.78	110.40	200.75	308.07	397.50	538.64
	4	82.21	115.70	202.41	351.10	443.55	566.39
Present (9-node; red.)	25	81.67	110.07	199.37	306.17	396.66	538.48
	100	81.50	109.90	199.52	303.02	392.17	537.89

coarse mesh of 25 elements is obvious and shown in Table 10.3. Better agreement is obtained especially for the higher modes. Also, the advantage of the 9-node over the 4-node element is confirmed in this case.

From Table 10.2 it is obvious that proposed model gives an accurate prediction of fundamental frequencies even for the coarse mesh of 25 layered finite elements, in comparison with the results obtained using the commercial software. Also, the proposed model implies a significantly lower number of nodal variables, which saves the computational time (note that proposed model implies two-dimensional FE mesh, in contrary to the conventional 3D FE models). In the case of coarse mesh, using of reduced integration for calculation of element matrices is necessary (because a/h ratio becomes large and we have thin plate situation), in order to avoid shear locking (see Table 10.3).

Example 10.2.3. Additional comparison is made with 16-layer plate with dimensions of $240 \times 180mm$ and a total thickness $h = 2.08mm$. Laminate is composed in

Table 10.3: Comparison of natural frequencies (Hz) of the intact (0/0/0/0)s free square plate using different numerical models, mesh densities and integration schemes (* – occur in pairs due – to the symmetry)

Source	FE	Mode					
		1	2	3	4	5	6
Alnefaie [65]	25	78.51	100.17	277.31	316.42	489.29	581.06
Yam et al. [61]	25	83.73	120.52	219.99	373.08	503.21	667.43
Lin et al. [62]	100	83.57	118.42	207.79	329.41	419.83	546.93
Present (9-node; full)	25	82.01	112.06	202.69	326.36	413.83	545.47
Present (9-node; red.)	25	81.67	110.07	199.37	306.17	396.66	538.48
Present (4-node; full)	25	85.13	157.93*	193.46*	252.29	475.12*	515.72
Present (4-node; red.)	25	80.23	116.22	206.38	372.85	441.63	568.94
Experimental [62]		81.50	107.40	196.60	285.50	382.50	531.00

(0/0/90/90/0/0/90/90)s lamination scheme, and each layer is made of material with the following mechanical characteristics: $E_1 = 125GPa, E_2 = E_3 = 8.5GPa, G_{12} = G_{13} = 4.5GPa, G_{23} = 3.27GPa, \nu_{12} = \nu_{13} = 0.30, \nu_{23} = 0.30, \rho = 1550kg/m^3$ [65].

Table 10.4 shows the natural frequencies of the first six modes for different numerical models. Results are compared with numerical results of Alnefaie [65] and numerical and experimental results of Wei et al. [63]. As shown in previous examples, computational time can be reduced using the proposed FE model.

Example 10.2.4. The final benchmark example in this section is concerned with a four-layer clamped circular composite plate with symmetric $(\theta/-\theta/-\theta/\theta)$ stacking sequence. The plate diameter is a, while the overall plate thickness is denoted as h. All laminas are of equal thickness. The following material parameters are assumed for orthotropic constitutive models of all laminas: $E_1/E_2 = 40, G_{12}/E_2 = G_{13}/E_2 = 0.6, G_{23}/E_2 = 0.5, \nu_{12} = \nu_{13} = \nu_{23} = 0.25, \rho = const$ [149].

The boundary conditions are prescribed along clamped boundaries by constraining all generalized displacements in edge nodes. The plate is discretized using two

Table 10.4: Comparison of natural frequencies (Hz) of the (0/0/90/90/0/0/90/90)s intact free composite plate using different numerical models and integration schemes

Source	FE	Mode					
		1	2	3	4	5	6
Alnefaie [65]	400	89.16	278.97	330.35	354.92	393.26	574.50
Wei et al. [63]	400	90.52	279.17	333.59	354.22	397.62	583.71
Present (9-node; red.)	25	88.51	281.22	332.54	356.48	397.42	578.67
Present (4-node; red.)	25	86.10	296.89	344.06	376.51	414.44	585.79
Experimental [63]		90	289	318	354	386	570

different unstructured mesh densities and two different element types (linear finite element denoted as **Q4** and quadratic finite element denoted as **Q9**, see Table 10.5) with reduced integration. The nondimenzionalized fundamental frequencies $\overline{\omega} = \omega \cdot a^2/h\sqrt{\rho/E_2}$ of intact laminated composite plates are calculated and compared with results obtained using different theories: transverse shear deformation theory [149], FSDT [150] and inverse trigonometric shear deformation theory [151]. The results are elaborated in Table 10.6.

Table 10.5: Properties of the numerical models used in Example 10.2.4.

FE	Mesh	FE Size	Number of FE	Number of Nodes
Q4	Mesh 1	$a/10$	303	335
	Mesh 2	$a/20$	931	994
Q9	Mesh 1	$a/10$	303	1275
	Mesh 2	$a/20$	931	3849

From Table 10.6 it is obvious that the proposed model is fully capable to predict the fundamental frequencies of circular laminated composite plates, even by using the quadrilateral elements to describe the circular plate geometry. It is shown that
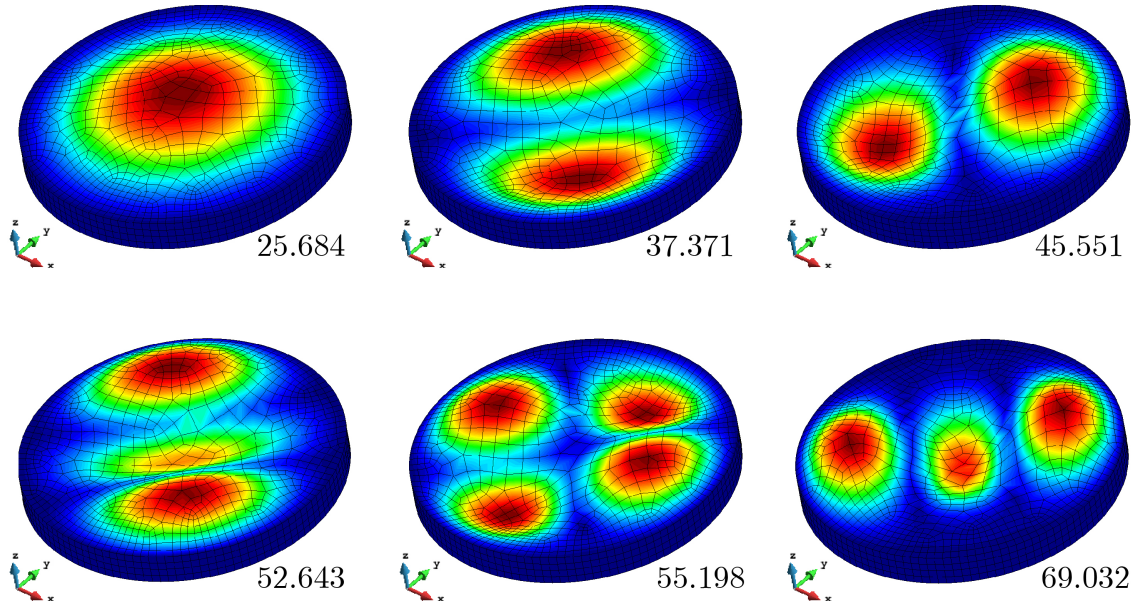
Figure 10.7: First 6 nondimenzionalized frequencies $\overline{\omega} = \omega \cdot a^2/h\sqrt{\rho/E_2}$ and corresponding mode shapes of 4-layer clamped $(45/-45/-45/45)$ angleply circular composite plate ($a/h = 10$, Q9, Mesh 2)

a slightly stiffer response (2-4 %) is obtained using all numerical models and that mesh refinement leads to the convergence of results, for all considered stacking sequences. The first 6 nondimenzionalized frequencies and the corresponding mode shapes plotted in GiD Post Processor for $(45/-45/-45/45)$ stacking sequence of the clamped circular laminated composite plate are illustrated in Figure 10.7.

Free Vibrations of Delaminated Plates

Obviously, the natural frequencies of a delaminated composite plate will decrease because of the loss in stiffness caused by the presence of delaminations [37]. In this section, effects of boundary conditions, delamination geometry and delamination position on natural frequencies and mode shapes are investigated numerically.

Example 10.2.1. An 8-layer square composite plate with symmetric $(0/90/45/90)s$ stacking sequence is considered, with all laminas of equal thickness. Overall plate height is $h = 2.12mm$. Each layer is made of material with following mechanical characteristics: $E_1 = 132GPa, E_2 = 5.35GPa, G_{12} = G_{13} = 2.79GPa, \nu_{12} = \nu_{13} = $

Table 10.6: The nondimenzionalized fundamental frequencies $\overline{\omega} = \omega \cdot a^2/h\sqrt{\rho/E_2}$ of the 4-layer clamped circular laminated composite plates with symmetric $(\theta/-\theta/-\theta/\theta)$ angle-ply stacking sequence $(a/h = 10)$

Numerical model	$\theta = 0^o$	$\theta = 15^o$	$\theta = 30^o$	$\theta = 45^o$
SDT [149]	23.130	23.308	24.063	24.557
MLSDQ-FSDT [150]	22.211	22.774	24.071	24.752
IGA-ITSDT [151]	23.578	23.609	24.208	24.661
Present, Q4, Mesh 1	23.174	23.918	25.333	25.903
Present, Q4, Mesh 2	22.984	23.747	25.175	25.750
Present, Q9, Mesh 1	22.914	23.677	25.108	25.685
Present, Q9, Mesh 2	22.913	23.676	25.107	25.684

$0.291, \nu_{23} = 0.30, \rho = 1446.2 kg/m^3$ [37]. Different boundary conditions are adopted in the analysis. Square delamination is located in the center of the mid-plane of the laminate, with delamination side of $a/2$ (where $a = 250mm$ is the side length of the plate). First 6 modes for intact and delaminated plates are listed in Table 10.7.

Results obtained using the proposed numerical model with 6×6 mesh of 9-node layered finite elements are compared with the existing data from the literature, elaborated in Table 10.7 and graphically interpreted in Figure 10.8. Reduced integration is adopted in all calculations to avoid shear locking.

The reduction of the fundamental frequency caused by the presence of the delamination is more pronounced for higher modes, for all four examined cases of boundary conditions. It is very important to highlight that shear deformation does not reduce the fundamental frequency (Mode 1) in the case of free and cantilever plate. In the case of simply supported or clamped plate, fundamental frequency is reduced, both for the intact and the delaminated plates.

Example 10.2.2. A five layer (0/90/core/0/90) anti-symmetric simply supported square sandwich plate is analyzed in this example. Plate is composed from the cross-ply rigid face sheets, each of thickness t_f and the soft core of thickness t_c. Face sheets are made of Graphite-Epoxy T300/934 with following mechanical char-

Table 10.7: Comparison of natural frequencies (Hz) of the intact and delaminated (0/90/45/90)s square plate with different boundary conditions, using different numerical models

BC	Source	Crack	Mode					
			1	2	3	4	5	6
FFFF	Ju et al.	-	73.31	202.59	243.37	264.90	306.34	444.80
	FSDT [37]	a/2	72.94	202.07	241.18	258.51	304.29	421.99
	Present	-	89.68	201.42	259.61	263.38	327.58	478.18
	6 × 6 FE	a/2	89.66	200.27	248.93	256.67	317.52	442.25
CFFF	Ju et al.	-	41.35	60.66	221.52	258.72	286.78	407.98
	FSDT [37]	a/2	40.26	60.77	220.02	249.69	285.26	395.33
	Present	-	41.07	68.17	226.26	257.49	299.74	435.58
	6 × 6 FE	a/2	40.29	68.08	221.31	248.23	293.90	403.85
SSSS	Ju et al.	-	164.37	404.38	492.29	658.40	854.17	1046.20
	FSDT [37]	a/2	161.58	348.27	371.19	637.48	704.72	837.45
	Present	-	169.81	409.78	504.22	672.69	855.48	1044.71
	6 × 6 FE	a/2	167.04	347.88	374.62	611.08	653.97	750.39
CCCC	Ju et al.	-	346.59	651.51	781.06	1017.20	1195.40	1487.00
	FSDT [37]	a/2	334.67	579.43	653.25	851.27	1074.07	1108.80
	Present	-	346.81	643.44	777.93	982.16	1170.83	1412.03
	6 × 6 FE	a/2	316.88	529.34	554.81	783.80	893.91	947.52
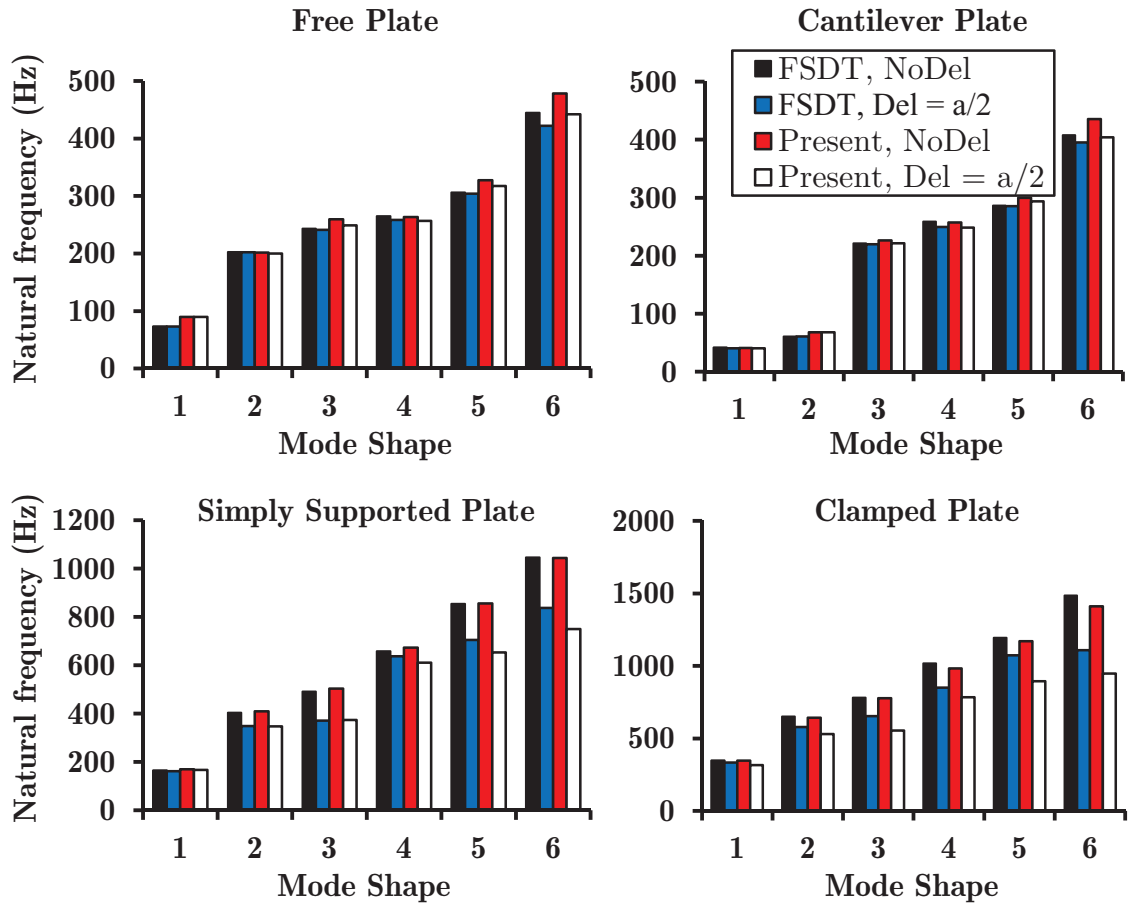
Figure 10.8: Natural frequencies (Hz) for intact and delaminated (0/90/45/90)s composite plates with different boundary conditions for the first six modes

acteristics: $E_1 = 131GPa, E_2 = E_3 = 10.34GPa, G_{12} = G_{23} = 6.895GPa, G_{13} = 6.205GPa, \nu_{12} = \nu_{13} = 0.22, \nu_{23} = 0.49, \rho = 1627kg/m^3$ [20]. Soft core is made of isotropic material with following mechanical characteristics: $E = 6.89MPa, G = 3.45MPa, \nu = 0, \rho = 1550kg/m^3$.

Results presented in Table 10.8 shows that excellent agreement is obtained using the proposed FE model, in comparison with the closed form solution (CFS) of Ćetković and Vuksanović [20]. Results are obtained using the reduced integration, and they are reliable both for the thick and thin plates. After the applicability of the proposed model for the intact plate is confirmed, a new parametric study is performed for delaminated plate, using the 4-node element, with 16×16 mesh. The goal was to study the influence of the delamination position through the thickness

Table 10.8: Non-dimenzionalized fundamental frequencies of symmetric intact simply supported (0/90/core/90/0) square sandwich plates with $t_c/t_f = 10$

a/h	Mode	ESL [64]	HSDT [64]	GLPT CFS [20]	Present; 9-node; 8×8 Mesh	Present; 4-node; 16×16 Mesh
	1,1	4.96	4.86	1.87	1.85	1.85
	1,2	8.19	8.02	3.29	3.23	3.25
	1,3	11.99	11.74	5.40	5.25	5.36
10	2,2	10.52	10.30	4.40	4.31	4.32
	2,3	13.75	13.47	6.30	6.12	6.21
	3,3	16.45	16.13	7.96	7.71	7.82
	1,1	15.55	15.51	12.11	11.95	11.97
	1,2	39.27	39.03	23.58	23.42	23.56
	1,3	73.50	72.76	36.31	36.21	36.71
100	2,2	55.15	54.76	31.15	30.96	31.05
	2,3	84.29	83.44	41.65	41.50	41.75
	3,3	106.59	105.38	49.98	49.50	49.42

Table 10.9: Non-dimenzionalized fundamental frequencies of $(0/90/core/90/0)$ simply supported square sandwich plate with $t_c/t_f = 10$ for different positions of square delamination of side length $a_{del} = a/2$

a/h	Mode	Intact	Mid-plane	Interface 1	Interface 2
	1,1	1.85	1.74	1.78	1.83
	1,2	3.25	2.82	2.89	3.18
	1,3	5.36	4.88	5.01	5.53
10	2,2	4.32	4.02	4.10	4.29
	2,3	6.21	5.86	5.96	6.18
	3,3	7.82	7.51	7.59	7.73
	Local 1	-	4.66	4.86	3.95
	Local 2	-	5.52	5.48	5.28
	1,1	1.85	1.74	1.78	1.83
	1,2	3.25	2.82	2.89	3.18
	1,3	5.36	4.88	5.01	5.53
100	2,2	4.32	4.02	4.10	4.29
	2,3	6.21	5.86	5.96	6.18
	3,3	7.82	7.51	7.59	7.73
	Local 1	-	4.66	4.86	3.95
	Local 2	-	5.52	5.48	5.28

on fundamental frequencies and mode shapes. Square delamination is located at the center of the plate. Three different positions of the delamination (of side length $a_{del} = a/2$) were studied: mid-plane delamination, delamination at the Interface 1 $(0/90/core//90/0)$ or at the Interface 2 $(0/90/core/90//0)$, where $//$ denotes the delamination position.

Non-dimenzionalized fundamental frequencies of SS square sandwich plate with the soft core for different delamination positions are presented in Table 10.9. It is obvious that if the delamination is closer to the mid-plane, fundamental frequency is more reduced, so the influence of delamination is higher. Also, if the plate is

delaminated, local mode shapes occur beside the global mode shapes. Global and local mode shapes for different delamination position are shown in Figure 10.9.
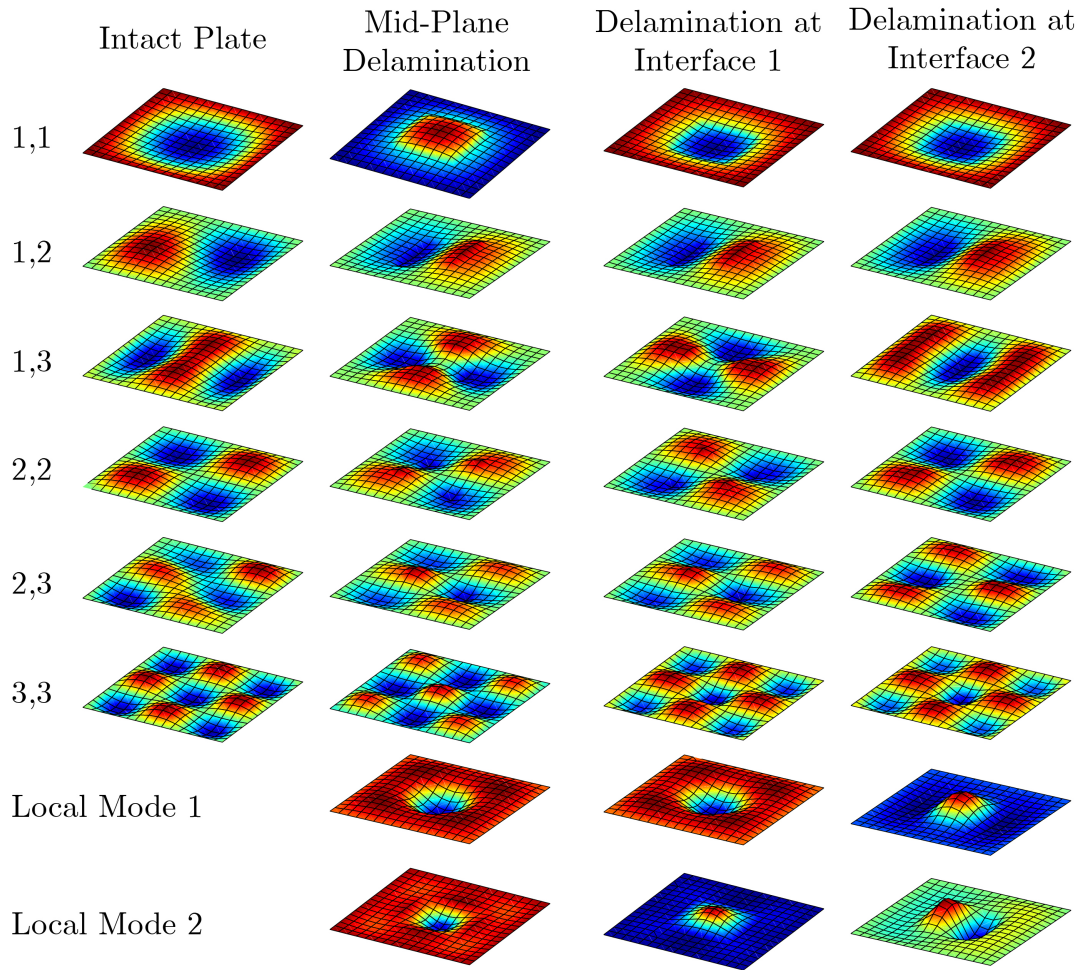
Figure 10.9: Global and local mode shapes of intact and delaminated sandwich plate with delamination in mid-plane, Interface 1 and Interface 2

From the performed numerical analysis it is obvious that delaminated segment of the plate oscillate independently from the intact rest of the plate with its own frequency. Generally, if the delamination is closer to the middle plane of the plate, local fundamental frequency is higher, because the segment which oscillates independently is of higher thickness than if the delamination is near the plate surface. On the other hand, in the thin plate situation (with $a/h = 100$, for example), it is shown that independent oscillation of delaminated segment can achieve second bending mode, too, as shown in Figure 10.9. This is the confirmation that delaminated segment can be treated as the independent plate connected with the rigid

intact rest of the plate, and it oscillates independently with its own frequency.

This example confirms that proposed model is able to accurately predict the natural frequencies both for the intact and delaminated sandwich and composite plates. Fundamental frequency of the delaminated segment can be derived in the same manner, too. This is very important feature, because it can serve as the basis for defining the new set of boundary conditions which can be incorporated on delamination boundaries. Accurate results obtained even for the coarse mesh shown that this method is not computationally expensive, which makes it the powerful tool for obtaining the fundamental dynamic characteristics of damaged laminar composites.

10.3   Linear Buckling

To derive the eigenvalue buckling problem and the corresponding matrices in the finite element model, energy approach in combination with the finite element formulation is used [9]. The following analysis assumes that a linear analysis gives a good approximation of the structural behavior up to the limit of stability.

If the prebuckling deformations can be accurately predicted by a linear solution (where nonlinear portion of the stiffness matrix is equal to zero), then for a fixed prescribed loading p_0 on the plate [9]:

$$\delta^2 \Pi = \left(\left[K^L \right] + \left[K^G \right] \right) \delta \{d\} = 0 \tag{10.3}$$

where $\{d\} = \{u \quad v \quad w\}^T$, and the second variation $\delta^2 \Pi$ indicates a critical point on the equilibrium path. Since a linear solution is used for the prebuckling deformations, the geometric stiffness matrix $\left[K^G \right]$ depends linearly on the load, for any load level λp_0 (where λ is the unknown constant). Then it follows:

$$\delta^2 \Pi = \left(\left[K^L \right] + \lambda \left[K^G \right] \right) \delta \{d\} = 0 \tag{10.4}$$

If any nontrivial perturbation $\delta \{d\}$ exists, then λp_0 is the buckling load, and the λ is obtained from the eigenvalue problem. The geometric stiffness matrix of the single layered finite element is given in Eq. (5.18), while its derivation is given in [9].

Critical Buckling Loads of Intact Plates

Example 10.3.1. The first example deals with the effects of incorporated shear deformation on critical buckling loads of intact laminated composite plates. Symmetric cross-ply lamination scheme and layers of equal thickness are adopted. The SS square plates are subjected to an in-plane uniform uniaxial compressive load.

Each layer is made of material with following mechanical characteristics: $G_{12}/E_2 = 0.6, G_{13}/E_2 = G_{23}/E_2 = 0.5, \nu_{12} = 0.25, \rho = 1.0$ [21]. The critical buckling load is presented in the non-dimenzionalized form $\overline{N} = \sigma_{cr}a^2/(E_2h^2)$. The effects of orthotropy and lamination scheme of simply supported cross ply laminated composite plates with $a/h = 10$ are presented in Table 10.10.

Table 10.10: Non-dimenzionalized critical buckling loads of the intact (0/90/0) simply supported square laminates with three and five orthotropic layers using different E_1/E_2 ratios

Source	Layers	E_1/E_2			
		3	10	20	30
Vuksanović - CLPT [21]		5.5738	11.4920	19.7120	27.9360
Owen and Li - Refined [38]		5.4026	9.9590	15.3201	19.6872
Vuksanović - HSDT [21]	3	5.3587	9.7133	14.5935	18.3890
Noor - 3D Elasticity [30]		5.3044	9.7621	15.0191	19.3040
Present (9-node; 5×5 FE)		5.3910	9.8427	14.9138	18.9099
Present (4-node; 10×10 FE)		5.4287	9.8989	14.6739	18.9684
Vuksanović - CLPT [21]		5.7538	11.4920	19.7120	27.9360
Owen and Li - Refined [38]		5.4208	10.1609	15.9976	20.9518
Vuksanović - HSDT [21]	5	5.3746	9.9714	15.4913	20.0732
Noor - 3D Elasticity [30]		5.3255	9.9603	15.6527	20.4663
Present (9-node; 5×5 FE)		5.3862	10.0001	15.5397	20.1323
Present (4-node; 10×10 FE)		5.4238	10.0593	15.6115	20.2039

Example 10.3.2. In the second example, simply supported sandwich plate loaded by uniformly distributed normal pressure N_x is analyzed. Plate is composed from cross-ply face sheets, each of thickness t_f, and the soft-core. Overall plate thickness is h. Plate has symmetric (0/90/0/90/0/core/0/90/0/90/0) stacking sequence. Sandwich plate is made of material with following mechanical characteristics [20]: For the face sheets: $E_{1f}/E_{2f} = 19, E_{2f} = E_{3f}, G_{12f}/E_{2f} = G_{13f}/E_{2f} = 0.52, G_{23f}/E_{2f} = 0.338, \nu_{12f} = \nu_{13f} = 0.32, \nu_{23f} = 0.49$, while for the soft-core: $E_1/E_{2f} = 3.2 \times 10^{-5}, E_2/E_{2f} = 2.9 \times 10^{-5}, E_3/E_{2f} = 0.4, G_{12}/E_{2f} = 2.4 \times 10^{-3}, G_{13}/E_{2f} = 7.9 \times 10^{-2}, G_{23}/E_{2f} = 6.6 \times 10^{-2}, \nu_{12} = 0.99, \nu_{13} = \nu_{23} = 0.3 \times 10^{-5}$. The critical buckling loads are presented in non-dimenzionalized form: $\overline{N_x} = N_{cr}b^2/(E_{2f}h^3)$.

Table 10.11: Non-dimenzionalized critical buckling loads of the intact simply supported (0/90/0/90/0/core/0/90/0/90/0) square sandwich plates with different geometries, using different t_f/h ratios

Source	a/h	t_f/t_c			
		0.025	0.050	0.075	0.100
Noor et al. - 3D Elasticity [30]		2.2081	3.7385	4.8307	5.6721
Sarath Baby et al. - FSDT [152]		2.2043	3.8662	5.2650	6.4930
Sarath Baby et al. - HSDT [152]	10	2.2122	3.7499	4.8643	5.7100
Ćetković et al. [20]		2.2639	3.7649	4.8302	5.6255
Present (4-node; 10 × 10 FE)		2.2766	3.7795	4.8431	5.6357
Present (9-node; 5 × 5 FE)		2.2642	3.7653	4.8305	5.6258
Noor et al. - 3D Elasticity [30]		2.5534	4.6460	6.4401	7.9352
Sarath Baby et al. - FSDT [152]		2.5437	4.7128	6.6156	8.2984
Sarath Baby et al. - HSDT [152]	20	2.5536	4.6756	6.4528	7.9512
Ćetković et al. [20]		2.5660	4.6817	6.4428	7.9184
Present (4-node; 10 × 10 FE)		2.5854	4.7136	6.4839	7.9656
Present (9-node; 5 × 5 FE)		2.5667	4.6822	6.4439	7.9196

From the results given in Table 10.11, it is obvious that the proposed model gives the accurate prediction of the critical buckling load, in comparison with the

close form solution of Ćetković et al.[20] and 3D elasticity solution of Noor et al. [30]. The accuracy is achieved even for the coarse mesh of 5×5 quadratic layered finite elements and the applicability of the proposed model for the intact plates is confirmed.

Critical Buckling Loads of Delaminated Plates

Example 10.3.3. The simply supported square 5-layer $(0/90/0/90/0)$ cross-ply laminated composite plate with layers of equal thickness is investigated. The plate is subjected to an in-plane uniform uniaxial compressive loading.

Each layer is made of material with following mechanical characteristics [21]: $G_{12}/E_2 = 0.6, G_{13}/E_2 = G_{23}/E_2 = 0.5, \nu_{12} = 0.25, \rho = 1.0$, while the critical buckling loading is presented in non-dimenzionalized form: $\overline{N} = \sigma_{cr}a^2/(E_2h^2)$.

The results of the parametric study are shown in Figure 10.10. Two cases of delaminated interface were examined and compared with the results for the midplane delamination. Centrally located square delamination of maximum area of 25% of the plate area was investigated. In Figure 10.10, Interface 1 represents $(0/90/0//90/0)$ delamination (where // denotes the delamination position), while Interface 2 represents $(0/90/0/90//0)$ delamination.
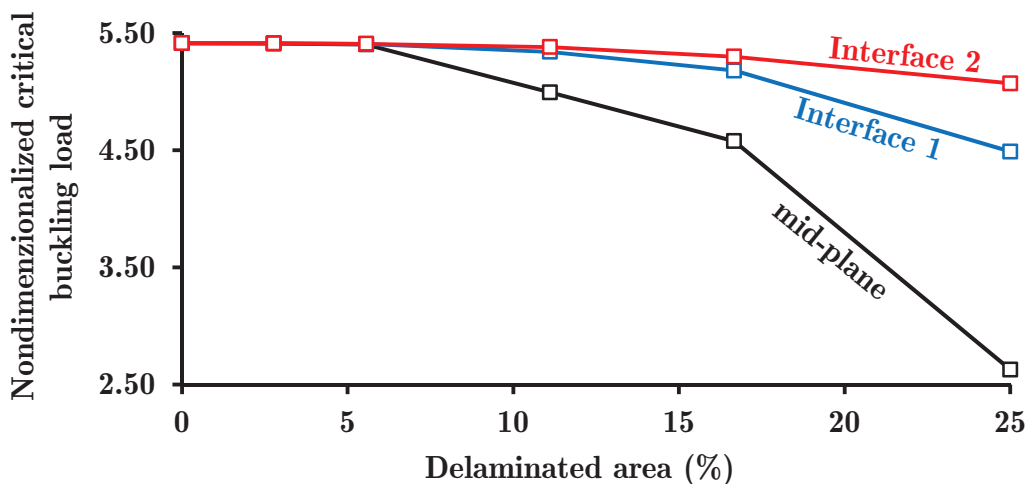

Figure 10.10: Critical non-dimenzionalized buckling loads for different delamination interfaces and different delamination positions in $(0/90/0/90/0)$ cross-ply laminated composite plate

From Figure 10.10 it is obvious that delaminated area up to the 6% of the plate area does not reduce the critical buckling load. For the mid-plane delamination, after increasing of the delaminated area, critical buckling load decreases down to 48.6% of the critical buckling load of the intact plate. If the delamination is located near the plate surface, it has the smaller influence on the results, because the intact rest of the plate is stiff enough to hold up to 82.9% or 93.7% of the critical buckling load for the delamination at the Interface 1 or at the Interface 2, respectively. On the other hand, delaminated segment is too small to buckle independently from the intact rest of the plate. Using the proposed numerical model, it is very easy to calculate the critical buckling loading for the damaged plate, with the delamination of arbitrary shape or arbitrary position through the plate thickness.

Example 10.3.2. The simply supported 11-layer (0/90/0/90/0/core/0/90/0/90/0) soft-core sandwich plate with rigid cross-ply face sheets was studied here to investigate the influence of delamination size and position on critical buckling loads. The plate is subjected to an in-plane uniform uniaxial compression. Three delaminated interfaces and two face-to-core-thickness ratios (t_f/t_c) were examined and compared.

Centrally located square delamination of maximum area of 25% of the plate area was considered. In Figure 10.11, Interfaces 1, 3 and 5 represent (0/90.../0/core//0/90.../0), (0/90.../0/core/0/90//0/90/0) and (0/90.../0/core/0/90/0/90//0) delaminations, respectively (where // denotes the delamination position).

The results of the parametric study are shown in Figure 10.11. The critical buckling loads are presented in non-dimenzionalized form: $\overline{N_x} = N_{cr}b^2/(E_{2f}h^3)$.

From the results shown in Figure 10.11 it is obvious that delaminated area up to the 6% of the plate area does not reduce the critical buckling loading, in all examined cases. For delamination located at Interface 1, uniaxially compressed sandwich plate loses the stability after the increasing of delamination area above the 6% of the plate area. The reason is that the rest of the plate does not have the enough in-plane stiffness, because the intact rest of the plate is composed from the face sheet at the bottom and the soft-core, while the face sheet at the top of the plate buckles independently.
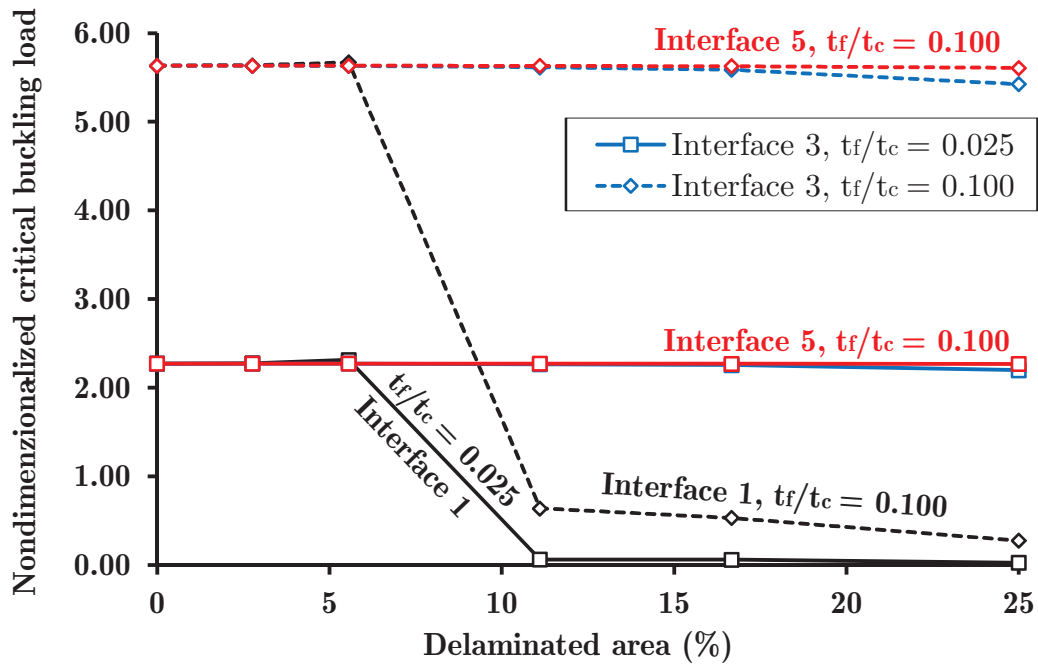
Figure 10.11: Critical non-dimenzionalized buckling loads for different delamination interfaces and different delamination sizes in sandwich plate with $a/h = 10$ and $(0/90/0/90/0/core/0/90/0/90/0)$ stacking sequence

On the other hand, if the delamination is located at the Interfaces 3 or 5, the reduction of the critical buckling load is negligible, because the intact rest of the plate is stiff enough to carry about the 97% of the critical buckling loading of the intact plate. Global and local buckling modes of soft-core sandwich plate with mechanical characteristics shown above, with $t_f/t_c = 0.1$ and $a/h = 0.1$, with the delamination at Interface 1, are shown on Figure 10.12. It is obvious that local mode exists if the delamination area is bigger than 6%, as stated above.

10.4 Transient Analysis

Proposed methodology of obtaining the transient response through the analytical and numerical solutions was investigated on several examples presented in this chapter. Homogeneous initial conditions (zero displacements and velocities) were assumed in all cases. Whenever possible, the obtained results are compared with the
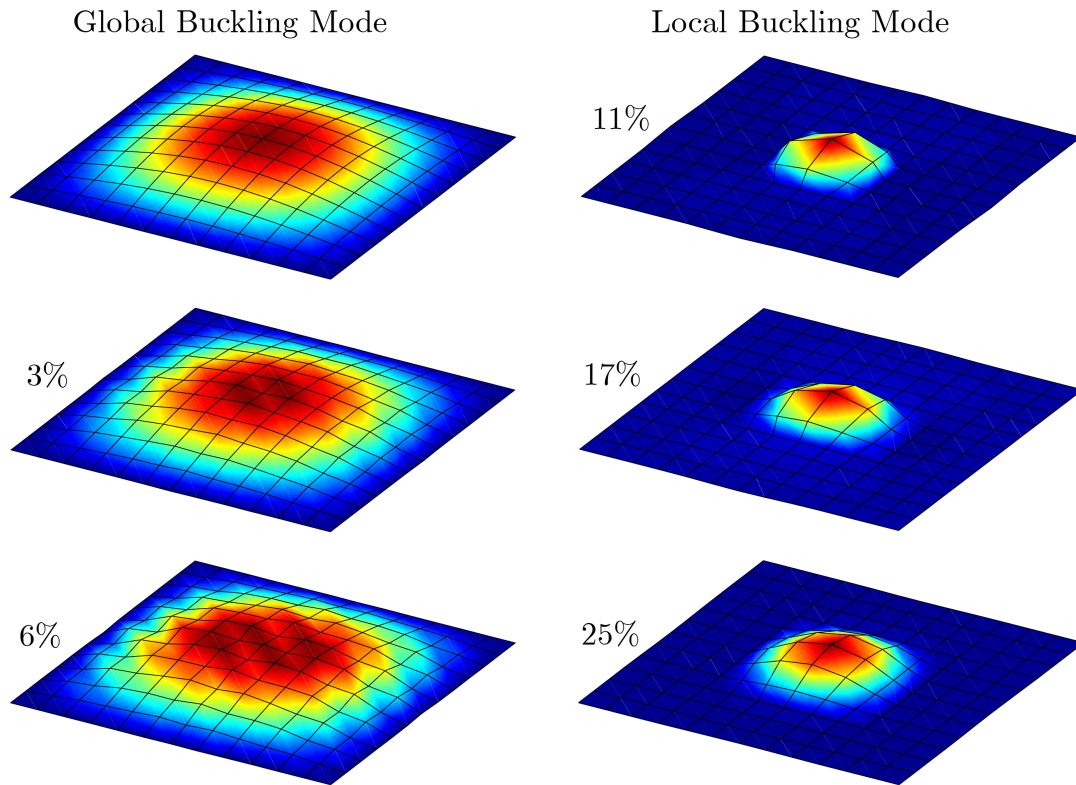
Figure 10.12: Global and local buckling modes of intact sandwich plate (top left corner) and sandwich plates with delaminations of different sizes in mid-plane

existing data from the literature. Some new results are presented as a benchmark for future investigations.

Linear and Geometrically Nonlinear Transient Analysis of Intact Plates

Example 10.4.1. In the preliminary calculation the influence of number of members in Fourier series on normalized transverse deflection is investigated. Simply supported cross-ply 2-layer laminate with $a = b = 25cm$ was examined and the analytical solution presented in **Chapter 4** is used for the calculation.

The following lamina properties are used: $E_1 = 52.5 \times 10^6 N/cm^2, E_2 = 2.1 \times 10^6 N/cm^2, \nu_{12} = 0.25, G_{12} = G_{13} = 0.5E_2, h = 1cm, \rho = 8 \times 10^{-6} Ns^2/cm^4$. The plate is subjected to the uniformly distributed loading q_0 in a form of the step pulse. Time increment is chosen as $\Delta t = 100\mu s$. Normalized center transverse deflection

Table 10.12: Normalized center transverse deflection at selective times, for different values of $m \times n$ members in Fourier series

$m \times n$	$t = 100\mu s$	200	300	400	500	600	700	800
1×1	0.4697	1.6270	2.8513	3.4860	3.1907	2.1239	0.8576	0.0708
3×3	0.4127	1.5855	2.8477	3.4173	3.1681	2.1080	0.7849	0.0667
5×5	0.4185	1.5864	2.8520	3.4202	3.1701	2.1130	0.7853	0.0727

is calculated as: $\overline{w} = w \cdot 100 E_2 h^3/(q_0 a^4)$. The results of the analytical solution are presented in Table 10.12.

Table 10.12 clearly shows that the number of members in double trigonometric series does not affect severely the transient response of laminated composite plate. According to this in all calculations it can be adopted that $m = n = 1$.

Example 10.4.2. Influence of the time increment was investigated numerically considering thin SS square cross-ply laminated composite plate composed of 4 layers in (0/90/0/90) stacking sequence. Side length of the plate is $a = 25cm$, while overall plate height is $h = 1cm$ ($a/h = 25$). All material layers are made of the material with the mechanical characteristics from the previous example.

Plate was exposed to the uniformly distributed step loading q_0 in the form of the step pulse, and solutions were obtained using both analytical and numerical methods. In the analytical solution, only the first member in the Fourier series is adopted. In the numerical solution, the plate was discretized using 10×10 4-node layered finite elements with reduced integration. Nondimenzionalized center transverse deflection is calculated as $\overline{w} = w \cdot 100 E_2 h^3/(q_0 a^4)$ and the time histories of the center transverse deflection are plotted in Figure 10.13.

From the conducted analysis it is obvious that increase of the time increment reduces the amplitude of oscillations, but increases the period, as showed in Figure 10.13. Maximum transient center transverse deflections in both cases are about two times that of the static center transverse deflection, as shown in Table 10.13.
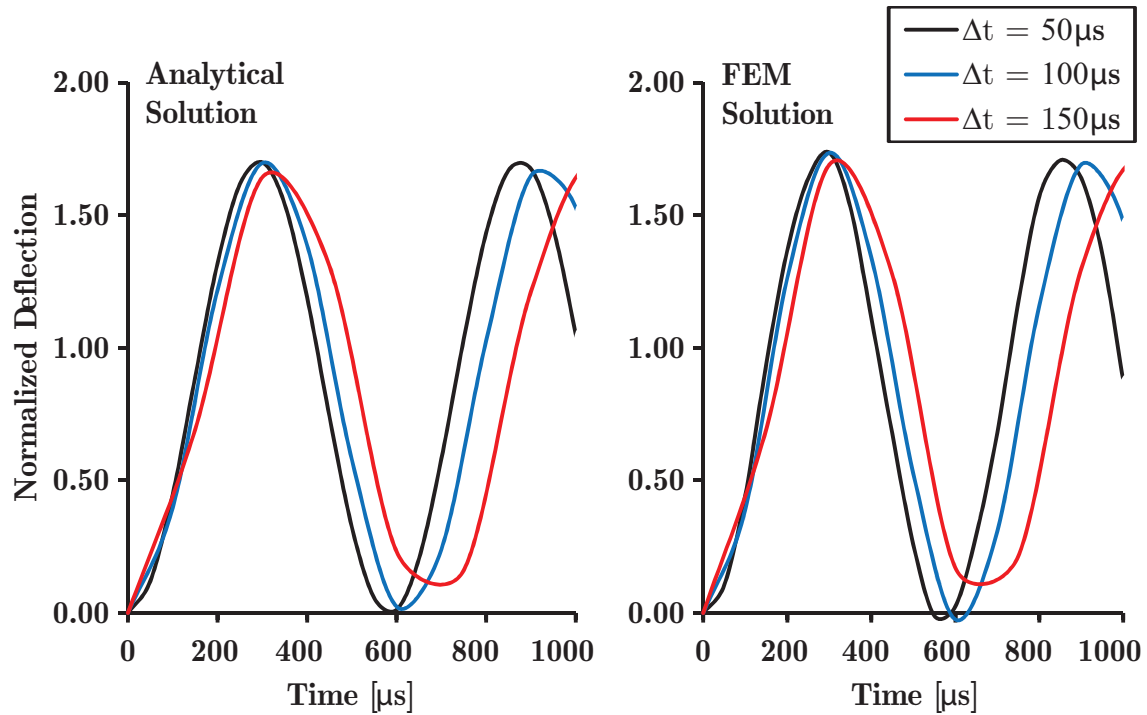
Figure 10.13: Analytical and FEM solutions for (0/90/0/90) laminate considering different time steps

Table 10.13: Comparison of normalized center transverse deflections in dynamic and static analysis, for different numerical models

Model	$\overline{w}_{max,dynamic}$	$\overline{w}_{max,static}$	Ratio
4-layer plate (Analytical)	1.6989	0.8936	1.9012
4-layer plate (FEM)	1.7360	0.8554	2.0295

Example 10.4.3. The influence of FE mesh refinement was investigated with 2 SS square cross-ply laminated plates made of 4 layers (0/90/0/90). Two side-to-thickness rations were used: $a/h = 5$ and $a/h = 25$, where $a = 25cm$ is the side length of the plate. All material layers are made of the material with the mechanical characteristics given in the previous examples.

Plates were exposed to the uniformly distributed step loading q_0 in the form of the step pulse. Time step of $\Delta t = 50\mu s$ was chosen in all calculations. The plate was discretized with 3 different mesh densities using 4-node layered finite elements with reduced integration. Nondimenzionalized center transverse deflection is calculated

as $\overline{w} = w \cdot 100 E_2 h^3 / q_0 a^4$.
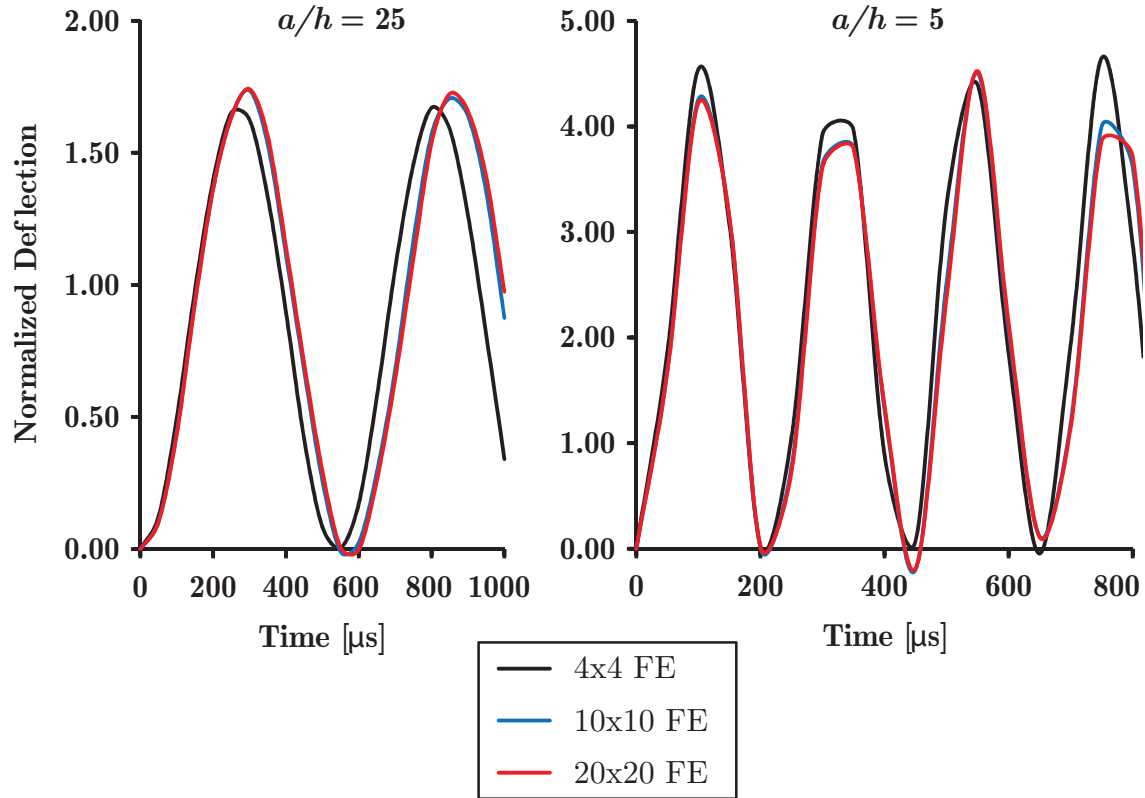
Figure 10.14: Nondimenzionalized deflection versus time for (0/90) laminate considering different mesh densities

Convergence of solution is reached with 10×10 FE mesh. Coarse mesh of 4×4 FE showed a little underestimation of the amplitude and the period in thin plate situation (Figure 10.14). In the thick plate situation coarse mesh overpredicted the amplitude of oscillations, and underpredicted the period slightly.

Example 10.4.4. The effect of the lamination scheme on the transient response of laminated structure is investigated using a cross-ply (0/90) laminates with different numbers of layers. Side length of the plate is $a = 25cm$, while overall plate thickness is $h = 1cm$ ($a/h = 25$). All material layers are made of the material with the mechanical characteristics given in the previous examples.

Plates were exposed to the uniformly distributed step loading q_0 in the form of the step pulse. Time step of $\Delta t = 50\mu s$ was chosen. In the numerical solution, the plate was discretized using 10×10 4-node layered finite elements with reduced

integration. Nondimenzionalized center transverse deflection is calculated as $\overline{w} = w \cdot 100 E_2 h^3 / q_0 a^4$ and plotted versus time in Figure 10.15, for the plate center. In
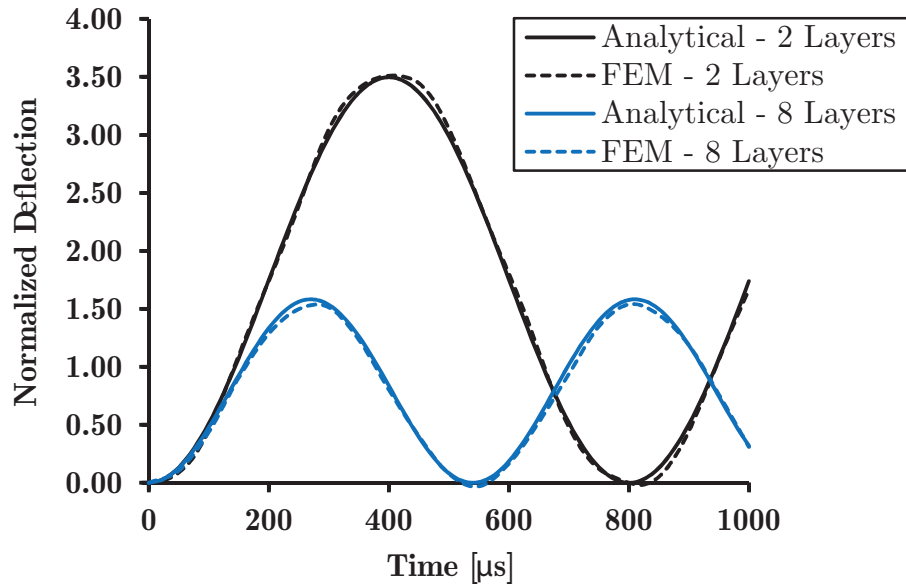
Figure 10.15: Normalized deflection versus time for cross-ply (0/90) laminates with $a/h = 25$, for different lamination schemes and different numerical models

addition, the time history of the nondimenzionalized normal stress $\overline{\sigma}_x = \sigma_x \cdot h^2 / (q_0 b^2)$ of the plate center, at the bottom of the laminate ($z = -h/2$) is plotted for different lamination schemes in Figure 10.16 ($\delta t = 10 \mu s$). The obtained results are compared with the analytical solution of Reddy [8], and excellent agreement was observed.

Figure 10.15 shows that reduction in the number of layers through the plate thickness leaded to the more flexible plate response it is increasing the amplitude as well as the period. By using more cross-ply layers through the same overall plate thickness, stiffer response is obtained. Very good agreement was obtained between analytical and numerical solution.

Finally, for the illustration, the stress distribution through the plate thickness for a $(0/90)_4$ laminate scheme is plotted for $t = 280 \mu s$ (the moment when the maximum normal stress σ_x is obtained, red lines in Figure 10.16), for $x = a/4, y = b/4$. The stress distribution is illustrated in Figures 10.17 and 10.18.

Example 10.4.5. The influence of different forcing functions which describe the
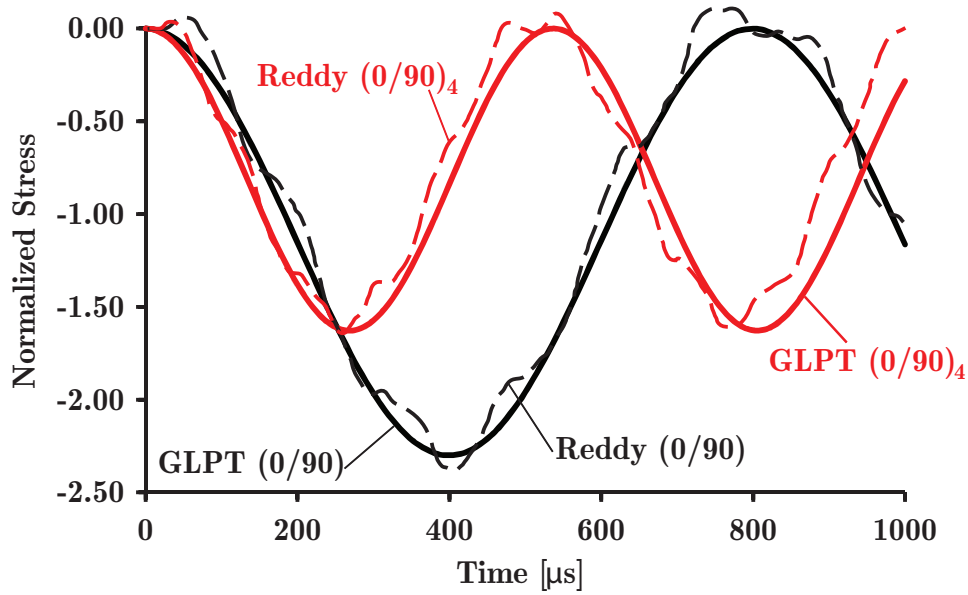
Figure 10.16: Normalized normal stress $\overline{\sigma}_x$ versus time for cross-ply (0/90) laminates with $a/h = 25$, for different lamination schemes and different numerical models
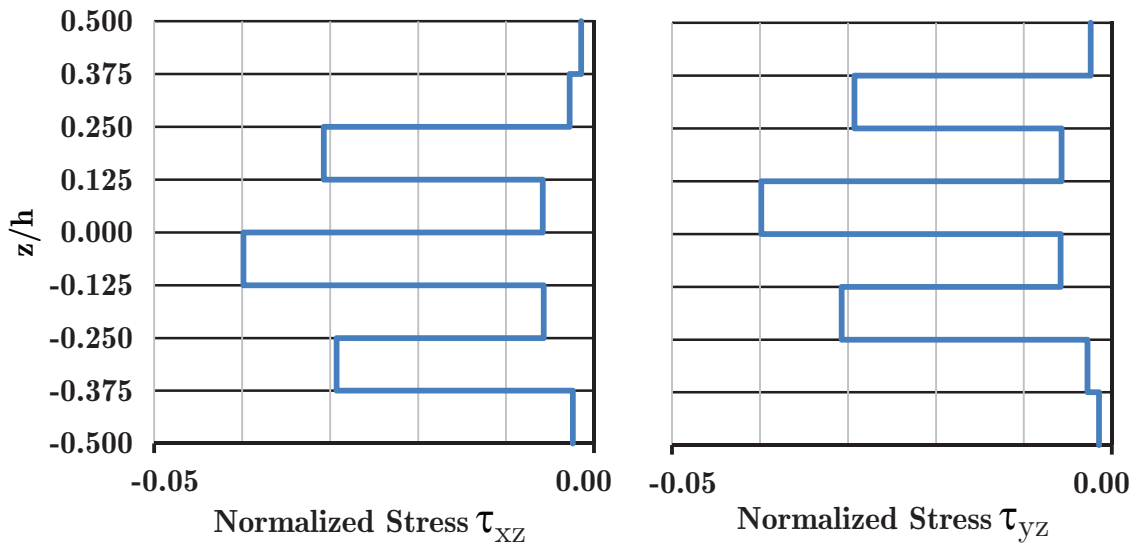
Figure 10.17: Variation of the normalized transverse shear stresses through a thickness of a eight-layer cross-ply $(0/90)_4$ laminate under uniformly distributed transverse load, in $x = a/4, y = b/4$

load change through time is analyzed in this example. Four different patterns of load change through the time are adopted as shown in Figure 10.19 and described as:

134
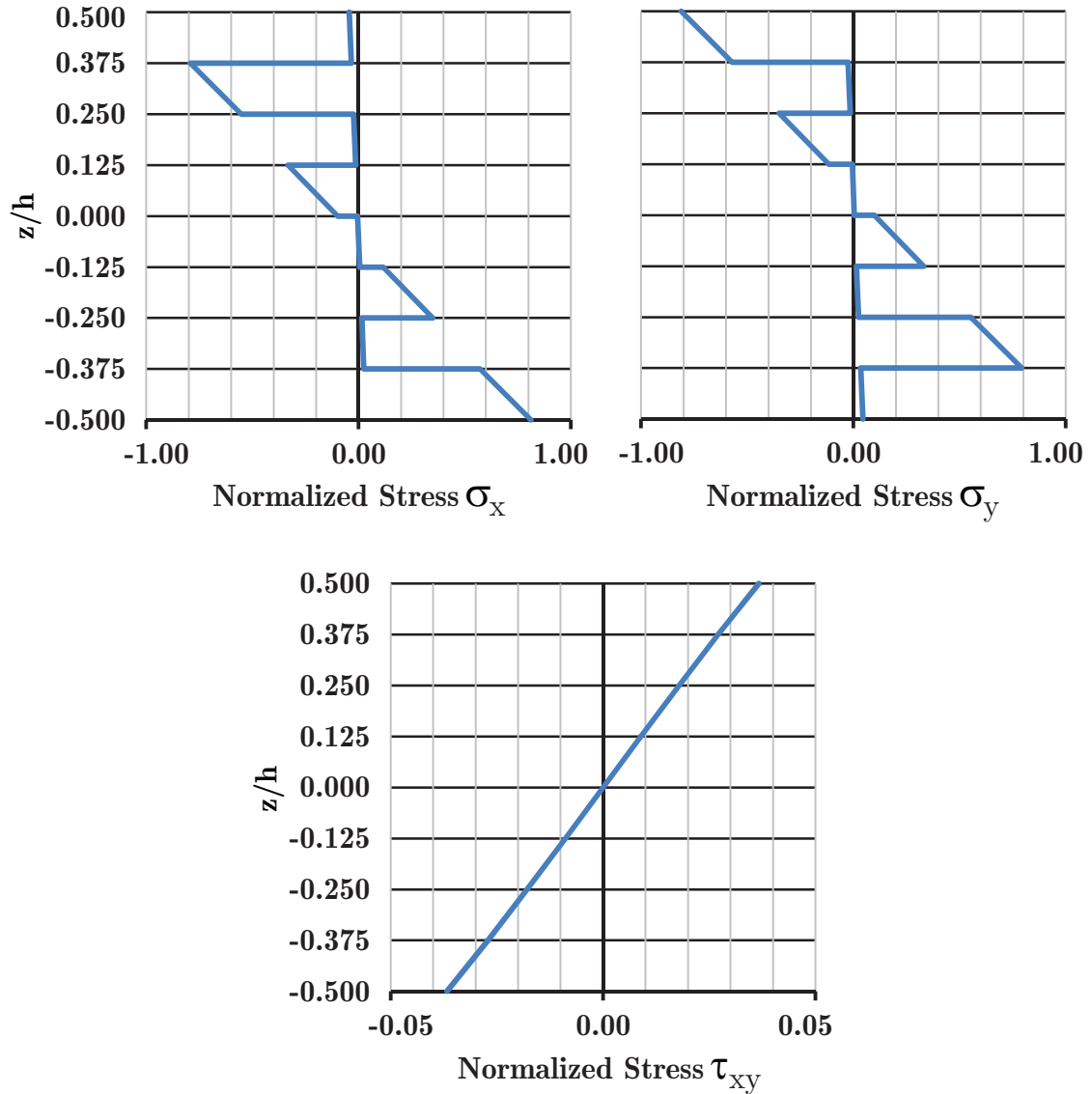
Figure 10.18: Variation of the normalized in-plane normal stresses through a thickness of a eight-layer cross-ply $(0/90)_4$ laminate under uniformly distributed transverse load, in $x = a/4, y = b/4$

1. Step Pulse: $F(t) = F_0$

2. Sine Pulse: $F(t) = F_0 \cdot sin(\pi t/T)$

3. Triangular Pulse: $F(t) = F_0 \cdot sin(1 - t/T)$

4. Exponential Pulse: $F(t) = F_0 \cdot e^{-\alpha t}$

F_0 represents the amplitude of the dynamic loading, t is the current time variable, T is the overall time in which loading acts and α is the damping parameter. For

135
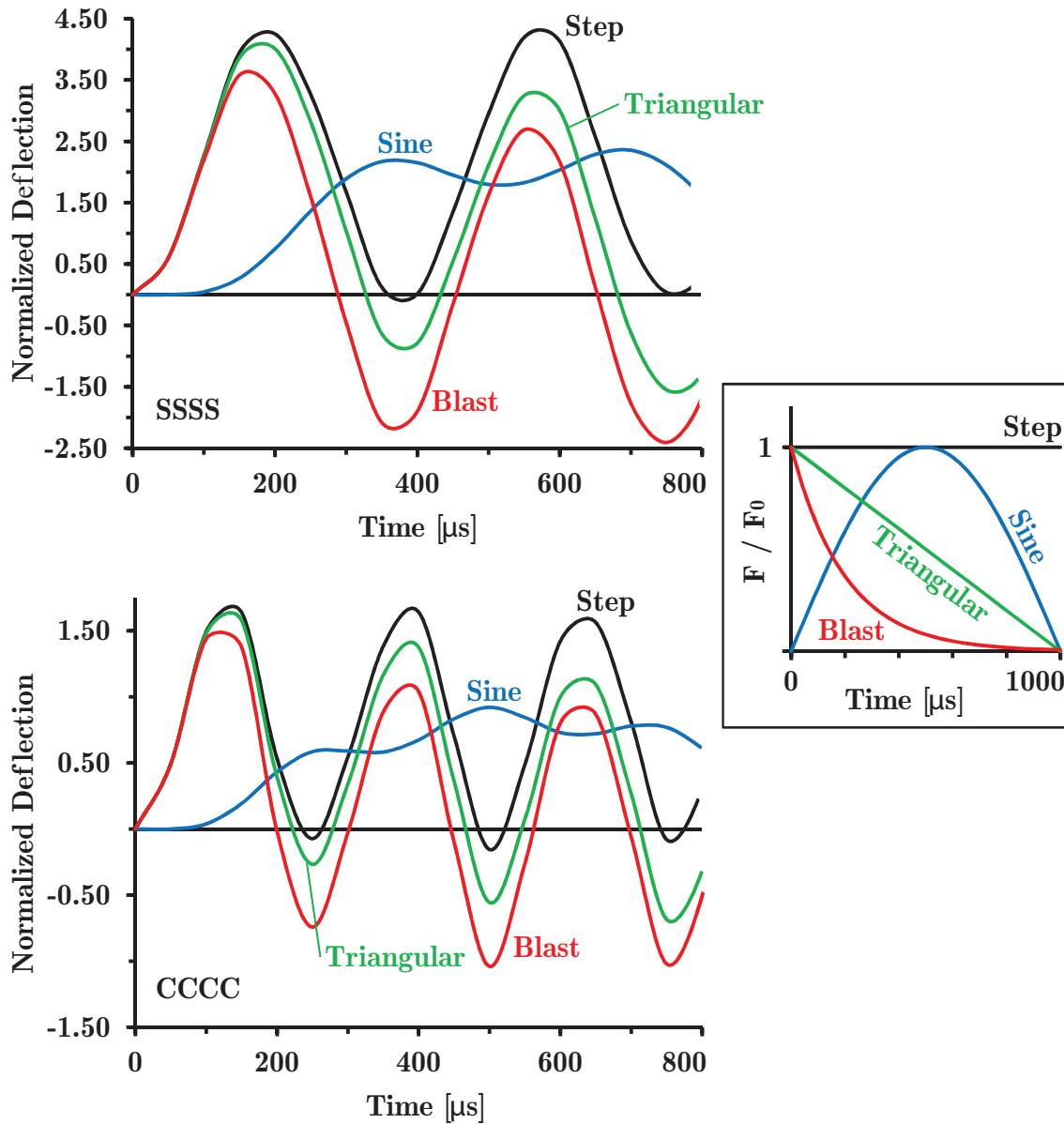
Figure 10.19: Normalized deflection versus time for (0/90) laminates with $a/h = 10$, different boundary conditions and different forcing functions

the purpose of this work, $\alpha = 0.005$ and $T = 1000\,\mu$s. Nondimenzionalized center transverse deflection is calculated as $\overline{w} = w \cdot 100E_2h^3/q_0a^4$.

The effect of the applied forcing functions on the transient response of laminated plate is investigated using a cross-ply (0/90) laminates with $a/h = 10$ and $a = b = 25$ cm. In all cases, uniformly distributed step loading was used. Results are obtained using FEM with 10×10 mesh, for SS and clamped laminated plates. Figure 10.19 illustrates the results of the calculation. Analytical solutions using Fourier

series and the convolution integral for simply supported Mindlin plates are in detail explained in previous work of Hinton and Vuksanović [153]. Also, FE results are given in work of Hinton and Vuksanović [154]. As stated in [153], triangular pulse is used to simulate a nuclear blast loading. The exponential pulse may be used to simulate a high explosive blast loading. Damping parameter α is adjusted to approximate the pressure curve from the blast test.

Example 10.4.6. This benchmark example [21] is concerned with a simply supported rectangular 3-layer composite plate, with one side length a and the other side length $b = \sqrt{a}$ and a side-to-thickness ratio $a/h = 0.1$. The top and bottom plies are identical, with $h^{(1)}/h = 0.1$, while the mid-layer has the thickness $h^{(2)}/h = 0.8$. Tho goal of this example is to illustrate the influence of the transverse shear deformation on the transient response of laminated composite plates.

The plate is subjected to a step pulse with uniformly distributed normalized loading $q_0 = 0.02$ over whole plate area. The following material parameters are assumed for orthotropic constitutive models of the top (bottom) and the middle layer: $E_1^{(1)} = 15, E_2^{(1)} = 7.878, G_{12}^{(1)} = 4.392, G_{13}^{(1)} = 2.6715, G_{23}^{(1)} = 4.458, \nu_{12}^{(1)} = 0.44, \rho^{(1)} = 5; E_1^{(2)} = 1, E_2^{(2)} = 0.5252, G_{12}^{(2)} = 0.2928, G_{13}^{(2)} = 0.1781, G_{23}^{(2)} = 0.2972, \nu_{12}^{(2)} = 0.44, \rho^{(2)} = 1$.

The plate is discretized by 10×10 4-node and, for comparison, with 9-node layered finite elements. The boundary conditions are prescribed along simply-supported edges as follows: at $x = 0$ and $x = a$: $v = w = v^I = 0$ and at $y = 0$ and $y = b$: $u = w = u^I = 0$.

The values of non-dimenzionalized center deflection $w_0 = w \cdot E_1^{(2)} h/q_0$ versus the non-dimenzionalized time $T_0 = T/a \cdot \sqrt{E_1^{(2)}/\rho^{(2)}}$ obtained from analyses using full and reduced integration are plotted and compared with the analytical results from the literature using different plate theories [21] (see Figure 10.20).

From Figure 10.20 it is obvious that ESL theories (CPT, FSDT and HSDT) underestimate the values of the transverse deflection, in comparison with the generalized laminated plate theory. It is obvious that incorporation of the transverse shear deformation reduces the natural frequency of the plate. While comparing dif-
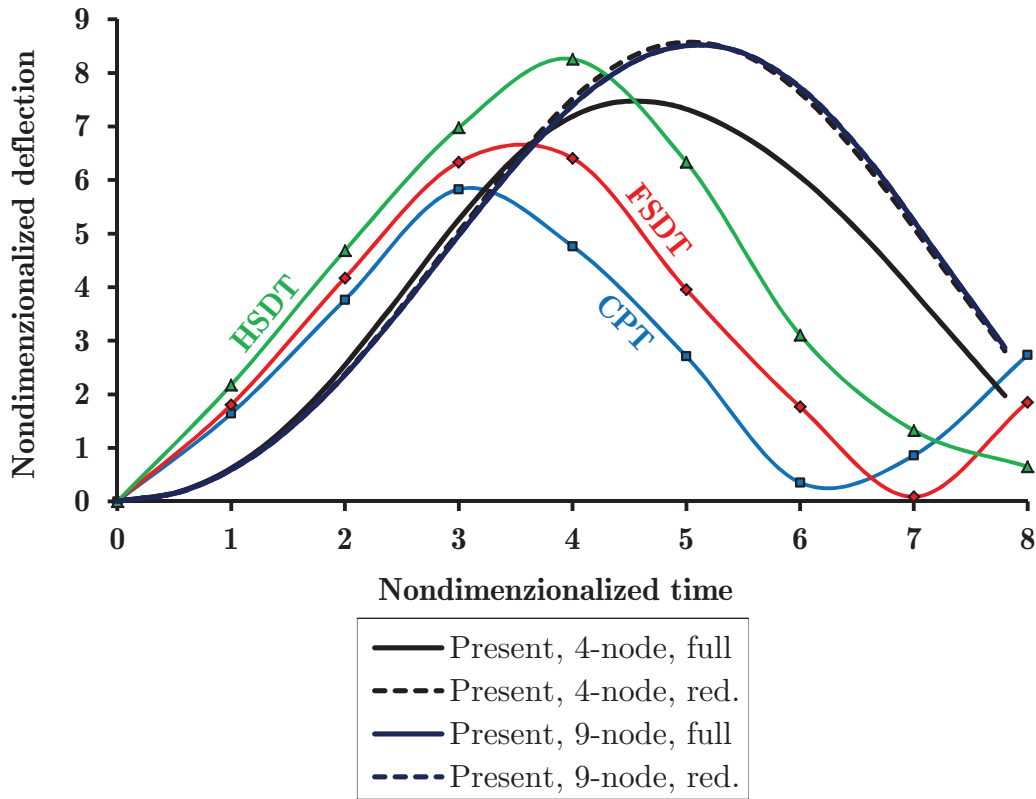
Figure 10.20: Time histories of center deflection using the proposed layered finite plate model in comparison with analytical solutions from different plate theories (CPT, FSDT and HSDT)

ferent layered finite element models, only in the case of full integration of 4-node element matrices, shear locking has occurred (solid black line in Figure 10.20).

Example 10.4.7. In the seventh benchmark example, the influence of the geometrical nonlinearity incorporated in the proposed finite plate model is investigated. A 8-layer simply supported intact square plate with a side length of $178mm$ and a total thickness of $1.58mm$ is discretized by 10×10 9-node layered finite elements with reduced integration. All plies are of 0° orientation. Eight laminas of equal thickness are assumed, with the following material parameters: $E_1 = 172.7GPa, E_2 = E_3 = 7.2GPa, G_{12} = G_{13} = 3.76GPa, G_{23} = 2.71GPa, \nu_{12} = \nu_{13} = 0.25, \nu_{23} = 0.33, \rho = 1566kg/m^3$ [65].

Uniformly distributed loading $q_0 = 1kN/m^2$ over the whole plate area is prescribed. The plate is subjected to step pulse loading lasting for $T = 5ms$. Time
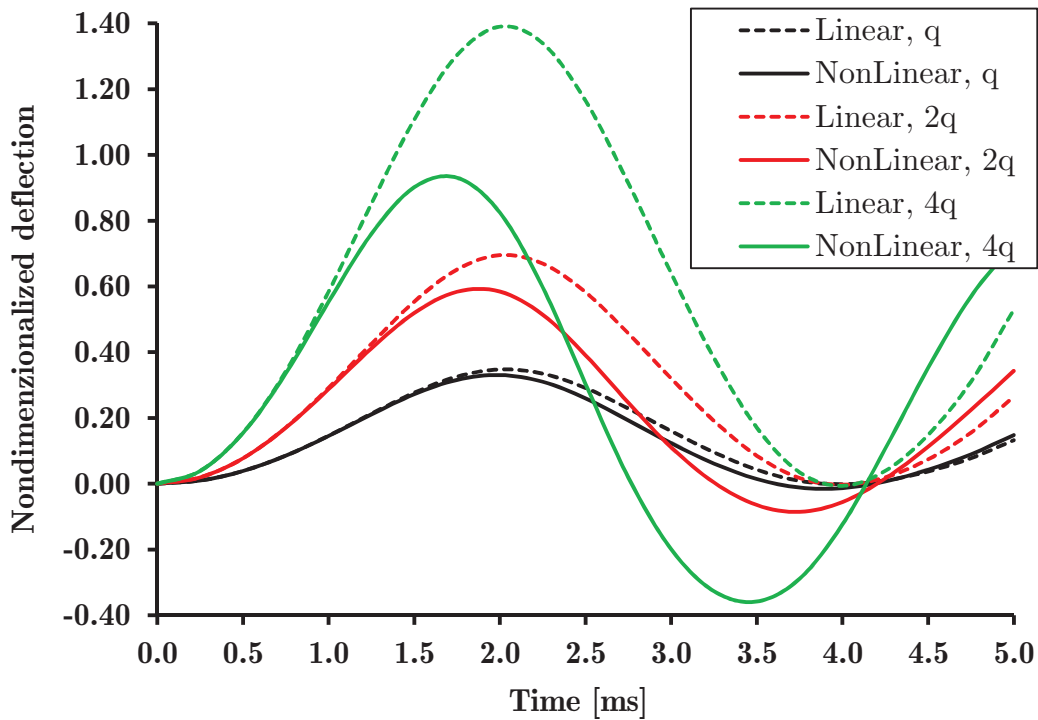
Figure 10.21: Linear and nonlinear transient responses of intact composite plate under different intensities of uniformly distributed step loads over whole plate area

increments $\Delta t = 0.25ms$ were chosen after computation of the natural frequencies of the laminate: $f_1 = 256.58Hz, f_2 = 349.51Hz$ and $f_3 = 579.75Hz$. The non-dimenzionalized center deflection is calculated as $w_0 = w \cdot E_1 h^3/q_0/a_4$ and the respective time histories are plotted in Figure 10.21.

Figure 10.21 illustrates the influence of load intensity and of the geometrical nonlinearity on the transient response of the intact composite plate. The linear and nonlinear responses are compared for three load intensities. It is shown that the amplitude and the period of oscillations decrease with increasing load levels. Furthermore, it is shown, that the influence of geometrical nonlinearity increases with increasing load levels. The values of negative peaks increase with the load [36].

Linear and Geometrically Nonlinear Transient Analysis of Delaminated Plates

Example 10.4.8. In this example the efficiency of the incorporated contact algorithm is investigated using the numerical model of SS square composite plate from Example 10.4.6. In the example, a centrally located square area of delamination covering 25% of the plate area is incorporated in the mid-plane.

Table 10.14: Natural frequencies (Hz) of the (0/0/0/0/0/0/0/0) simply supported square composite plates for different mesh densities

Mesh	f_1 (Hz)	f_2 (Hz)	f_3 (Hz)
Mesh 1 - Intact plate	256.58	349.51	579.75
Mesh 2 - Intact plate	255.15	345.65	555.08
Mesh 1 - Delaminated plate	254.40	322.61	503.40
Mesh 2 - Delaminated plate	253.81	323.91	500.12

The plate is discretized using two different finite element mesh densities: a 12×12 mesh using 4-node layered finite elements (Mesh 1) and a 6×6 mesh using 9-node (Mesh 2) finite elements with reduced integration. Uniformly distributed loading $q_0 = 1kN/m^2$ is prescribed. The plate is subjected to step pulse loading lasting for $T = 5ms$. Time increments and loading duration used in the Newmark's integration scheme are selected after the calculation of natural frequencies of the laminate, as given in Table 10.14.

The results from the analyses are evaluated based upon the normalized COD calculated as $\delta_0 = \delta \cdot E_1 h^3 \cdot 10^3 / q_0 / a^4$. The time history of the COD in the centroid of the delaminated area is plotted in Figure 10.22. As shown, contact algorithm successfully "corrects" the interlaminar penetration during the transient response of the delaminated composite plate both in the linear and geometrically nonlinear analysis. The influence of interlaminar penetration is more pronounced in the geometrically nonlinear response under step loading. The delaminated segment oscillates independently from the intact rest of the plate with its own frequency ($f_{del} \sim 1000Hz$),
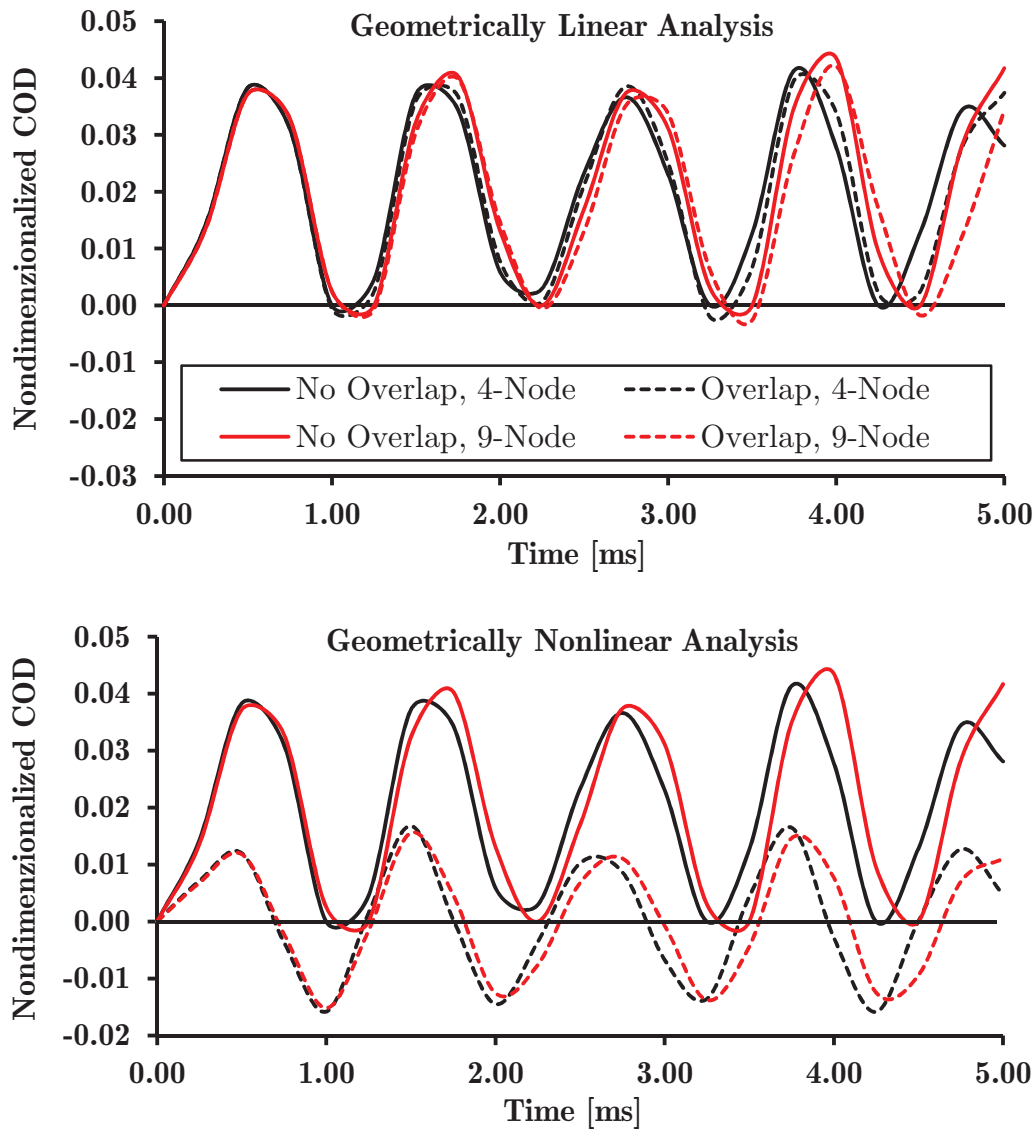
Figure 10.22: Temporal evolution of the normalized COD in the centroid of the delaminated area for two different discretizations

which is much higher than the natural frequency of the laminate.

Example 10.4.9. This example illustrates the linear and geometrically nonlinear transient response of a delaminated composite plate under step pulse. An 8-layer simply supported cross-ply (0/90/0/90/0/90/0/90) plate with the same geometry (side length a) and mechanical characteristics as used in Example 10.4.7. is analyzed. The influence of delamination size and position on transient response is investigated numerically for two cases: (a) mid-plane delamination of a square region considering

141

two different sizes ($a/3$ and $2a/3$) of the delaminated area as shown in Figure 10.23 and (b) delamination of a square region with side length $a/3$ located in three different positions along the height, as shown in Figure 10.23.
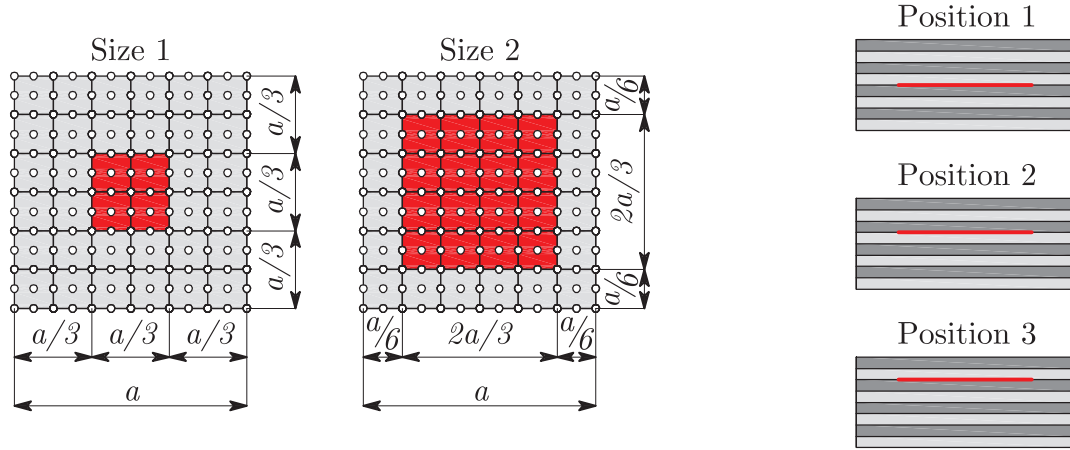
Figure 10.23: FE mesh with different sizes of a centrally located delamination within a square region in the mid-plane (left) and different positions of the delaminated zone along the plate thickness (right)

The plate is discretized by means of 6×6 quadratic layered finite elements with reduced integration. Uniformly distributed loading $q_0 = 4kN/m^2$ is prescribed over whole plate area. The plate is subjected to a step pulse loading. The total loading duration of $T = 10ms$ is discretized into time increments $\Delta t = 0.25ms$ using the Newmark's scheme for time integration. The natural frequencies for the analyzed plate are presented in Table 10.15. The normalized center transverse deflection of the plate is calculated as $\delta_0 = \delta \cdot E_1 h^3 \cdot 10^3 / q_0 / a^4$. The time history of the plate center is plotted in Figures 10.24 and 10.25.

Figure 10.24 illustrates the influence of the size of the delaminated zone on the response predicted by a linear and a geometrically nonlinear transient analysis of the delaminated composite plate. For the smaller size of the delamination area (Size 1) a marginal increase of the amplitude and period of the oscillations is observed for the linear analysis, while in the case of geometrically nonlinear analysis the period of oscillations is slightly reduced because of the added bending stiffness of the plate. The incorporated contact algorithm does not affect the linear response

Table 10.15: Natural frequencies (Hz) of the (0/90/0/90/0/90/0/90) SS square composite plate with different sizes and positions of the delaminated area

Size	Position	f_1 (Hz)	f_2 (Hz)	f_2 (Hz)
Intact Plate		255.15	345.65	555.08
Size 1	Mid-Plane	250.21	635.21	977.00
Size 2		237.76	428.47	535.05
	Position 1	250.21	635.21	977.00
Size 1	Position 2	250.23	636.33	666.17
	Position 3	249.69	667.41	808.77

severely, while in the geometrically nonlinear case this influence is more pronounced (solid blue line in Figure 10.24). For the larger size of the delaminated area (Size 2, see Figure 10.23), the amplitudes and the period of the oscillations of the laminate are significantly increased due to the reduced bending stiffness. The incorporated contact algorithm has only a minor effect in the linear transient response. However, in the geometrically nonlinear analysis, the delamination and its closure has a considerable influence on the time history of the transverse deflection (Figure 10.24). The results from the analysis considering contact of the delaminated layers (solid red line) differ considerably from the plots obtained for the analysis with consideration of contact (dashed line).

Figure 10.25 illustrates the influence of the delamination position on the results from a linear and a geometrically nonlinear transient analysis of the delaminated composite plate. In the linear analysis, changing the position of the delamination zone along the plate thickness does not have a large effect on the frequency of the oscillations. If the delamination is closer to the top of the plate, the amplitude of the oscillations is slightly reduced, because the thickness (and rigidity) of the intact rest of the plate increases. Changing the position of delamination in the geometrically nonlinear analysis is not affecting the transient response if the interlaminar penetration of delaminated layers is not prevented. However, if penetration is suppressed by

143
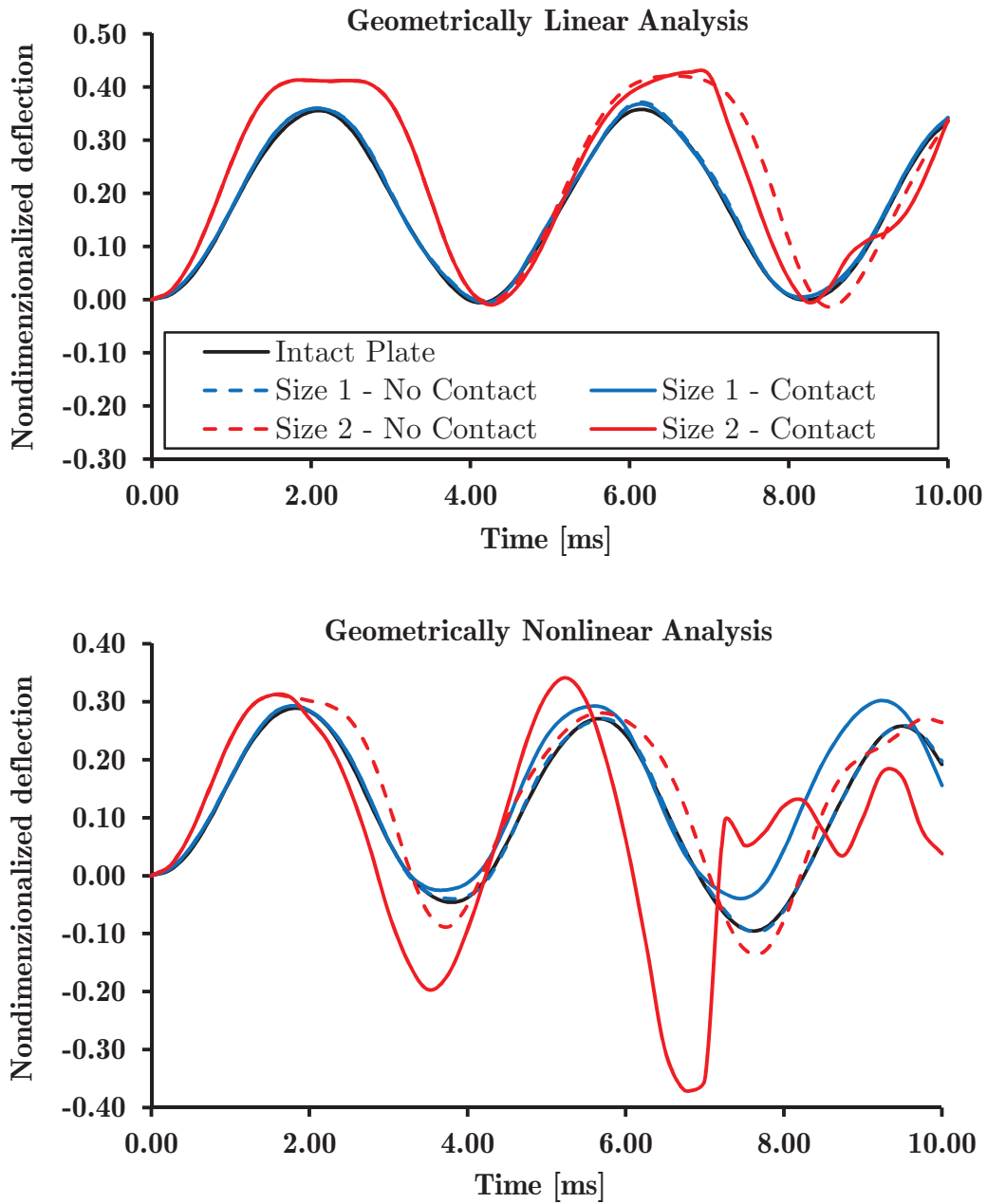
Figure 10.24: Temporal evolution of the central transverse deflection of the plate considering different sizes of the delaminated area

means of the activating the interlaminar contact algorithm, a large influence of the position of the delaminated region is observed (solid lines in Figure 10.25, down). The highest amplitudes are calculated for the delamination located in position 3.

Example 10.4.10. This benchmark example is concerned with a simply supported square 8-layer composite plate with $(0/90/45/90)s$ stacking sequence. The plate is

144
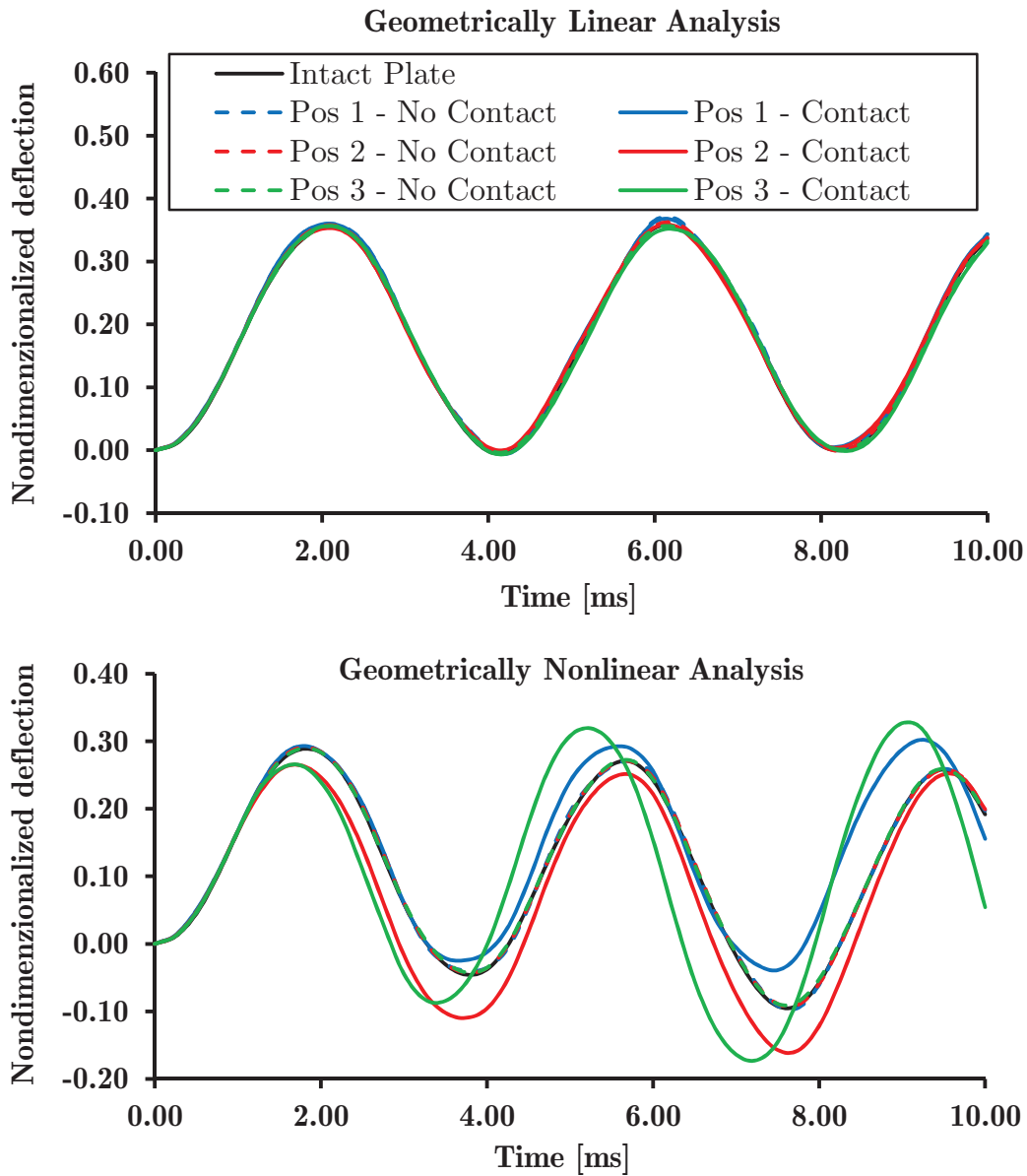
Figure 10.25: Temporal evolution of the central transverse deflection of the plate considering different positions of the delaminated area

analyzed to check the applicability of the proposed model for linear and geometrically nonlinear transient analysis of delaminated plates subjected to a triangular pulse loading. Also, the purpose of this example is to illustrate the capability of the proposed model to successfully replicate the independent motions of adjacent delaminated interfaces. The plate has a side length $a = 250mm$ and a height $h = 2.12mm$. Each layer has an identical thickness and material parameters: $E_1 = 132GPa, E_2 = 5.35GPa, G_{12} = G_{13} = 2.79GPa, \nu_{12} = \nu_{13} = 0.291, \nu_{23} = 0.30, \rho = 1446.2kg/m^3$.

Table 10.16: Natural frequencies (Hz) of the (0/90/45/90/90/45/90/0) simply supported square composite plate considering different delamination sizes and different delamination positions

Size	Position	f_1 (Hz)	f_2 (Hz)	f_2 (Hz)
Intact Plate		170.81	419.92	517.66
Size 1	Position 1	170.41	395.37	459.33
Size 2		151.14	294.41	297.61
Size 1	Position 2	170.29	398.61	460.99

The plate is subjected to a triangular pulse loading $q(t) = q_0(1 - t/T)$, with a uniformly distributed loading $q_0 = 10kN/m^2$ over whole area of the plate. The duration of the triangular pulse is $T = 15ms$. Time increments $\Delta t = 0.25ms$ are used in the Newmark's time integration. The plate is discretized using 12×12 linear layered finite elements with reduced integration. The previously explained contact algorithm is activated. The natural frequencies of the analyzed plate obtained for the different delamination scenarios are summarized in Table 10.16.

The normalized center deflections of selected delaminated interfaces are calculated as $\delta_0 = \delta \cdot E_1 h^3 \cdot 10^3 / q_0 / a^4$. The transient analyses are performed for delamination sizes 1 and 2 and delamination positions 1 and 2, according to Figure 10.23. The corresponding time histories of the central deflection of two adjacent layers 4 and 5 obtained from the different scenarios are plotted in Figures 10.26 and 10.27.

Figure 10.26 illustrates the influence of the delamination size on the results from linear and geometrically nonlinear transient analyses of delaminated composite plate. For the smaller size of the delaminated region (Size 1), the plate oscillates as one homogeneous structure with negligible relative displacements between adjacent layers 4 and 5 if linear analysis is employed (Figure 10.26). In the geometrically nonlinear analysis only a slightly larger influence of the delamination is observed for the small delamination size, resulting in only little relative displacements between the adjacent layers 4 and 5. For the larger size of the delaminated area (size 2), however, the amplitudes and the period of oscillations are considerably increased
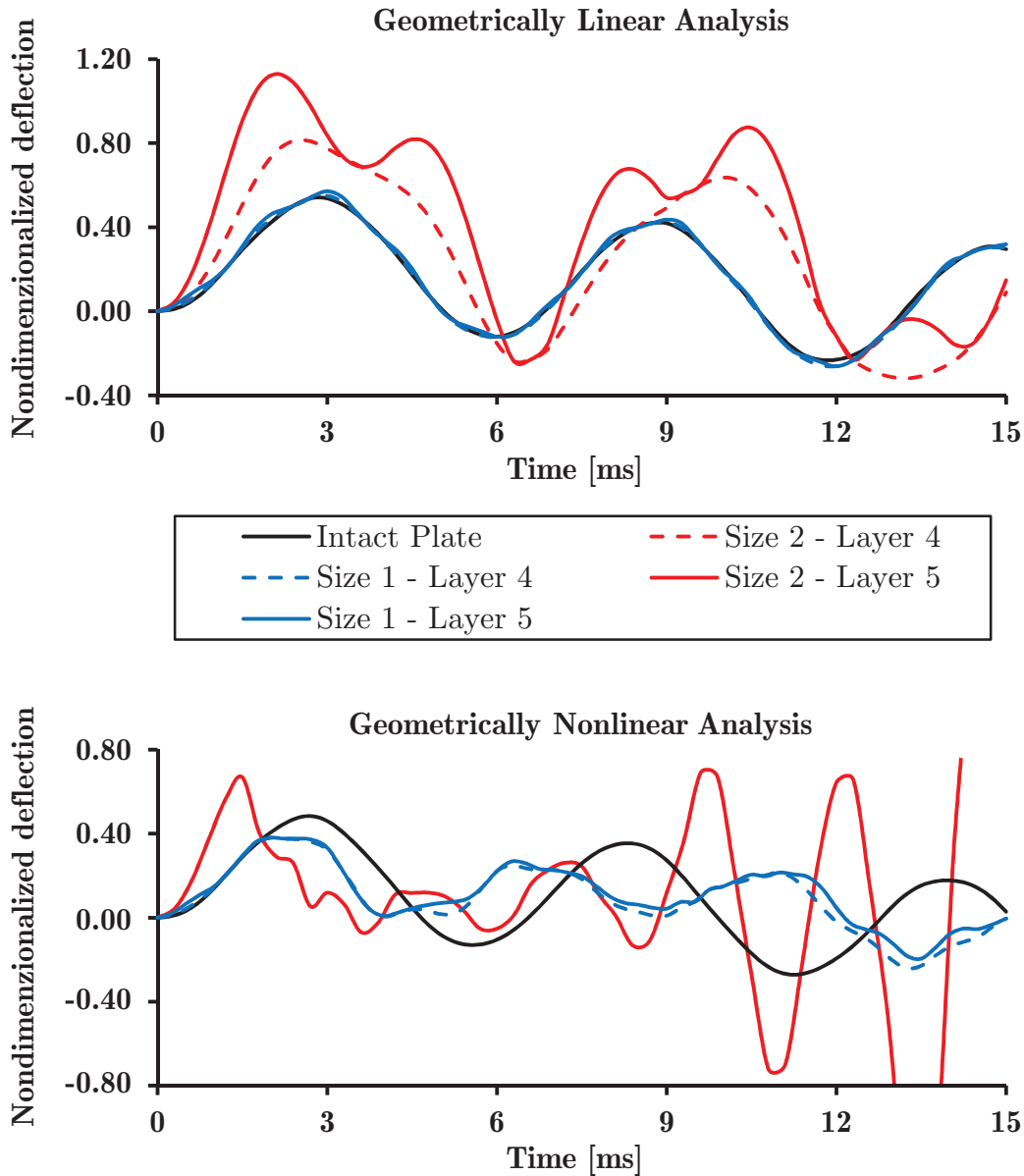
Figure 10.26: Temporal evolution of the central transverse deflection of two adjacent layers 4 and 5 considering different sizes of the delaminated area

(red lines in Figure 10.26). The mid-plane delamination of size 2 actually splits the laminate into two portions and reduces its bending stiffness dramatically. The crack opening displacement is the difference between the temporal central deflections of Layers 4-5 (the difference between the solid and dashed red lines in Figure 10.26).

Figure 10.27 illustrates the influence of the delamination position on the linear and geometrically nonlinear transient response of the investigated delaminated
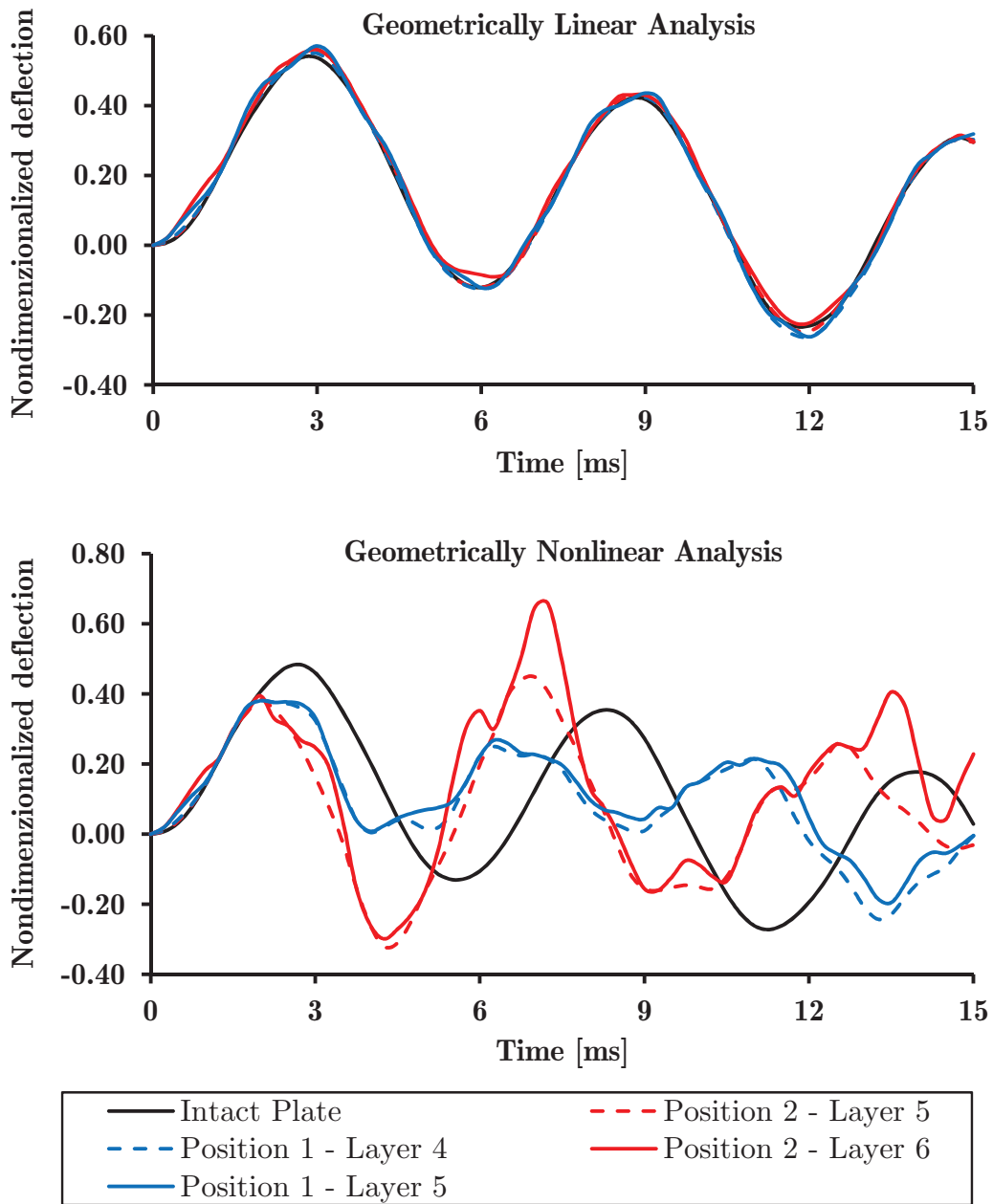
Figure 10.27: Temporal evolution of the central transverse deflection of two adjacent layers 4 and 5 considering different positions of the delaminated area

composite plate subjected to a pulse loading. In the linear analysis, changing the position of the delamination along the plate thickness does not lead to significant changes of the frequency and amplitudes of the oscillations. In the geometrically nonlinear transient response the position of the delaminated area has a large effect (Figure 10.27). The crack opening displacements are higher if the delamination is

closer to the top of the laminate (red lines in Figure 10.27). The transient response of the delaminated segment is characterized by contributions with higher frequency compared to the overall laminate.

Two previous examples demonstrate that the proposed model is capable to compute the transient response of laminated composite plates with embedded delaminated regions under different types of transient pulse loading. The model very efficiently replicates the motions of adjacent separated layers with reasonable computational cost. In the next example the same modeling strategy will be applied to the numerical analysis of the soft-core sandwich plates with embedded delamination.

Example 10.4.11. This benchmark example illustrates the linear and geometrically nonlinear transient responses of a delaminated sandwich plate under exponential blast pulse loading. The purpose of this example is to illustrate the capability of the proposed model to successfully represent the independent motions of adjacent delaminated interfaces in a sandwich panel. A five layer (0/90/core/0/90) anti-symmetric SS square sandwich plate is analyzed. The plate is composed from cross-ply rigid face sheets, with thickness t_f and a soft core with thickness t_c, where $t_c/t_f = 10$. The side length of the plate is $a = 250mm$ and its height is $h = 2.50mm$ $(a/h = 100)$.
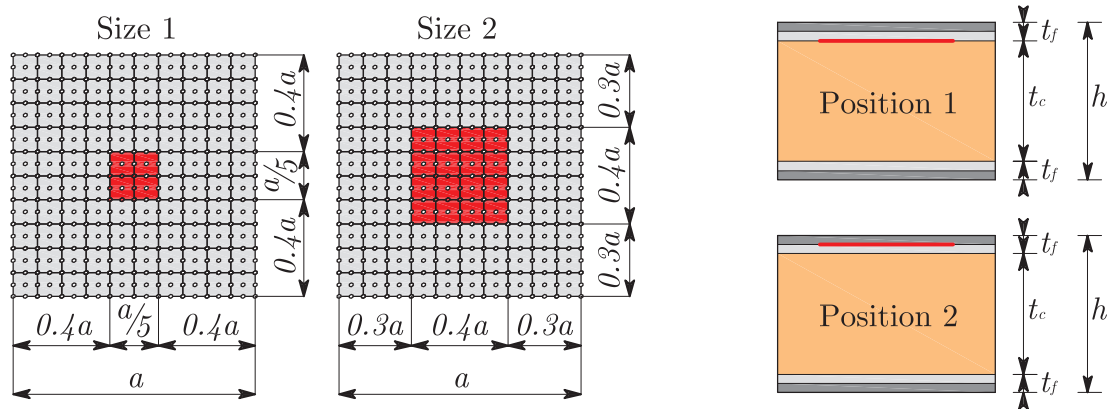
Figure 10.28: Soft-core sandwich plate with different sizes and positions of an embedded delamination zone

The face sheets are assumed to be made of Graphite-Epoxy T300/934 with the following mechanical characteristics: $E_{1,f} = 131GPa, E_{2,f} = E_{3,f} = 10.34GPa, G_{12,f} =$

Table 10.17: Natural frequencies (Hz) of the (0/90/core/0/90) simply supported square sandwich plate with different delamination sizes and different delamination positions

Size	Position	f_1 (Hz)	f_2 (Hz)	f_2 (Hz)
Intact Plate		191.72	375.82	496.92
Size 1	Position 1	190.67	334.46	489.78
Size 2		129.75	156.98	205.42
Size 1	Position 1	190.67	334.46	489.78
	Position 2	191.28	372.72	410.91

$G_{23,f} = 6.895 GPa, G_{13,f} = 6.205 GPa, \nu_{12,f} = \nu_{13,f} = 0.22, \nu_{23,f} = 0.49, \rho_f = 1627 kg/m^3$. For the isotropic soft-core the following material parameters are adopted: $E_c = 6.89 MPa, G_c = 6.895 MPa, \nu_c = 0, \rho_c = 1550 \, \text{kg/m}^3$ [20].

The plate is discretized using a 10×10 mesh of quadratic layered finite elements with reduced integration. Again, a uniformly distributed loading $q_0 = 1kN/m^2$ is prescribed over the whole plate area as an exponential pulse loading $q(t) = q_0 \times e^{-\alpha t}$. The duration of the exponential pulse loading is $T = 24ms$, using $\alpha = 150s^{-1}$ as a fictitious damping factor. The time increment was chosen as $\Delta t = 0.8ms$. The proposed contact algorithm is activated.

The normalized center transverse deflection is calculated as $w_0 = w \cdot E_{1,f} h^3 / q_0 / a^4$. The natural frequencies for the analyzed plate are summarized in Table 10.17 for the different delamination scenarios. The transient response obtained for the delamination sizes 1 and 2 and delamination positions 1 and 2 as illustrated in Figure 10.28 is plotted in Figures 10.29 and 10.30.

Figure 10.29 illustrates the influence of the position of the delaminated zone on the results of a linear and geometrically nonlinear transient analysis of the delaminated sandwich plate. The sandwich plate is highly vulnerable to embedded delamination between the soft-core and rigid face sheets, when subjected to exponential blast pulse loading (blue lines in Figure 10.29). The global amplitudes of the intact rest of the plate are increased because of the splitting. The crack opening

Geometrically Linear Analysis

Geometrically Nonlinear Analysis
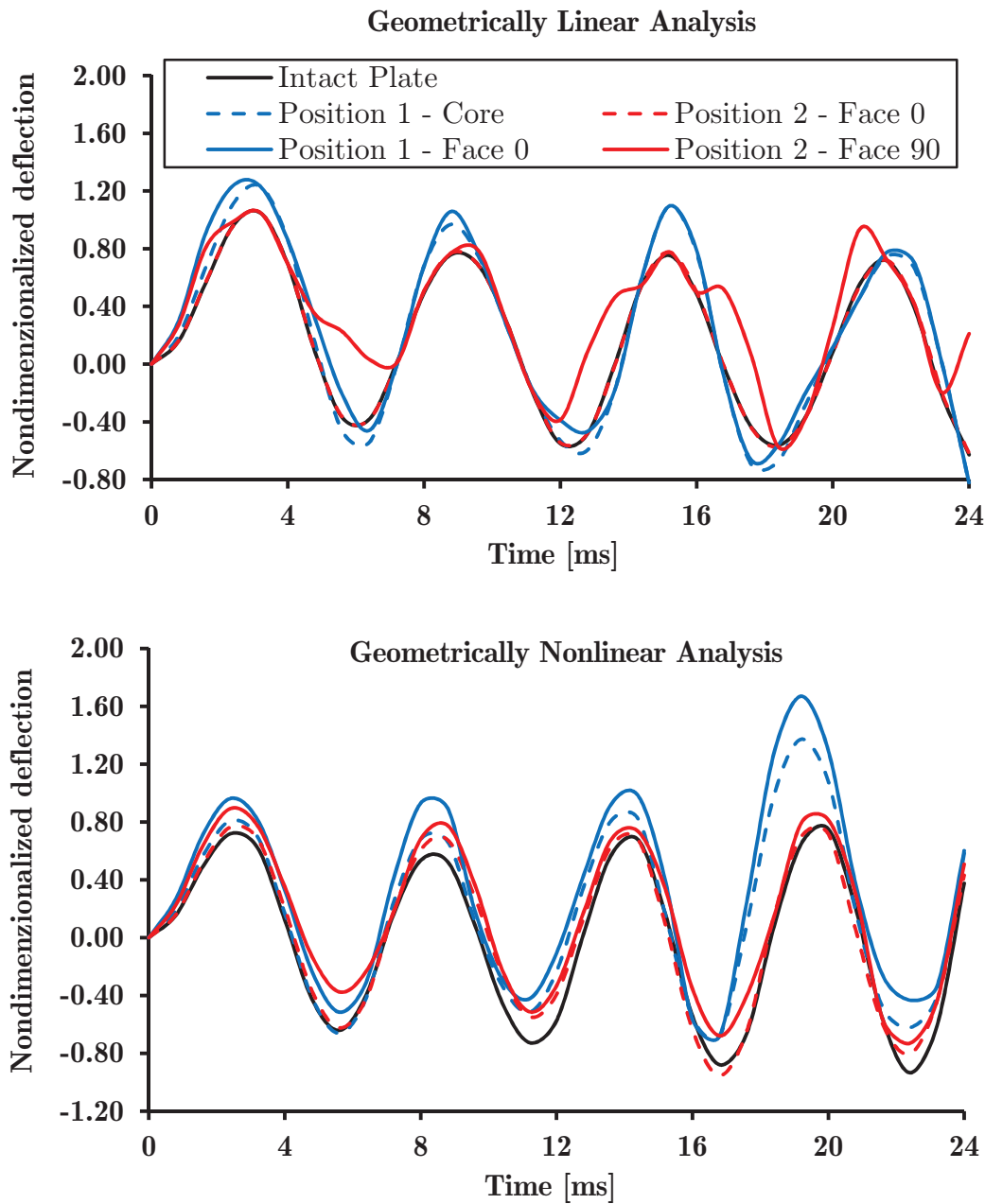
Figure 10.29: Temporal evolution of the central transverse deflection of two adjacent delaminated interfaces between the core and the face layer of a sandwich plate considering different positions of the delaminated area

displacements are small in the linear and slightly higher in the geometrically nonlinear analysis. On the other hand, if the delamination occurs between the (0/90) layers within the rigid face sheet, the global amplitudes of the intact rest of the plate are nearly the same as for the intact plate, because the undamaged part has the
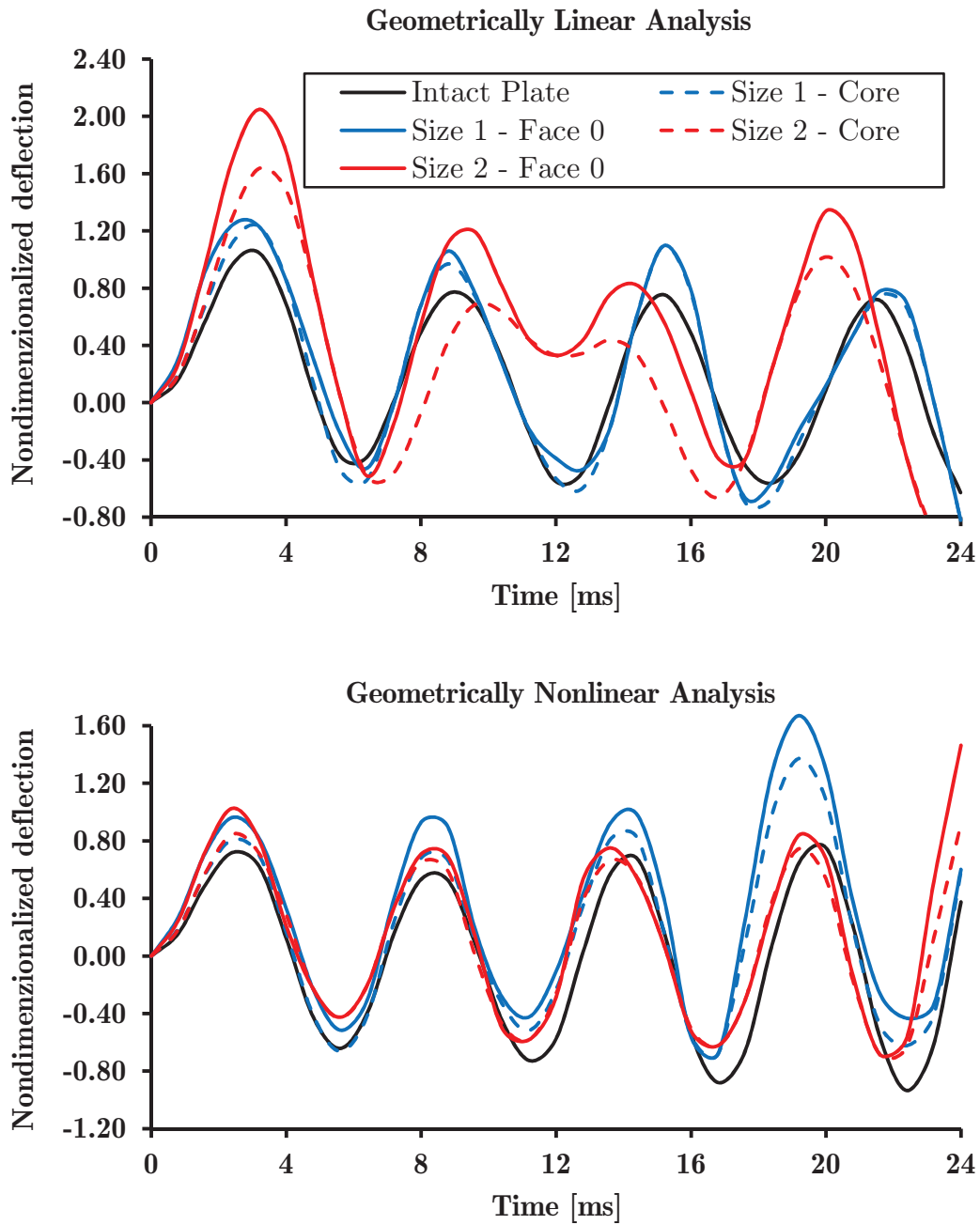
Figure 10.30: Temporal evolution of the central transverse deflection of two adja-
cent delaminated interfaces between the core and the face layer of
a sandwich plate considering different sizes of the delaminated area

more or less the same bending stiffness as the intact plate (red lines in Figure 10.29)
due to the small thickness of the face layers. However, the delaminated segment
(face 90) strongly oscillates locally with its own local frequency, causing relatively
large crack opening displacements (differences between solid and dashed red lines in

Figure 10.29).

Figure 10.30 shows the influence of the size of the delaminated zone on the linear and geometrically nonlinear transient response of the delaminated sandwich plate, with debonding assumed between the face sheet and the soft core. When the delamination area is small (blue lines in Figure 10.30), the face-core debonding is negligible and does not severely influence the overall linear transient response. The CODs are slightly higher in the geometrically nonlinear transient analysis (differences between solid and dashed blue lines in Figure 10.30, down). The highest amplitudes and crack opening displacements are reached after $16ms$, when the blast pulse intensity is almost decreased to zero and the free vibration phase is about to start. After increase of the delaminated area (red lines in Figure 10.30), however, the global linear plate motion significantly changes and becomes more complex, with increased amplitudes due to the reduction of the plate stiffness. The crack opening displacements are also increased (differences between solid and dashed red lines in Figure 10.30, up). In the geometrically nonlinear response of the sandwich plates (Figure 10.30, down), the added bending stiffness leads to a reduction of the crack opening displacements (differences between solid and dashed red lines in Figure 10.30, down) as compared to the linear case. The highest amplitudes and crack opening displacements are reached at $24ms$ corresponding (almost) to the end of blast pulse and start of free vibration phase.

Linear Transient Analysis of Plates with a Propagating Delamination

Example 10.4.12. In this benchmark example, the influence of the imposed delamination propagation algorithm on transient response of laminated composite plate is investigated numerically. A 4-layers fully clamped square plate with a side length $a = 600mm$ and a total thickness $h = 10mm$ ($h/a = 0.0333$) is considered. All layers are of equal thickness $h_k = 2.5mm$ and they are composed in the symmetric stacking sequence with the fibers orientations (0/90/90/0). The material parameters for all layers are taken from [107] and they correspond to the carbon/epoxy:

$E_1 = 109.34GPa$, $E_2 = E_3 = 8.82GPa$, $G_{12} = G_{13} = 4.32GPa$, $G_{23} = 3.20GPa$, $\nu_{12} = \nu_{13} = 0.342$, $\nu_{23} = 0.520$, $\rho = 1500kg/m^3$, $G_{Ic} = 306N/m$, $G_{IIc} = 632N/m$ and $G_{IIIc} = 817N/m$.
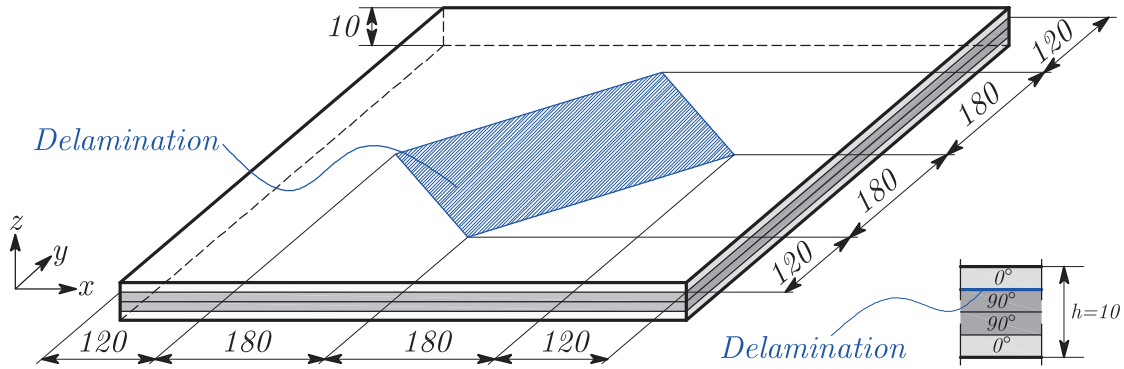
Figure 10.31: 4-layers $0^o/90^o/90^o/0^o$ laminated composite plate with embedded delamination

Uniformly distributed transverse pressure $q = 75kPa$ over the whole plate area is prescribed in the form of the step pulse lasting for $T = 16ms$, while the time increments are varied to check the influence of the time step: $\Delta t = 0.5ms$ and $\Delta t = 1.0ms$. The natural frequency of the intact plate is $f_1 = 259.062Hz$. A square delamination is prescribed between layer 3 and layer 4 (top layer of the plate), as shown in Figure 10.31.

The plate is discretized using 4-node quadrilateral finite elements with five different mesh densities. The average mesh size varies between 30 (Mesh 1) and 5 mm (Mesh 5). The numerical models are generated using again the GiD® Pre- and Post-processing program. Figure 10.32 shows the nodes corresponding to the prescribed embedded delamination zone as red nodes. The characteristic element matrices and vectors are calculated using the reduced Gauss-Legendre quadrature to avoid shear locking.

Influence of the time step and the incorporated algorithm for delamination propagation

In the first part of this example the influence of the time step for different scenarios in regards to the embedded delamination zone is checked. The plate is discretized
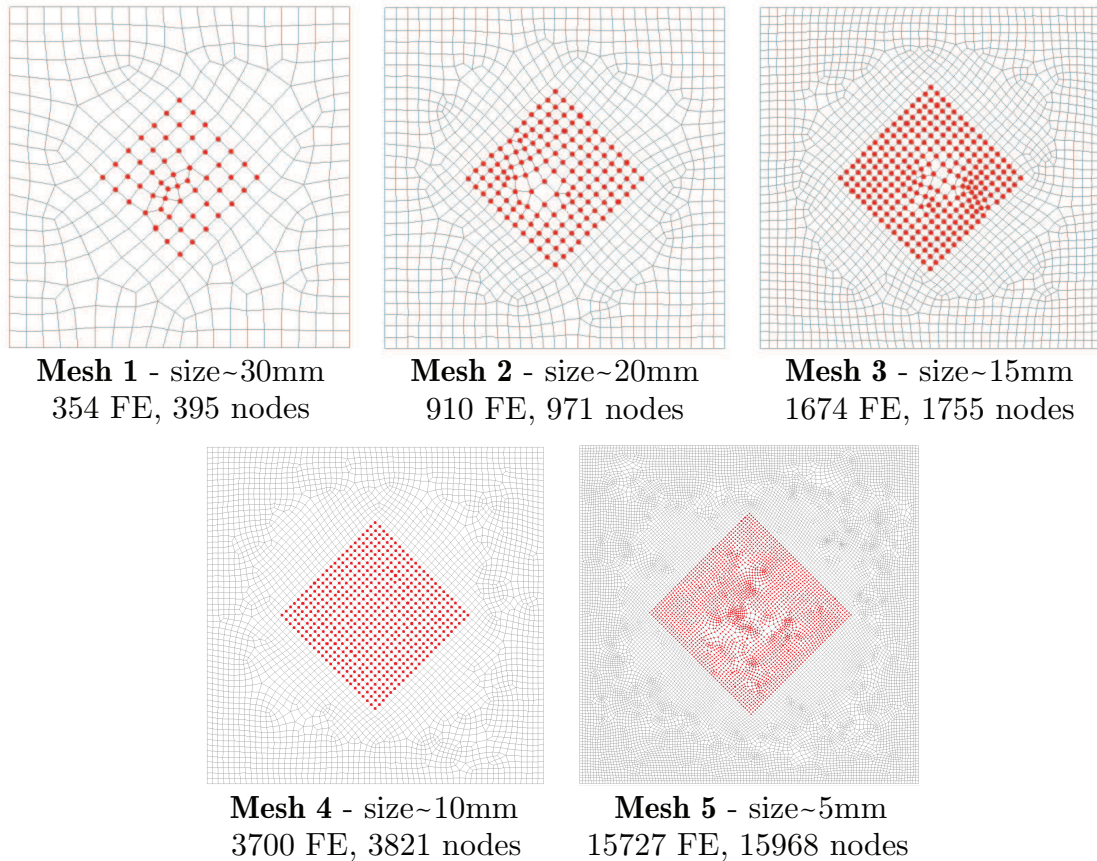
Figure 10.32: Different discretizations of the laminated composite plate with embedded delamination (GiD) and the properties of the models

using Mesh 1 (see Figure 10.32). The transient response is analyzed numerically for the following situations: i) intact composite plate without delamination (black lines in Figure 10.33), ii) the plate with an delaminated zone, allowing for delamination growth (red lines) and, for comparison, iii) the plate with an delaminated zone, suppressing, however, further delamination (red dashed lines). This case has been analyzed recently in [94].

The time histories of the transverse deflection of the plate center are plotted in Figure 10.33 for two different time steps, for the intact plate and the plate with an embedded delamination zone allowing and suppressing further delamination. Considering case ii), the delamination zone changes considerably during the transient motion of the plate. In Figure 10.33, these stages are indicated by green circles. The red bullet in Figure 10.33 indicates the onset of delamination growth.
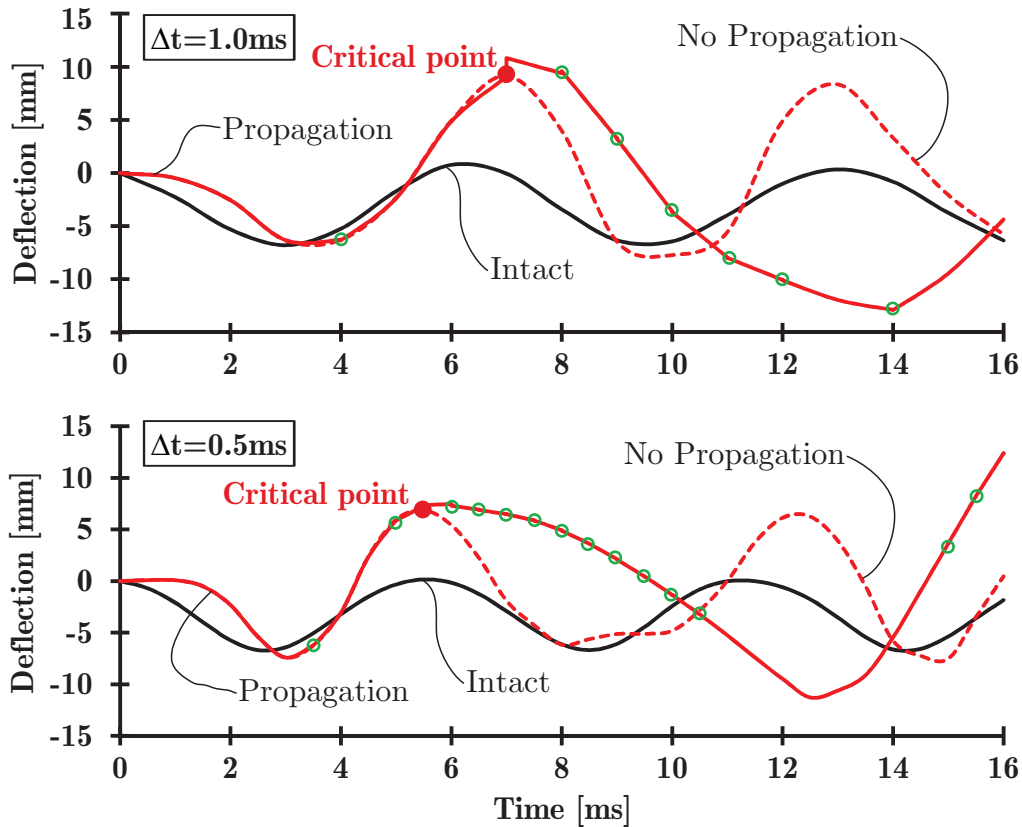
Figure 10.33: Temporal evolution of the central transverse deflection of the delaminated top layer (layer-4) of the composite plate considering three scenarios w.r.t. delamination zone and two different sizes of time increments (red bullet - onset of the delamination growth, green circles - time points in which the delamination shape is changed)

From the performed computational analysis, conclusions can be drawn:

- Reduction of the time step reduces the period of oscillations for all considered cases, while the amplitudes are constant.

- Due to the presence of an embedded delamination zone, in the case without delamination propagation as well as in the case, in which delamination growths is enabled, the debonded layer oscillates independently from the intact rest of the plate. This results in the increase of the amplitudes and the reduction of the frequency in comparison with the intact plate.

- The incorporation of the delamination propagation algorithm severely influences the overall response of the delaminated plate in comparison with the previously presented model [94] with stationary delamination zones in plates. In the moment of the extension of the delaminated zone, the transient response of the delaminated layer changes considerably. This is visualized in Figure 10.33 by the difference between the the solid and dashed red lines, connected with the reduction of the frequency and an increase of the amplitude resulting from the stiffness degradation.

Influence of the mesh density

Figures 10.34, 10.35 and 10.36 show the temporal change of the shape of the delamination zone for three different spatial discretizations (Mesh 1, Mesh 3 and Mesh 4). The time step is $\Delta t = 0.5ms$ in all cases. The trend of the extension of the embedded rectangular delamination zone to form an elliptically shaped zone is the same for all three meshes. The node-to-node propagation algorithm evidently leads to differences in the final delamination shape. While a smooth delamination front is obtained for Mesh 3 and Mesh 4, a polygon-shaped front is obtained for Mesh 1. In this case, the delamination zone reaches the plate boundary.
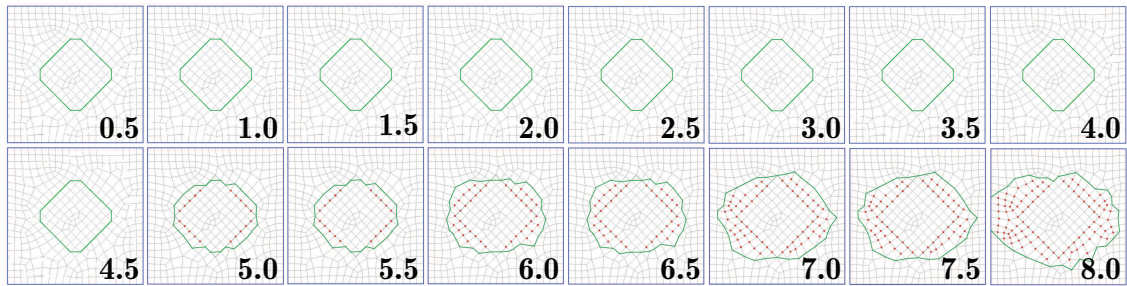
Figure 10.34: Different phases of delamination propagation for Mesh 1 and $\Delta t = 0.50ms$ (numbers indicate time in ms, while red dots are newly created delaminated nodes)
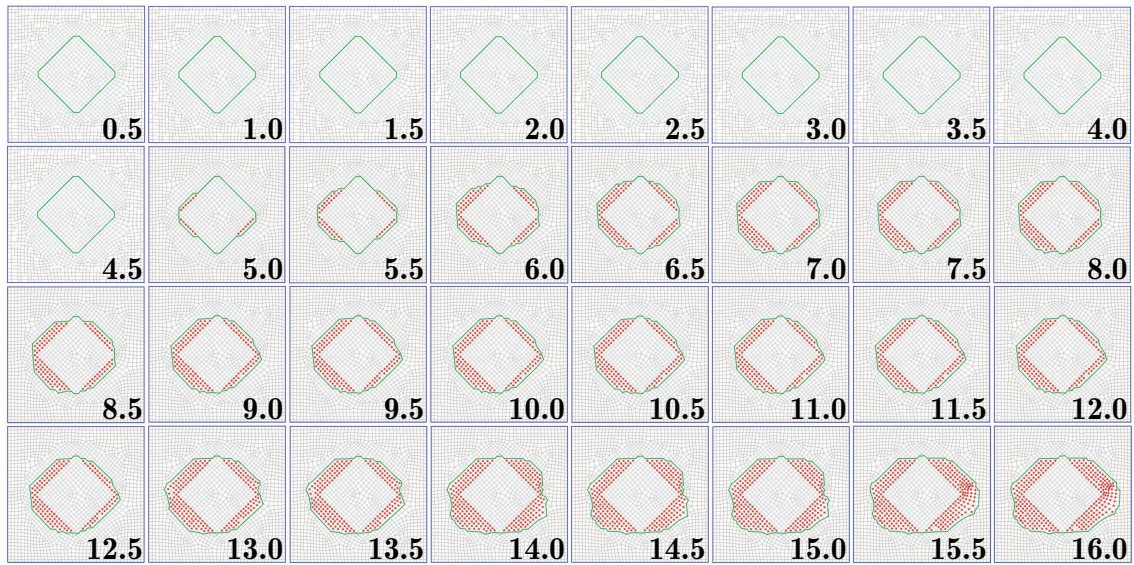
Figure 10.35: Different phases of delamination propagation for Mesh 3 and $\Delta t =$ $0.50ms$ (numbers indicate time in ms, while red dots are newly created delaminated nodes)
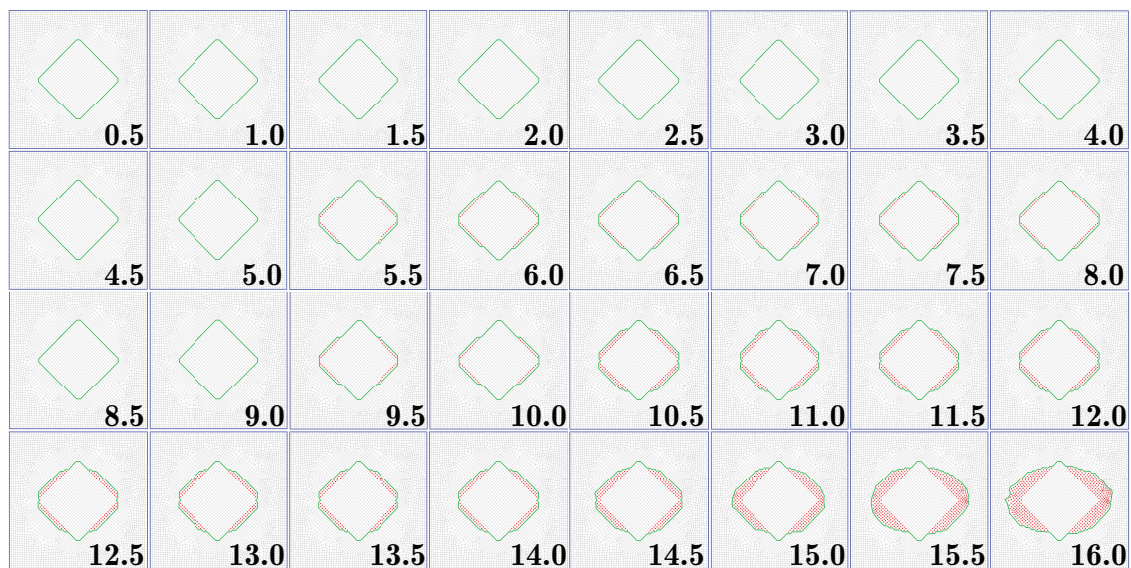
Figure 10.36: Different phases of delamination propagation for Mesh 4 and $\Delta t =$ $0.50ms$ (numbers indicate time in ms, while red dots are newly created delaminated nodes)

Finally, the time histories of the transverse deflection of the plate center are plotted in Figure 10.37 for different mesh densities, varying from coarse to a very

fine mesh, considering delamination growth of the delaminated zone (solid lines). For comparison, also the results from the respective analyses, in which the growth of the delamination zone is suppressed, is included in this Figure (dashed lines). The size of the time increment is $\Delta t = 0.5ms$ in all calculations.
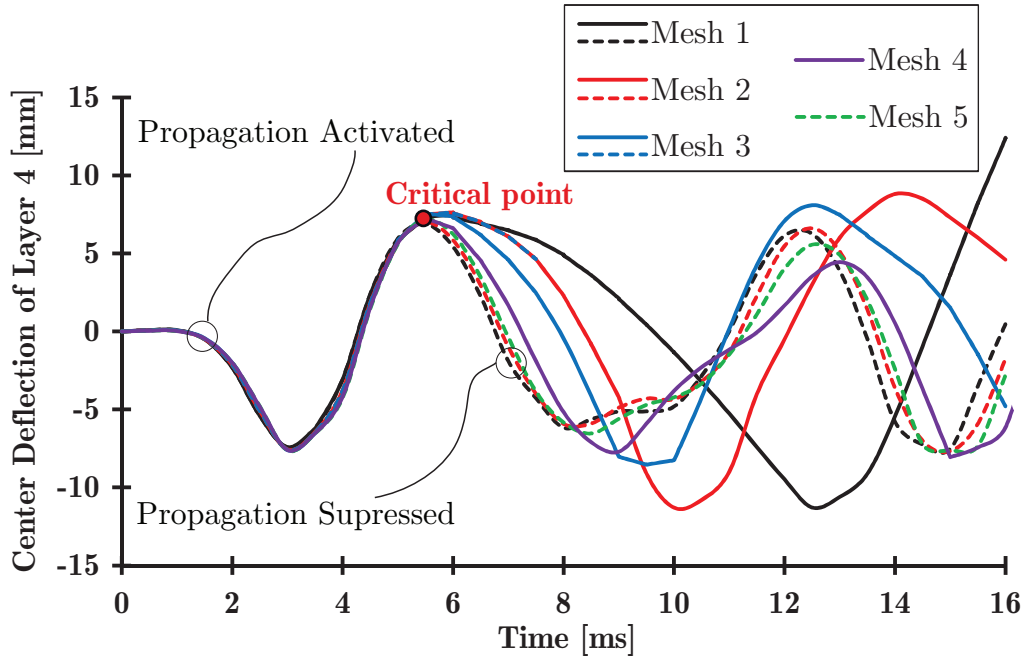
Figure 10.37: Temporal evolution of the central transverse deflection of the delaminated plate obtained for different mesh densities and $\Delta t = 0.5ms$ (solid lines - with delamination growth, dashed lines - without delamination growth, red bullet - onset of the delamination growth)

From Figure 10.37 it is observed, that the mesh refinement does not have a strong influence on the transient response if delamination propagation algorithm is not included. Only a slight reduction of the frequency of oscillations is detected (difference between dashed lines of different colors in Figure 10.37). This confirms that the accurate transient response can be obtained even by using a very coarse mesh, if a delamination propagation algorithm is not activated.

In case of the analysis, in which delamination propagation is considered, the mesh density influences the results severely after the new delaminated zone is created. Delamination growth starts at $\approx 5.5ms$ (for all considered mesh densities), indicated by a red bullet in Figure 10.37. Mesh refinement results in lower ampli-

tudes and higher frequencies of the oscillations of the delaminated segment. The fine mesh leads to a smooth step-by-step change of the delaminated zone (see Figures 10.35-10.36), while in the case of coarse mesh (Mesh 1, see Figure 10.34) the more abrupt extension of the delaminated area leads to a stronger change of the plate motion. Comparing the series of solid lines in Figure 10.37 associated with the activated delamination propagation algorithm, one observes convergence of the computed response with mesh refinement.

10.5 Free Vibrations of Laminated Composite Shells

Free Vibrations of Intact Shells

Example 10.5.1. The first benchmark example is concerned with the cylindrical cross-ply laminated composite shells clamped along both ends. The goal is to check the influence of the mesh refinement on natural frequencies. The length of the analyzed shells is $L = 12m$, and the shell radius is $R = 3m$. The shells are composed from three orthotropic layers, each of thickness $h_k = 0.02m$, so the total shell thickness is $h = 0.06m$ (length-to-radius ratio $L/R = 4$ and thickness-to-radius ratio $h/R = 0.02$, which is related to thin and moderately long shells). The material parameters (Graphite-Epoxy) for all layers are assumed as: $E_1 = 138GPa, E_2 = E_3 = 8.96GPa, G_{12} = G_{13} = 7.1GPa, G_{23} = 3.45GPa, \nu_{12} = 0.30, \rho = 1645kg/m^3$ [59].

Layered triangular finite elements with 3-nodes are used. The shells are discretized using two different mesh densities and two different meshing strategies (structured and unstructured mesh). The boundary conditions are prescribed along clamped edges by constraining all generalized displacements in edge nodes: $u = v = w = u^I = v^I = 0$. The properties of the numerical models are given in Table 10.18, while the finite element meshes generated in GiD are presented in Figure 10.38. The values of non-dimenzionalized frequency parameters $\Omega = \omega \cdot 100R(\rho/E_2)^{1/2}$ are compared with the results by Narita et al. [155] using 2D ring FE model and Ich

Table 10.18: Properties of the numerical models used in Example 10.5.1.

Unstructured mesh	Element size	Number of FE	Number of nodes
Mesh 1	$0.75m$	1080	588
Mesh 2	$0.50m$	2360	1252

Structured mesh	Number of cells per edge	Number of FE	Number of nodes
Mesh 1	10	800	420
Mesh 2	20	3200	1640

Thinh et al. [59] using continuous element constructed from the dynamic stiffness matrix. The results for fundamental frequencies are presented in Table 10.19 and graphically interpreted in Figure 10.39, for different symmetric lamination schemes.

Unstructured Mesh   Structured Mesh
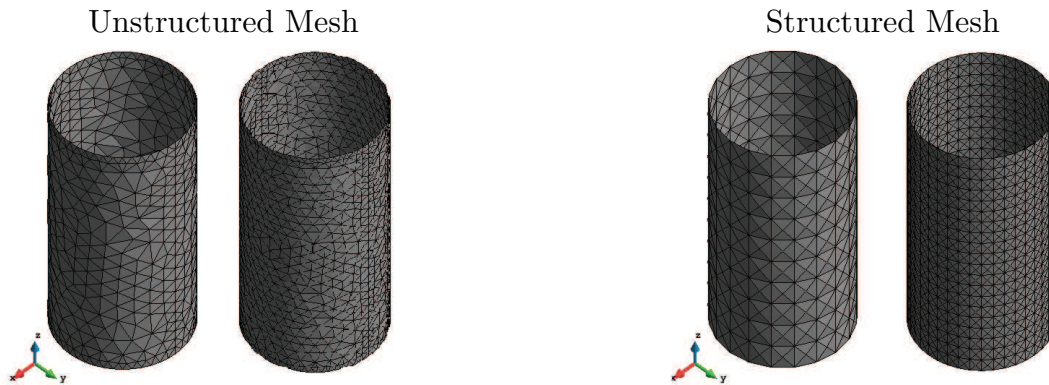
Figure 10.38: Unstructured and structured meshes of triangular layered finite elements

From Figure 10.39 it is obvious that mesh refinement leads to the lower values of frequency parameter, which then converge to the exact solution from Ref. [59], both for the structured and unstructured FE mesh. In the case of the structured mesh, slightly higher frequency parameters are obtained because of the higher influence of clamped edges in boundary conditions (see Figure 10.39). The best agreement with the exact solution (grey bars in Figure 10.39) is obtained for the Unstructured Mesh 2 (green bars in Figure 10.39), and these results are commented as follows:

1. For the (0/0/0) and (0/90/0) cross-ply lamination schemes, excellent agreement is obtained for the first three modes, while in the higher modes the fre-

Table 10.19: Comparison of frequency parameters $\Omega = \omega \cdot 100 R(\rho/E_2)^{1/2}$ of cross-ply cylindrical shells clamped at both ends obtained using different numerical models ($h/R = 0.02$, $L/R = 4$, * - due to the symmetry)

Scheme	Numerical model	Ω_1	Ω_2	Ω_3	Ω_4	Ω_5
0/0/0	Narita et al.[155]	18.14	18.87	21.52	22.97	29.43
	Ich Thinh et al.[59]	18.10	18.84	21.49	22.91	29.33
	Mesh 1 - Unstructured	21.48	22.27	23.68	24.93	29.58
	Mesh 2 - Unstructured	17.66	18.75	20.80	22.02	23.27
	Mesh 1 - Structured	28.33*	28.39*	31.09*	38.24*	49.85*
	Mesh 2 - Structured	18.91*	19.90*	22.56*	27.98*	29.77*
0/90/0	Narita et al.[155]	18.69	20.95	21.51	26.94	30.31
	Ich Thinh et al.[59]	23.71	24.36	25.76	27.81	30.75
	Mesh 1 - Unstructured	19.18	20.89	21.65	26.13	27.05
	Mesh 2 - Unstructured	17.66	18.75	20.80	22.02	23.27
	Mesh 1 - Structured	28.04*	28.09*	29.81*	38.82*	47.87*
	Mesh 2 - Structured	18.61*	19.03*	22.65*	26.37*	30.18*
90/0/90	Narita et al.[155]	25.54	29.63	35.25	42.70	43.60
	Ich Thinh et al.[59]	25.44	29.59	34.96	42.51	43.24
	Mesh 1 - Unstructured	23.76	27.47	32.32	39.14	40.23
	Mesh 2 - Unstructured	17.66	22.02	23.27	30.20	36.32
	Mesh 1 - Structured	27.28*	27.98*	39.01*	45.15*	53.43*
	Mesh 2 - Structured	17.88*	22.29*	24.60*	30.13*	36.37*
90/90/90	Narita et al.[155]	21.37	23.07	34.12	34.33	38.82
	Ich Thinh et al.[59]	21.26	22.98	33.89	34.04	38.48
	Mesh 1 - Unstructured	21.94	23.89	34.09	36.40	38.33
	Mesh 2 - Unstructured	18.34	20.44	24.54	30.14	35.32
	Mesh 1 - Structured	25.03*	26.03*	38.97*	40.49*	48.93*
	Mesh 2 - Structured	16.80*	21.50*	30.09*	33.31*	38.09*
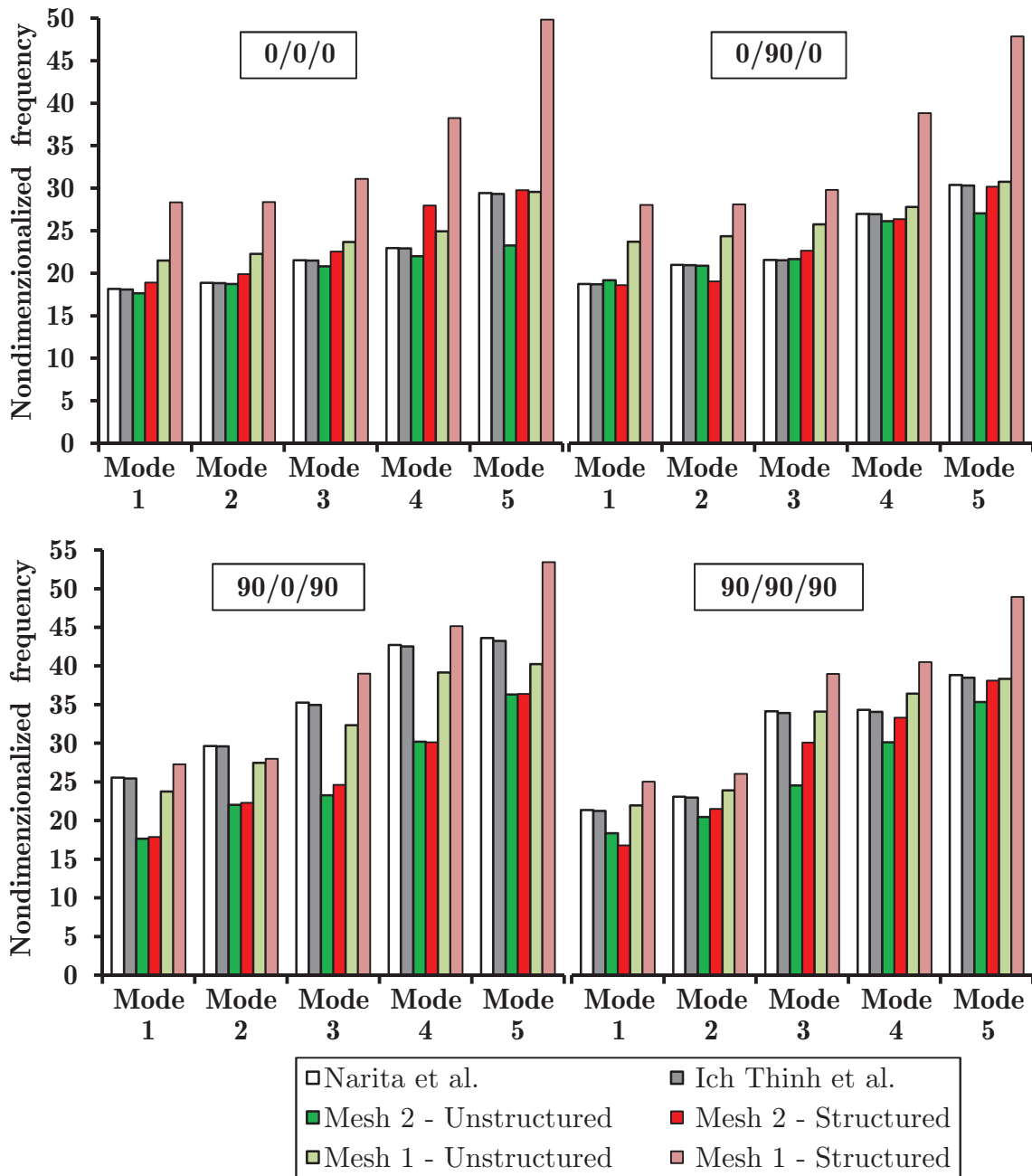
Figure 10.39: Comparison of frequency parameters $\Omega = \omega \cdot 100 R(\rho/E_2)^{1/2}$ of cross-ply cylindrical shells clamped at both ends obtained using different numerical models ($h/R = 0.02, L/R = 4$)

quency parameters obtained using the proposed model are lower. The reason is the influence of the transverse shear deformation, which effects are simplified in the FSDT [59], as well as because of the idealizations related to the application of the plate finite elements in the modeling of curved geometry of

composite shells.

2. For the (90/0/90) and (90/90/90) schemes, the lower frequency parameters are obtained for all modes, because of the influence of the transverse shear deformation and the idealizations regarding the shell geometry.

Example 10.5.2. The second benchmark example is concerned with the cylindrical cross-ply laminated composite shells with different boundary conditions. The goal is to check the influence of the incorporated shear deformation and variable boundary conditions on natural frequencies. The length of the analyzed shells is $L = 2m$, the shell radius is $R = 1m$, while the total shell thickness is $h = 0.2m$ (length-to-radius ratio $L/R = 2$ and thickness-to-radius ratio $h/R = 0.2$, which is related to the thick and moderately long shells). The shells are composed from orthotropic layers of equal thickness, in two different stacking sequences: (0/90), where $h_1 = h_2 = 0.1m$, and (0/90/0), where $h_1 = h_2 = h_3 = 0.0667m$.

The material parameters (Graphite-Epoxy) for all layers are assumed as [59]: $E_1 = 40GPa, E_2 = E_3 = 1GPa, G_{12} = 0.6GPa, G_{13} = G_{23} = 0.5GPa, \nu_{12} = 0.25, \rho = 1600kg/m^3$.

Layered triangular elements with 3-nodes are used. The boundary conditions are prescribed along clamped edges by constraining all generalized displacements in edge nodes: $u = v = w = u^I = v^I = 0$. Along the simply supported edges, boundary conditions are prescribed by constraining the vertical mid-plane displacement $w = 0$, as well as by assigning the rigid springs in tangential direction (local coordinate system) in each boundary node along the simply supported edge. This is performed by the penalty method, where $k_{spring} = 100 \cdot k_{max}$, where k_{spring} is the spring stiffness to be assigned in the local coordinate system, while k_{max} is the absolute maximal value from the global stiffness matrix. This operation is performed during the assembly of the global stiffness matrix, after the transformation of the spring stiffness matrix (truss element) from the local to the global coordinate system.

The shell is afterwards discretized using two different mesh densities and two different meshing strategies. The properties of the numerical models are given in

Table 10.20: Properties of the numerical models used in Example 10.5.2.

Unstructured mesh	Element size	Number of FE	Number of nodes
Mesh 1	$0.175m$	1160	648
Mesh 2	$0.100m$	3460	1854

Structured mesh	Number of cells per edge	Number of FE	Number of nodes
Mesh 1	10	800	420
Mesh 2	15	1800	930

Table 10.20, while the FE meshes are presented in Figure 10.40.

Unstructured Mesh   Structured Mesh
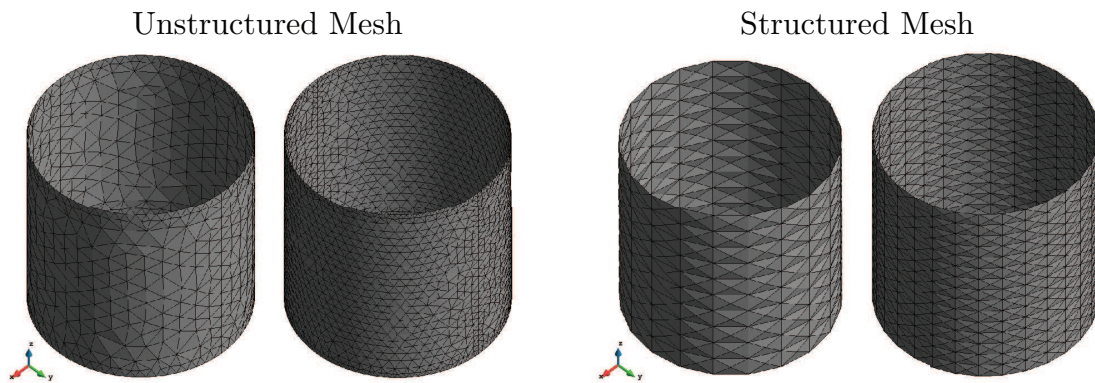
Figure 10.40: Unstructured and structured meshes of triangular layered FE

The values of non-dimenzionalized frequency parameters $\Omega = \omega \cdot L^2 (\rho/E_2)^{1/2}/h$ obtained from analyses are compared with the results by Khdeir et al. [44] using different theories and Ich Thinh et al. [59] using continuous element constructed from the dynamic stiffness matrix. The results for fundamental frequencies are presented in Table 10.21 and graphically interpreted in Figure 10.41, for different symmetric lamination schemes. Also, fundamental mode shapes and corresponding frequency parameters of cross-ply cylindrical shells with various boundary conditions are illustrated in Figures 10.42 - 10.43.

From the results given in Table 10.21 it is obvious that mesh refinement leads to the lower values of frequency parameter, both for the structured and unstructured mesh. In the case of structured mesh, higher frequency parameters are obtained because of the higher influence of constrained edges (see Figure 10.40). In the

Table 10.21: Comparison of frequency parameters $\Omega = \omega \cdot L^2 (\rho/E_2)^{1/2}/h$ of cross-ply cylindrical shells with various boundary conditions obtained using different numerical models ($h/R = 0.2$, $L/R = 2$, * - symmetry)

Scheme	Numerical model	CF	SS	CS	CC
0/90	Khdeir et al. - CLPT [44]	9.38	16.30	18.41	21.20
	Khdeir et al. - FSDT [44]	9.14	15.52	16.97	18.76
	Khdeir et al. - HSDT [44]	9.21	15.66	17.26	19.28
	Ich Thinh et al. [59]	8.72	15.19	16.61	17.37
	Mesh 1 - Unstructured	7.63	16.13	17.86	19.98
	Mesh 2 - Unstructured	7.29	15.47	16.97	18.82
	Mesh 1 - Structured	8.71*	17.62*	20.71*	24.62*
	Mesh 2 - Structured	8.54*	17.59*	20.24*	23.48*
0/90/0	Khdeir et al. - CLPT [44]	10.99	20.73	26.62	33.38
	Khdeir et al. - FSDT [44]	9.88	17.79	19.45	21.29
	Khdeir et al. - HSDT [44]	9.95	17.77	19.72	21.91
	Ich Thinh et al. [59]	8.72	17.22	19.50	20.83
	Mesh 1 - Unstructured	7.75	14.10	16.05	19.03
	Mesh 2 - Unstructured	7.41	13.77	15.58	18.14
	Mesh 1 - Structured	9.92*	20.09*	20.67*	23.74*
	Mesh 2 - Structured	9.67*	15.94*	16.67*	19.34*

following, the results obtained for the Unstructured Mesh 2 (green bars in Figure 10.41) are commented:

1. For the (0/90) cross-ply lamination scheme, excellent agreement is obtained for SS and CS boundary conditions. For the cantilever shell the fundamental frequency is lower (as expected) in comparison with [59], while in the case of clamped shell the fundamental frequency is slightly higher than expected, because of the idealizations regarding the curved geometry of composite shells and the highly constrained boundaries.

2. For the (0/90/0) scheme (higher level of orthotropy), the lower frequency pa-
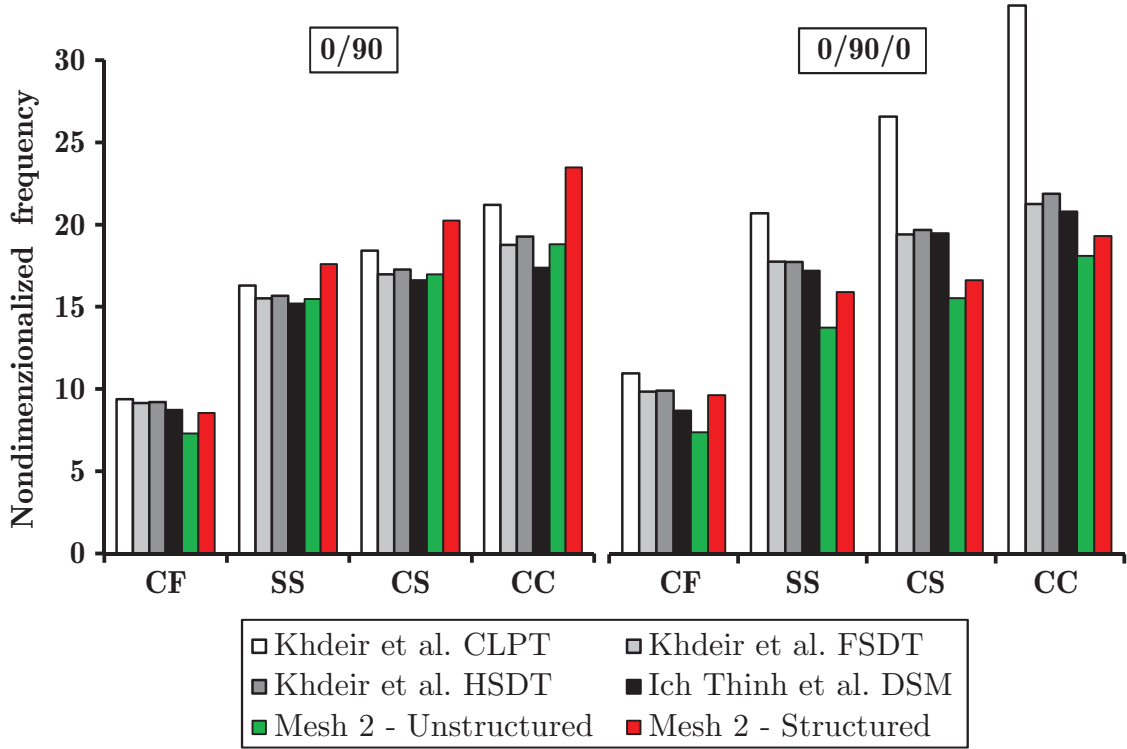
Figure 10.41: Comparison of frequency parameters $\Omega = \omega L^2 \cdot (\rho/E_2)^{1/2}/h$ of cross-ply cylindrical shells with various boundary conditions obtained using different numerical models ($h/R = 0.2, L/R = 2$)

CF - 7.29	**SS** - 15.47	**CS** - 16.97	**CC** - 18.82
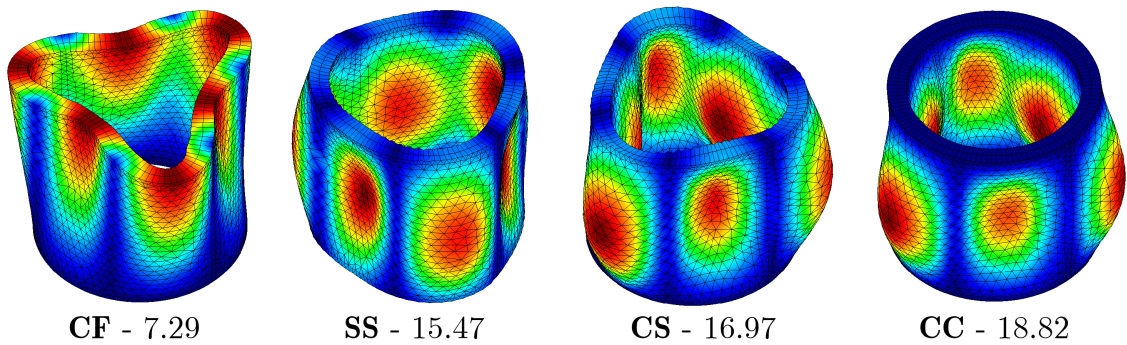
Figure 10.42: Fundamental mode shapes and corresponding frequency parameters $\Omega = \omega \cdot L^2(\rho/E_2)^{1/2}/h$ of 2-layer (0/90) cross-ply cylindrical shells with various boundary conditions ($h/R = 0.2, L/R = 2$)

rameters are obtained for all boundary conditions, because of the high influence of the transverse shear deformation (which is more pronounced for thick shells).

Example 10.5.3. The third benchmark example is concerned with the conical

CF - 7.41   **SS** - 13.77   **CS** - 15.58   **CC** - 18.14
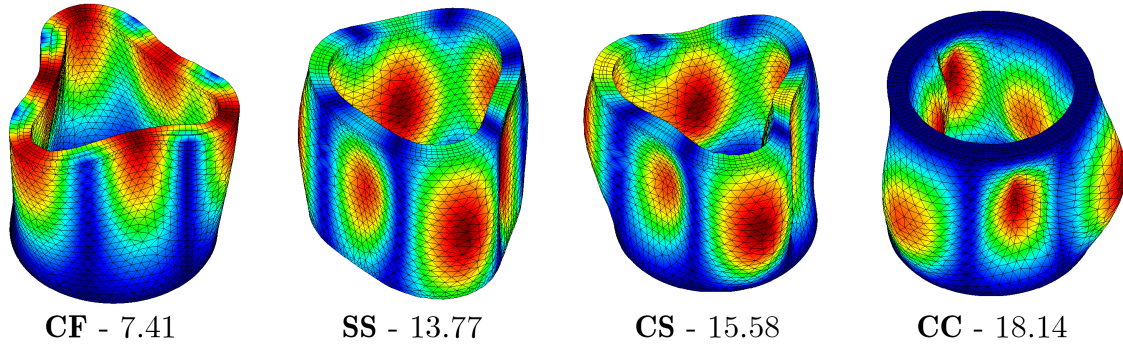
Figure 10.43: Fundamental mode shapes and corresponding frequency parameters $\Omega = \omega \cdot L^2(\rho/E_2)^{1/2}/h$ of 3-layer (0/90/0) cross-ply cylindrical shells with various boundary conditions ($h/R = 0.2, L/R = 2$)

Table 10.22: Properties of the numerical models used in Example 10.5.3.

Mesh	Element size	Number of FE	Number of nodes
Mesh 1	$0.15m$	516	327
Mesh 2	$0.10m$	942	576
Mesh 3	$0.07m$	1698	1002

cross-ply laminated composite shells with various boundary conditions (see Figure 10.44). The goal is to check the influence of the mesh refinement and incorporated shear deformation on natural frequencies of laminated composite conical shells. The cone length along its generator is $L = 0.5m$, $R_0 = 0.75m$ and $R_1 = 1.00m$ are the cone radii at its small and large edges, respectively, while $\alpha_0 = 30^o$ is the semi vertex angle of the cone. The shells are composed from two orthotropic layers, each of thickness $h_k = h/2$, with the cross-ply stacking sequence (0/90). The total shell thickness is denoted as h. Ten different h/R_1 ratios are investigated numerically, covering the range from thin ($h/R_1 = 0.01$) to thick ($h/R_1 = 0.10$) shell situations.

The material parameters for all layers are assumed as: $E_1 = 150GPa, E_2 = E_3 = 10GPa, G_{12} = 5GPa, G_{13} = G_{23} = 3.846GPa, \nu_{12} = 0.25, \rho = 1500kg/m^3$ [58]. Layered triangular elements with 3-nodes are used. The shell is discretized using three different unstructured mesh densities (see Table 10.22 and Figure 10.45).

The values of non-dimenzionalized frequency parameters $\Omega = \omega \cdot R_1(\rho h/A_{11})^{1/2}$

Table 10.23: Comparison of frequency parameters $\Omega = \omega \cdot R_1(\rho h/A_{11})^{1/2}$ of clamped-clamped cross-ply conical shells with various h/R_1 ratios obtained using different numerical models

h/R_1	Model					
	Shu [50]	Wu et al. [52]	Jin et al. [58]	Mesh 1	Mesh 2	Mesh 3
0.01	0.2986	0.3045	0.2966	0.6295	0.5069	0.4538
0.02	0.4625	0.4504	0.4504	0.7435	0.6459	0.5899
0.03	0.6210	0.5834	0.5835	0.8541	0.7809	0.7154
0.04	0.7752	0.6986	0.6987	0.9585	0.8899	0.8239
0.05	0.9331	0.7967	0.7971	1.0477	0.9807	0.9170
0.06	1.0843	0.8810	0.8817	1.1204	1.0544	0.9941
0.07	1.2344	0.9476	0.9480	1.1787	1.1139	1.0583
0.08	1.3845	1.0010	1.0017	1.2254	1.1631	1.1118
0.09	1.5206	1.0457	1.0466	1.2627	1.2037	1.1566
0.10	1.5737	1.0831	1.0843	1.2932	1.2376	1.1938

Table 10.24: Comparison of frequency parameters $\Omega = \omega \cdot R_1(\rho h/A_{11})^{1/2}$ of SS cross-ply conical shells with various h/R_1 ratios obtained using different numerical models

h/R_1	Model			
	Jin et al. [58]	Mesh 1	Mesh 2	Mesh 3
0.02	0.3771	0.4869	0.4227	0.3914
0.03	0.4710	0.5322	0.4809	0.4495
0.04	0.5538	0.5715	0.5316	0.5010
0.05	0.6321	0.5632	0.5650	0.5396
0.06	0.7067	0.5521	0.5567	0.5353
0.07	0.7663	0.5441	0.5506	0.5316
0.08	0.8212	0.5381	0.5461	0.5290
0.09	0.8713	0.5336	0.5427	0.5270
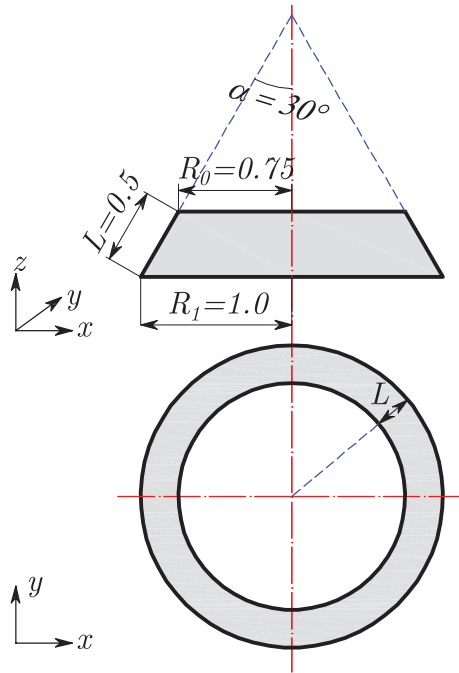
Figure 10.44: The geometry of the conical shells in Example 10.5.3.
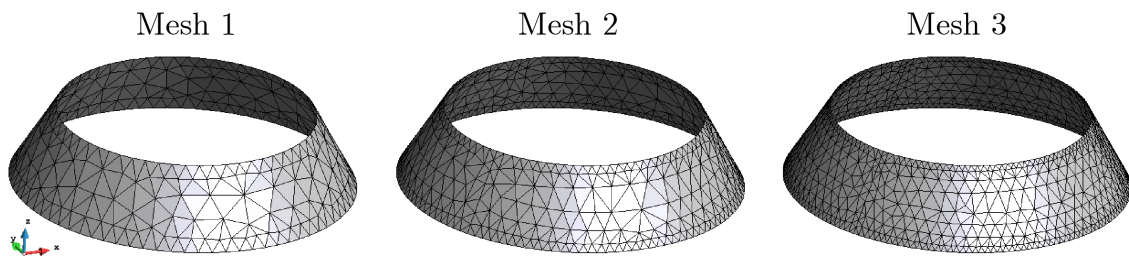
Figure 10.45: Unstructured meshes of triangular layered finite elements

(where $A_{11} = \sum\limits_{k=1}^{n} \overline{Q}_{11}^{k} \cdot h_k = \frac{h}{2} \cdot \left(\overline{Q}_{11}^{0} + \overline{Q}_{11}^{90} \right)$) obtained from performed analyses are compared with the exact solution by Jin et al. [58] using a Fourier series, as well as with the solution of Shu [50] using the generalized differential quadrature based on the classical plate theory and the differential quadrature solution of Wu and Lee [52] based on the FSD Theory. The results for fundamental frequencies are presented in Tables 10.23 - 10.24 and graphically interpreted in Figure 10.46, for different h/R_1 ratios. Also, fundamental mode shapes of conical shells with various h/R_1 ratios and various boundary conditions are illustrated in Figures 10.47-10.48.

From Figure 10.46 it is obvious that mesh refinement leads to the lower values of frequency parameter. For the CC laminated composite conical shell it is shown that the present model (green bars in Figure 10.46, left) gives an accurate prediction of
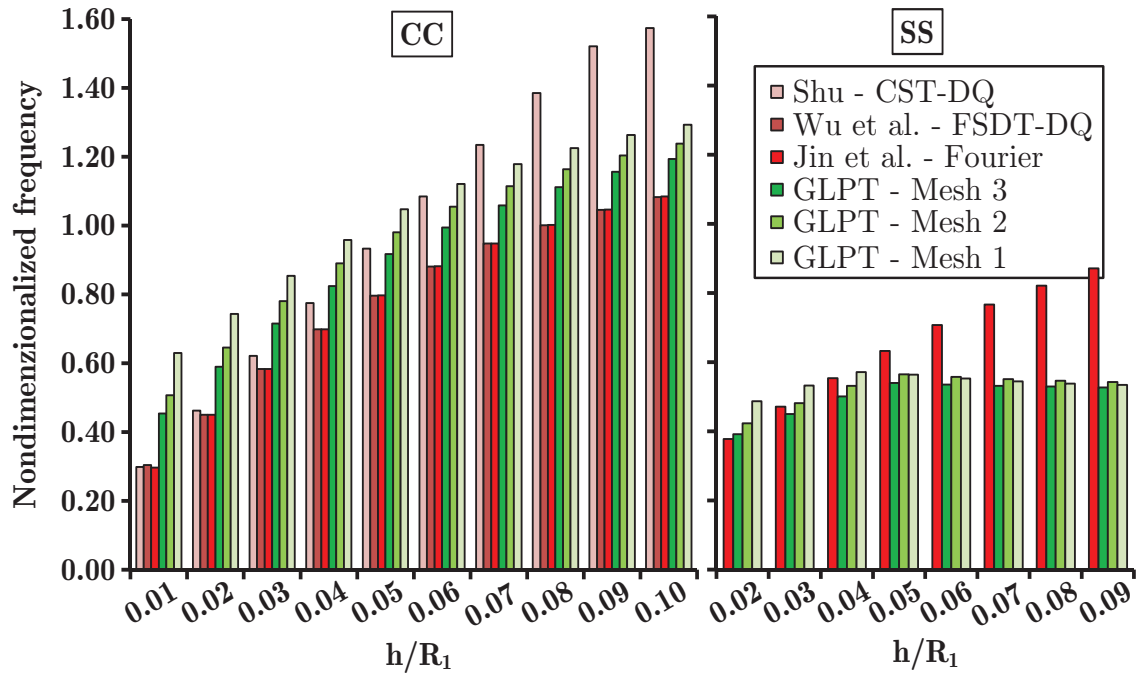
Figure 10.46: Comparison of frequency parameters $\Omega = \omega \cdot R_1(\rho h/A_{11})^{1/2}$ of cross-ply conical shells with various h/R_1 ratios and various boundary conditions, obtained using different numerical models
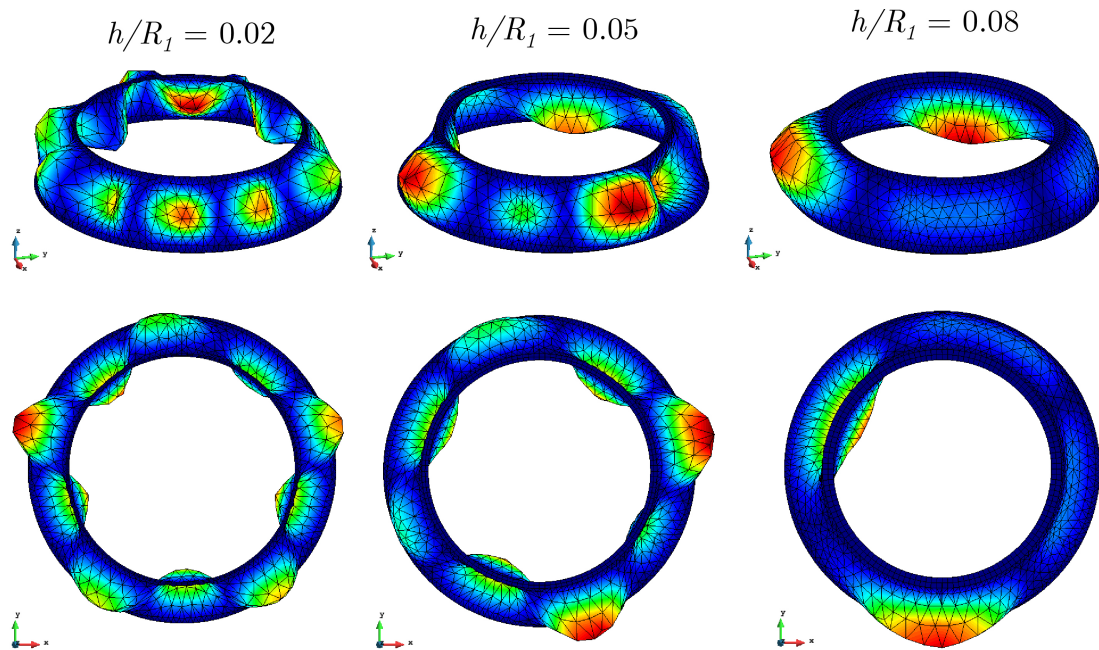
Figure 10.47: Fundamental mode shapes of CC 2-layer (0/90) cross-ply conical shells with various h/R_1 ratios

the frequency parameter. For all h/R_1 ratios a stiffer response is obtained because of the geometry idealization using the flat triangular finite elements for the generation
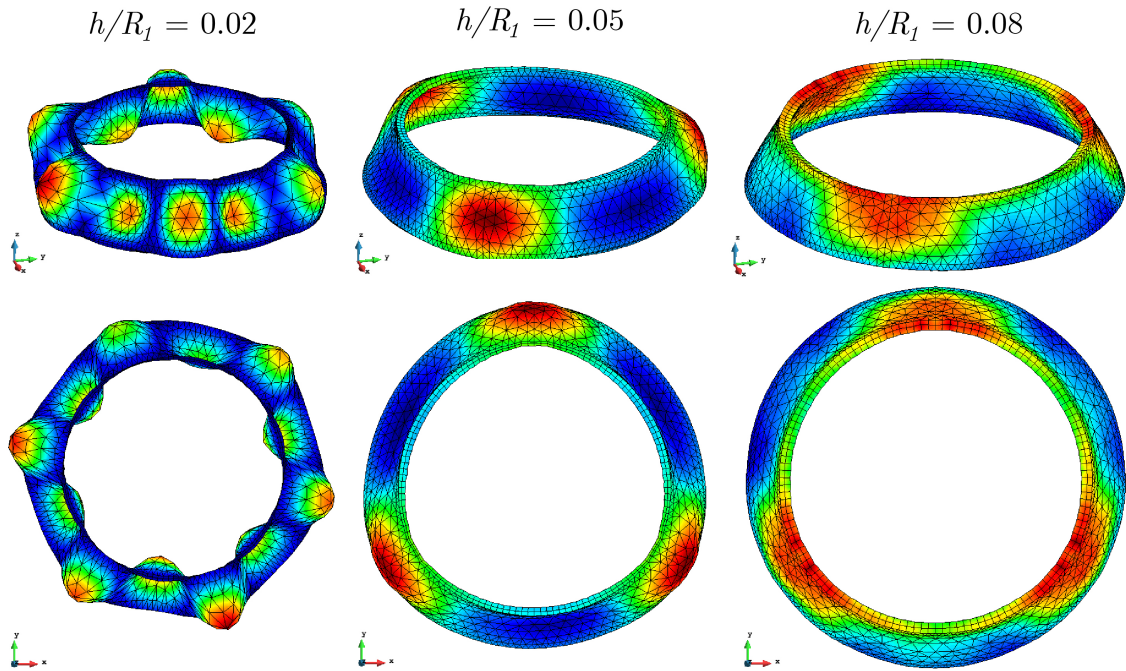
Figure 10.48: Fundamental mode shapes of SS 2-layer (0/90) cross-ply conical shells with various h/R_1 ratios
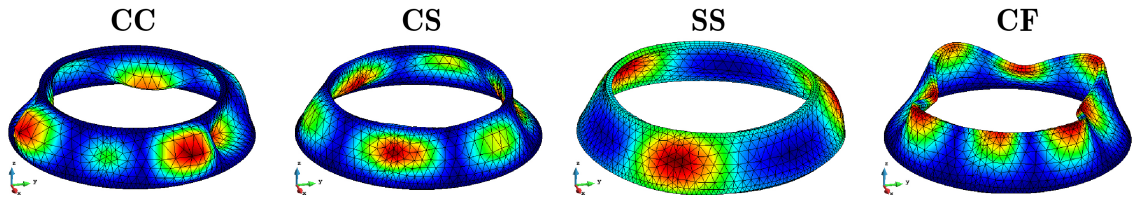
Figure 10.49: Fundamental mode shapes of 2-layer (0/90) cross-ply conical shells with various boundary conditions, for $h/R_1 = 0.05$

of curved surfaces. For thin shells, the present model gives the moderately higher values of natural frequency in comparison with the Equivalent-Single-Layer shell theories. In the case of the thick shells, the result obtained using the classical shell theory is too stiff, because of the neglection of the transverse shear deformation. In this case the present model gives only the slightly higher results for natural frequencies, and this can be overcome by the further mesh refinement. This is the confirmation that the proposed model is appropriate for the analysis of thick laminated composite shells.

For the SS laminated composite conical shell it is shown that the present model (green bars in Figure 10.46, right) is capable to accurately calculate the natural

frequencies for the moderately thin shells ($h/R_1 < 0.04$), while in the case of thick shells the obtained results diverge from the exact solution by Jin et al. [58].

The **Examples 10.5.1. - 10.5.3.** clearly show that the mesh refinement leads to the lower values of frequency parameter (convergence to the exact solution), both for the structured and unstructured mesh. Higher frequency parameters are obtained in the case of the structured mesh, because of the higher influence of constrained edges. This is more pronounced for the numerical models with highly constrained boundaries (CS, CC). The transverse shear deformation severely influences the fundamental dynamic characteristics of cylindrical and conical laminated composite shells, both for the high and low length-to-thickness ratios (thin and thick shell situations). This influence is higher for the shells with the higher level of orthotropy. Also, the influence is higher for the higher modes of oscillation, leading to the lower values of frequency parameter.

Example 10.5.4. The fourth benchmark example is concerned with the cross-ply (0/90/0) cylindrical and spherical laminated composite panels with various boundary conditions. The length of the analyzed panels is $a = 2m$, while the radius is $R = 10m$. The panels are composed from three orthotropic layers, each of thickness $h_k = 0.0667m$, so the total thickness is $h = 0.20m$ (length-to-radius ratio $a/R = 0.2$ and thickness-to-radius ratio $h/R = 0.10$, which is related to thick shells). The material parameters for all layers are assumed as: $E_1 = 25GPa, E_2 = 1GPa, G_{12} = G_{13} = 0.5GPa, G_{23} = 0.2GPa, \nu = 0.25, \rho = 1000kg/m^3$ [1].

Figure 10.50: The geometry of the cylindrical and spherical panels

The shells are discretized using unstructured mesh of 3-node triangular elements. Element size is $0.1m$ (1130 FE, 633 nodes). The finite element meshes generated in

Table 10.25: Comparison of frequency parameters $\Omega = 0.02\omega$ of cross-ply cylindrical and spherical shallow panels obtained using different numerical models ($a/R = 0.2$, $h/R = 0.10$)

Model	BC	Cylindrical	Spherical
Ferreira - FSDT [156]		12.214	12.417
Ferreira - HSDT [156]	SSSS	11.851	12.063
Fazzolari - DSM HSDT [1]		11.846	12.054
Present	CCCC	11.391	10.970
	CCCF	10.227	7.320

GiD are presented in Figure 10.51. The boundary conditions are prescribed along clamped edges by constraining all generalized displacements in edge nodes. The values of non-dimenzionalized frequency parameters $\Omega = \omega \cdot \frac{a^2}{h}(\rho/E_2)^{1/2} = 0.02\omega$ are compared with the results by Ferreira et al. [156] using a sinusoidal shear deformation theory and Fazzolari [1] using the dynamic stiffness method based on the HSDT. The results for fundamental frequencies are presented in Table 10.25.

Cylindrical Panel   Spherical Panel

Figure 10.51: Unstructured meshes of triangular layered finite elements

From the results shown in Table 10.25 it is obvious that the proposed model does not predict the fundamental frequencies of the shallow shells adequately. The discrepancy arises because of the co-planar finite elements meeting in a node, which lead to the singular assembled system of equations (see Section 8.5). The obtained results for the clamped-clamped case are in agreement with the data from [1] and [156] for SS case. This means that the proposed model gives too soft results for natural frequencies of shallow shells.

By taking the remarks from **Examples 10.5.1. - 10.5.4.** into account, the presented model is capable to accurately predict the fundamental frequencies of intact

laminated composite shells of different shapes. After the verification of the proposed model for intact shells, the parametric study of the influence of delamination size on natural frequencies will be discussed in the next subsection.

Free Vibrations of Delaminated Shells

Example 10.5.5. This benchmark example is concerned with the cylindrical cross-ply laminated composite shells (see **Example 10.5.2.** for the review of shell geometry and mechanical properties of the laminas), with previously imposed rectangular delaminated area (see Figure 10.52). In all numerical models, delaminations are imposed in the mid-surface of the shell. The goal of this example is to check the influence of the delamination size on the natural frequencies of laminated composite shells.

The cross-ply shells are composed from the orthotropic layers of equal thickness, in $(0/90)$ stacking sequence, where $h_1 = h_2 = 0.1m$ are layer thicknesses. Layered triangular elements with 3-nodes are used. The shell is discretized using the structured mesh with two different mesh densities (see Figure 10.40). The properties of the numerical models are given in Table 10.20. The values of non-dimenzionalized frequency parameters $\Omega = \omega L^2 \sqrt{\rho/E_2}/h$ obtained from analyses are graphically interpreted in Figure 10.53 for laminated composite cylindrical shells with two different boundary conditions (CC and CF).
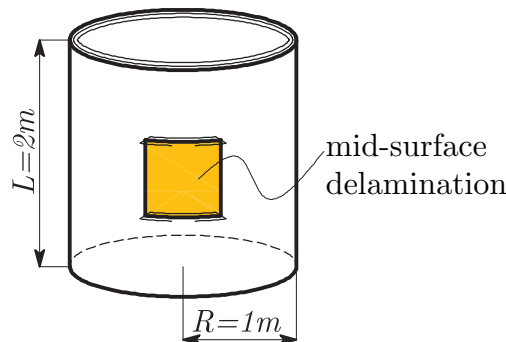
Figure 10.52: The geometry of the cylindrical shell with embedded delamination

Figure 10.53 illustrates the frequency reduction curves due-to the presence of mid-surface delamination. For the CC laminated shells investigated in this example, the natural frequency is reduced severely after the increase of the delaminated area
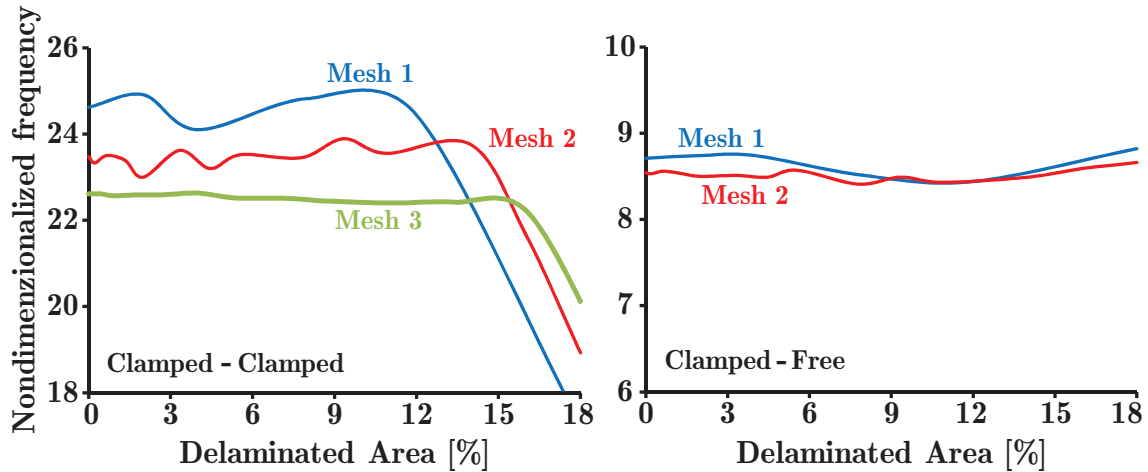
Figure 10.53: Influence of the delaminated area on nondimenzionalized funda-
mental frequencies $\Omega = \omega L^2 \sqrt{\rho/E_2}/h$ of 2-layer (0/90) cross-ply
cylindrical shells with various boundary conditions ($h/R = 0.2$,
$L/R = 2$)

above 12% of the shell area. This critical delamination area is influenced slightly
by the mesh density (15% for Mesh 2 and 16% for Mesh 3). The mesh density
influences the frequency reduction curves by reducing the natural frequency with
the increase of number of elements used for the discretization.

For the CF laminated shells, the increase of mesh density does not influence the
natural frequencies severely. Also, it is shown that the increase of delaminated area
does not reduce the fundamental frequency. It can be concluded that for the numer-
ical models with highly constrained boundaries, the influence of the delamination
area on natural frequencies is higher (see Figure 10.53).

11 Conclusions

Triangular and quadrilateral layered finite elements with varying levels of interpolation capable to incorporate the independent motion of adjacent delaminated interfaces are recalled based upon the Generalized Laminated Plate Theory of Reddy. The numerical model of layered plate finite element is further extended for the analysis of free vibration response of delaminated composite shells. The extension is made using simple geometrical considerations which are easy to implement into the previously derived finite element code. Due to some simplifications of the shell kinematics some limitations of the model have arise and they are highlighted in this study. Geometrical nonlinearity is accounted based upon the von Kármán assumptions. Interlaminar penetration between delaminated layers has not been enabled by activating the contact conditions between the individual layers. A novel delamination propagation algorithm has been implemented based on the Virtual Crack Closure Technique to allow for the change of the previously imposed delaminated zone during the static and dynamic motion of the plate.

The proposed models have been verified and their accuracy is demonstrated using the variety of benchmark examples, for bending, free vibration, buckling and transient analysis of laminated composite and sandwich plates. The accuracy of the models is proved both for intact and delaminated composite plates. The differences between the models considering only the stationary delamination and the models allowing for delamination propagation have been highlighted. From the number of numerical analyses, the following conclusions are drawn:

- The simplifications regarding the transverse shear deformation which are employed in the ESL theories cause the underestimation of the transverse deflections and the overestimation of the fundamental frequencies of laminated composite plates, when compared to the GLPT. When the delamination is present, the influence of the transverse shear deformation is higher for the

plates with highly constrained boundaries. While comparing different finite element models, in the case of full integration of 4-node element matrices, shear locking has occurred, thus the reduced integration is necessary in thin plate situation to prevent the negative effects of spurious transverse shear stiffness. In addition, the transverse shear deformation severely influences the fundamental dynamic characteristics of cylindrical and conical laminated composite shells, both for the thin and thick shell situation. This influence is higher for the shells with the higher level of orthotropy, as well as for the higher modes of oscillation.

- It is documented that the proposed model is capable to accurately predict the fundamental frequencies of intact laminated composite plates of different shapes, even by using the quadrilateral elements for approximation of the circular plate geometry. The results obtained using the proposed model are in agreement with the numerical results from the commercial software and the experimental data, with reduced computational cost and obvious convergence of results due to the mesh refinement. A slightly better performance of quadratic elements is detected in the prediction of higher modes of vibration.

- The reduction of the fundamental frequency of the laminated composite plates caused by the presence of the delamination is more pronounced for higher modes of vibration. The position of the embedded delamination through the plate thickness plays an important role by significantly reducing the global fundamental frequency of the delaminated plate (both composite and sandwich) for mid-plane delamination, and otherwise having an marginal effect when near-surface delamination is employed. In this case, the delaminated segment oscillate independently from the intact rest of the plate with its own frequency. In the thin plate situation the independent oscillation of delaminated segment can achieve even the second bending mode, too.

- Author's attempt to describe the free vibration response of composite shell structures using a very robust numerical model based on the flat layered triangular finite elements showed that the mesh refinement, as expected, reduces

the natural frequencies of the CC cross-ply cylindrical and conical shells, with the convergence to the exact solution both for the structured and unstructured mesh and shell thicknesses varying from thin to thick situation. For the (0/0/0) and (0/90/0) schemes excellent agreement is obtained in lower modes, while in higher modes of vibration the frequency parameters are lower in comparison with the existing data from the literature. For the (90/0/90) and (90/90/90) schemes, the lower frequency parameters are obtained for all modes. Because of the geometry idealization using the flat triangular finite elements for the generation of curved surfaces, a stiffer response then expected is obtained in the case of conical shells, for all thicknesses. Finally, the proposed model does not predict the fundamental frequencies of the shallow shells adequately due to the co-planar finite elements meeting in a node leading to the singular assembled system of equations. The proposed model gives too soft results for natural frequencies of shallow panels.

- When the delamination is present within a shell structure the natural frequency is reduced severely after the increase of the delaminated area above 12% of the shell area. This critical delamination area is influenced slightly by the mesh density, which influences the frequency reduction curves by reducing the natural frequency with the increase of number of elements used for the discretization. For the numerical models with highly constrained boundaries, the influence of the delamination area on natural frequencies is higher.

- The proposed model accurately predicts the critical buckling load of laminated composite plates, in comparison with the existing close form and 3D elasticity solutions. The accuracy is proven even for the coarse mesh, leading to the reduced computational cost. It is documented that the delaminated area up to the 6% of the plate area does not reduce the critical buckling load. When the delamination position within a plate is considered, near-surface delamination has smaller influence to the results, because the intact rest of the plate is stiff enough to hold the majority of the critical buckling loading. The similar trend is observed for the uniaxially compressed sandwich plates, having in mind that

thin delaminated layer will buckle independently from the rest of the plate.

- The activation of the contact algorithm during the transient analysis of laminated composite plates showed to have only a minor effect on linear transient response. However, in the geometrically nonlinear analysis the delamination has a considerable influence, thus the results from the analysis considering contact of the delaminated layers differ considerably from the plots obtained for the analysis without consideration of contact. As an illustration, changing the position of delamination in the geometrically nonlinear analysis is not affecting the transient response if the contact algorithm is not activated. However, if penetration is suppressed by means of the activating the contact algorithm, a large influence of the position of the delaminated region is observed.

- Transient analysis of delaminated composite and sandwich plates showed that when a small delamination area is present within a laminate only a marginal increase of the amplitude and the period of oscillations is observed in linear analysis. The plate still oscillates as one homogeneous structure with negligible relative displacements between adjacent layers. However, in the case of geometrically nonlinear transient analysis the period of oscillations is slightly reduced because of the added bending stiffness of the plate, as expected. For the larger size of the delaminated area the amplitudes and the period of oscillations of the laminate are significantly increased due to the significant stiffness degradation. Changing the position of the delamination zone through the plate thickness does not have a large effect on the frequency of the oscillations in the linear analysis.

- The sandwich plates are highly vulnerable to embedded delamination between the soft-core and rigid face sheets when subjected to exponential blast pulse loading. The global amplitudes of the intact rest of the plate are increased because of the splitting. The crack opening displacements are small in the linear and slightly higher in the geometrically nonlinear analysis. On the other hand, if the delamination occurs within the rigid face sheet, the global amplitudes of the intact rest of the plate are nearly the same as for the intact

plate, because the undamaged part has the more or less the same bending stiffness as the intact plate. When the delamination area is small the face-core debonding is negligible. The CODs are slightly higher in the geometrically nonlinear transient analysis. After increase of the delaminated area, however, the global linear plate motion significantly changes and becomes more complex, with increased amplitudes due to the reduction of the plate stiffness. In the geometrically nonlinear response of the sandwich plates the added bending stiffness leads to a reduction of the crack opening displacements as compared to the linear case. The highest amplitudes and crack opening displacements are reached at the end of blast pulse and start of free vibration phase.

- Incorporation of the delamination propagation algorithm severely influences the transient response of the delaminated plate. In the moment of delamination extension the response of the delaminated layer is changed considerably leading to the reduction of the frequency because of the stiffness degradation and increase of the amplitudes. The general trend of the delamination extension is independent of the mesh density, but the final shape of the delamination is mesh-dependent by means of creation of smooth delamination front for fine mesh and polygon-shaped front for coarse mesh. The considerable change in the transient response of delaminated plates occurs nearly in the same time point regardless of the mesh density. The mesh refinement results in the lower amplitudes of oscillations of the delaminated segment, with higher frequencies, due to the fact that fine mesh allows for smooth step-by-step change in the delaminated zone, which is a robust and elegant, but also a very simple approximation of the real behavior of the delaminated structure. The mesh dependence is caused by a node-to-node delamination propagation algorithm, which implies two main approximations: (1) the node-to-node approximation of a virtually closed area A and, (2) the node-to-node approximation of the movement of the delamination front. It was also shown that the computed transient response converges with increasing mesh density. The reason is that the selection of a mesh size causes the previously described approximations to be more or less violated, further leading to the convergence of the results.

- On the other hand, when static bending analysis of laminated plates is performed with activated delamination propagation algorithm, it has been found that linear finite elements result in the slightly higher values of the calculated reaction force in the displacement-control analysis of the DCB, in comparison with the quadratic elements. The distribution of the G_I along the plate width calculated using the linear elements is nearly constant in contrast with the quadratic elements for which the distribution is curved. The mesh refinement in width direction does not significantly influence the G_I distribution, while the reduction of the displacement increment leads to the convergence of numerical solution.

12 Future Work

Based upon the assumptions and restrictions which served as a basis for the presented model, as well as based on the main conclusions of this work, recommendations for further research are specified below:

1. Initiation of delamination was not in the scope of this study. There are several possibilities to simulate the creation of the first debonded node pair within the finite element model, based on the strength or deformation criteria of the material. It would be interesting to incorporate these criteria in the presented model, to simulate the structural behavior of the intact laminated structure under different types of loading, and to track the behavior from the initiation of delamination, its propagation until the final collapse.

2. The plane stress model incorporated in this study impose the inextensibility of the transverse normal, which leads to zero transverse normal deformation. Considering that transverse normal stress could be relevant for the delamination study, the full 3D constitutive model can be considered. However, the full 3D constitutive model can lead to the shear locking because of the spurious transverse normal stiffness, so the solution to overcome this issue should also be found, for example using the selective integration techniques.

3. The computational cost could be reduced by using some simpler definitions of the finite elements for the simulation of the composite laminate. The ESL-based finite elements derived upon the CLPT or FSDT plate theories can be combined with the GLPT-based layered finite elements, discretizing the different subregions of the considered domain. For example, the intact part of the analyzed domain can be accurately modeled using the FSDT-based elements, while in the delaminated subregion enriched layered elements should be used. In addition, the conditions to provide the compatibility of the degrees-of-freedom in the adjacent nodes between different elements should be provided.

4. The proposed model assumes that the ideal bonding exist between the node pair until the fracture criterion is satisfied. After the new delaminated area is created, there is no cohesion within the previously bonded node pair, which is the very robust idealization. Therefore the incorporated frictionless contact algorithm should be improved by introducing a cohesive law between adjacent delaminated interfaces. The convergence problems which can arise in the cohesive models should also be investigated.

5. The application of the plate layered finite elements for the analysis of laminated composite shells is done by the simple transformations of the coordinates presented in this study. However, the discontinuity of the curvatures at elements' connections leads to some irregularities in the results. The more sophisticated model could be developed by introducing the patch of triangular elements [157] to overcome the discontinuity-of-rotations-problem, and afterwards the obtained results could be compared with these presented within this study.

6. The interfacial material properties (critical energy release rates) are the experimental parameters which are not always easy to obtain. These properties are generally assumed based on the strength limits of the bulk material using the simple analytical models. The statistical variation of the interfacial strength can be implemented in the proposed model to more realistically approximate the behavior of the real structure.

7. Piezoelectric materials are very interesting due to their potential use in actively controlling of the elastic deformations of structures in civil engineering. They exhibit elastic deformations when subjected to an applied electric field. Due to their compact size and light weight, many of these piezoelectric patches can be attached to the structure without greatly changing the mechanical properties of the structure. Therefore, the mechanical and piezoelectric coupling should be incorporated in the constitutive relations to extend the proposed theory for the analysis of the laminated structure with piezoelectric layers.

8. In the proposed model the delamination is modeled as a node-to-node dis-

continuity. It can be also treated as the sum of the contributions of every delaminated node particularly. For this reason it would be interesting to calculate the transient response of the laminate with the single delaminated node and to calculate some quantity which describe the vulnerability of the single-delaminated-node-structure. Then the statistical distribution of the damage (influence surface) within a plate can be plotted, discovering the dangerous positions of the damage in the plate for different loading situations, boundary conditions or plate geometries.

9. Environmental effects (thermal effects, humidity) are not accounted in the presented study. These aspects should be considered by means of the influence of the environmental effects on the dynamic properties of the laminates, especially on the natural frequencies.

Appendix

`layerwiseFE.cnd` file

```
CONDITION: Laminate_Definition
  CONDTYPE: over surface
  CONDMESHTYPE: over elems
  CANREPEAT: no
  QUESTION: Properties(Thickness,Angle,Material)
  VALUE:#N# 3 0.0 0 "Material_1"
END CONDITION
CONDITION: Distributed_Loadings
  CONDTYPE: over surface
  CONDMESHTYPE: over elems
  CANREPEAT: no
  QUESTION: X_Direction:
  VALUE: 0.0
  QUESTION: Y_Direction:
  VALUE: 0.0
  QUESTION: Z_Direction:
  VALUE: 0.0
END CONDITION
CONDITION: Nodal_Forces
  CONDTYPE: over points
  CONDMESHTYPE: over nodes
  CANREPEAT: no
  QUESTION: X_Direction:
  VALUE: 0.0
  QUESTION: Y_Direction:
  VALUE: 0.0
  QUESTION: Z_Direction:
  VALUE: 0.0
END CONDITION
CONDITION: Crack_Opening_Displacement
  CONDTYPE: over points
  CONDMESHTYPE: over nodes
  CANREPEAT: no
  QUESTION: Value:
  VALUE: 0.0
END CONDITION
```

```
CONDITION: Clamped_Edge
  CONDTYPE: over lines
  CONDMESHTYPE: over nodes
  CANREPEAT: yes
END CONDITION
CONDITION: Simply_Supported_Edge
  CONDTYPE: over lines
  CONDMESHTYPE: over body elements
  CANREPEAT: yes
END CONDITION
CONDITION: Delaminated_Node
  CONDTYPE: over points
  CONDMESHTYPE: over nodes
  CANREPEAT: yes
END CONDITION
```

layerwiseFE.mat file

```
BOOK: Orthotropic_Lamina
  MATERIAL: Material_1
  TITLE: Modules_of_Elasticity
    QUESTION: E1:
     VALUE: 0.0
     HELP: Elasticity module in direction 1
    QUESTION: E2:
     VALUE: 0.0
     HELP: Elasticity module in direction 2
    QUESTION: E3:
     VALUE: 0.0
     HELP: Elasticity module in direction 3
  TITLE: Poisson_Ratios
    QUESTION: ni12
     VALUE: 0
     HELP: Poisson ratio 12
    QUESTION: ni13
     VALUE: 0
     HELP: Poisson ratio 13
    QUESTION: ni23
     VALUE: 0
     HELP: Poisson ratio 23
  TITLE: Shear_Modules
    QUESTION: G12:
     VALUE: 0.0
     HELP: Shear module 12
    QUESTION: G13:
```

```
     VALUE: 0.0
     HELP: Shear module 13
    QUESTION: G23:
     VALUE: 0.0
     HELP: Shear module 23
  TITLE: Other
    QUESTION: SelfWeight
     VALUE: 0
     HELP: Mass Density of the Material
  END MATERIAL
```

layerwiseFE.prb file

```
PROBLEM DATA
TITLE: Analysis
  QUESTION:Analysis_Type:#CB#(Bending_Analysis,Transient_Analysis,
  Free_Vibration_Analysis,Initial_Stability_Analysis)
    VALUE: Bending_Analysis
    HELP: Choose the type of Analysis
    DEPENDENCIES:(Bending_Analysis, RESTORE,Contact_Algorithm,
    #CURRENT#, RESTORE,Geometric_NonLinearity,#CURRENT#,
    RESTORE,Crack_Propagation,#CURRENT#, HIDE,Multiplicator,
    #CURRENT#,HIDE,Number_of_Mode_Shapes,#CURRENT#,HIDE,
    Number_of_Buckling_Modes,#CURRENT#,HIDE,Nx,#CURRENT#,HIDE,Ny,
    #CURRENT#,HIDE,Nxy,#CURRENT#,HIDE,Pulse_Type:,#CURRENT#,HIDE,
    Time_Step:,#CURRENT#, HIDE,Total_Time:,#CURRENT#,HIDE,
    Damping_Factor:,#CURRENT#)
    DEPENDENCIES:(Transient_Analysis, RESTORE,Contact_Algorithm,
    #CURRENT#, RESTORE,Geometric_NonLinearity,#CURRENT#,RESTORE,
    Crack_Propagation,#CURRENT#, HIDE,Multiplicator,#CURRENT#,HIDE,
    Number_of_Mode_Shapes,#CURRENT#,HIDE,Number_of_Buckling_Modes,
    #CURRENT#, HIDE,Nx,#CURRENT#, HIDE,Ny,#CURRENT#, HIDE,Nxy,
    #CURRENT#,RESTORE,Time_Step:,#CURRENT#,RESTORE,Total_Time:,
    #CURRENT#,RESTORE,Pulse_Type:,#CURRENT#,HIDE,Damping_Factor:,
    #CURRENT#)
    DEPENDENCIES:(Free_Vibration_Analysis,HIDE,Contact_Algorithm,
    #CURRENT#,HIDE,Geometric_NonLinearity,#CURRENT#,HIDE,
    Crack_Propagation,#CURRENT#,HIDE,Critical_EnergyReleaseRate_1,
    #CURRENT#, HIDE,Critical_EnergyReleaseRate_2,#CURRENT#,HIDE,
    Critical_EnergyReleaseRate_3,#CURRENT#, HIDE,Tolerance,#CURRENT#,
    HIDE,Number_of_Steps,#CURRENT#, HIDE,Max_Iterations,#CURRENT#,
    HIDE,Non_Linear_Solver,#CURRENT#, RESTORE,Multiplicator,#CURRENT#,
    RESTORE,Number_of_Mode_Shapes,#CURRENT#,HIDE,
    Number_of_Buckling_Modes,#CURRENT#, HIDE,Nx,#CURRENT#,HIDE,Ny,
    #CURRENT#, HIDE,Nxy,#CURRENT#, HIDE,Time_Step:,#CURRENT#,HIDE,
```

```
    Total_Time:,#CURRENT#, HIDE,Pulse_Type:,#CURRENT#,HIDE,
    Damping_Factor:,#CURRENT#)
    DEPENDENCIES:(Initial_Stability_Analysis,HIDE,Contact_Algorithm,
    #CURRENT#, HIDE,Geometric_NonLinearity,#CURRENT#,HIDE,
    Crack_Propagation,#CURRENT#,HIDE,Critical_EnergyReleaseRate_1,
    #CURRENT#, HIDE,Critical_EnergyReleaseRate_2,#CURRENT#,HIDE,
    Critical_EnergyReleaseRate_3,#CURRENT#, HIDE,Tolerance,#CURRENT#,
    HIDE,Number_of_Steps,#CURRENT#, HIDE,Max_Iterations,#CURRENT#,
    HIDE,Non_Linear_Solver,#CURRENT#, RESTORE,Multiplicator,#CURRENT#,
    HIDE,Number_of_Mode_Shapes,#CURRENT#,RESTORE,
    Number_of_Buckling_Modes,#CURRENT#, RESTORE,Nx,#CURRENT#,RESTORE,
    Ny,#CURRENT#, RESTORE,Nxy,#CURRENT#, HIDE,Time_Step:,#CURRENT#,
    HIDE,Total_Time:,#CURRENT#, HIDE,Pulse_Type:,#CURRENT#,HIDE,
    Damping_Factor:,#CURRENT#)
QUESTION: Delaminated_Interface:
    VALUE: 2
    HELP: Interface in which Delamination occurs
QUESTION: Gauss_Quadrature:#CB#(FULL,RED)
    VALUE: RED
    HELP: Type of Gauss-Legendre Quadrature
QUESTION: Contact_Algorithm#CB#(YES,NO)
    VALUE: YES
    HELP: Include Contact Algorithm in the Analysis
QUESTION: Geometric_NonLinearity#CB#(YES,NO)
    VALUE: NO
    HELP: Von Karman Geometrical Nonlinear Analysis
    DEPENDENCIES:(YES, RESTORE,Non_Linear_Solver,#CURRENT#,RESTORE,
    Tolerance,#CURRENT#, RESTORE,Max_Iterations,#CURRENT#,RESTORE,
    Number_of_Steps,#CURRENT#)
    DEPENDENCIES:(NO, HIDE,Non_Linear_Solver,#CURRENT#,HIDE,Tolerance,
    #CURRENT#,HIDE,Max_Iterations,#CURRENT#,HIDE,Number_of_Steps,
    #CURRENT#)
QUESTION: Non_Linear_Solver:#CB#(Picard_Method,Newton-Raphson_Method)
    VALUE:Newton-Raphson_Method
    HELP: Type of the Non Linear Solver
QUESTION: Tolerance:
    VALUE: 0.001
    HELP: Convergence Criterium
QUESTION: Max_Iterations:
    VALUE: 10
    HELP: Max Number of Iterations in Geometric Nonlinear Analysis
QUESTION: Number_Of_Steps:
    VALUE: 10
    HELP: Max Number of Steps
QUESTION: Crack_Propagation#CB#(YES,NO)
    VALUE: NO
```

```
  HELP: Include Crack Propagation in the Analysis
  DEPENDENCIES:(YES,RESTORE,Number_of_Steps,#CURRENT#,RESTORE,
  Critical_EnergyReleaseRate_1,#CURRENT#,RESTORE,
  Critical_EnergyReleaseRate_2,#CURRENT#,RESTORE,
  Critical_EnergyReleaseRate_3,#CURRENT#)
  DEPENDENCIES:(NO,HIDE,Number_of_Steps,#CURRENT#,HIDE,
  Critical_EnergyReleaseRate_1,#CURRENT#,HIDE,
  Critical_EnergyReleaseRate_2,#CURRENT#,HIDE,
  Critical_EnergyReleaseRate_3,#CURRENT#)
QUESTION: Critical_EnergyReleaseRate_1:
  VALUE: 10000
  HELP: Critical Value of ERR in Mode 1 of Delamination
QUESTION: Critical_EnergyReleaseRate_2:
  VALUE: 100
  HELP: Critical Value of ERR in Mode 2 of Delamination
QUESTION: Critical_EnergyReleaseRate_3:
  VALUE: 100
  HELP: Critical Value of ERR in Mode 3 of Delamination
QUESTION: Multiplicator:
  VALUE: 1
  HELP: Multiplicator for Non-Dimenzionalized Natural Frequencies
  or Critical Loads
QUESTION: Number_of_Mode_Shapes:
  VALUE: 6
  HELP: Number of Mode Shapes to be calculated
QUESTION: Number_of_Buckling_Modes:
  VALUE: 6
  HELP: Number of Buckling Modes to be calculated
QUESTION: Nx:
  VALUE: 1
  HELP: Initial Normal Force in X-Direction
QUESTION: Ny:
  VALUE: 1
  HELP: Initial Normal Force in Y-Direction
QUESTION: Nxy:
  VALUE: 0
  HELP: Initial Shear Force
QUESTION: Pulse_Type:#CB#(STEP,SINE,TRIANGULAR,EXPONENTIAL)
  VALUE: STEP
  HELP: Choose the type of transient pulse loading
  DEPENDENCIES:(STEP, HIDE,Damping_Factor,#CURRENT#)
  DEPENDENCIES:(SINE, HIDE,Damping_Factor,#CURRENT#)
  DEPENDENCIES:(TRIANGULAR, HIDE,Damping_Factor,#CURRENT#)
  DEPENDENCIES:(EXPONENTIAL, RESTORE,Damping_Factor:,#CURRENT#)
QUESTION: Time_Step:
  VALUE: 0.1
```

```
      HELP: Time Step in Newmark Integration
   QUESTION: Total_Time:
      VALUE: 100
      HELP: Total Time in Newmark Integration
   QUESTION: Damping_Factor:
      VALUE: 100
      HELP: Damping Factor for Exponential Pulse

TITLE: Project
   QUESTION: Project_Title:
      VALUE:
   QUESTION: Author:
      VALUE:
   QUESTION: Supervisor:
      VALUE:
   QUESTION: Company:
      VALUE:
   QUESTION: Date:
      VALUE:
END PROBLEM DATA
```

layerwiseFE.bas file

```
INTEGRATION = '*GenData(Gauss_Quadrature:)';
GEOMETRICNONLINEARITY = '*GenData(Geometric_NonLinearity)';
SOLVERTYPE = '*GenData(Non_Linear_Solver:)';
TOLERANCE = *GenData(Tolerance:);
NUMBEROFSTEPS = *GenData(Number_of_Steps:);
NUMBEROFITERATIONS = *GenData(Max_Iterations:);
CONTACTALGORITHM = '*GenData(Contact_Algorithm)';
ANALYSISTYPE = '*GenData(Analysis_Type:)';
multiplicator = *GenData(Multiplicator:);
ModeNumber = *GenData(Number_of_Mode_Shapes:);
ModeNumberBuckling = *GenData(Number_of_Buckling_Modes:);
CRACKPROPAGATION = '*GenData(Crack_Propagation)';
Nx = *GenData(Nx:);
Ny = *GenData(Ny:);
Nxy = *GenData(Nxy:);
id = *GenData(Delaminated_Interface:);
TIMESTEP = *GenData(Time_Step:);
TIMETOTAL = *GenData(Total_Time:);
PULSETYPE = '*GenData(Pulse_Type:)';
ERR1 = *GenData(Critical_EnergyReleaseRate_1:);
ERR2 = *GenData(Critical_EnergyReleaseRate_2:);
ERR3 = *GenData(Critical_EnergyReleaseRate_3:);
```

```
DAMPINGFACTOR = *GenData(Damping_Factor:);
TITLE = '*GenData(Project_Title:)';
AUTHOR = '*GenData(Author:)';
SUPERVISOR = '*GenData(Supervisor:)';
COMPANY = '*GenData(Company:)';
DATE = '*GenData(Date:)';

*set var countmat = 0
*loop materials *notused
*set var countmat = countmat+1
*end materials
MATERIALS = cell(*countmat,11);
*set var counter = 1
*loop materials *notused
MATERIALS(*counter,1) = {'*matprop(0)'};
MATERIALS(*counter,2:11) = {
*format "%10.3f %10.3f %10.3f %5.3f %5.3f %5.3f %10.3f %10.3f %10.3
%10.3f"
*matprop(1) *matprop(2) *matprop(3) *matprop(4) *matprop(5) *matprop(6)
*matprop(7) *matprop(8) *matprop(9) *matprop(10)};
*set var counter = counter+1
*end materials

*Set Cond Laminate_Definition
*loop elems *OnlyInCond
STACKING = ' *cond ';
*end elems

splitstring = textscan(STACKING,'%s');
splitstring = splitstring{1};
clear STACKING
STACKING = splitstring;
clear splitstring;
last = size(STACKING,1);
STACKINGNEW = STACKING(3:last-1);
Nlayer = size(STACKINGNEW,1)/3;
STACKING = cell(Nlayer,3);
for i = 1:Nlayer
    STACKING(i,1) = STACKINGNEW((i-1)**3+1,1);
    STACKING(i,2) = STACKINGNEW((i-1)**3+2,1);
    STACKING(i,3) = STACKINGNEW((i-1)**3+3,1);
end

layers = zeros(size(STACKING,1),1);
angles = zeros(size(STACKING,1),1);
for i = 1:size(STACKING,1)
```

```
    layers(i) = str2num(cell2mat(STACKING(i,1)));
    angles(i) = str2num(cell2mat(STACKING(i,2)));
end
clear i STACKINGNEW last

*if(nnode==3)
Elem_Shape = 'Triangular'; Interpolation = 'Linear';
elemstring = 'Prism'; plotnodes = 6;
*endif
*if(nnode==6)
Elem_Shape = 'Triangular'; Interpolation = 'Quadratic';
elemstring = 'Prism'; plotnodes = 6;
*endif
*if(nnode==4)
Elem_Shape = 'Quadrilateral'; Interpolation = 'Linear';
elemstring = 'Hexahedra'; plotnodes = 8;
*endif
*if(nnode==9)
Elem_Shape = 'Quadrilateral'; Interpolation = 'Quadratic';
elemstring = 'Hexahedra'; plotnodes = 8;
*endif

nodescoord = [
*loop nodes
*format "%12.5f %12.5f %12.5f"
*NodesCoord(1) *NodesCoord(2) *NodesCoord(3);
*end nodes ];

connectivity = [
*loop elems
*if(ElemsType==2)
*if(ElemsNnode==3)
*format "%6i %6i %6i"
*ElemsConec;
*endif
*if(ElemsNnode==6)
*format "%6i %6i %6i %6i %6i %6i"
*ElemsConec;
*endif
*endif
*if(ElemsType==3)
*if(ElemsNnode==4)
*format "%6i %6i %6i %6i"
*ElemsConec;
*endif
*if(ElemsNnode==9)
```

```
*format "%6i %6i %6i %6i %6i %6i %6i %6i %6i"
*ElemsConec;
*endif
*endif
*end elems ];

nelem = size(connectivity,1);
nnode = *npoin;

*set cond Distributed_Loadings *elems
Distributed_Loadings = zeros(*nelem,3);
*loop elems *OnlyInCond
*format "%6i %12.5f"
Distributed_Loadings(*ElemsNum,1) = *cond(1);
*format "%6i %12.5f"
Distributed_Loadings(*ElemsNum,2) = *cond(2);
*format "%6i %12.5f"
Distributed_Loadings(*ElemsNum,3) = *cond(3);
*end elems
*set cond Nodal_Forces *nodes
Nodal_Forces = zeros(*npoin,3);
*loop nodes *OnlyInCond
*format "%6i %12.5f"
Nodal_Forces(*NodesNum,1) = *cond(1);
*format "%6i %12.5f"
Nodal_Forces(*NodesNum,2) = *cond(2);
*format "%6i %12.5f"
Nodal_Forces(*NodesNum,3) = *cond(3);
*end nodes
*set cond Crack_Opening_Displacement *nodes
CODs = zeros(*npoin,2);
*loop nodes *OnlyInCond
*format "%6i"
CODs(*NodesNum,1) = *NodesNum;
*format "%6i %12.5f"
CODs(*NodesNum,2) = *cond(1);
*end nodes

delete=[];
for i = 1:size(CODs,1)
if CODs(i,1) == 0
delete = vertcat(delete,i);
end
end
CODs(delete,:)=[];
```

```
*set cond Clamped_Edge *nodes
CC = zeros(*npoin,1);
*loop nodes *OnlyInCond
*format "%6i"
CC(*NodesNum,1) = *NodesNum;
*end nodes
CC = CC(CC~=0);

SSpreliminary = [
*set cond Simply_Supported_Edge
*loop elems *onlyInCond
*if(ElemsNnode==2)
*set var i=0
*for(i=1;i<=2;i=i+1)
*ElemsConec(*i) ;
*end
*endif
*if(ElemsNnode==3)
*set var i=0
*for(i=1;i<=2;i=i+1)
*ElemsConec(*i) ;
*end
*endif
*end elems ];

SSrecords = size(SSpreliminary,1)/2;
SS = zeros(SSrecords , 2);
for i = 1:SSrecords
SS(i,:) = SSpreliminary(2**i-1:2**i);
end

*set cond Delaminated_Node *nodes
DEL = zeros(*npoin,1);
*loop nodes *OnlyInCond
*format "%6i"
DEL(*NodesNum,1) = *NodesNum;
*end nodes
DEL = DEL(DEL~=0);

%%MATLAB SYNTAX
%Creation of the Node Objects in MATLAB
Nodes(nnode) = Node();
for i = 1:nnode
    Nodes(i) = Node(i,nodescoord);
end
```

```
%Creation of all Materials
Materials(size(MATERIALS,1)) = Orthotropic();
for i = 1:length(Materials)
    E1 = cell2mat(MATERIALS(i,2));
    E2 = cell2mat(MATERIALS(i,3));
    E3 = cell2mat(MATERIALS(i,4));
    ni12 = cell2mat(MATERIALS(i,5));
    ni13 = cell2mat(MATERIALS(i,6));
    ni23 = cell2mat(MATERIALS(i,7));
    G12 = cell2mat(MATERIALS(i,8));
    G13 = cell2mat(MATERIALS(i,9));
    G23 = cell2mat(MATERIALS(i,10));
    ro = cell2mat(MATERIALS(i,11));
    Materials(i) = Orthotropic(E1,E2,E3,ni12,ni13,ni23,G12,G13,G23,ro);
    clear E1 E2 E3 ni12 ni13 ni23 G12 G13 G23 ro
end

Laminas(Nlayer) = OrthotropicLaminaPlaneStress();
for i = 1:Nlayer
    Laminas(i) = OrthotropicLaminaPlaneStress(i,angles(i),layers(i));
end

%Assignment of the Materials to Laminas
for i = 1:Nlayer
    for j = 1:size(MATERIALS,1)
        if strcmp( STACKING(i,3) , MATERIALS(j,1) ) == 1
            Laminas(i) = Laminas(i).assignMat(Materials(j));
        end
    end
end
```

`MakePostRes.m` **file**

```
function make_post_res(file_name, MyModel, elements, SOLVER)

%INITIALIZATION
res_file = strcat(file_name(1:end-4),'.post.res');
fid = fopen(res_file,'w');
fprintf(fid,'GiD Post Results File 1.0 \n');

%GAUSS POINTS
if strcmp(MyModel.ElemString,'Prism') == 1
    fprintf(fid,'GaussPoints "Gauss_Points_Prism" Elemtype Prism \n');
    fprintf(fid,'Number of Gauss Points: 6        \n');
    fprintf(fid,'Natural Coordinates: Give        \n');
    fprintf(fid,'0.166666666667 0.166666666667 0  \n');
    fprintf(fid,'0.666666666667 0.166666666667 0  \n');
    fprintf(fid,'0.166666666667 0.666666666667 0  \n');
    fprintf(fid,'0.166666666667 0.166666666667 1  \n');
    fprintf(fid,'0.666666666667 0.166666666667 1  \n');
    fprintf(fid,'0.166666666667 0.666666666667 1  \n');
else
    fprintf(fid,'GaussPoints "Gauss_Points_Hexahedra"
    Elemtype Hexahedra \n');
    fprintf(fid,'Number of Gauss Points: 8        \n');
    fprintf(fid,'Natural Coordinates: Given       \n');
    fprintf(fid,'-0.577350269189626 -0.577350269189626 -1 \n');
    fprintf(fid,' 0.577350269189626 -0.577350269189626 -1 \n');
    fprintf(fid,' 0.577350269189626  0.577350269189626 -1 \n');
    fprintf(fid,'-0.577350269189626  0.577350269189626 -1 \n');
    fprintf(fid,'-0.577350269189626 -0.577350269189626  1 \n');
    fprintf(fid,' 0.577350269189626 -0.577350269189626  1 \n');
    fprintf(fid,' 0.577350269189626  0.577350269189626  1 \n');
    fprintf(fid,'-0.577350269189626  0.577350269189626  1 \n');
end
fprintf(fid,'end GaussPoints \n');

%% FREE VIBRATIONS AND BUCKLING
if strcmp(SOLVER.ResultType, 'Mode Shape') == 1
    result = MyModel.DeformedShape;
    records = size(result, 4);
    for rec = 1:records
        fprintf(fid,'Result "Mode Shape" "Eigen Value Analysis"
        %6i Vector OnNodes \n', SOLVER.NatFreq(rec));
        fprintf(fid,'ComponentNames "X", "Y", "Z" \n');
        fprintf(fid,'Values \n');
```

```
        for j = 1:length(MyModel.NodesNumericalZ)
            for i = (j-1)*MyModel.NumNode+1 : j*MyModel.NumNode
                realnode_plane = i - (j-1)*MyModel.NumNode;
                fprintf(fid,'%6i %12.5f %12.5f %12.5f \n', i,
                result(j, 1:3, realnode_plane,rec));
            end
        end
        fprintf(fid,'End Values \n');
    end
elseif strcmp(SOLVER.ResultType, 'Buckling Mode') == 1
    result = MyModel.DeformedShape;
    records = size(result, 4);
    for rec = 1:records
        fprintf(fid,'Result "Buckling Mode" "Eigen Value Analysis"
        %6i Vector OnNodes \n', SOLVER.CritLoad(rec));
        fprintf(fid,'ComponentNames "X", "Y", "Z" \n');
        fprintf(fid,'Values \n');
        for j = 1:length(MyModel.NodesNumericalZ)
            for i = (j-1)*MyModel.NumNode+1 : j*MyModel.NumNode
                realnode_plane = i - (j-1)*MyModel.NumNode;
                fprintf(fid,'%6i %12.5f %12.5f %12.5f \n', i,
                result(j, 1:3, realnode_plane,rec));
            end
        end
        fprintf(fid,'End Values \n');
    end
end

%% TRANSIENT ANALYSIS
if strcmp(SOLVER.ResultType, 'Deformed Shapes') == 1
    result = MyModel.DeformedShape;
    records = size(result, 4);
    for rec = 1:records
        fprintf(fid,'Result "Total Displacement" "Transient
        Analysis" %6i Vector OnNodes \n', rec);
        fprintf(fid,'ComponentNames "X", "Y", "Z" \n');
        fprintf(fid,'Values \n');
        for j = 1:length(MyModel.NodesNumericalZ)
            for i = (j-1)*MyModel.NumNode+1 : j*MyModel.NumNode
                realnode_plane = i - (j-1)*MyModel.NumNode;
                fprintf(fid,'%6i %12.5f %12.5f %12.5f \n', i,
                result(j, 1:3, realnode_plane, rec));
            end
        end
        fprintf(fid,'End Values \n');
    end
```

```
    if strcmp(MyModel.ElemString,'Prism') == 1
        for rec = 1:records
            fprintf(fid,'Result "Stresses" "Transient Analysis" %6i
            Vector OnGaussPoints "Gauss_Points_Prism"  \n', rec);
            fprintf(fid,'ComponentNames "SigmaX","SigmaY","SigmaXY" \n');
            fprintf(fid,'Values \n');
            for layer = 1:MyModel.NumLayer
                for elem = 1:MyModel.NumEl
                    elemID = (layer-1)*MyModel.NumEl + elem;
                    fprintf(fid,'%6i %12.5f %12.5f %12.5f \n',elemID,
                    FiniteElements(elem).Stress_In_Plane(1,:,layer,rec));
                    for gaus = 2:6
                        fprintf(fid,'%12.5f %12.5f %12.5f \n',
                        FiniteElements(elem).Stress_In_Plane
                        (gaus, :, layer, rec));
                    end
                end
            end
            fprintf(fid,'End Values \n');
        end
    else
        for rec = 1:records
            fprintf(fid,'Result "Stresses" "Transient Analysis" %6i
            Vector OnGaussPoints "Gauss_Points_Hexahedra" \n', rec);
            fprintf(fid,'ComponentNames "SigmaX","SigmaY","SigmaXY" \n');
            fprintf(fid,'Values \n');
            for layer = 1:MyModel.NumLayer
                for elem = 1:MyModel.NumEl
                    elemID = (layer-1)*MyModel.NumEl + elem;
                    fprintf(fid,'%6i %12.5f %12.5f %12.5f \n',elemID,
                    elements(elem).Stress_In_Plane(1,:,layer, rec));
                    for gaus = 2:8
                        fprintf(fid,'%12.5f %12.5f %12.5f \n',
                        elements(elem).Stress_In_Plane(gaus,:,layer,rec));
                    end
                end
            end
            fprintf(fid,'End Values \n');
        end
    end
end


%% LINEAR SOLVER
if strcmp(SOLVER.ResultType, 'Deformed Shape') == 1
    %DISPLACEMENTS
    result = MyModel.DeformedShape;
```

```
    fprintf(fid,'Result "Total Displacement" "Load Analysis"
    %6i Vector OnNodes \n', 1);
    fprintf(fid,'ComponentNames "X", "Y", "Z" \n');
    fprintf(fid,'Values \n');
    for j = 1:length(MyModel.NodesNumericalZ)
        for i = (j-1)*MyModel.NumNode+1 : j*MyModel.NumNode
            realnode_plane = i - (j-1)*MyModel.NumNode;
            fprintf(fid,'%6i %12.5f %12.5f %12.5f \n', i,
            result(j,1:3,realnode_plane,1));
        end
    end
    fprintf(fid,'End Values \n');

    %STRESSES
    if strcmp(MyModel.ElemString,'Prism') == 1
        fprintf(fid,'Result "Stresses" "Load Analysis" %6i Vector
        OnGaussPoints "Gauss_Points_Prism" \n', 1);
        ngaus=6;
    else
        fprintf(fid,'Result "Stresses" "Load Analysis" %6i
        Vector OnGaussPoints "Gauss_Points_Hexahedra"  \n', 1);
        ngaus=8;
    end
    fprintf(fid,'ComponentNames "SigmaX","SigmaY","SigmaXY" \n');
    fprintf(fid,'Values \n');
    for layer = 1:MyModel.NumLayer
        for elem = 1:MyModel.NumEl
            elemID = (layer-1)*MyModel.NumEl + elem;
            fprintf(fid,'%6i %12.5f %12.5f %12.5f \n', elemID,
            elements(elem).Stress_In_Plane(1, :, layer));
            for gaus = 2:ngaus
                fprintf(fid,'%12.5f %12.5f %12.5f \n',
                elements(elem).Stress_In_Plane(gaus, :, layer));
            end
        end
    end
    fprintf(fid,'End Values \n');
end


%% NONLINEAR SOLVER
if strcmp(SOLVER.ResultType, 'Deformed Shape NL') == 1
    result = MyModel.DeformedShape;
    records = size(result, 4);
    %DISPLACEMENTS
    for rec = 1:records
        fprintf(fid,'Result "Total Displacement" "Load Analysis"
```

```
        %6i Vector OnNodes  \n', rec);
        fprintf(fid,'ComponentNames "X","Y","Z"  \n');
        fprintf(fid,'Values \n');
        for j = 1:length(MyModel.NodesNumericalZ)
            for i = (j-1)*MyModel.NumNode+1 : j*MyModel.NumNode
                realnode_plane = i - (j-1)*MyModel.NumNode;
                fprintf(fid,'%6i %12.5f %12.5f %12.5f  \n', i,
                result(j, 1:3, realnode_plane, rec));
            end
        end
        fprintf(fid,'End Values  \n');
    end


    %STRESSES
    for rec = 1:records
        if strcmp(MyModel.ElemString,'Prism') == 1
            fprintf(fid,'Result "Stresses" "Load Analysis" %6i
            Vector OnGaussPoints "Gauss_Points_Prism"  \n', rec);
            ngaus = 6;
        else
            fprintf(fid,'Result "Stresses" "Load Analysis" %6i
            Vector OnGaussPoints "Gauss_Points_Hexahedra" \n', rec);
            ngaus = 8;
        end
        fprintf(fid,'ComponentNames "SigmaX","SigmaY","SigmaXY"  \n');

        fprintf(fid,'Values  \n');
        for layer = 1:MyModel.NumLayer
            for elem = 1:MyModel.NumEl
                elemID = (layer-1)*MyModel.NumEl + elem;
                fprintf(fid,'%6i %12.5f %12.5f %12.5f \n', elemID,
                elements(elem).Stress_In_Plane(1, :, layer, rec));
                for gaus = 2:ngaus
                    fprintf(fid,'%12.5f %12.5f %12.5f \n',
                    elements(elem).Stress_In_Plane(gaus, :,
                    layer, rec));
                end
            end
        end
        fprintf(fid,'End Values \n');
    end
end
fclose(fid);
end
```

MakePostMsh.m file

```
function make_post_msh(file_name, MyModel)
msh_file = strcat(file_name(1:end-4),'.post.msh');
fid = fopen(msh_file,'w');
fprintf(fid,'MESH dimension %6i elemtype %s nnode %6i \n', 3,
MyModel.ElemString, MyModel.PlotNodes);

fprintf(fid,'coordinates \n');
for j = 1:length(MyModel.NodesNumericalZ)
    for i = (j-1)*MyModel.NumNode+1 : j*MyModel.NumNode
        realnode_plane = i-(j-1)*MyModel.NumNode;
        fprintf(fid,'%6i %12.5f %12.5f %12.5f \n', i,
        MyModel.StartCoord(j,1:3,realnode_plane) );
    end
end
fprintf(fid,'end coordinates \n');

elements = zeros(MyModel.GiDNumEl,MyModel.PlotNodes);
SubArray = zeros(MyModel.NumLayer,2);
SubArray(1,:) = [1 2];
counter = 1;
for i = 2:length(MyModel.NodesNumericalZ)-1
    if MyModel.NodesNumericalZ(i) < MyModel.NodesNumericalZ(i+1)
        counter = counter+1;
        SubArray(counter,:) = i:i+1;
    end
end

switch MyModel.NodesPerElem
    case 3
        connew = zeros(MyModel.NumEl,3,length(MyModel.NodesNumericalZ));
        for i = 1:length(MyModel.NodesNumericalZ)
            connew(:,:,i) = MyModel.ConnectivityInPlane(:,:)
            + MyModel.NumNode*(i-1);
        end
    case 6
        connew = zeros(MyModel.NumEl,3,length(MyModel.NodesNumericalZ));
        for i = 1:length(MyModel.NodesNumericalZ)
            connew(:,:,i) = MyModel.ConnectivityInPlane(:,1:3)
            + MyModel.NumNode*(i-1);
        end
    case 4
        connew = zeros(MyModel.NumEl,4,length(MyModel.NodesNumericalZ));
        for i = 1:length(MyModel.NodesNumericalZ)
```

```matlab
            connew(:,:,i) = MyModel.ConnectivityInPlane(:,:)
            + MyModel.NumNode*(i-1);
        end
    case 9
        connew = zeros(MyModel.NumEl,4,length(MyModel.NodesNumericalZ));
        for i = 1:length(MyModel.NodesNumericalZ)
            connew(:,:,i) = MyModel.ConnectivityInPlane(:,1:4)
            + MyModel.NumNode*(i-1);
        end
end

for i = 1:MyModel.NumEl
    for j = 1:MyModel.NumLayer
        elements((j-1)*MyModel.NumEl+i , :) = [connew(i,:,SubArray(j,1))
                                                connew(i,:,SubArray(j,2))];
    end
end

%Make New Connectivity for Every Element according to GiD Customization
fprintf(fid,'elements \n');
switch MyModel.PlotNodes
    case 8
        for i = 1:MyModel.GiDNumEl
            fprintf(fid,'%6i %6i %6i %6i %6i %6i %6i %6i %6i \n',
            i, elements(i,:));
        end
    case 6
        for i = 1:MyModel.GiDNumEl
            fprintf(fid,'%6i %6i %6i %6i %6i %6i %6i \n', i,
            elements(i,:));
        end
end
fprintf(fid,'end elements');
fclose(fid);
end
```

List of Abbreviations

2D two-dimensional

3D three-dimensional

CC clamped-clamped

CCT Crack Closure Technique

CF clamped-free

CFRP carbon-fiber-reinforced polymers

COD Crack Opening Displacement

CPT classical plate theory

CS clamped-simply supported

DCB Double-Cantilever-Beam

DOF degree-of-freedom

DSM Dynamic Stiffness Method

ESL Equivalent-Single-Layer

F free

FE finite element

FRP fiber-reinforced polymers

FSDT First-Order Shear Deformation Theory

GLPT Generalized Laminated Plate Theory

GRP glass-reinforced plastic

HSDT Higher-Order Shear Deformation Theory

L linear

NL non-linear

OO object-oriented

SERR Strain Energy Release Rate

SS simply-supported

VCCT Virtual Crack Closure Technique

Bibliography

[1]   F. A. Fazzolari. "A refined dynamic stiffness element for free vibration analysis of cross-ply laminated composite cylindrical and spherical shallow shells". In: *Composites Part B: Engineering* 62 (2014), pp. 143–158.

[2]   T. C. Triantafillou and L. J. Gibson. "Debonding in foam-core sandwich panels". In: *Materials and Structures* 22 (1989), pp. 64–69.

[3]   V. N. Burlayenko and T. Sadowski. "Finite element nonlinear dynamic analysis of sandwich plates with partially detached facesheet and core". In: *Finite Elements in Analysis and Design* 62 (2012), pp. 49–64.

[4]   I. W. Obreimoff. "The splitting strength of mica". In: *Proceedings of the Royal Society of London: Series A - Mathematical and Physical Sciences* 127A (1930), pp. 290–297.

[5]   V. V. Bolotin. "Mechanics of Delaminations in Laminate Composite Structures". In: *Mechanics of Composite Materials* 37.5 (2001), pp. 367–380.

[6]   L. M. Kachanov. "Layering in glass-fiber pipes subjected to external pressure". In: *Polymer Mechanics* 11.6 (1975), pp. 947–949.

[7]   V. V. Bolotin. "Delaminations in composite structures: its origin, buckling, growth and stability". In: *Composites Part B: Engineering* 27 (1996), pp. 129–145.

[8]   J. N. Reddy. *Mechanics of laminated composite plates: theory and analysis.* CRC Press, 1997.

[9]   E. J. Barbero and J. N. Reddy. "Modeling of Delamination in Composite Laminates using a Layer-Wise Plate Theory". In: *International Journal of Solids and Structures* 28.3 (1991), pp. 373–388.

[10] T. von Kármán. "Festigkeits Versuche unter allseitigem Druck". In: *Verhandlungen der Deutchen Ingenieurwesen* 55 (1911), pp. 1749–1757.

[11] E. J. Barbero and J. N. Reddy. "The Jacobian Derivative Method for Three-Dimensional Fracture Mechanics". In: *Communications in Applied Numerical Methods* 6 (1990), pp. 507–518.

[12] P. Tong, H. P. P. Pian, and S. J. Lasry. "A Hybrid-element Approach to Crack Problems in Plane Elasticity". In: *International Journal for Numerical Methods in Engineering* 7 (1973), pp. 297–308.

[13] I. S. Raju. "Calculation of strain-energy release rates with higher order and singular finite elements". In: *Engineering Fracture Mechanics* 28.3 (1987), pp. 251–274.

[14] J. R. Rice. "A Path Independent Integral and the Approximate Analysis of Strain Concentrations by Notches and Cracks". In: *Journal of Applied Mechanics* 35 (1968), pp. 379–386.

[15] S. K. Chan, I. S. Tuba, and W. K. Wilson. "On the Finite Element Method in Linear Fracture Mechanics". In: *Engineering Fracture Mechanics* 2 (1970), pp. 1–17.

[16] T. K. Hellen. "On the Method of Virtual Crack Extensions". In: *International Journal for Numerical Methods in Engineering* 9 (1975), pp. 187–207.

[17] E. F. Rybicki and M. F. Kanninen. "A finite element calculation of stress intensity factors by a modified crack closure integral". In: *Engineering Fracture Mechanics* 9 (1977), pp. 931–938.

[18] A. Szekrényes. "Interlaminar stresses and energy release rates in delaminated orthotropic composite plates". In: *International Journal of Solids and Structures* 49.18 (2012), pp. 2460–2470.

[19] A. Szekrényes. "Stress and fracture analysis in delaminated orthotropic composite plates using third-order shear deformation theory". In: *Applied Mathematical Modelling* 38.15-16 (2014), pp. 3897–3916.

[20] D. Vuksanović and M. Ćetković. "Bending , free vibrations and buckling of laminated composite and sandwich plates using a layerwise displacement model". In: *Composite Structures* 88 (2009), pp. 219–227.

[21] D. Vuksanović. "Linear analysis of laminated composite plates using single layer higher-order discrete models". In: *Composite Structures* 48 (2000), pp. 205–211.

[22] S. Kapuria, P. C. Dumir, and N. K. Jain. "Assessment of zig-zag theory for static loading, buckling, free and forced response of composite and sandwich beams". In: *Composite StructuresComposite Structures* 64 (2004), pp. 317–327.

[23] D. K. Rao and Y. M. Desai. "Analytical solutions for vibrations of laminated and sandwich plates using mixed theory". In: *Composite Structures* 63 (2004), pp. 361–373.

[24] W. Zhen, C. Wanji, and R. Xiaohui. "An accurate higher-order theory and C0 finite element for free vibration analysis of laminated composite and sandwich plates". In: *Composite Structures* 92.6 (2010), pp. 1299–1307.

[25] G. H. Staab. *Laminar composites*. Butterworth-Heinemann, 1999.

[26] D. Gay, S. V. Hoa, and S. W. Tsai. *Composite materials: design and applications*. CRC Press, 2003.

[27] A. W. Leissa. *Vibration of shells (NASA SP-288)*. Washington DC: US Government Printing Office, 1973.

[28] E. Carrera, S. Brischetto, and P. Nali. *Plates and shells for smart structures: classical and advanced theories for modeling and analysis*. John Wiley & Sons, 2011.

[29] N. J. Pagano. "Exact solutions for composite laminates in cylindrical bending". In: *Journal of Composite Materials* 3 (1967), pp. 398–411.

[30] A. K. Noor. "Free vibrations of multilayered composite plates". In: *AIAA Journal* 11 (1973), pp. 1038–1039.

[31] M. S. Qatu. *Vibration of laminated shells and plates*. San Diego: Elsevier Ltd, 2004.

[32] M. S. Qatu. "Recent research advances in dynamic behavior of shells: 1989-2000. Part 1: laminated composite shells". In: *Applied Mechanics Reviews* 55.4 (2002), pp. 325–349.

[33] M. S. Qatu. "Recent research advances in dynamic behavior of shells: 1989-2000. Part 2: homogeneous shells". In: *Applied Mechanics Reviews* 55.5 (2002), pp. 415–434.

[34] M. S. Qatu, R. W. Sullivan, and W. Wang. "Recent research advances in dynamic behavior of composite shells: 2000-2009". In: *Composite Structures* 93 (2010), pp. 14–31.

[35] N. Nanda and J. N. Bandyopadhyay. "Geometrically nonlinear transient analysis of laminated composite shells using the finite element method". In: *Journal of Sound and Vibration* 325.1-2 (2009), pp. 174–185.

[36] J. N. Reddy. "Geometrically Nonlinear Transient Analysis of Laminated Composite Plates". In: *AIAA Journal* 21.4 (1983), pp. 621–629.

[37] F. Ju, H. P. Lee, and K. H. Lee. "Finite element analysis of free vibration of delaminated composite plates". In: *Composites Part B: Engineering* 5.2 (1995), pp. 195–209.

[38] D. R. J. Owen and Z. H. Li. "A refined analysis of laminated plates by finite element displacement methods-II. Vibration and stability". In: *Computers & Structures* 26.6 (1987), pp. 915–923.

[39] J. N. Reddy. "A simple higher-order theory for laminated composite plates". In: *Journal of Applied Mechanics* 51 (1984), pp. 745–752.

[40] Y. Baar, Y. Ding, and R. Schultz. "Refined shear-deformation models for composite laminates with finite rotations". In: *International Journal of Solids and Structures* 30.19 (1993), pp. 2611–2638.

[41] A. K. Nayak, R. A. Shenoi, and S. S. J. Moy. "Transient response of initially stressed composite sandwich plates". In: *Finite Elements in Analysis and Design* 42 (2006), pp. 821–836.

[42] A. K. Nayak, R. A. Shenoi, and S. S. J. Moy. "Transient response of composite sandwich plates". In: *Composite Structures* 64 (2004), pp. 249–267.

[43] J. N. Reddy. "Bending of laminated anisotropic shells by a shear deformable finite element". In: *Fibre Science and Technology* 17 (1982), pp. 9–24.

[44] A. A. Khdeir, J. N. Reddy, and D. Frederick. "A Study of Bending, Vibration and Buckling of Cross-Ply Circular Cylindrical Shells". In: *International Journal of Engineering Science* 27.11 (1989), pp. 1337–1351.

[45] R. Bellman and J. Casti. "Differential quadrature and long-term integration". In: *Journal of Mathematical Analysis and Applications* 34 (1971), pp. 235–238.

[46] R. Bellman, B. G. Kashef, and J. Casti. "Differential quadrature: a technique for the rapid solution of nonlinear partial differential equations". In: *Journal of Computational Physics* 10 (1972), pp. 40–52.

[47] C. Shu. "Generalized differential-integral quadrature and application to the simulation of incompressible viscous flows including parallel computation". PhD. University of Glasgow, 1991.

[48] C. Shu and B. E. Richards. "Application of generalized differential quadrature to solve two-dimensional incompressible Navier-Stokes equations". In: *International Journal for Numerical Methods in Fluids* 15 (1992), pp. 791–798.

[49] C. Shu and B. E. Richards. "Parallel simulation of incompressible viscous flows by generalized differential quadrature". In: *Computing Systems in Engineering* 3 (1992), pp. 271–281.

[50] C. Shu. "Free Vibration Analysis of Composite Laminated Conical Shells by Generalized Differential Quadrature". In: *Journal of Sound and Vibration* 194 (1996), pp. 587–604.

[51] C. P. Wu and C. H. Wu. "Asymptotic differential quadrature solutions for the free vibration of laminated conical shells". In: *Computational Mechanics* 25 (2000), pp. 346–357.

[52]   C. Wu and C. Lee. "Differential quadrature solution for the free vibration analysis of laminated conical shells with variable stiffness". In: *International Journal of Mechanical Sciences* 43 (2001), pp. 1853–1869.

[53]   M. Talebitooti. "Three-dimensional free vibration analysis of rotating laminated conical shells: layerwise differential quadrature (LW-DQ) method". In: *Archive of Applied Mechanics* 83.5 (2012), pp. 765–781.

[54]   L. Tong. "Free vibration of composite laminated conical shells". In: *International Journal of Mechanical Sciences* 35.1 (1993), pp. 47–61.

[55]   L. Tong. "Free vibration of laminated conical shells including transverse shear deformation". In: *International Journal of Solids and Structures* 31.4 (1994), pp. 443–456.

[56]   G. Jin et al. "An exact solution for the free vibration analysis of laminated composite cylindrical shells with general elastic boundary conditions". In: *Composite Structures* 106 (2013), pp. 114–127.

[57]   G. Jin et al. "A unified approach for the vibration analysis of moderately thick composite laminated cylindrical shells with arbitrary boundary conditions". In: *International Journal of Mechanical Sciences* 75 (2013), pp. 357–376.

[58]   G. Jin et al. "A general Fourier solution for the vibration analysis of composite laminated structure elements of revolution with general elastic restraints". In: *Composite Structures* 109 (2014), pp. 150–168.

[59]   T. Ich Thinh and M. C. Nguyen. "Dynamic stiffness matrix of continuous element for vibration of thick cross-ply laminated composite cylindrical shells". In: *Composite Structures* 98 (2013), pp. 93–102.

[60]   M. Marjanović and D. Vuksanović. "Layerwise solution of free vibrations and buckling of laminated composite and sandwich plates with embedded delaminations". In: *Composite Structures* 108 (2014), pp. 9–20.

[61]   L. H. Yam et al. "Numerical analysis of multi-layer composite plates with internal delamination". In: *Computers & Structures* 82.7-8 (2004), pp. 627–637.

[62]   D. X. Lin, R. G. Ni, and R. D. Adams. "Prediction and measurement of the vibrational damping parameters of carbon glass fiber-reinforced plastics plates". In: *Journal of Composite Materials* 18 (1984), pp. 132–152.

[63]   Z. Wei, L. H. Yam, and L. Cheng. "Detection of internal delamination in multi-layer composites using wavelet packets combined with modal parameter analysis". In: *Composite Structures* 64 (2004), pp. 377–387.

[64]   W. Zhen and C. Wanji. "Free vibration of laminated composite and sandwich plates using globallocal higher-order theory". In: *Journal of Sound and Vibration* 298.1-2 (2006), pp. 333–349.

[65]   K. Alnefaie. "Finite element modeling of composite plates with internal delamination". In: *Composite Structures* 90.1 (2009), pp. 21–27.

[66]   Y. Baar, M. Itskov, and A. Eckstein. "Composite laminates: nonlinear interlaminar stress analysis by multi-layer shell elements". In: *Computer Methods in Applied Mechanics and Engineering* 185 (2000), pp. 367–397.

[67]   Y. Baar and M. H. Omurtag. "Free-vibration analysis of thin/thick laminated structures by layer-wise shell models". In: *Computers & Structures* 74.4 (2000), pp. 409–427.

[68]   S. Botello, E. Onate, and J. M. Canet. "A layer-wise triangle for analysis of laminated composite plates and shells". In: *Computers & Structures* 70.6 (1999), pp. 635–646.

[69]   A. Ghoshal et al. "Effect of delamination on transient history of smart composite plates". In: *Finite Elements in Analysis and Design* 41 (2005), pp. 850–874.

[70]   A. Chattopadhyay, H. S. Kim, and A. Ghoshal. "Non-linear vibration analysis of smart composite structures with discrete delamination using a refined layerwise theory". In: *Journal of Sound and Vibration* 273 (2004), pp. 387–407.

[71] H. Schwarts-Givli, O. Rabinovitch, and Y. Frostig. "High-order nonlinear contact eects in the dynamic behavior of delaminated sandwich panels with a flexible core". In: *International Journal of Solids and Structures* 44 (2007), pp. 77–99.

[72] S. Klinkel, F. Gruttmann, and W. Wagner. "A continuum based 3D shell element for laminated structures". In: *Computers & Structures* 71 (1999), pp. 43–62.

[73] W. Sprenger, F. Gruttmann, and W. Wagner. "Delamination growth analysis in laminated structures with continuum-based 3D-shell elements and a viscoplastic softening model". In: *Computer Methods in Applied Mechanics and Engineering* 185 (2000), pp. 123–139.

[74] E. J. Barbero, J. N. Reddy, and J. Teply. "An accurate determination of stresses in thick laminates using a generalized plate theory". In: *International Journal for Numerical Methods in Engineering* 29 (1990), pp. 1–14.

[75] B. W. R. Forde, R. O. Foschi, and S. F. Stiemer. "Object-oriented finite element analysis". In: *Computers & Structures* 34.3 (1990), pp. 355–374.

[76] J. R. Filho and P. R. B. Devloo. "Object oriented programming in scientific computations: the beginning of a new era". In: *Engineering Computations* 8.1 (1991), pp. 81–87.

[77] G. R. Miller. "An object-oriented approach to structural analysis and design". In: *Computers & Structures* 40.1 (1991), pp. 75–82.

[78] R. I. Mackie. "Object oriented programming of the finite element method". In: *International Journal for Numerical Methods in Engineering* 35.2 (1992), pp. 425–436.

[79] T. Zimmermann, Y. Dubois-Pelerin, and P. Bomme. "Object-oriented finite element programming: I: Governing principles". In: *Computer Methods in Applied Mechanics and Engineering* 98.2 (1992), pp. 291–303.

[80] Y. Dubois-Pelerin, T. Zimmermann, and P. Bomme. "Object-oriented finite element programming: II: a prototype program in smalltalk". In: *Computer Methods in Applied Mechanics and Engineering* 98.3 (1992), pp. 361–397.

[81] Y. Dubois-Pelerin and T. Zimmermann. "Object-oriented finite element programming: III: An efficient implementation in c++". In: *Computer Methods in Applied Mechanics and Engineering* 108.1-2 (1993), pp. 165–183.

[82] P. Menetrey and T. Zimmermann. "Object-oriented non-linear finite element analysis: application to j2 plasticity". In: *Computers & Structures* 49.5 (1993), pp. 767–773.

[83] R. M. V. Pidaparti and A. V. Hudli. "Dynamic analysis of structures using object-oriented techniques". In: *Computers & Structures* 49.1 (1993), pp. 149–156.

[84] B. Raphael and C. S. Krishnamoorthy. "Automating finite element development using object-oriented techniques". In: *Engineering Computations* 10.3 (1993), pp. 267–278.

[85] G. R. Miller. "Coordinate-free isoparametric elements". In: *Computers & Structures* 49.6 (1994), pp. 1027–1035.

[86] G. R. Miller, S. Banerjee, and K. Sribalaskandarajah. "A framework for interactive computational analysis in geomechanics". In: *Computers and Geotechnics* 17.1 (1995), pp. 17–37.

[87] G. C. Archer. "Object-Oriented Finite Element Analysis". PhD. University of California at Berkeley, 1996.

[88] G. C. Archer, G. Fenves, and C. Thewalt. "A new object-oriented finite element analysis program architecture". In: *Computers & Structures* 70.1 (1999), pp. 63–75.

[89] A. Cardona, I. Klapka, and M. Geradin. "Design of a new finite element programming environment". In: *Engineering Computations* 11.4 (1994), pp. 365–381.

[90] B. Patzak and Z. Bittnar. "Object oriented finite element modeling". In: *Acta Polytechnica* 39.2 (1999), pp. 99–113.

[91] P. Dadvand. "Framework for developing nite element code for Multi-Disciplinary Applications". PhD. 2007.

[92] P. Dadvand, R. Rossi, and E. Onate. "An Object-oriented Environment for Developing Finite Element Codes for Multi-disciplinary Applications". In: *Archives of Computational Methods in Engineering* 17.3 (2010), pp. 253–297.

[93] M. Ćetković. "Nonlinear behavior of laminated composite plates". PhD thesis. University of Belgrade, 2010.

[94] M. Marjanović, D. Vuksanović, and G. Meschke. "Geometrically nonlinear transient analysis of delaminated composite and sandwich plates using a layerwise displacement model with contact conditions". In: *Composite Structures* 122 (2015), pp. 67–81.

[95] M. Marjanović and D. Vuksanović. "Transient Response of Cross-Ply Laminated Composite Plates". In: *Proceedings of International Symposium for Students of Doctoral Studies in the fields of Civil Engineering, Architecture and Environmental Protection*. Niš, 2012, pp. 345–352.

[96] M. Marjanović and D. Vuksanović. "Linear Transient Analysis of Laminated Composite Plates using GLPT". In: *Proceedings of First international conference for PhD students in Civil Engineering*. Vol. 381. 0. Cluj-Napoca, 2012, pp. 169–176.

[97] M. Marjanović and D. Vuksanović. "Linear Transient Analysis of Laminated Composite Plates using GLPT". In: *cta Technica Napocensis: Civil Engineering & Architecture* 56.2 (2013), pp. 58–71.

[98] N. Newmark. "A method of computation for structural dynamics". In: *Journal of the Engineering Mechanics Division - ASCE* 85 (1959), pp. 67–94.

[99] O. C. Zienkiewicz and R. L. Taylor. *The Finite Element Method Volume 2: Solid Mechanics*. Butterworth-Heinemann, 2000.

[100] G. Meschke. *Finite Element Methods in Linear Structural Mechanics. Part III: Geometric Nonlinearity (Lecture Notes)*. Ruhr University Bochum - Institute for Structural Mechanics, 2011.

[101] A. K. Chopra. *Dynamics of structures: theory and applications to earthquake engineering*. Prentice Hall, 1995.

[102] R. W. Clough and J. Penzien. *Dynamics of structures*. McGraw-Hill, 1975.

[103] P. Wriggers. *Nonlinear Finite Element Methods*. Springer, 2008.

[104] M. Marjanović and D. Vuksanović. "Transient analysis of laminated composite and sandwich plates with embedded delaminations using GLPT". In: *Proceedings of 9th International Conference on Structural Dynamics EURODYN 2014*. July. Porto, 2014, pp. 3373–3380.

[105] M. Marjanović and D. Vuksanović. "Geometrically nonlinear transient analysis of delaminated composite plates". In: *Zbornik radova Graevinskog fakulteta Subotica* 25 (2014), pp. 465–471.

[106] D. Xie and S. B. Biggers. "Strain energy release rate calculation for a moving delamination front of arbitrary shape based on the virtual crack closure technique. Part I: Formulation and validation". In: *Engineering Fracture Mechanics* 73.6 (2006), pp. 771–785.

[107] D. Xie and S. B. Biggers. "Strain energy release rate calculation for a moving delamination front of arbitrary shape based on the virtual crack closure technique. Part II: Sensitivity study on modeling details". In: *Engineering Fracture Mechanics* 73.6 (2006), pp. 786–801.

[108] M. Marjanović and D. Vuksanović. "Linear Analysis of Single Delamination in Laminated Composite Plate using Layerwise Plate Theory". In: *Proceedings of 4th International Congress of Serbian Society of Mechanics*. June. Vrnjačka Banja, 2013, pp. 443–448.

[109] H. Chai, C. D. Babcock, and W. G. Knauss. "One-dimensional modeling of failure in laminated plates by delamination buckling". In: *International Journal of Solids and Structures* 17 (1981), pp. 1069–83.

[110] H. Chai and C. D. Babcock. "Two-dimensional modeling of compressive failure in delaminated laminates". In: *Journal of Composite Materials* 19 (1985), pp. 67–98.

[111] P. Robinson, F. Javidrad, and D. Hitchings. "Finite element modelling of delamination growth in the DCB and edge delaminated DCB specimens". In: *Composite Structures* 32 (1995), pp. 275–285.

[112] R. T. Tenchev and B. G. Falzon. "A pseudo-transient solution strategy for the analysis of delamination by means of interface elements". In: *Finite Elements in Analysis and Design* 42.8-9 (2006), pp. 698–708.

[113] Y. Mi, M. A. Crisfield, and G. A. O. Davies. "Progressive Delamination using Interface Elements". In: *Journal of Composite Materials* 32.14 (1998), pp. 1246–1272.

[114] M. Meo and E. Thieulot. "Delamination modelling in a double cantilever beam". In: *Composite Structures* 71 (2005), pp. 429–434.

[115] F. Shen, K. H. Lee, and T. E. Tay. "Modeling delamination growth in laminated composites". In: *Composites Science and Technology* 61.9 (2001), pp. 1239–1251.

[116] K. N. Shivakumar, P. W. Tan, and J. C. Newman Jr. "A virtual crack-closure technique for calculating stress intensity factors for cracked three dimensional bodies". In: *International Journal of Fracture* 36 (1988), pp. 43–50.

[117] R. Krueger. "The virtual crack closure technique: history, approach and applications". In: *Applied Mechanics Reviews* 57 (2004), pp. 109–143.

[118] T. E. Tay et al. "Mesh design in finite element analysis of post-buckled delamination in composite laminates". In: *Composite Structures* 47.1999 (2000), pp. 603–611.

[119] P. Robinson and D. Q. Song. "A modified DCB specimen for mode-I testing of multidirectional laminates". In: *Journal of Composite Materials* 26 (1992), pp. 1554–1577.

[120]   D. Hitchings, P. Robinson, and F. Javidrad. "A finite element model for delamination propagation in composites". In: *Computers & Structures* 60.6 (1996), pp. 1093–1104.

[121]   J. D. Whitcomb and K. N. Shivakumar. "Strain-Energy Release Rate Analysis of a Laminate with a Postbuckled Delamination". In: *NASA Technical Memorandum* 89091 (1987).

[122]   H. Hosseini-Toudeshky, S. Hosseini, and B. Mohammadi. "Buckling and Delamination Growth Analysis of Composite Laminates Containing Embedded Delaminations". In: *Applied Composite Materials* 17.2 (2009), pp. 95–109.

[123]   H. Hosseini-Toudeshky, S. Hosseini, and B. Mohammadi. "Delamination buckling growth in laminated composites using layerwise-interface element". In: *Composite Structures* 92.8 (2010), pp. 1846–1856.

[124]   H. Hosseini-Toudeshky, S. Hosseini, and B. Mohammadi. "Progressive delamination growth analysis using discontinuous layered element". In: *Composite Structures* 92.4 (2010), pp. 883–890.

[125]   Y. X. Zhang and S. Wang. "Buckling, post-buckling and delamination propagation in debonded composite laminates. Part 1 : Theoretical development". In: *Composite Structures* 88.1 (2009), pp. 121–130.

[126]   S. Wang and Y. X. Zhang. "Buckling, post-buckling and delamination propagation in debonded composite laminates. Part 2 : Numerical applications". In: *Composite Structures* 88.1 (2009), pp. 131–146.

[127]   F. Aymerich, F. Dore, and P. Priolo. "Prediction of impact-induced delamination in cross-ply composite laminates using cohesive interface elements". In: *Composites Science and Technology* 68.12 (2008), pp. 2383–2390.

[128]   L. Zhao et al. "Simulation of delamination growth in multidirectional laminates under mode I and mixed mode I/II loadings using cohesive elements". In: *Composite Structures* 116.1 (2014), pp. 509–522.

[129] A. C. Orifici et al. "Development of a Finite-Element Analysis Methodology for the Propagation of Delaminations in Composite Structures". In: *Mechanics of Composite Materials* 43.1 (2007), pp. 9–28.

[130] R. de Borst. "Numerical aspects of cohesive-zone models". In: *Engineering Fracture Mechanics* 70.14 (2003), pp. 1743–1757.

[131] A. C. Orifici et al. "Development of a degradation model for the collapse analysis of composite aerospace structures". In: *Proceedings of the 3rd European Conference on Computational Mechanics: Solids, Structures and Coupled Problems in Engineering*. Ed. by C. A. Mota Soares. Lisbon, Portugal, 2006.

[132] D. Vuksanović and M. Marjanović. "Application of layered finite elements in the numerical analysis of laminated composite and sandwich structures with delaminations". In: *Building Materials and Structures* 58 (2015), pp. 59–76.

[133] M. Marjanović and D. Vuksanović. "Free vibrations of laminated composite shells using the rotation-free plate elements based on Reddys layerwise discontinuous displacement model". In: *Composite Structures* (2016).

[134] S. P. Timoshenko and S. Woinowsky-Krieger. *The Theory of Plates and Shells*. McGraw-Hill, 1964.

[135] J. N. Reddy. *Theory and Analysis of Elastic Plates and Shells*. CRC Press, 2006.

[136] F. K. Bogner, R. L. Fox, and L. A. Schmit. "A cylindrical shell element". In: *AIAA Journal* 5 (1966), pp. 745–750.

[137] J. Connor and C. Brebbia. "Stiffness matrix for shallow rectangular shell element". In: *Proceedings of the American Society of Civil Engineers* 93 (1967), pp. 43–65.

[138] G. Cantin and R. W. Clough. "A curved, cylindricall shell finite element". In: *AIAA Journal* 6 (1968), pp. 1057–1062.

218

[139] G. R. Cowper, G. M. Lindberg, and M. D. Olson. "A shallow shell finite element of triangular shape". In: *International Journal of Solids and Structures* 6 (1970), pp. 1133–1156.

[140] G. Dupuis and J. J. Goel. "A curved finite element for thin elastic shells". In: *International Journal of Solids and Structures* 6 (1970), pp. 987–996.

[141] G. Meschke. *Finite Element Methods in Linear Structural Mechanics. Part II: Finite Element Methods for Slabs and Plates, Finite Volume Elements (Lecture Notes)*. Ruhr University Bochum - Institute for Structural Mechanics, 2011.

[142] E. Onate. *Structural Analysis with the Finite Element Method. Linear Statics. Volume 1. Basis and Solids*. Springer, 2009.

[143] *GiD - The Personal Pre And Post Processor, www.gidhome.com*.

[144] A. J. M. Ferreira. *MATLAB Codes for Finite Element Analysis Solids and Structures*. Springer, 2009.

[145] Y. W. Kwon and K. Bang. *The Finite Element Method using MATLAB*. CRC Press, 1997.

[146] D. Vuksanović and M. Marjanović. "Free vibrations of delaminated composite and sandwich plates". In: *Proceedings of 5th International Conference Civil Engineering Science and Practice*. February. Žabljak, 2014, pp. 363–370.

[147] G. H. Qing, Y. H. Liu, and D. H. Li. "A semi-analytical model for the energy release rate analyses of composite laminates with a delamination". In: *Finite Elements in Analysis and Design* 47.9 (2011), pp. 1017–1024.

[148] Z. Jiang et al. "Determination of mode-I fracture toughness and non-uniformity for GFRP double cantilever beam specimens with an adhesive layer". In: *Engineering Fracture Mechanics* 128 (2014), pp. 139–156.

[149] K. P. Soldatos. "A transverse shear deformation theory for homogenous monoclinic plates". In: *Acta Mechanica* 94 (1992), pp. 195–220.

[150] K. M. Liew, Y. Q. Huang, and J. N. Reddy. "Vibration analysis of symmetrically laminated plates based on FSDT using the moving least squares dierential quadrature method". In: *Computer Methods in Applied Mechanics and Engineering* 192 (2003), pp. 2203–2222.

[151] H. T. Chien et al. "Isogeometric analysis of laminated composite and sandwich plates using a new inverse trigonometric shear deformation theory". In: *European Journal of Mechanics - A/Solids* 43 (2014), pp. 89–108.

[152] C. Sarath Babu and T. Kant. "Two shear deformable finite element models for buckling analysis of skew fiber-reinforced composite and sandwich panels". In: *Composite Structures* 46 (1999), pp. 115–124.

[153] E. Hinton and D. Vuksanović. "Closed form solutions for dynamic analysis of simply supported Mindlin plates". In: *Numerical Methods and Software for Dynamic Analysis of Plates and Shells*. Ed. by E. Hinton. Swansea: Pineridge Press, 1988, pp. 1–47.

[154] E. Hinton and D. Vuksanović. "Explicit transient dynamic finite element analysis of initially stressed Mindlin plates". In: *Numerical Methods and Software for Dynamic Analysis of Plates and Shells*. Ed. by E. Hinton. Swansea: Pineridge Press, 1988, pp. 205–259.

[155] Y. Narita, Y. Ohta, and M. Saito. "Finite element study for natural frequencies of cross-ply laminated cylindrical shells". In: *Composite Structures* 26 (1993), pp. 55–62.

[156] A. J. M. Ferreira, C. M. C. Roque, and R. M. N. Jorge. "Static and free vibration analysis of composite shells by radial basis functions". In: *Composites Part B: Engineering* 30.9 (2006), pp. 719–733.

[157] E. Onate and F. Zarate. "Rotation-free triangular plate and shell elements". In: *International Journal for Numerical Methods in Engineering* 47 (2000), pp. 557–603.

Biography

Miroslav Marjanović was born on January 8th 1986 in Užice, Republic of Serbia, where he finished elementary school and Gymnasium, receiving the "*Vuk Karadžić*" Award both during the elementary and the high school. He completed the BSc (2005-2009) and the MSc studies (2009-2010) at the Faculty of Civil Engineering in Belgrade, with the highest average grade in his class at Module Structures. Miroslav Marjanović won the Prize of the Faculty of Civil Engineering in Belgrade (*Professor Dušan Krajčinović Foundation*) and the *Prize of the Regional Chamber of Commerce Užice* in 2008.

Miroslav Marjanović enrolled the PhD studies at the Faculty of Civil Engineering in Belgrade in 2010. Since December 2010 he has been working at the Faculty of Civil Engineering in Belgrade as a Teaching Assistant, teaching exercises in several subjects from the field of Theory of Structures. He has awarded several scholarships for the success achieved during regular studies. In four occasions he participated in seminars organized in collaboration of the University of Belgrade and German universities. Since 2011, Miroslav Marjanović participates as the Scholarship Holder in the international PhD program *SEEFORM*, in which he stayed at Ruhr-Universität Bochum, Institute for Structural Mechanics for 7 months and has also participated in several seminars for PhD students in Serbia and abroad. He is also engaged as a researcher on the Project of the Ministry of Education, Science and Technological Development of Serbia N^0 TR-36048.

Miroslav Marjanović completed the professional exam (Serbian Chamber of Engineers) for the construction industry in 2014. He is a member of the Association of Structural Engineers of Serbia and the Serbian Society of Mechanics. He speaks and writes English and Russian language. He is married.

Contributions

International Journal Papers

1. **Marjanović M**, Meschke G, Vuksanović Dj (**2016**). A finite element model for propagating delamination in laminated composite plates based on the virtual crack closure method. *Composite Structures, submitted.*

2. **Marjanović M**, Vuksanović Dj (**2016**). Free vibrations of laminated composite shells using the rotation-free plate elements based on Reddy's layerwise discontinuous displacement model. *Composite Structures, in press.*

3. Vuksanović Dj, **Marjanović M** (**2015**). Application of layered finite elements in the numerical analysis of laminated composite and sandwich structures with delaminations. *Building Materials and Structures*, 58:59-76.

4. **Marjanović M**, Vuksanović Dj, Meschke G (**2015**). Geometrically nonlinear transient analysis of delaminated composite and sandwich plates using a layerwise displacement model with contact conditions. *Composite Structures*, 122:67-81.

5. **Marjanović M**, Vuksanović Dj (**2014**). Layerwise solution of free vibrations and buckling of laminated composite and sandwich plates with embedded delaminations. *Composite Structures*, 108:9-20.

International Conferences

1. Vuksanović Dj, **Marjanović M**, Kovačević D (**03/2016**). Finite element modeling of free vibration problem of delaminated composite plates using Abaqus CAE. 6th International Conference Civil Engineering - Science and Practice. Žabljak, Montenegro, *in press.*

2. **Marjanović M**, Vuksanović Dj (**07/2014**). Transient analysis of laminated composite and sandwich plates with embedded delaminations using GLPT. 9th International Conference on Structural Dynamics EURODYN 2014. Porto, Portugal, 3373-3380.

3. Vuksanović Dj, **Marjanović M** (**02/2014**). Free vibrations of delaminated composite and sandwich plates. 5th International Conference Civil Engineering - Science and Practice. Žabljak, Montenegro, 363-370.

4. **Marjanović M**, Vuksanović Dj (**06/2013**). Linear Analysis of Single Delamination in Laminated Composite Plate using Layerwise Plate Theory. 4th International Congress of Serbian Society of Mechanics. Vrnjačka Banja, Serbia, 443-448.

5. **Marjanović M**, Vuksanović Dj (**11/2012**). Linear Transient Analysis of Laminated Composite Plates using GLPT. First international conference for PhD students in Civil Engineering. Cluj-Napoca, Romania, 169-176.

6. **Marjanović M**, Vuksanović Dj (**09/2012**). Transient Response of Cross-Ply Laminated Composite Plates. International Symposium for Students of Doctoral Studies in the fields of Civil Engineering, Architecture and Environmental Protection. Niš, Serbia, 345-352.

National Journal Papers

1. **Marjanović M**, Vuksanović Dj (**2014**). Geometrically nonlinear transient analysis of delaminated composite plates. *Zbornik radova Gradjevinskog fakulteta Subotica*, 25:465-471.

2. **Marjanović M**, Vuksanović Dj (**2013**). Linear Transient Analysis of Laminated Composite Plates using GLPT. *Acta Technica Napocensis: Civil Engineering & Architecture*, 56(2):58-71.

Прилог 1.

Изјава о ауторству

Потписани   Мирослав С. Марјановић

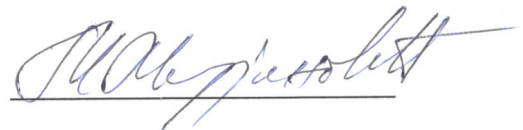број индекса 901/2010.

Изјављујем

да је докторска дисертација под насловом

NONLINEAR ANALYSIS OF LAMINATED COMPOSITE PLATES AND SHELLS WITH DELAMINATIONS USING FINITE ELEMENT METHOD

- резултат сопственог истраживачког рада,
- да предложена дисертација у целини ни у деловима није била предложена за добијање било које дипломе према студијским програмима других високошколских установа,
- да су резултати коректно наведени и
- да нисам кршио/ла ауторска права и користио интелектуалну својину других лица.

Потпис докторанда

У Београду, март 2016.

Прилог 2.

Изјава о истоветности штампане и електронске верзије докторског рада

Име и презиме аутора	Мирослав Марјановић, мастер инж. грађ.
Број индекса	901/2010.
Студијски програм	Грађевинарство
Наслов рада	NONLINEAR ANALYSIS OF LAMINATED COMPOSITE PLATES AND SHELLS WITH DELAMINATIONS USING FINITE ELEMENT METHOD
Ментори	Проф. др Ђорђе Вуксановић Универзитет у Београду, Грађевински факултет
	Prof. Dr.techn. Günther Meschke Ruhr University Bochum, Institute for Structural Mechanics

Потписани/а   **Мирослав Марјановић, мастер инж. грађ.**

Изјављујем да је штампана верзија мог докторског рада истоветна електронској верзији коју сам предао/ла за објављивање на порталу **Дигиталног репозиторијума Универзитета у Београду.**

Дозвољавам да се објаве моји лични подаци везани за добијање академског звања доктора наука, као што су име и презиме, година и место рођења и датум одбране рада.

Ови лични подаци могу се објавити на мрежним страницама дигиталне библиотеке, у електронском каталогу и у публикацијама Универзитета у Београду.

Потпис докторанда

У Београду, март 2016.

Прилог 3.

Изјава о коришћењу

Овлашћујем Универзитетску библиотеку „Светозар Марковић" да у Дигитални репозиторијум Универзитета у Београду унесе моју докторску дисертацију под насловом:

NONLINEAR ANALYSIS OF LAMINATED COMPOSITE PLATES AND SHELLS WITH DELAMINATIONS USING FINITE ELEMENT METHOD

која је моје ауторско дело.

Дисертацију са свим прилозима предао/ла сам у електронском формату погодном за трајно архивирање.

Моју докторску дисертацију похрањену у Дигитални репозиторијум Универзитета у Београду могу да користе сви који поштују одредбе садржане у одабраном типу лиценце Креативне заједнице (Creative Commons) за коју сам се одлучио/ла.

1. Ауторство

2. Ауторство - некомерцијално

3. Ауторство – некомерцијално – без прераде

4. Ауторство – некомерцијално – делити под истим условима

5. Ауторство – без прераде

6. Ауторство – делити под истим условима

(Молимо да заокружите само једну од шест понуђених лиценци, кратак опис лиценци дат је на полеђини листа).

Потпис докторанда

У Београду, март 2016.

1. Ауторство - Дозвољавате умножавање, дистрибуцију и јавно саопштавање дела, и прераде, ако се наведе име аутора на начин одређен од стране аутора или даваоца лиценце, чак и у комерцијалне сврхе. Ово је најслободнија од свих лиценци.

2. Ауторство – некомерцијално. Дозвољавате умножавање, дистрибуцију и јавно саопштавање дела, и прераде, ако се наведе име аутора на начин одређен од стране аутора или даваоца лиценце. Ова лиценца не дозвољава комерцијалну употребу дела.

3. Ауторство - некомерцијално – без прераде. Дозвољавате умножавање, дистрибуцију и јавно саопштавање дела, без промена, преобликовања или употребе дела у свом делу, ако се наведе име аутора на начин одређен од стране аутора или даваоца лиценце. Ова лиценца не дозвољава комерцијалну употребу дела. У односу на све остале лиценце, овом лиценцом се ограничава највећи обим права коришћења дела.

4. Ауторство - некомерцијално – делити под истим условима. Дозвољавате умножавање, дистрибуцију и јавно саопштавање дела, и прераде, ако се наведе име аутора на начин одређен од стране аутора или даваоца лиценце и ако се прерада дистрибуира под истом или сличном лиценцом. Ова лиценца не дозвољава комерцијалну употребу дела и прерада.

5. Ауторство – без прераде. Дозвољавате умножавање, дистрибуцију и јавно саопштавање дела, без промена, преобликовања или употребе дела у свом делу, ако се наведе име аутора на начин одређен од стране аутора или даваоца лиценце. Ова лиценца дозвољава комерцијалну употребу дела.

6. Ауторство - делити под истим условима. Дозвољавате умножавање, дистрибуцију и јавно саопштавање дела, и прераде, ако се наведе име аутора на начин одређен од стране аутора или даваоца лиценце и ако се прерада дистрибуира под истом или сличном лиценцом. Ова лиценца дозвољава комерцијалну употребу дела и прерада. Слична је софтверским лиценцама, односно лиценцама отвореног кода.